A ROLE FOR TOPOISOMERASE II ALPHA IN CHROMOSOME DAMAGE IN HUMAN CELL LINES

Samantha Terry

A Thesis Submitted for the Degree of PhD
at the
University of St. Andrews

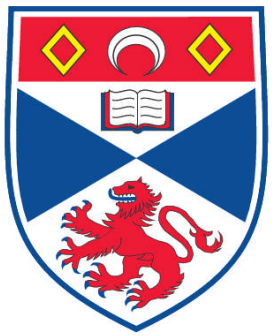

2009

A ROLE FOR TOPOISOMERASE II ALPHA IN CHROMOSOME DAMAGE IN HUMAN CELL LINES

Samantha Terry, BSc

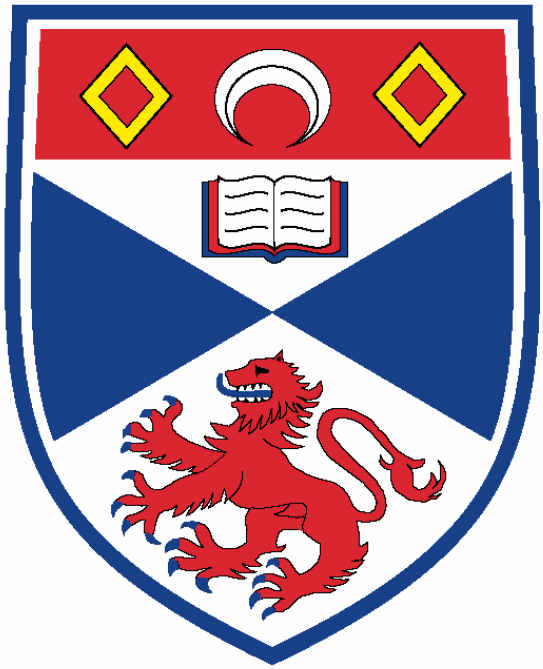

A thesis submitted to the University of St. Andrews for
the degree of

DOCTOR OF PHILOSOPHY

School of Medicine

September 2009

Declarations

I, Samantha Terry, hereby certify that this thesis, which is approximately 52,000 words in length, has been written by me, that it is the record of work carried out by me and that it has not been submitted in any previous application for a higher degree.

I was admitted as a research student in October 2006 and as a candidate for the degree of PhD in October 2007; the higher study for which this is a record was carried out in the University of St Andrews between 2006 and 2009.

Date Signature of candidate

…… …….

I hereby certify that the candidate has fulfilled the conditions of the Resolution and Regulations appropriate for the degree of Doctor of Philosophy in the University of St Andrews and that the candidate is qualified to submit this thesis in application for that degree.

Date Signature of supervisor

…… …….

In submitting this thesis to the University of St Andrews we understand that we are giving permission for it to be made available for use in accordance with the regulations of the University Library for the time being in force, subject to any copyright vested in the work not being affected thereby. We also understand that the title and the abstract will be published, and that a copy of the work may be made and supplied to any bona fide library or research worker, that my thesis will be electronically accessible for personal or research use, and that the library has the right to migrate my thesis into new electronic forms as required to ensure continued access to the thesis. We have obtained any third-party copyright permissions that may be required in order to allow such access and migration.

The following is an agreed request by candidate and supervisor regarding the electronic publication of this thesis:

Access to printed copy and electronic publication of thesis through the University of St Andrews.

Date Signature of candidate Signature of supervisor

…… ……. ……

Acknowledgements

I would like to thank Francis McCarthy and Georg Haehner at the School of Chemistry at the University of St Andrews with whom I collaborated to study chromosomal damage after hydrogen peroxide treatment with atomic force microscopy.

A big ‘cheers’ must go to everyone on E-floor and especially Elaine Campbell, Andrew Riches and the Bute Champagne Club, including the many females who have left the office to go have babies. A special thanks must go to my supervisor Peter Bryant for ‘hanging around’ in my final year and not giving up on either me or chromatid breaks.

Finally, the ultra cheesy part. Thank you Kirsty for providing me with tea, food and a couch. I also could not have completed this body of work without the constant support of my parents and my sister Becky, who were always available on the other end of the phone and last, but definitely not least, a BIG thanks to Dr Dan for just being there and sending flowers.

Publications

Terry, S.Y., Riches, A.C. & Bryant, P.E. Suppression of topoisomerase II alpha expression and function in human cells decreases chromosomal radiosensitivity. *Mutation Research*, **663**, 40-45 (2009).

Terry, S.Y., Riches, A.C. & Bryant, P.E. A role for topoisomerase II alpha in the formation of radiation-induced chromatid breaks. *Br J Cancer*, **99**, 670-4 (2008).

PE Bryant, AC Riches, S Terry, O Shovman, D Adamson. Topoisomerase II expression as a determinant of chromosomal radiosensitivity and possible susceptibility in breast cancer. *Breast Cancer Research* **10** (Suppl 2):P5 (2008).

Abstract

Human response to ionising radiation (IR) shows a wide variation. This is most clearly seen in the radiation-response of cells as measured by frequencies of chromosomal aberrations. Different frequencies of IR-induced aberrations can be conveniently observed in phytohaemagglutin-stimulated peripheral blood T-lymphocytes from both normal individuals and sporadic cancer cases, in either metaphase chromosomes or as micronuclei in the following cell cycle. Metaphase cells show frequent chromatid breaks, defined as chromatid discontinuities or terminal deletions, if irradiated in the G_2-phase of the cell cycle. It has been shown that the frequency of chromatid breaks in cells from approximately 40% of sporadic breast cancer patients, are significantly higher than in groups of normal individuals. This suggests that elevated radiation-induced chromatid break frequency may be linked with susceptibility to breast cancer.

It is known that chromatid breaks are initiated by a double strand break (DSB), but it appears that the two are linked only indirectly as repair kinetics for DSBs and chromatid breaks do not match. Therefore, the underlying causes of the wide variation in frequencies of chromatid breaks in irradiated T-lymphocytes from different normal individuals and from sporadic breast cancer cases are still unclear but it is unlikely to be linked directly to DSB rejoining.

My research has focused on the mechanism through which chromatid breaks are formed from initial DSBs. The lack of a direct association suggested that a signalling process might be involved, connecting the initial DSB and resulting chromatid break. The signal model, suggested that the initial DSB is located within a chromatin loop that leads to an intra- or interchromatid rearrangement resulting in incomplete mis-joining of chromatin ends during the decatenation of chromatids during G_2. It was therefore proposed that topoisomerase II alpha (topo IIα) might be involved, mainly because of its ability to incise DNA and its role in sister chromatid decatenation.

During my PhD research I have used a strategy of altering topo II activity or expression and studying whether this alters IR-induced chromatid break frequency. The first approach involved cell lines that varied in topo IIα expression. The frequency of IR-induced chromatid breaks was found to correlate positively with topo IIα expression level, as measured in three different cell lines by immunoblotting, i.e. two cell lines with lower topo IIα expression exhibited lower chromatid break frequency. Topo II activity in these three cell lines was also estimated indirectly by the ability of a topo IIα poison to activate the G_2/M checkpoint, and this related well with topo IIα expression. A second approach involved 'knocking down' topo IIα protein expression by silencing RNA (siRNA). Lowered topo IIα expression was confirmed by immunoblotting and polymerase chain reaction. SiRNA-lowered topo IIα expression correlated with a decreased IR-induced chromatid break frequency. In a third series of

experiments cells were treated with ICRF-193, a topo IIα catalytic inhibitor. It was shown that inhibition of topo IIα also significantly reduced IR-induced chromatid breaks. I also showed that lowered chromatid break frequency was not due to cells with high chromatid break frequencies being blocked in G_2 as the mitotic index was not altered significantly in cells with lowered topo IIα expression or activity. These experiments show that topo IIα is involved in IR-induced chromatid break formation.

The final experiments reported here attempted to show how topo II might be recruited in the process of forming IR-induced chromatid breaks. Hydrogen peroxide was used as a source of reactive oxygen species (reported to poison topo IIα) and it was shown that topo IIα under these conditions is involved in the entanglement of metaphase chromosomes and formation of chromatin 'dots' as well as chromatid breaks. Experiments using atomic force microscopy attempted to confirm these dots as excised chromatin loops.

The possible role of topo IIα in both radiation- and hydrogen peroxide-induced primary DNA damage was also tested. It was shown that topo IIα does not affect radiation-induced DSBs, even though it does affect chromatid break frequency. Also, topo IIα does not affect hydrogen peroxide-induced DNA damage at low doses. The results support the idea that topo IIα is involved in the conversion of DSBs to chromatid breaks after both irradiation and treatment with hydrogen peroxide at a low concentrations.

I have demonstrated that topo IIα is involved in forming IR-induced chromatid breaks, most likely by converting the initial DSBs into chromosomal aberrations as suggested by the signal model.

TABLE OF CONTENTS

List of figures

Figure **Page**

Chapter 6

List of tables

Abbreviations

3D	3-dimensional
53BP1	p53 binding protein 1
^{137}Cs	^{137}Caesium
γH_2AX	phosphorylated form of histone H_2AX
ADP	adenosine diphosphate
AFM	atomic force microscopy
ALL	acute lymphoblastic leukemia
AML	acute myeloid leukemia
APL	acute promyelocytic leukemia
APS	ammonium persulphate
Ara A	9-β-D-arabinosyladenine or adenine arabinoside
AT	ataxia telangiectasia
ATCC	American type culture collection
ATM	ataxia telangiectasia mutated protein
ATM	ataxia telangiectasia mutated gene
ATP	adenosine triphosphate
ATR	ATM-related protein
Bcr	breakage cluster region
BPB	bromophenol blue
BRCA1 or 2	Breast cancer protein 1 or 2
BRCA1 or *2*	Breast cancer gene 1 or 2
BRCT	C-terminal domain of breast cancer proteins
BS	Bloom's syndrome
BSA	bovine serum albumin
CA	chromosome aberration
cdc2	cyclin-dependent kinase 2
cdc25	cyclin-dependent phosphatase 25
CDK1	cyclin-dependent kinase 1
cDNA	complement DNA
Chk1	checkpoint kinase 1
CISH	chromogenic *in situ* hybridisation
DAPI	4',6-diamidino-2-phenylindole
DSB	double strand break
DMEM-F12	a 1:1 mixture of Dulbecco's Modified Eagle's medium and Ham's F12 medium
DMSO	dimethyl sulfoxide
DNA	deoxyribonucleic acid
DNA-PK_{cs}	DNA-dependent protein kinase catalytic subunit

dNTP	deoxynucleoside triphosphates
DTT	dithiothreitol
ECL	enhanced chemiluminescence
E. coli	*Eschericia coli*
EDTA	ethylenediaminetetraacetic acid
FA	Fanconi's anaemia
FCS	foetal calf serum
FDR	fraction of DNA released
FISH	fluorescent *in situ* hybridisation
G_0	quiescent gap phase of cell cycle
G_1	gap phase of cell cycle before DNA replication
G_2	gap phase of cell cycle before mitosis
G-segment	gated DNA double helix segment
H_2O_2	hydrogen peroxide
HCl	hydrogen chloride
HL60	human promyelocytic leukemic cell line
HRR	homologous recombination repair
hTERT-RPE1	human telomerase reverse transcriptase-transformed retinal pigment epithelial 1 cell line
ICRF-193	Imperial Cancer Research Fund-193
IR	ionising radiation
KCl	potassium chloride
kDNA	kinetoplast DNA
LET	linear energy transfer
LiCl	lithium chloride
LiDS	lithium dodecyl sulphate
LMP	low melting point
mAMSA	amsacrine hydrochloride or amsacrine or 4'-(9-acridinylamino)methanesulfon-m-aniside
MAR	matrix-associating region
MDC1	mediator of DNA damage checkpoint protein 1
$MgCl_2$	magnesium chloride
MLL	mixed-lineage leukemia
MPF	mitosis promoting factor
mRNA	messenger RNA
MRN	protein complex including hMRE11, hRad50 and NBS1
MX1 or 2	mitoxantrone-resistant cells 1 or 2
NaCl	sodium chloride
NADPH	nicotinamide adenine dinucleotide phosphate (reduced)
NaOH	sodium hydroxide
NBN	nibrin protein

NBS1	Nijmegen breakage syndrome protein 1 or NBN
NCBI	National Center for Biotechnology Information
NES	nuclear export signal
NHEJ	non-homologous end-joining repair mechanism
NLS	nuclear localisation signal
PBL	peripheral blood lymphocyte
PBS	phosphate-buffered saline
PBST	phosphate-buffered saline and Triton X-100
PCR	polymerase chain reaction
PHA	phytohaemagglutinin
PI	propidium iodide
Pi	inorganic phosphate
RISC	RNA-induced silencing complex
RNA	ribonucleic acid
ROS	reactive oxygen species
RPA	replication protein A
rpm	rotations per minute
RPMI-1640	Royal Park Memorial Institute medium
RT	reverse transcriptase
SAR	scaffold-associating region
SC1	scaffold protein 1
SCE	sister chromatid exchange
SDS	sodium dodecyl sulphate
SDS-PAGE	SDS-polyacrylamide gel electrophoresis
siRNA	silencing RNA or short inhibitory RNA
SMC	structural maintenance of chromosomes proteins
S-phase	DNA replication or synthesis phase of the cell cycle
SSB	single strand break
TAE	tris acetate EDTA
TBE	tris borate EDTA
TEMED	10 μl N,N,N',N'-tetramethylethylenediamine
topo	topoisomerase
TopBP1	topoisomerase II-binding protein 1
T-segment	transferred DNA double helix segment
UV	ultraviolet
WRN	protein affected in Werner's syndrome
XRCC	X-ray repair cross-complementing protein
xrs	X-ray sensitive cell line

CHAPTER 1

INTRODUCTION

1.1 Aim

The aim of my thesis was to further investigate chromosomal aberrations induced by gamma-radiation and how they arise from deoxyribonucleic acid (DNA) damage. More specifically to investigate how chromatid breaks form from double strand breaks (DSBs). The process behind chromatid break formation is unclear. Here the role of topoisomerase IIα in chromatid break induction was investigated and as it is known that DNA DSBs are the initiating lesions, the importance of induction and rejoining of DSBs in chromatid break formation was also tested.

1.2 Ionising radiation-induced DNA damage

The purpose of a cell is to replicate its DNA as accurately as possible and pass it on to daughter cells, avoiding DNA and chromosome damage. DNA and chromosome damage can come in many different forms, including single strand breaks (SSBs) and DSBs as well as chromosomal exchanges and breaks. The focus of this thesis is on chromosome damage caused by low linear energy transfer (LET) ionising radiation (IR), namely γ-rays, and more specifically on induction of chromatid breaks.

Firstly it is important to define low LET IR. IR is so-named as it can carry enough energy per quantum to ionise atoms or molecules. IR can be categorised in to either high or low LET with high LET referring, for example, to alpha particles that are more densely ionising but do not penetrate very far in biological material as their positive charge interacts with the DNA. Thus they deposit most of their energy within the volume of one cell. However, low LET IR encompasses X-rays, beta particles and gamma rays; the latter being the type of radiation used in all experiments described in this thesis. Gamma rays are emitted by radioactive isotopes (here ^{137}Caesium or ^{137}Cs) resulting from excess energy released as the unstable nucleus decays [1].

Ionising radiation is a well-known carcinogen as determined from many human studies [1]. It, more specifically X-rays, was also the first environmental agent shown to be mutagenic in *Drosophila melanogaster* [2]. We are all exposed to ionising radiation as either background irradiation from for example cosmic rays, or medical uses such as radiography. Damage to the DNA by ionising radiation can occur either directly or indirectly (Figure 1.1). Direct damage refers to IR ionising components of the DNA, whereas indirect damage occurs when IR interacts with water molecules in the vicinity of DNA producing free radicals that in turn diffuse short distances to reach the DNA molecule and lead to DNA damage. It is thought that low LET radiation, such as γ-rays, mainly acts on DNA indirectly through the production of radicals [3]. Ionised water (H_2O^+) reacts with other water molecules (H_2O) surrounding it which results in the formation of the hydroxyl radical $^{\cdot}OH$ (as well as H_3O^+). Free radicals attack

hydrogen bonds in the DNA double helix, causing DNA damage [4] and hydroxyl radicals are thought to play a major role in IR-induced DNA damage [1,3].

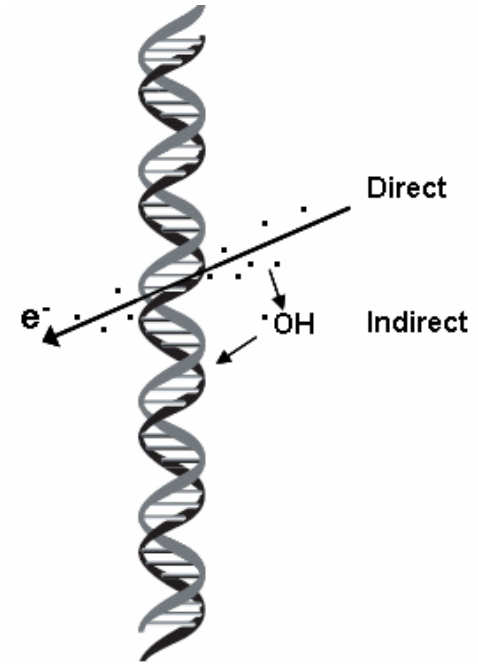

Figure 1.1: Mechanisms of radiation-induced DNA damage: the direct and indirect actions of ionising radiation. Ionising radiation can affect DNA both indirectly, where photons ionise water to form hydroxyl radicals ·OH, and directly. Adapted from Hall (1994) [1].

A source of DNA and chromosomal damage other than γ-radiation used in this thesis is hydrogen peroxide (H_2O_2). H_2O_2 also forms ·OH radicals in the presence of ferrous ions and its action is known to be radiomimetic [5]. H_2O_2 is produced endogenously and is a key cellular signalling molecule [6].

Ionising radiation results in a wide range of DNA lesions including SSBs, DSBs, base damage, DNA-DNA crosslinks, protein-DNA crosslinks and sugar damage [7]. A SSB refers to breakage of one phosphodiester backbone. Double strand breaks, the lesion most relevant to the experiments here, can be described as the breakage of both phosphodiester strands at sites less than four nucleotides apart. This DSB is regarded as the most important initial lesion and, unlike SSBs, has been associated with cell death [8,9]. DSBs can be classified as either blunt- (with no or few bases overlapping) or sticky-ended (with cohesive free ends of many bases) and the type of DSB determines the ability for it to cause chromosomal aberration [10]. It is known that per cell approximately 36 - 40 DSBs arise per Gy of low LET IR [11,12].

IR can also induce partial destruction or alteration of bases which can include up to 20 different modifications of molecular structure for each of the 4 bases [7,13]. As well as base

damage IR also causes sugar damage leading to base loss (abasic site), SSBs and crosslinking of DNA with itself (interstrand cross-links) or with proteins [1]. So far all IR-induced lesions have been explained as individual IR effects. However, due to its indirect effect, ionising radiation can also induce complex lesions where SSBs, DSBs and damaged bases are localised within one helical turn (1-10 base pairs). These complexes were termed locally multiply damaged sites in 1985 by Ward [14] and are referred to as complex DSBs within this thesis.

It is important to understand that simply the presence of single or double strand breaks, or other types of DNA lesions does not automatically lead to aberrant cell growth or disease progression as under normal circumstances these breaks would be repaired.

1.3 DNA repair

The "molecule of the year" goes to … DNA repair systems! [15]

DNA repair is an essential process to ensure integrity of genetic material before it is replicated and passed on to daughter cells. Single strand breaks caused by IR can be repaired through many proteins also involved in base excision repair [16]. This requires the base as well as the deoxyribose phosphate in the backbone to be excised, the DNA to be re-synthesised and finally sealed with a DNA ligase.

1.3.1 Double strand break repair

Double strand breaks are repaired through two major pathways, namely homologous recombination (HRR) and non-homologous end-joining (NHEJ) repair (Figure 1.2) [17,18]. Double strand breaks can also be repaired by single strand annealing (Figure 1.2), which is activated when a DSB is located between two repeat sequences. It repairs the DSB through pairing up sequences of direct repeats with the intervening repeats and other DNA being lost, followed by DNA synthesis by DNA polymerase and DNA ligation [19]. This repair process does not conserve the DNA sequence and involves the activity of RAD50 and some proteins, such as hMRE11, that are also involved in homologous recombination repair [19] of double strand breaks (see next section). SSA is therefore often thought of as a special form of HRR.

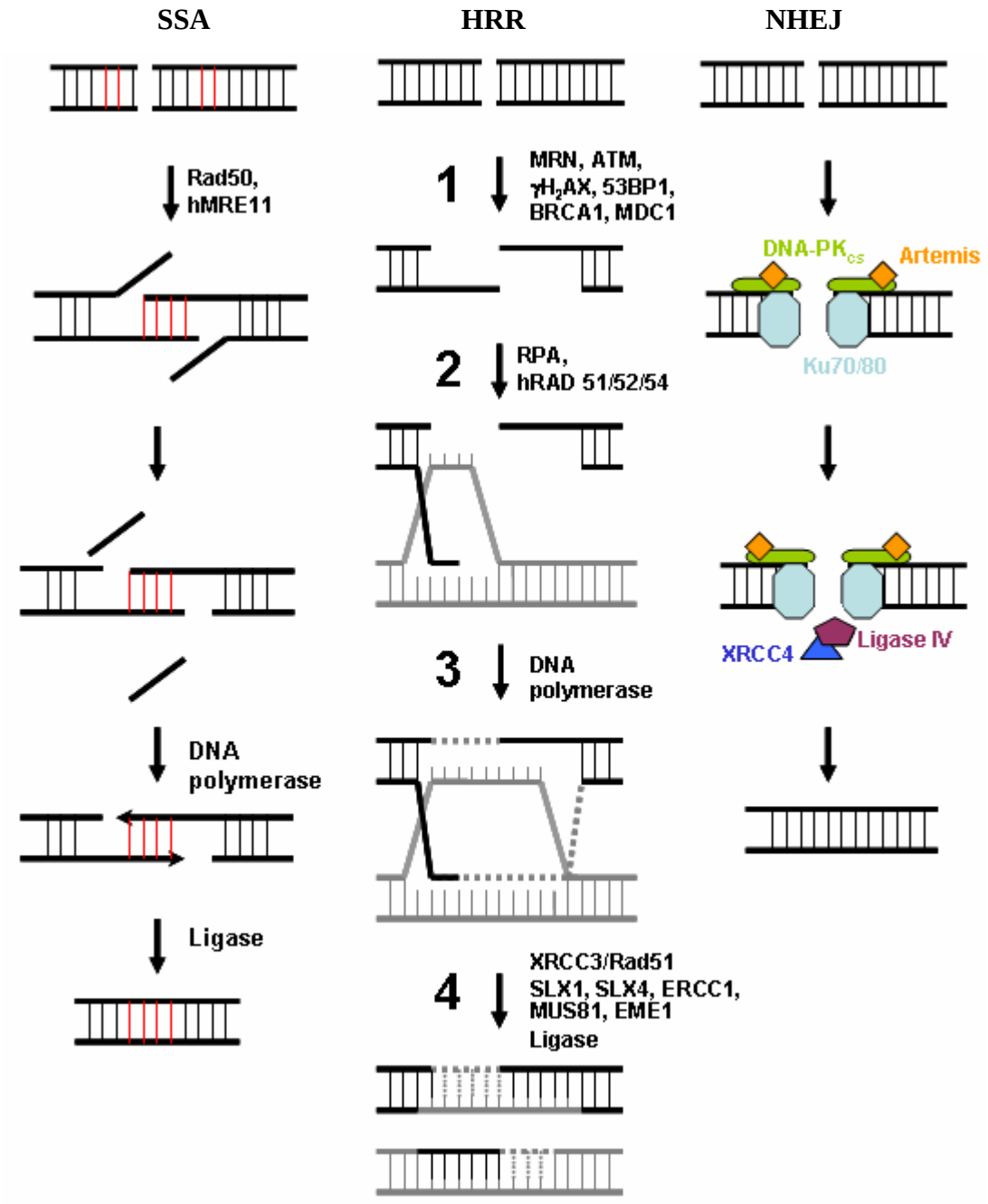

Figure 1.2 DSB repair systems simplified. Single strand annealing (SSA, left) and homologous recombination (HRR, middle) require homologous sequences. The red sequences shown as part of SSA refer to direct repeat sequences. The grey sequences shown as part of HRR are homologous sequences. Non-homologous end-joining (NHEJ, right) is able to repair DSBs by resection of the DNA ends and then ligation of the two blunt DSBs without maintaining genomic integrity. For full description see text. Protein XLF is also associated with NHEJ as it interacts directly with the XRCC4/Ligase IV complex [20].

Firstly, as the name suggests, homologous recombination repair (HRR) requires the presence of homologous sequences in order to repair the DSB; it needs around 200 bp overlap [21]. In HRR of IR-induced DSBs in mammalian cells, the DSB is first processed by the eukaryotic MRN complex (hMRE11, hRad50 and NBS1 (Nijmegen Breakage Syndrome protein 1, also known as Nibrin or NBN) [22], which 'cuts back' or removes damaged DNA sequences next to the DSB (Step 1, Figure 1.2). The MRN complex then recruits ATM (Ataxia Telangiectasia Mutated), which in turn phosphorylates histone H_2AX at serine 139 [23]. The phosphorylated form of H2AX is termed γ-H_2AX and it forms foci at and around (up to several megabases) the DSB [24]. The protein mediator of DNA damage checkpoint protein 1 (MDC1) is recruited to the site and increases γH_2AX foci formation either by decreasing phosphatase or increasing kinase activity [25]. γH_2AX ubiquitination results in the recruitment of BRCA1 (BReast CAncer 1) and p53 binding protein 1 (53BP1) to the damaged DNA site [25,26]. BRCA1 is a crucial DNA repair protein due to its function as an E3-ubiquitin ligase [27] that attaches subsequent repair proteins to the damaged site [28]. Proteins with the C-terminal domain of breast cancer proteins (BRCT regions) are known to be involved in cell cycle regulation and DNA repair. BRCA1 and 2, two such BRCT proteins, are no exception and are able to regulate hRad51 as well as the G_2 checkpoint [29,30]. It is known that mutations in these two BRCA proteins are associated with an increased risk of breast cancer [31]. 53BP1 on the other hand activates p53 and cell cycle checkpoints ultimately resulting in cell cycle arrest [32]. Therefore shortly after IR γ-H_2AX, MRN, MDC1, 53BP1, ATM and BRCA1 can all be visualised at the DSB site by immunocytochemistry [22,33,34]. Also, γH_2AX foci recruit chromatin remodelling complexes that allow access to the DSB by other repair proteins [35]. Another important consequence of IR-induced DNA damage is the recruitment of the cohesin complex via the phosphorylation of SMC1 (structural maintenance of chromosome protein 1, part of the cohesin complex) by ATM [35,36]. This tethers the sister chromatid in place to allow for HRR.

After the DSB has been processed, the proteins 'search' for a homologous sequence (Step 2, Figure 1.2), which then allows base pairing and strand exchange by the eukaryotic proteins hRAD51/52/54 and replication protein A (RPA) [37-40]. Interestingly, in murine cells where Rad54 is absent, cells will repair by single strand annealing rather than HRR [41], which as mentioned earlier is not conservative as large sequences can be deleted.

The two ends of homologous sequences in HRR invade each other and serve as primers for DNA synthesis by a DNA polymerase (Step 3, Figure 1.2). These Holliday junctions are then resolved by X-ray repair cross-complementing protein XRCC3/Rad51 [38] as well as SLX1, SLX4, ERCC1, MUS81 and EME1 proteins [42-44]. Finally the gaps are filled by an as yet unknown ligase (Step 4, Figure 1.2).

In addition to HRR, DSB rejoining can also be accomplished by NHEJ which is non-conservative and can occur in the absence of homologous sequences. In eukaryotes, NHEJ

requires the recruitment of the ku70/80 heterodimer, which recognise the damaged site, DNA-dependent protein kinase catalytic subunit (DNA-PK_{cs}) and XRCC4/DNA ligase IV [18,45]. Together ku70/80 and DNA-PK_{cs} are referred to as DNA-PK. The ATM kinase used as part of HRR also has a role in regulating the activity of the NHEJ protein Artemis, which is bound to DNA-PK. Hyperphosphorylation of Artemis by ATM activates the Artemis/DNA-PK complex, which results in nuclease (trimming) activity on the DSB [46] followed by the ligation of the DNA by the XRCC4/DNA ligase IV complex [47]. Several NHEJ proteins are also involved in V(D)J recombination in maturing B and T lymphocytes [48].

It is now not only known that HRR mainly repairs IR-induced double strand breaks in the G_2 phase of the cell cycle [49,50], as it requires the availability of homologous sequences, but also that NHEJ can occur in all phases of the cell cycle including G_2 [50]. The HRR pathway appears to be regulated mainly through ATM signalling [51]. The phosphorylation of CtIP and recruitment of BRCA1 during S and G_2 phases of the cell cycle can also influence the type of DSB repair mechanism [52]. Also, the type of DSB can lead to 'selection' of the repair pathway as more complex DSBs created by ionising radiation are rejoined by HRR, whereas simple DSBs (e.g. bleomycin-induced) are repaired via NHEJ as determined by the lack of recruitment of the HRR protein RAD51 [53].

1.3.2 Cell cycle checkpoints

Another effect of DNA damage is the activation of cell cycle checkpoints. Most DNA repair proteins mentioned in the previous section affect and 'slow down' or arrest the cell cycle to allow time for DNA damage to be repaired and to ensure that DNA damage does not get passed on to daughter cells. The cell cycle (Figure 1.3) consists of a gap (G_1) phase where cells prepare for DNA replication or synthesis in S phase. Gap phase 2 (G_2) prepares the cells for the equal segregation of DNA in each daughter cell. The G_2/M cell cycle checkpoint is located between G_2 and mitosis (M), after DNA replication. This G_2/M checkpoint is crucial in halting cells in G_2 when DNA has been damaged or is not yet decatenated to ensure correct sister chromatid separation at anaphase [54,55]. G_1/S and anaphase checkpoints are also in place, however as these are irrelevant to this thesis, they will not be covered.

In G_2, both cyclin A and B expression levels are altered, although only cyclin B is involved in the G_2/M checkpoint. Cyclin B binds to the kinase p^{34}, also known as cyclin-dependent kinase 2 (cdc2) and cyclin-dependent kinase 1 (CDK1). Together cyclin B and p^{34} are termed the mitosis promoting factor (MPF). At G_2 MPF, although present, is inactive until the phosphatase cdc25 is activated by checkpoint protein 1 (Chk1). Cdc25 now activates MPF which in turn targets lamins that are part of the inner nuclear envelope (lamina). MPF also activates condensins that allows chromosome condensation and proteins that promote spindle formation. Decreased nuclear expression of cyclin B due to ubiquitination or

localisation to the cytoplasm defines the onset of anaphase. This signalling pathway has been reviewed by many groups [56-58].

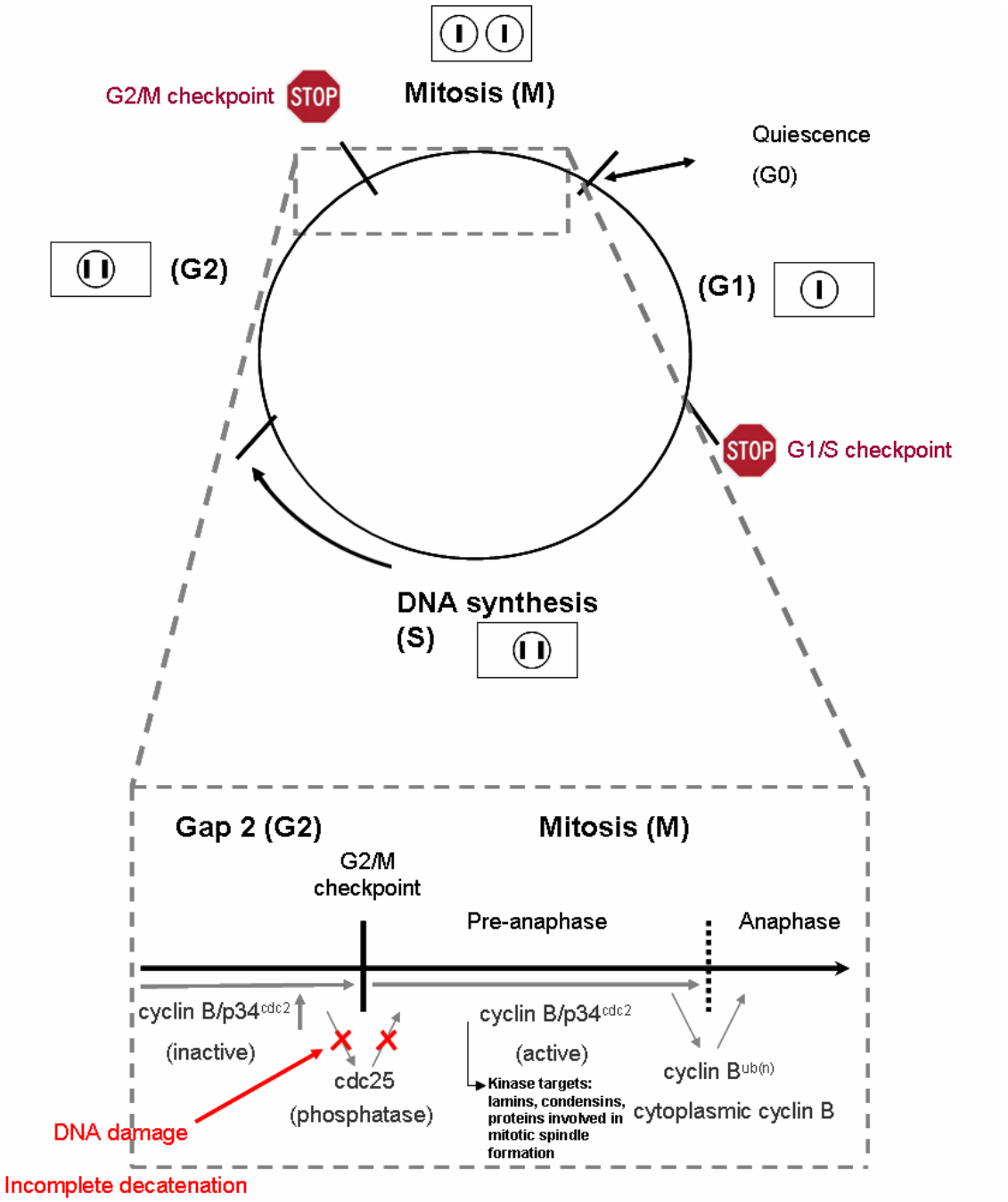

Figure 1.3: Cell cycle and G_2/M checkpoint control. Cells cycle from S phase, where DNA is replicated, to G_2, where cells prepare for mitosis, and finally mitosis where the genetic material is split evenly in to daughter cells. If the environment is unfavourable, such as lack of nutrients, cells will go into quiescence (G_0) and can start cycling again when the milieu has recovered. The G_1/S checkpoint stops cells from going into S phase if DNA is damaged. The grey box shows a more detailed time-line of the G_2/M checkpoint. For a full description of the G_2/M checkpoint see text.

As mentioned, both DNA damage and lack of DNA decatenation activate the G_2/M checkpoint and halt cells in G_2. The mechanism behind this involves a complex signalling cascade involving many repair proteins as well as the ultimate checkpoint protein p53 [58-60], which is activated by ATM [61]. This ultimately inhibits cdc25 and keeps the MPF in an inactive state until DNA repair has taken place.

1.4 Chromosomal damage

1.4.1 Types of chromosomal damage

Chromosomal damage can be categorised into either chromosome or chromatid aberrations. As mentioned earlier, the aim of this thesis was to find out more about the mechanism behind chromatid damage (breaks). The difference between chromosome and chromatid breaks is illustrated in Figure 1.4.

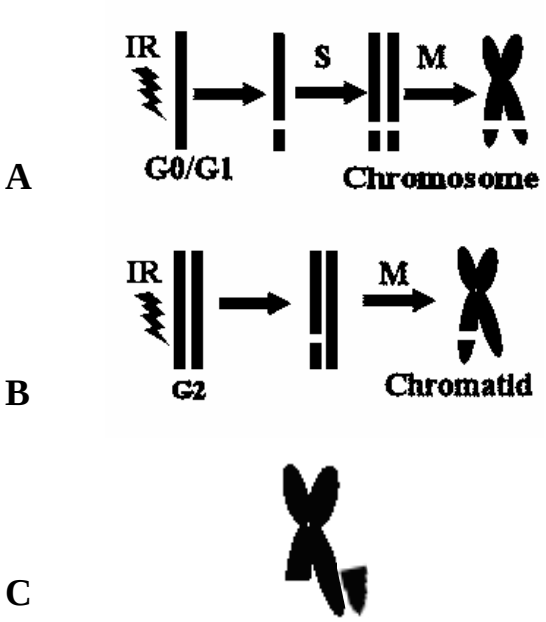

Figure 1.4 Difference between chromosome **(A)** and chromatid **(B)** breaks. DNA damage acquired through ionising radiation (IR) in the G_0 or G_1 phase of the cell cycle will result in chromosome breaks when viewed in mitosis (M) after replication of the DNA in S phase. Chromatid breaks arise from DNA damage acquired by IR in the G_2 phase of the cell cycle. **(C)**: chromatid break with displacement of broken segment.

Chromosome aberrations (Figure 1.4A) refer to damage accumulated in the G_0/G_1 phase of the cell cycle. If left unrepaired, the initial DNA damage is replicated in S phase and manifests itself as breaks (or gaps) in both chromatid arms. These chromosome breaks can be seen in metaphase, a phase of mitosis where chromosomes are condensed but have not yet separated into daughter cells. In most cases however, the initial damage would have been

repaired by NHEJ or HRR (section 1.3.1). It should be noted that chromosome aberrations other than breaks also include telomeric deletions (end of chromosomes deleted), interstitial deletions (deletions not at terminus), translocations and dicentrics (exchanges between different chromosomes), rings (exchanges within a single chromosome), chromosome insertions, inversions and duplications.

Chromatid aberrations (Figure 1.4B) include chromatid gaps, breaks and exchanges. Unlike chromosome aberrations, chromatid breaks are classified as breaks in only one of the two chromatid arms and result from IR-induced DNA damage acquired during the G_2 phase of the cell cycle. Classically, chromatid 'breaks' were considered to be discontinuities larger than the width of the chromatid, whereas 'gaps' were those smaller than the chromatid width. However, Sandford *et al.* counted chromatid breaks as chromatid discontinuities with displacement of the broken segment (Figure 1.4C) and gaps as aligned breaks [62]. It was therefore unclear whether or not 'gaps', defined as discontinuities smaller than the width of the chromatid, should be included when calculating chromatid break frequency. A study in which the size of chromatid discontinuity was compared to their frequency displayed a continuous pattern of sizes [63]. If gaps and breaks do arise from different mechanisms, two peaks in the distribution would be expected, referring to either type of chromatid discontinuity [63]. However, as no two clear peaks were detected, it can be assumed that gaps and breaks are not two qualitatively different types of discontinuity [63]. Also, in another study the kinetics of the disappearance of both the gaps and breaks after IR were comparable [64], again suggesting that breaks and gaps can be regarded as a similar type of chromatid discontinuity.

In this thesis, following the example of Bryant *et al.* [65], chromatid breaks are defined as any type of chromatid discontinuity, including chromatid 'gaps', where aligned discontinuities are smaller than the width of the chromatid, and 'breaks' where discontinuities are larger than the width of the chromatid. It is thought that the displacement of the broken segment occurs in a random fashion during sample preparation and these were therefore also included during analysis.

Terminal fragments (Figure 1.4) are kept close to the chromatid break due to cohesion of the two sister chromatids mediated by the cohesin complex [66]. Cohesins are proteins that maintain 'sister chromatid' adhesion after replication and it is generally accepted that they do this by encircling the DNA [66,67]. This cohesin complex includes Smc1 and 3, which belong to the structural maintenance of chromosomes (SMC) protein family, as well as Scc1 [66,67]. Before metaphase most cohesin complexes are removed from chromosome arms, resulting in the well known X-shaped chromosome. If sister chromatids were not still slightly cohesed at metaphase, chromatid breaks would not be visible as the structures shown in Figure 1.4B. Instead these breaks would cause the end of the chromatid to separate completely from the chromosome and be lost as a telomeric deletion in the preparation of the sample. How then

do these chromatid breaks still allow all homologous sections of the chromosome to remain 'attached' to each other in metaphase? Although chromosome arms in metaphase are often visibly separated, i.e. appear in optical microscopy to be only connected via the centromere, some arm cohesion nevertheless persists throughout metaphase and is sufficient to maintain sister chromatid cohesion [68]. How arm cohesion is maintained until metaphase is still unknown although small amounts of cohesin can be detected in the interchromatid region of metaphase chromosome arms.

1.4.2 Chromosomal radiosensitivity

Radiosensitivity is formally defined as $1/D_0$ of a cell survival curve with D_0 representing the dose required to reduce the surviving fractions by 63% along the exponential portion of the curve. Here however, the term 'high radiosensitivity' is used to refer to cells responding sensitively to ionising radiation and resulting in an elevated frequency of chromatid breaks or other types of chromosomal damage.

Wide intra-individual differences have been found in the radiosensitivity of phytohaemagglutinin (PHA)-stimulated peripheral blood samples from normal donors and inter-individual G_2 values ranged from 86 to 154 chromatid gaps and breaks per 100 metaphases [69]. This wide range in normal donors was also seen in studies by other groups, where the G_2 score, or number of chromatid breaks per 100 cells, varied from 15 to 115 [70] and from 80 to 120 [71], in all cases showing a Gaussian distribution. Some of the differences in values found between different studies could probably be attributed to what is defined as a chromatid break. Nonetheless, it is clear that significant inter-individual differences between peripheral blood samples of normal donors exist. The mechanism underlying the inter- and intra-individual variations is as yet unclear.

High cellular and chromosomal radiosensitivity is seen in cells from ataxia telangiectasia (AT) patients. AT is an autosomal, homozygous recessive condition with ataxia (inability to coordinate voluntary muscle movements) and ocular and cutaneous telangiectasia (small dilated blood vessels). Other symptoms include progressive neural degeneration, severe immunodeficiency, spontaneous chromosomal instability, predisposition to cancer and high cellular and chromosomal radiosensitivities after IR. Studies with skin fibroblasts [62,72] and PHA-stimulated lymphocytes [71,73] from AT heterozygotes showed a higher chromatid break frequency than in normal individuals after irradiation. These studies also found that AT homozygotes showed a further increased radiosensitivity [62,72,73].

As mentioned, the protein mutated in AT (ATM) is required for normal repair of DSBs and thus it logically follows that AT cells might be radiosensitive due to deficient repair. However, in AT lymphoblastoid cell lines, γ-irradiated cells do not show a higher number of radiation-

induced DSBs [74]. However, a two-fold increase in chromosomal damage was seen in AT cells in G_1 or G_2 suggesting that AT cells have a higher rate of conversion of DSBs into chromosomal aberrations [74]. One group incorrectly assumed a DNA repair defect from data that showed higher chromatid break frequency in cells of AT patients four hours after irradiation [75], as this was not substantiated by specific DSB experiments. As in AT lymphoblast cells [74], no difference in DSB induction after γ-irradiation of fibroblast AT cells was seen [76,77]. In these studies it was also reported that radiation-induced DSB repair was normal [76] or more rapid then normal [77].

Cell cycle irregularities in AT have also been suggested to cause radiosensitivity. Interestingly, X-irradiation of AT cells caused a linear decrease in % DNA synthesis, whereas normal diploid cells showed first a steep followed by a shallow decline seen in AT cells [78]. It was postulated that AT cells lack a response to strand replication initiation. Another group showed that γ-irradiation of lymphoblastoid AT cells did not affect the mitotic index, unlike in normal cells [55]. It therefore appeared that the G_2 block response (Section 1.3.2) is inactive in AT cells [55,79]. Also AT cells, when treated with calyculin A, which condenses cells in G_2, showed the same IR-induced chromatid break frequency as AT cells treated with colcemid and allowed to enter mitosis. Control cells however showed a decrease in chromatid break frequency in cells treated with colcemid rather than calyculin A, suggesting that the G_2 block found in control cells is inactive in AT cells [55].

In this thesis colcemid, also known as demecolcine, is also used to block cells in mitosis. It was derived from colchicine, originally extracted from the *Colchicum autumnale* plant. It maintains cells in prometaphase by depolymerising microtubules and inhibiting new microtubule formation. Cells are thus kept in prometaphase as a lack of spindle fibres inhibits correct seperation of sister chromatids [80].

Treatment of cells with caffeine, which abrogates checkpoint activity, does not affect chromatid break frequency in AT cells, though it does increase chromatid break frequency in control cells [55]. The data thus shows that the G_2/M checkpoint is not fully functional in homozygous AT cells. High radiosensitivity has also been attributed to altered G_2/M cell cycle checkpoint in non-AT cells as chromosomal damage in G_2 was no different in radiosensitive compared to radioresistant cells however, radiosensitive cells did show higher chromosomal damage in mitosis [81]. Data implying that altered radiosensitivity is not linked with altered G_2/M checkpoint activity [82,83] however suggest that abnormal G_2/M checkpoint control does not necessarily result in increased chromatid breakage.

As previously discussed AT chromatid radiosensitivity is not necessarily due to lowered DNA repair [76,77,84] and therefore might be due to increased DNA damage or altered conversion of DSBs to chromatid breaks. For example, it has been shown that the kinetics of DSB and

chromatid break disappearance in Chinese hamster ovary cells do not correspond since treatment of cells with the nucleoside analogue 9-β-D-arabinosyladenine (ara A or adenine arabinoside) inhibits chromatid break rejoining while DSB repair remains unaltered [85] suggesting a conversion stage between DSBs and chromatid breaks.

Several studies by Scott's group [71,86-88] showed that irradiated PHA-stimulated peripheral blood lymphocytes (PBLs) of breast cancer patients also showed elevated frequencies of chromatid breaks in comparison to controls. More specifically, it was determined that 40% of breast cancer patients showed increased radiosensitivity compared to 10% in healthy controls [71]. High radiosensitivity of breast cancer PBLs has been confirmed by several other groups after either X- or γ-irradiation [70,81,89-92]. However, the largest and most recent of this type of study, encompassing 211 breast cancer patients and 170 control cases, did not show any significant difference in radiosensitivity between breast cancer cases and normal controls [93]. This study did however suggest increased radiosensitivity in women (both with and without breast cancer) with a strong family history of breast cancer, suggesting a link between radiosensitivity and risk of breast cancer in heritable cases [93].

It has been hypothesised that this increase in radiosensitivity in breast cancer patients is due to aberrant or lack of DNA repair [94,95]. It is known that certain genes mutated in breast cancer, namely *BRCA1* and *2*, are involved in DNA repair [29-31]. These proteins are associated with many DNA repair proteins mentioned in section 1.3 and are also known to activate the G_2/M checkpoint (see reviews Bucher and Britten [56], Lobrich and Jeggo [57] and Stark and Taylor [58]). In these studies [94,95] however, DNA repair was extrapolated indirectly from measurements of the number of chromosomal breaks and gaps left unrepaired at a certain time point. Also *BRCA1* and *BRCA2* gene mutations are found in only a low percentage of inherited breast cancer cases and breast cancer patients or cell lines derived from patients with *BRCA1* and *BRCA2* mutations did not show significant radiosensitivity as measured by the G_2 assay [96].

As *BRCA1* and *2* mutations account only for a small proportion of the overall familial risk of breast cancer [97] and the mutations are not necessarily associated with increased radiosensitivity [96], the radiosensitivity seen in breast cancer patients must be due to other factors. One study [88] showed that high radiosensitivity was heritable and, alongside data suggesting that increased radiosensitivity is also found in young cancer patients (<20 years old) [98], substantiated the idea that inter-generational transmission of cancer predisposing genes of low penetrance allows this familial inheritance. Also in one study 62% of first-degree relatives of radiosensitive breast cancer patients were themselves radiosensitive, compared to 7% of first-degree relatives of breast cancer patients with normal G_2 scores [88]. A more recent study has also shown the heritability of radiosensitivity in peripheral blood samples of childhood and adolescent cancer survivors (52%) and their offspring (53%) [99]. All these results led to speculation on the presence of genes of low penetrance. It seems that breast

cancer susceptibility is largely polygenic, where a large number of low-penetrance genes confer small risks individually that then act in combination to cause a wide variation in risk in the population [100]. The penetrance of a disease-causing mutation is the proportion of individuals with the mutation who exhibit clinical symptoms. Thus a low penetrance gene will only sometimes result in clinical symptoms. Interestingly, *ATM* has been associated with intermediate risk (two-fold increase) of breast cancer and can be classified as one of these low-penetrance genes [101].

The associated risk of (breast) cancer found in individuals with high radiosensitivity, has also tentatively been connected with risk of other types of cancer, such as colorectal cancer [87], head and neck cancer [102,103], and cancer of the larynx [104].

1.5 Models of chromatid aberrations

1.5.1 Breakage-and-reunion model

An early study of the formation of X-ray-induced chromatid breaks was made by Sax in 1938 using pollen from *Tradescantia*, where chromosomes are few in number and large in size. Sax' model regards chromosome breaks as both the initial and final lesion as a consequence of single ('one-hit') interactions of ionising tracks with chromosomes [105]. A modified form of Sax' 'breakage-and-reunion' model [106], proposed that polynucleotide breaks or abasic lesions modified into strand breaks were the initiating lesions [107]. These breaks would then be rejoined, left unrepaired or mis-joined such that genetic material between different chromosomes is exchanged (Figure 1.5).

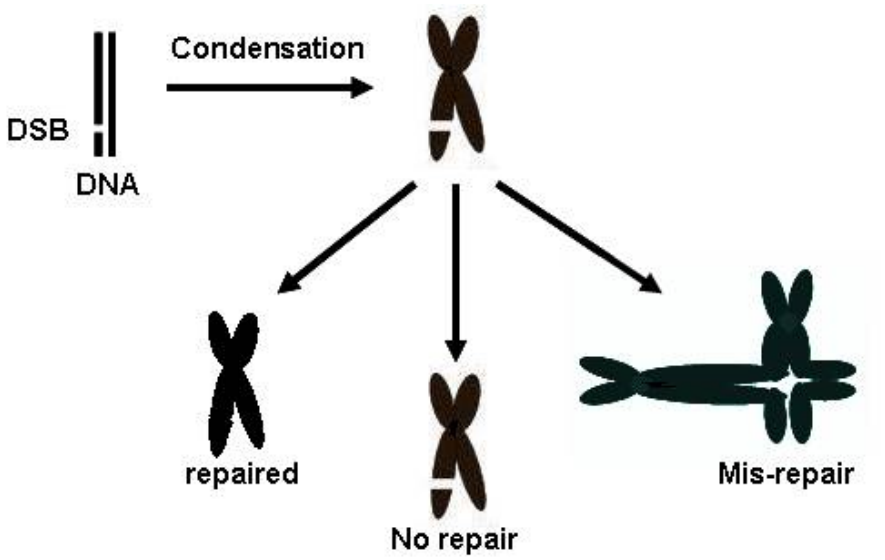

Figure 1.5 Breakage-and-reunion model of chromatid break formation. The initial strand break, now known to be a double strand break (DSB), results in a chromatid break in mitosis after chromosome condensation. This DSB is repaired, mis-repaired or left unrepaired. The diagram is based on Bryant 1998 [108].

Studies using restriction endonuclease-induced DSBs showed that the initiating lesion in the formation of chromatid breaks was a DSB [10,109,110]. Previously, studies combining *Neurospora* endonuclease and X-rays had shown that conversion of single strand damage to a DSB increased chromatid aberration frequency, although the initial damage would have been a mix of single and double strand breaks [111]. Therefore the strand breaks proposed to be involved in chromatid breakage by Bender are actually now known to be DSBs.

Chromatid breaks can be up to 40 Mbp in size (based on human haploid genome size of around 3000 Mbp [112,113]). Bender's model [107] would implicate two strand breaks that interact with each other, deleting the region in between the two and thus predicts a quadratic rather than linear relationship between radiation dose and chromatid breaks. The probability of two strand breaks occurring near each other on the same chromatid is unlikely, especially at the low doses used in many chromatid break studies, namely 0.25 – 1 Gy as it can be inferred that 0.25 Gy will induce about ten DSBs per diploid cell (based on 40 DSBs per Gy [11,12]). Even more unlikely is finding two DSBs on one chromosome in control (unirradiated) cells, where a low number of chromatid breaks can also be found. This might instead result from massive exonuclease activity surrounding the initiating strand break or due to extensive condensation of the chromatin at the end of the break, although both are rather unlikely. This breakage-and-reunion model therefore does not explain how the strand break, with no genetic material lacking, increases in size to become a chromatid break.

It was shown by Sax that chromatid breaks yielded a linear relationship with radiation dose [105,106]. This linear dose response was also found in other cell types [108,112]. Experiments with carbon K-shell ultrasoft X-rays, the range of which is very short so they affect only one double helix, show that chromatid breaks still occur when only one DSB is formed [114]. These results suggest that one DSB is enough to cause a chromatid break, which does not correspond with the two DSBs required to induce a chromatid break as proposed with the breakage-and-reunion model. If two DSBs were involved, a quadratic, and not a linear, relationship between radiation dose and chromatid break induction would occur and therefore an interaction of two DSBs to form a chromatid break seems even more unlikely.

1.5.2 Exchange model

Another theory of chromatid break formation is the 'exchange model' proposed by Revell [115] (Figure 1.6). It suggests that chromatid breaks are formed or seen only as a result of the partial failure of exchanges within and between sister chromatids. Thus, if the process of exchanging genetic material were halted or interrupted after irradiation, chromatid breaks could be seen. The exchange was proposed to occur at the base of looped chromatin regions where IR could have caused 'initiating lesions'. Revell classified the types of chromatid breaks as colour-switch and non-colour-switch (Figure 1.6), where exchange between or within

chromatids had occurred respectively. Colour-switches can be observed through Harlequin staining which involves treatment of cells with bromodeoxyuridine [116] or tritiated thymidine [117,118]. Cells are then allowed to proceed through two cell cycles, halted at metaphase with colchicine and finally stained with Giemsa [117] or Giemsa plus Hoechst [116]. The darker chromatid will have been through more cycles than the lighter sister chromatid.

The colour switches seen by Harlequin staining correspond to the exchange of genetic material between chromatids. Revell's model predicted that 40% of chromatid breaks involve colour-switches assuming exchanges were equally probable as (D+E)/(A+B+C+D+E) = 40% (Figure 1.6). A value close to this, 38%, was in fact found in rat kangaroo cells [118]. However, later studies on X-irradiated or endonuclease-treated Chinese hamster cells showed a lower percentage of chromatid-exchange breaks, namely 15-18% [112,117,119]. Thus it appears the ratio of colour-switch to non-colour-switch breaks is species-dependent.

The looped domains mentioned in Revell's model are thought to be associated with transcription 'factories' [120] and might be surrounded by RNA (ribonucleic acid) polymerases, other transcription factors or DNA processing enzymes such as helicases and topoisomerases (topos). Evidence for transcription 'factories', formed from large loop domains that interact within the nucleus, came from studies where the incorporation of biotin-labelled CTP or UTP as well as the localisation of ribonucleoprotein and RNA polymerase II was detected by either light or electron microscopy and shown to appear in overlapping clusters [120]. It is also known that topo II is located at the base of chromatin loops [121].

As with the 'breakage-and-reunion' model, the 'exchange' model assumes two lesions are formed close to each other which is not only unlikely at the low radiation doses used in experiments, but also does not conform to the linear dose-effect relationship [106,108,112]. However, Harlequin staining has shown that exchange between two chromatids occurs.

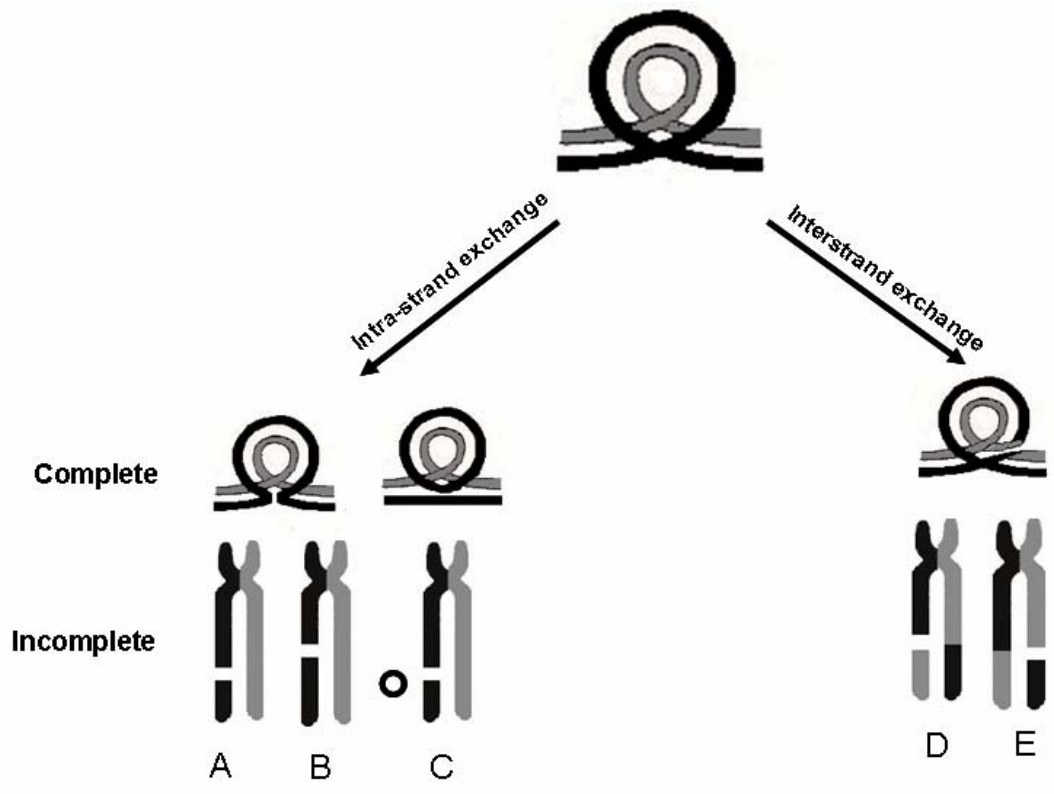

Figure 1.6: Revell's exchange model of chromatid break formation. The diagram is based on a figure from Heddle *et al.* 1969 [118]. Only the types that include chromatid breaks have been included. Chromosomes have been stained through Harlequin staining (tritiated thymidine). According to this model the proportion of chromatid breaks showing colour-switches is equal to (D+E)/(A+B+C+D+E) = 40% assuming the exchanges are equally probable.

A second exchange model was proposed by Radford [122]. His transcription-based model proposed that one DSB is brought into contact with a topoisomerase I molecule via transcription and results in a cleavage complex that interacts with another topoisomerase I molecule within the same chromosome (intra-strand) or a transcription 'factory' located nearby on a different chromosome (inter-strand). He proposed this would result in strand exchanges, cleavage and formation of an exchange aberration, more specifically non-colour-switch and colour-switch chromatid breaks depending on intra- or inter-strand exchange respectively [122].

The transcription-based model [122] fits with data suggesting a linear relationship between chromatid break induction and IR dose, as only one IR-induced DSB is proposed to initiate exchange aberrations. According to this model, the initial radiation-induced DSB would be located in a transcription factory close to the area of mis-exchange and chromatid breakage. However, no direct evidence exists that supports this model.

The 'exchange' model proposed by Revell implies a quadratic relationship between chromatid breaks and radiation dose since the probability of two lesions occurring close together would increase with dose. As mentioned previously, it is unlikely at the low radiation doses used in

chromatid break experiments that two DSBs would occur close enough to each other to interact and form a chromatid break [112].

1.5.3 Signal model

Unlike Sax' and Revell's models, the signal model does accommodate the linear relationship between chromatid break induction and radiation dose [108,112]. The signal model proposes that a single DSB, as suggested by the carbon K-shell ultrasoft X-rays study [114], initiates a signal ultimately leading to the formation of chromatid breaks.

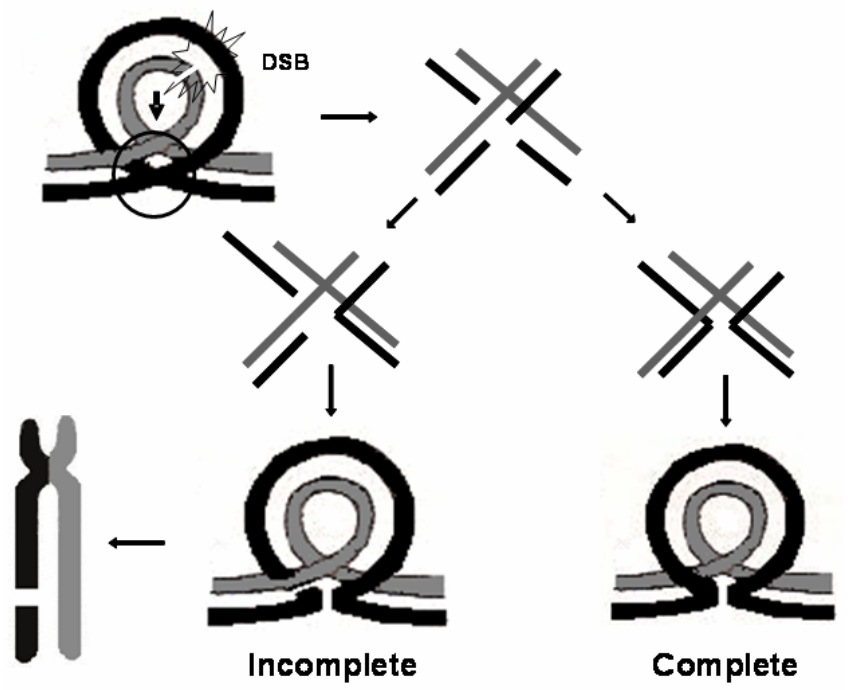

Figure 1.7: Signal model of chromatid break formation. The diagram is based on a figure from Bryant 1998 [112]. A single DSB is induced by ionising radiation in the chromosomal loop. This causes a signalling cascade to the base of chromatin loop, causing a mis-exchange during chromatid decatenation resulting in the formation of an omega loop. The initial DSB is repaired and the omega loop presents itself as a non-colour-switch chromatid break if not completed.

The signal model (Figure 1.7) is based on Revell's model in that the mis-exchange of genetic material is suggested to take place at the base of chromatin loops where they cross over. Thus chromatid breaks are, under the signal model, incomplete exchange aberrations [112]. According to the signal model, a single DSB is hypothesised to be induced somewhere within the chromatin loop, rather than the base of the chromatin loops. It was later confirmed that a single initiating DSB can create a chromatid break when cells were treated with a Meganuclease 'targeted' to a single I-SceI restriction enzyme site [119]. Interestingly, it also suggests that the disappearance of chromatid breaks with time is simply the completion of the exchange, rather than the repair of the initial DSB. The signal model would also explain why

the number of chromatid breaks found in cells is substantially less than the DSB frequency as the signal might only be produced in actively transcribed areas where the DNA is accessible [112]. Omega loops as suggested by both the exchange (Figure 1.6) and signal model (Figure 1.7) have also been observed in cells treated with ICRF-193 (Imperial Cancer Research Fund-193) for several hours [123]. Cells escaping the G_2 block induced by this agent showed omega figures as well as multiple chromatid breaks. Mis-joining of chromatin strands at the base of loops following γ-radiation could reflect a similar mechanism.

1.5.4 Topoisomerase II and the signal model

The signal model proposes that the DSB formed by irradiation is repaired, but a 'signal' triggers the formation of a transient chromatid break that can be seen in metaphase when the exchange of chromatin ends is abruptly halted by cell fixation. The nature of the signal is unknown. However, it might for example result from a distortion of the chromatin loop domain due to the presence of an initial DSB [112]. Possible candidates playing a role in this signalling pathway include DNA-PK, ATM or ku80 [108,112].

Another candidate for producing a chromatid break is topo IIα. Topoisomerase II is an enzyme that can cut both DNA strands as part of chromatid decatenation [124] and as such is a perfect candidate to play a role in the formation of chromatid breaks after irradiation. Other reasons include its location at the base of chromatin loops [121,125], its ability to excise these loops [126], its role in exchanges [127], cell cycle expression patterns [128] and it is the target of many endogenous and exogenous compounds that lead to a change in activity resulting in an excess of DSBs. Experiments in a hamster-human hybrid cell line also showed that topo II is capable of excising loops as amsacrine-induced deletions in the MICI locus on the human chromosome 11 resulted in the loss of 1.5 – 2 megabases [129]. Topo II-targeting drugs in histone-depleted nuclei and native chromatin resulted in similar DNA cleavage patterns suggesting that these drugs mainly target matrix-associated topo II and that DNA close to these regions is preferentially damaged by topo II [130]. Also, after precise ultraviolet-A (UV-A) - treatment, topo IIα and β localise to that specific irradiated area [131], which suggests that topo II is either involved in DNA damage repair or, is signalled to mis-join DNA ends. The normal role of topo IIα and its characteristics will be discussed in more detail in the following section.

1.6 Topoisomerase II

1.6.1 Introduction

"DNA topoisomerases are the magicians of the DNA world" [132]

Topoisomerases are so named for their role in changing the topology of DNA into different isomers. Their role in the cell is extremely important and in some cases even essential for cell survival. Through their action, topoisomerases control many processes including replication, transcription and most importantly mitosis in which daughter chromosomes are decatenated. For reviews see Wang 1985 [133], 1996 [134] and 2002 [132], Gellert 1981 [135], Watt and Hickson 1994 [136] and Deweese and Osheroff 2009 [137]. There is much interest in topoisomerases on account of the drugs that are used clinically that target them and the role of topoisomerases in DNA topology. Topoisomerases are classified as either type I or II according to their ability to cause either single [138,139] or double [140,141] strand breaks and changing the linking number by 1 or 2 respectively (Figure 1.8). The linking number represents the number of times two strands are intertwined. Type I topoisomerase cuts a single DNA strand, allowing the DNA to unwind by one linking number, and then rejoins the break [138]. This activity is employed ahead of the replication fork where DNA is overwound, also known as positively supercoiled (Figure 1.8). Topo I is required alongside helicases at the replication fork as helicases alone would only separate, and not unwind, DNA strands. In the absence of topo I this would then lead to overwound strands which would inhibit replication fork progression. Topo I is therefore required to unwind these strands so replication can continue. A similar requirement for topo I is found during transcription and even chromosome condensation [132].

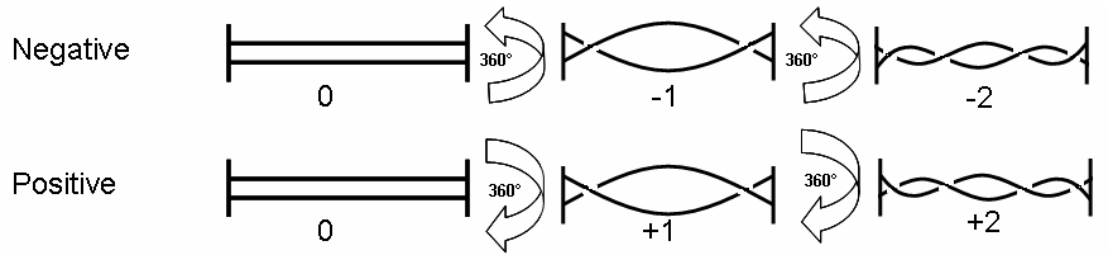

Figure 1.8: Negative (-) and positive (+) supercoiling. Numbers represent the linking number.

Although topo I has important roles in cellular processes, it is not essential as yeast mutation studies have shown. If topo I is absent, topo II, a type II topoisomerase, can replace its cellular function [142,143].

1.6.2 Topoisomerase II isoforms

There are two different isoforms of topo II present in mammalian cells, topo IIα and β. These are present in all higher eukaryotes, excluding *Drosophila* which only encodes one isoform most reminiscent of topo IIα [144]. The topo IIα gene, located on chromosome 17q21-22 as determined through cloning its complement DNA (cDNA) from human cells (HeLa and Raji-HN2 Burkitt's lymphoma) [145,146], codes for a 172 kDa protein that is immunologically distinct from the 180 kDa protein [147-149] encoded by the topo IIβ gene on chromosome 3p24 [146,150]. Topo IIα and β also vary in the number of exons coding the proteins; topo IIα has 35 and topo IIβ 36 exons [151,152]. The two isoforms show 72% identity and contain highly conserved regions apart from the N-terminus and a large proportion of the C-terminus [150]. It is thought that as their intron-exon arrangement is very similar, the two isoforms have arisen by gene duplication [151,152]. Topo IIβ has two differentially spliced forms of mRNA (messenger RNA), one leading to a protein that has TFLDQ inserted following valine at position 23 [153]. The role of this insertion is unclear, but it might alter subcellular localisation or post-translational modification. As well as two topo IIβ mRNA forms, cells also express a novel 160 kDa protein form of topo IIα that was discovered in mitoxantrone-resistant cells [154-156].

More interest has been placed on topo IIα for several reasons. Not only was it the first of the two to be purified in mammalian cells in 1981 [140] , six years before topo IIβ [148], but it was also the first to be cloned [145]. Also its expression patterns suggest a more functional role. Whereas topo IIβ is expressed at a constant level throughout the cell cycle, increased only during cell quiescence, topo IIα expression peaks at the G_2/M phase before decreasing during G_0/G_1 and increasing again at S phase [128]. In human PBLs it was also shown that topo IIα was required less in resting cells [157]. Expression of both isoforms increased to comparable levels after PHA stimulation, although topo IIβ, not topo IIα, expression was lowered by 50% after longer PHA stimulation [157]. This increased topo IIβ expression in cycling cells contradicts previous findings [128] and is thought to be due to different methodology and antibodies. Topo IIα is also thought to be the dominant isoform as Chinese hamster lung cells, in which topo IIβ has been inactivated to confer resistance to 9-OH-ellipticine, are still viable [158]. Cells can only temporarily survive a knockdown of topo IIα expression which can be circumvented by using temperature-sensitive topo IIα mutants [124,142]. Topo IIα expression is also increased in transformed cells, suggesting it could be a marker for cell proliferation [159]. Interestingly, topo IIα expression is increased in breast tumours where erbB (Her2), the target for the drug Herceptin, is amplified in tandem arrangement [160].

One main question that as yet lies unanswered is: 'Why does the cell encode two isoforms that are structurally and mechanistically very similar?'

1.6.3 Functions

Topo II has many cellular functions including replication and transcription. As negative and positive supercoils (Figure 1.8) form behind and ahead of both the replication and transcription complex respectively, topo II is required to relax these supercoils or else the complexes cannot proceed or be removed [161-164]. As replication is topology dependent [165], topo IV, an *Eschericia coli* homologue of human topo II, is necessary to ensure together with DNA gyrase ahead of the complex that enough, but not too much, negative supercoiling is present to initiate replication, as well as transcription [166]. In human cells, topo I and II both function ahead of the complex and only topo II is found to act behind it [161,166,167] as it is able to relax duplex DNA by transporting one strand through the other [140,141], whereas topo I can only act within, rather than between, duplex DNA [139].

After newly replicated strands are untangled by topo II, they are still kept slightly catenated until closer to mitosis. However, nearer to mitosis, these catenations must be removed by topo II to allow for chromosome condensation in prophase [124], although it appears topo II stabilises rather than initiates condensation [168,169].

Cells might survive without topo IIα if it were not for its role in sister chromatid decatenation at mitosis [168-172]. If topo II is inhibited, G_2 checkpoint activation (section 1.3.2) prevents cells from entering mitosis, or if already in mitosis, a different checkpoint prevents cells from entering anaphase. Cell cycle progression is resumed only when cells are capable of decatenating sister chromatids as if this is not ensured DNA damage can occur after the chromatids are pulled to either side of the cell in anaphase. Topo II has also been associated with apoptosis [173].

All functions mentioned above have been attributed mostly to topo IIα. Topo IIβ cannot adopt the mitotic function in human cells [174], even though both isoforms can substitute yeast type II topoisomerase in mitosis [175]. Although it has been suggested that topo IIβ can act at the transcription complex too [176], the only functions this isoform has been convincingly associated with are ageing [177], differentiation [178,179] and neuronal development [180]. In some cases topo II activity is thought to be decreased in differentiated cells [181], however this is most likely influenced by a decrease in topo IIα not β activity.

Whereas topo IIα preferentially binds AT rich domains [147] such as those found at the nuclear scaffold [182]; topo IIβ preferentially binds GC rich areas such as in nucleolar DNA suggesting a role in ribosomal RNA transcription [147] .

1.6.4 Localisation

Although topo IIα and β activity is similar mechanistically, how is it that their cellular functions vary? Perhaps tissue, cellular and chromosomal localisation might be a key to this.

Tissues

Topo IIα expression is high in highly proliferating tissues such as the spleen, testes and proliferating endometrium [183,184]. Topo IIα mRNA levels are also high in the spleen, testes, thymus, bone marrow and intestine [185]. Interestingly, although low amounts of topo IIα protein are found in the liver, it appears to be inactive as after purification it cannot decatenate kinetoplast DNA (kDNA). This might be because the liver proliferates only during acute injury, so perhaps topo IIα levels and activity increases only after injury [184]. Topo IIβ protein on the other hand is generally distributed in differentiated or lowly proliferative tissues such as the brain [177]. It can therefore be concluded that the tissue distribution does suggest that topo IIα is mostly required in proliferative tissues and that only after differentiation does topo IIβ become the primary isoform.

Cellular

Although topo II might be active, if it is not located near DNA, one would not expect it to function on a cellular level. Cellular localisation is determined by both nuclear localisation sequences and nuclear export sequences (NES), located between the breakage/reunion and nuclear localisation domains (in the C-terminus),q of topo IIα and β [186]. Topo IIα is rarely in the cytoplasm, except in the plateau phase of cell growth [187], again suggesting that it is the more dominant and functional isoform. Nuclear localisation sequences (NLS) found in the C-terminus of topo II bind importin α, which ensures nuclear localisation of the protein [187]. It has been suggested that topo IIα does not shuttle constantly between the cytoplasm and nucleus in proliferating cells, but only becomes cytoplasmic after certain signals allowing for the active export of this protein [187].

In interphase, topo IIα and β are expressed in the nucleolus and nucleoplasm [185,188-191]. However, due to its role in the decatenation of sister chromatids, most of the focus has been placed on cellular localisation during mitosis. In most phases of mitosis topo IIα is associated with chromosomes [190,192]. It is thought that topo IIα has a role in human condensation in prophase as it is located on chromosomes [193,194]. In late anaphase and telophase, topo IIα starts moving to the cytoplasm, with foci appearing in the reforming nucleoli [188]. It is thought that *Drosophila* has three separate mitotic topo II pools, which all leave the nucleus at different stages of the cell cycle. In human cells this would mostly relate to the topo IIα isoform. The first topo II pool in *Drosophila* dissociates at prophase, which might infer a role in condensation, another leaves at metaphase, after chromosome segregation, and the rest remains attached to chromosomes which suggest a structural role [195]. Topo IIβ on the other

hand is mostly cytoplasmic during mitosis with little to none found on chromosomes; perhaps because topo IIβ is pushed out of the nucleolus due to either higher affinity of topo IIα to DNA [185,192], or through active export [192]. It was thought that as topo IIβ was not bound to chromosomes during mitosis [178] that it could not be involved in the mitotic function usually associated with topo II.

Chromosomal

The association of topo II with chromosomes is essential for its activity in decatenating sister chromatids. The overall paradigm is that topo IIα is chromosome-bound during mitosis [125,191]. However, where on the chromosome does topo IIα bind? Results are varied due perhaps to species type [189], fixation methods or stage of mitosis. What is certain is topo IIα's location at the base of chromatin loops [121,125,182,196].

It was shown that after histone-depletion the DNA is still highly folded suggesting other proteins must be holding it together, collectively forming an X-shaped central proteinaceous scaffold from which DNA radiates as a halo [197,198]. Scanning electron microscopy data confirmed this radial loop model [199]. Other data suggests that these radial loops coexist with helical coils in metaphase [200]. It was quickly determined that the main non-histone protein present was scaffold protein 1 (SC1) at 1-2% of total mitotic chromosomal protein and this was established to be the 170,000 molecular weight protein, topo IIα [121,125,201]. Average loop size in HeLa metaphases is 70,000 bases [198] and the matrix/scaffold-associating region (MAR/SAR) found at the bases of these loops are preferential binding sites for topo II [125,182,196,201,202]. Topo II is known to excise these chromatin loops suggesting that poisoning topo II can result in the loss of these genetic areas [130].

The precise areas of the chromosomes bound by topo IIα varies according to the stage of mitosis. In prophase, topo IIα is nucleolar with some bound at kinetochores [188], in prometaphase and metaphase it moves to areas along the central axis of the chromosomal arms [193] and in anaphase less is expressed at the centromere, with some still present on the arms [203]. Other groups have also determined that topo IIα is bound in mitosis to chromosome arms [192]. It was also concluded that the 13S condensing complex and topo IIα together show a barberpole appearance with one being expressed, then the other [194], substantiating a role for topo IIα in chromosome condensation.

As well as binding chromosomally during mitosis topo IIα is also bound during interphase, as is topo IIβ. Chromosomal localisation of topo IIβ in mitosis [203] however is quite controversial as it does not decatenate sister chromatids [174]. It was determined that some topo IIβ localises at centromeres only in early mitosis and at chromosome arms until telophase [203]. Studies with biofluorescent chimera of topo IIβ also determined low levels of topo IIβ bound to

chromosomes at metaphase, yet topo IIα is still the main isoform present on chromosomes during mitosis [191]. It therefore seems that the main isoform involved in mitotic topo II activity is topo IIα.

In the same study it was suggested that some chromosome-associated human topo IIα remains non-motile after photobleaching suggesting a structural role [191]. This structural role was also proposed after experiments using pBR322 DNA relaxation studies showed that topo II activity was reduced in mitosis yet topo IIα still bound to chromosomes in mitosis [190,192]. However, in *in vitro* studies of *Xenopus* cells topo II was easily extracted and chromosome shape did not change, suggesting that topo II is not involved structurally [204]. Also the rapid exchange between the cytoplasm and chromosome of topo IIα does not support a structural role, although the authors do allow the possibility of some topo IIα remaining bound to chromosomes [188]. Although topo IIβ is present at low levels on chromosomes in mitotis, it is more likely that topo IIα is the active isoform in this stage of the cell cycle.

1.6.5 Structure

Currently, no complete crystal structure of human topo II has been determined. A large amount of the information regarding mammalian topo II structure has been determined from studies on bacterial DNA gyrase and topo IV, *Schizosaccharomyces pombe* and *Saccharomyces cerevisiae* topo II, and archeal topo VI as their primary sequences are homologous [205]. Human topo II mostly forms a homodimer [140] and occasionally a heterodimer [206], thus when looking into topo II isoform localisation, expression or regulation, it is important to note that heterodimers might act differently.

Topoisomerase II has three functional domains. Firstly, the N-terminal domain contains an adenosine triphosphate (ATP) binding site and is capable of ATP hydrolysis and dimerisation [205,207]. Secondly, a highly conserved part of the enzyme, the central region, includes the catalytic tyrosine residue as well as the breakage and reunion activity. Finally, the C-terminus includes another DNA binding site as well as dimerisation, nuclear localisation/export sequences and posttranslational modification sites, including serine/threonine phosphorylation sites [187,205,208]. These three domains correspond with those found in type II topoisomerases of *Schizosaccharomyces pombe, Saccharomyces cerevisiae* [136,166]. For instance, *E. coli* DNA gyrase regions Gyr A and B are similar not only to the Par C and Par E subunits of *E. coli* topo IV respectively, but also to the central domain and N-terminus of eukaryotic topo II [136,205].

Interestingly the N-terminus is the most conserved domain of type II topoisomerases. The central region is still quite highly conserved, but the C-terminus appears to be the area of most variability [136].

1.6.6 Mechanism

Much of topo II's mechanism (Figure 1.9) has been determined from various dimer intermediates crystallised with a DNA duplex or nucleotide. There is a high sequence homology between human, yeast and *Drosophila* topo II [145] and as mentioned human topo II can replace yeast topo II mechanistically [175]. It is therefore logical that in the absence of a full human topo II crystal structure, data derived from yeast or *Drosophila* type II topoisomerases such as the following can be applied to human topo II. The first mechanistic step involves the dimer binding a duplex DNA, also called the gated segment (G-segment) as it forms a gate through which the other duplex DNA is transported (T-segment). The affinity of topo II to the G-segment is increased when magnesium ions are bound [209] or when the DNA sequence is a specific topo II-targeting sequence although topo II activity is also affected by DNA structure and bendability [210,211]. When the G-segment binds topo II, this dimer changes structurally resulting in its two catalytic tyrosine residues to become located close to each other [210]. This change in protein structure also renders these tyrosine residues and the magnesium ions close to the DNA duplex. This DNA duplex becomes bent at an angle of 150° when bound to topo II.

After the DNA (G-segment) is bound, it is in an equilibrium state between cleavage and religation [210,212]. Cleavage of DNA involves each monomer of topo II creating a single strand break and remaining linked to a 5' end of DNA by phosphotyrosine on opposite strands, 4 base pairs apart [212-216]. This covalent bond keeps the dimerised topo II bound to the DNA ensuring that the genetic material of the G-segment is maintained as accurately as possible and is often referred to as the cleavable complex.

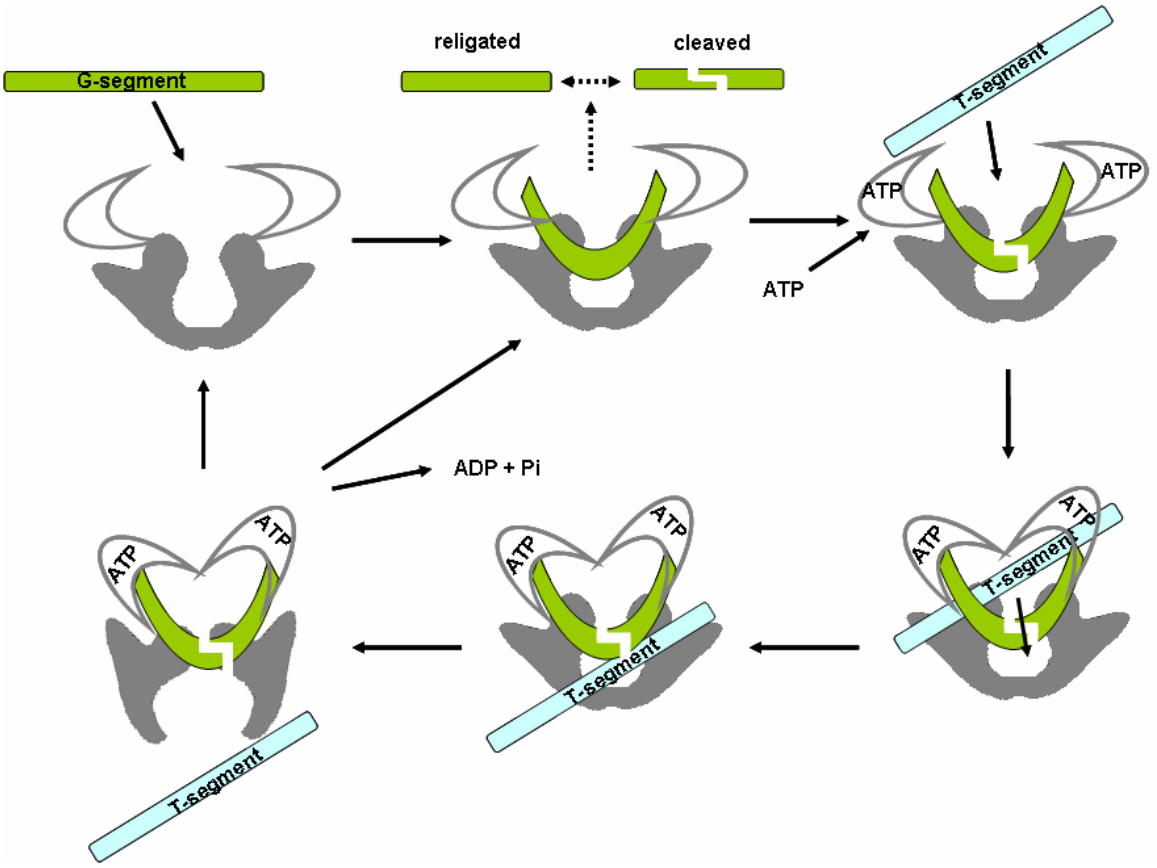

Figure 1.9: Mechanism of topoisomerase II. The enzyme dimer binds the gate segment DNA double helix (G-segment) and is in an equilibrium state between cleavage and religation. When ATP is bound, the transported double helix (T-segment) is able to bind and pass through the G-segment and be released. ATP hydrolysis to ADP and Pi allows for the recycling of the dimer.

Once one ATP molecule binds each monomer, the dimer undergoes a conformational change resulting in DNA (T-segment) strand passage [212]. This strand passage allows for the decatenation of daughter duplex DNA [123,170,217]. Interestingly, although the use of non-hydrolysable ATP analogues suggests a role for ATP in protein turnover, no ATP is required for the cleavage-religation equilibrium of the G-segment [218,219]. After ATP hydrolysis to adenosine diphosphate (ADP) and inorganic phosphate Pi, another conformational change occurs resulting in the opening of the C-terminal gate through which the T-segment can now be released [212]. DNA binding alone also results in the opening of the C-terminal gate, suggesting that the T-segment does not need to be present [210].

It is now predominantly accepted that, as suggested by the two-gate model, the T-segment enters the topo II dimer through the ATP-containing N-terminal domain and leaves through the C-terminal domain [220,221].

1.6.7 Poisons and inhibitors

As already pointed out, topo II is involved in many important cellular processes. For this reason, many drugs used clinically target topo II and affect its activity, resulting ultimately in cell (tumour) death. Similar drugs are being used as antibiotics, such as the quinolones nalidixic acid and ciprofloxacin [222,223]. Topo II-targeting drugs can be classified into either catalytic inhibitors or poisons, with most clinical drugs falling in the latter category. These poisons however are mostly referred to as topo II inhibitors in the literature. Here, for the sake of clarity, they will be referred to as topo II poisons.

As already explained (section 1.6.6) topo II activity requires the binding of a G-segment, which when cleaved, will form the gate through which the T-segment is moved. This T-segment is released, the G-segment is religated and ultimately the DNA linking number has changed by a factor of 2 [140,141]. A drug is generally considered a 'topo II poison' when it interferes with topo II activity in such a way that the G-segment is still cleaved and DSBs are still formed. This is unlike catalytic inhibitors, which do not cause DSB.

Inhibitors

Although many type II topoisomerase inhibitors exist, the only inhibitor used in this thesis is the bis (2,6-dioxopiperazine) derivative ICRF-193. This inhibitor is known to target type II topoisomerases [224]. As a true catalytic inhibitor ICRF-193 does not stabilise a cleavable complex, instead inhibiting protein activity by trapping the enzyme as a closed protein clamp. It maintains this closed clamp formation only in the presence of ATP [224]. As topo II activity is inhibited, chromosome segregation will no longer occur in anaphase and to prevent further damage cells are blocked through the G_2/M checkpoint in G_2 [54].

Most non-intercalating drugs affect one isoform more than the other. ICRF-193 is no exception as it preferably targets topo IIα rather than β [225]. Although the definition of catalytic inhibitors suggests that they do not cause DNA damage, at high drug concentrations ICRF-193 can [226]. However, as the concentrations used here are low, this should not be the case in the experiments performed here.

Exogenous poisons

The most clinically used drug is etoposide, also known as VP-16, which is classified as a topo II poison and has been used in the last 20 years for the treatment of leukemias, lymphomas and several solid tumours [227]. Topo II poisons are used alongside radiotherapy as they sensitise cells to the effects of radiation and thus increase cell death and tumour size diminishment. They are considered tumour specific as cells, such as breast cancer cells, generally have a higher topo II level and therefore are more sensitive to the topo II-targeting drugs [160,228,229]. Other antitumour topo II-targeting drugs exist although the only one relevant

to this thesis is amsacrine hydrochloride; also known as mAMSA or 4'-(9-acridinylamino)methanesulfon-m-aniside [222,230]. It acts on topo II in a similar way to etoposide, stabilising the cleavable complex [231] and ultimately inducing cell death.

mAMSA is an intercalator that stabilises the cleavable complex, which defines the DNA duplex bound to the topo II dimer [230]. Generally, when a drug is bound to the cleavable complex, it is referred to as the ternary complex. Stabilising the cleavable complex, in this case by inhibiting religation, increases the number of DSBs formed by topo II [230,231]. Unlike ICRF-193, mAMSA targets both topo IIα and β equally [225].

Other exogenous poisons that are relevant, though which have not been used experimentally in this thesis include quinones. Quinones, such as 1,4-benzoquinone found in cigarette smoke, bind topo II and trap the G-segment causing DSBs and have been associated with the t(8;21) translocation found in acute myeloid leukemias [232] and translocations involving 11q23 often associated with infant leukemias.

As well as inhibiting topo II catalytic activity, many topo II inhibitors also affect topo II poison activity. If added before the addition of topo II poisons, such as etoposide or mAMSA, ICRF-193 and other inhibitors can prevent the cleavable complex from forming in the first place, thus decreasing DNA damage [233-235].

Endogenous poisons

As part of the signal model it is possible that topo II activity, if involved in chromatid break formation, is affected by endogenous topo II poisons. Both topo IIα and β activity can be affected by DNA lesions and they can locate one in a background of several 1000 undamaged base pairs [236]. Oxidized and mono-alkylated DNA adducts fall into this category [236] and show the general 'positional specificity' [237] found with all endogenous poisons, where they only affect activity if located between the four base pair scissile bonds of topo II. This 'positional specificity' could be regarded as a 'signalling' mechanism to topo II. 8-oxoguanine is an endogenous topo II poison that is found in normal tissues at 7500 per genome, though levels in smokers are 50% higher [236]. O6-methylguanine is normally found at 20,000/genome in people who smoke or have occupational exposure to alkylating agents. Neither affect DNA religation by topo II [236].

DNA lesions such as abasic sites, which are normally found during excision repair, recombination or after ionising radiation or reactive oxygen species, can be more potent than etoposide. Abasic sites, and more specifically apurinic sites, do not interfere with religation and are considered more than 2000 times more potent than etoposide. Although they can be quickly removed, if repair is faulty or a few sites are left behind, they can dramatically increase the formation of topo II-induced DSBs [237-239].

Bioflavonoids such as quercetin and genistein, which are normally recommended as part of a healthy diet due to their antioxidant content, are associated with mainly infant leukaemia. In these cases, although the infant had not come into contact with topo II-targeting drugs *in utero,* they still developed leukemia as their mother's dietary intake of bioflavonoids during pregnancy had affected topo II activity [240,241]. One might question why topo II is allowed to cause such levels of DNA damage if the alterations could be mutagenic. Perhaps it acts as a "cellular barometer for genomic damage", causing cell death when the level of damage is too high and repair is unfeasible [242].

Another endogenous topo II poison is the hydroxyl radical. This is important to mention as in Chapter 6 hydrogen peroxide is used to question the role of topo II in forming DNA and chromosomal damage via $^{\cdot}OH$ radicals and it will be discussed later in this thesis.

1.7 Topo II and DNA or chromosomal damage

1.7.1 Topo II in chromosomal aberrations

Although normal topo II action involves DSB induction, the DSBs are protein-associated and the DSB is usually religated soon after, so no overall damage will have occurred. One can assume that if something goes wrong during this process, a DSB might either remain unrepaired or topo II might mis-join the ends of the DSB. In S-phase, the replication fork can collide with the topo II cleavable complex, where the DSB is still bound to the dimer. This results in the enzyme being released from the DSB and this damage can cause sister chromatid exchanges (SCEs) and chromosome aberrations (CAs) [243]. Here, chromosome aberrations refer to breaks or gaps on both sister chromatids as well as dicentrics, rings and multi-centric chromosomes. Other groups have also shown that topo II poisons, such as amsacrine, etoposide, doxorubicin and ellipticine can produce CAs and SCEs [127,244] as the cleavable complex is often stabilised and DSB induction rather than religation is favoured. The SCE induction by these drugs is known to be formed through topo II activity because in drug-resistant cells, in which topo II activity and expression is reduced, CAs or SCEs were not created [127,244].

It has also been shown that the presence or absence of a cleavable complex can determine the type of chromosomal damage, whether chromosome or chromatid aberrations. As explained earlier, chromatid aberrations refer to damage to only one sister chromatid, whereas chromosome aberrations refer to damage to both chromatids. If the drug used causes the formation of a cleavable complex, CAs can often be found in drug-sensitive, but not drug-resistant, cells [245]. Topo II poisons that stabilise cleavable complexes such as etoposide, adriamycin and mitoxantrone induce CAs [246]. Aclarubicin, a topo II inhibitor, rather than poison, does not stabilise the cleavable complex and actually decreases the number of

poison-induced CAs [246,247]. Although these studies do also mention chromatid aberrations after 6 or 24 hours of continuous drug treatment, the focus has always remained on chromosome aberrations and the definition of chromatid aberrations is ill-defined. It was also suggested that the stage within the cell cycle as well as the presence of a cleavable complex determines the type of chromosomal damage. If this complex is formed before replication, CAs occur and if after, only chromatid aberrations, such as breaks, exchanges and gaps, can be seen; the cleavable complex however is not, unlike for chromosomal aberrations, always required in the formation of chromatid aberrations [245].

1.7.2 Topo II in translocations

Cell death occurs when topo II expression and activity is either too low or high [232]. Minimum activity is required mainly for the decatenation of sister chromatids in mitosis. A maximum topo II activity threshold is also in place as without it, the cell will accumulate far more DNA damage than it can repair and tolerate. However, if the topo II level is in between these two thresholds it is evident from its involvement in CAs and SCEs that higher than normal activity levels may lead to disease states [232].

More specifically, topo II can cause translocations at the chromosomal location 11q23 resulting in MLL where differentiation of pluripotent hematopoietic stem cells or committed myeloid or lymphoid stem cells is affected [232]. This is thought to be due to the replication or transcription complex colliding with the cleavable complex creating a permanent, non-reversible DSB to which topo II is no longer covalently bound [232,240]. Most *MLL* rearrangements occur within a 8.3 kb region that contains putative topo II cleavage recognition sequences and it is thought that topo II causes the initial DSB. Mis-repair of these DSBs by either the nonhomologous end-joining or single strand annealing repair pathways results in the translocations [240,248].

As mentioned earlier, etoposide is the most commonly prescribed anticancer drug and 2-12% of patients treated with etoposide-based regimens result in therapy-related leukemia and 50% of these show translocations in the *MLL* gene breakpoint cluster region [249]. 11q23 translocations have also been associated with infant leukemias even in the absence of these drugs. It is now thought that endogenous topo II poisons, such as abasic sites, or maternal consumption of bioflavanoids are the cause [232,240]. Other topo II poisons consumed maternally during pregnancy linked to infant acute myeloid leukemia (AML, t(8:21)) include legumes, soy, apples, onions, berries and caffeine [240].

As well as etoposide, teniposide is also used clinically for treatment of lung cancer in adults and pediatric acute lymphoblastic leukemia (ALL) [240]. Also mitoxantrone and anthracyclines are used for breast cancer treatment resulting in acute promyelocytic leukemia (APL).

Cigarette and wood smoke include phenols, catechols, hydroquinones and benzene which cause chromosomal abnormalities at 11q23 in amniocytes from foetuses of smoking mothers. Another topo II poison involved in infant ALL caused by the translocation t(4;11) is p-benzoquinone that is normally detoxified by nicotinamide adenine dinucleotide phosphate (reduced) (NADPH) quinine reductase except when its gene is inactivated by a polymorphism [240].

It has been suggested that topo II activates the NHEJ pathway and mis-repair causes the secondary leukemias [250], though NHEJ does not appear defective in AML patients [251]. It is likely that topo II can become error prone, resulting in the mis-repair of topo II-induced DSBs, which ultimately lead to various types of leukemia. This is substantiated in experiments where purified topo II was shown to be able to cleave the translocation hotspot *MLL* breakpoint cluster *in vitro* [240]. Mis-repair or mis-recombination has also been suggested as a mechanism of chromatid break induction [252].

1.7.3 Topo II in syndromes showing high radiosensitivity

As well as looking into the role of topo II in leukemia-related translocations, many groups question if topo II levels or activity can be a marker for early cancer diagnosis or even predict the outcome of topo II-targeting drug treatment. In ovarian, cervical, colon and non-small-cell lung cancer both topo IIα and β are upregulated and overall topo II activity is higher [253,254]. In precancerous and cancerous lesions of the oral mucosa immunohistochemical detection of topo IIα was increased when compared to normal squamous epithelium and is related to disease stage progression and prognosis [255]. It is also known that topo II autoantibodies are produced in systemic lupus erythematosus [223]. However, what I am interested in is the role of topo II in chromatid breaks and in this next section I will focus on topo II and syndromes of high radiosensitivity as these show higher than normal numbers of chromatid breaks after ionising irradiation.

As mentioned previously, in many disease states, such as breast cancer, deficient repair is thought to be a predisposing factor leading to high radiosensitivity. As the area of interest in this thesis is the role of topo IIα in chromatid break formation, this section focuses on topo IIα expression in syndromes of high radiosensitivity. In primary breast cancer cases, topo IIα gene status is increased as determined by fluorescent or chromogenic *in situ* hybridisation (FISH or CISH) [256]. Topo IIα expression was also increased as determined by immunohistochemistry, although in these cases gene amplification did not correlate with anthracycline response [256]. This amplification was also seen in two out of five Her-2/neu-positive breast cancer cell lines, although interestingly one cell line also showed a deletion of the *top2a* gene. Here, in primary breast cancer carcinomas it was also determined that this gene amplification or deletion, determined by FISH, was associated with altered topo II

expression as well as doxorubicin (anthracycline) sensitivity and resistance respectively in Her-2/neu-positive breast cancer cells [160]. It was confirmed elsewhere that topo II gene status as determined by FISH might be a marker of anthracycline response *in vivo* as assessed by pathological complete remission, here in non-endocrine response breast cancer cases overexpressing Her-2/neu [229]. In human breast cancer cell lines, sensitivity to amsacrine and etoposide correlated with topo IIα and β expression respectively, as determined by western blotting [228]. As well as determining drug response, topo II expression can also be related to the histological grade and lymph node status in breast ductal invasive carcinomas [257]. It has also been suggested that unlike Her-2 or topo II gene status or expression, topo II mRNA levels cannot act as a marker for anthracyclines, etoposide, amsacrine or taxane sensitivity of breast tumours or in breast cancer cell lines [228]. This is unexpected as topo IIα expression is linked with Her-2 expression even though both topo IIα and Her-2 are found on chromosome 17q and this area is often overamplified together in breast cancer [160].

The role of topo II in AT is still unclear. AT is thought to be due to mainly increased topo II expression and activity found in AT cell lines [258,259] though others suggest that a defect in repair might be behind the high radiosensitivity of AT cells [75,260]. The mechanism behind radiosensitivity and the role of normal cell cycle and DNA repair function is unclear but perhaps topo II is involved. This role however is uncertain as in some cases topo II activity is lowered rather than increased, suggesting that the AT phenotype is not topo II-dependent [261].

Fanconi's anaemia (FA) cells are hypersensitive to crosslinking agents and show increased spontaneous chromosome aberrations and Bloom's syndrome (BS) cells show an increased number of SCEs. This was thought to be due to decreased topo II activity which originally might have provided access to repair proteins to the damaged site. However, topo II activity was not altered in FA or BS cells as topo II-targeting drugs did not contribute to this hypersensitivity [262,263].

As already mentioned, many topo II-targetting drugs are used clinically, as the amount of DNA damage they cause often leads to apoptosis of tumour cells. However, it is possible that topo II can cause DNA damage that ultimately does not lead to cell death and if maintained might even contribute to disease initiation or progression as stated above. If this is the case, it is possible that topo II can be poisoned and its activity become aberrant in such a way that chromatid breaks, initiated by DSBs, are formed.

1.7.4 Repair of topo II-induced breaks

A puzzling mechanism is the repair of topo II-induced DSBs. Cells incubated with a topo II poison cause cleavable complexes and thus topo II–induced DSBs. These can be repaired by NHEJ [264,265]. In fact, two separate NHEJ pathways have been suggested for the repair of topo II-induced DSBs, namely with and without DNA-PK_{cs} [266]. However how do NHEJ repair proteins gain access to topo II-induced DSBs as the topo II poison etoposide for example stabilises the cleavable complex with topo II still linked to the DSB [267]? This would leave the DSB inaccessible to repair proteins and the site of damage could therefore not be accessed by DNA-PK, which is dependent on the binding of the Ku70 and 80 proteins to single strand DNA ends for recruitment [268]. It appears that the protein-bound DSB complicates matters when trying to determine how they are repaired.

One way in which topo II-linked DSBs might become 'visible' to repair proteins is through collision of the protein with a replication fork [269]. Stalled replication forks allow RPA to bind single strand DNA, thus recruiting ATR (ATM-related protein) and all the Rad proteins eventually phosphorylating Chk1 and halting DNA replication allowing for DNA repair [270]. Although replication forks are not present in the G_2 phase, where the initial damage of chromatid breaks are formed, one can imagine that transcription complexes might act in a similar fashion.

It has also been shown that cleavable complexes caused by topo II poisons can be proteolytically degraded by proteasomes [271,272]. It therefore appears most likely that cleavable complexes are degraded leaving DSBs accessible to NHEJ proteins for repair.

1.7.5 Role of topo II in DNA repair

Due to the mechanistic action in which DSBs are created and repaired, topo II has already been implicated in SCEs [127] and illegitimate recombination [273] and a role in DNA repair has been suggested. For example, it has been proposed that topo II creates a DSB, thus altering chromatin structure and allowing access for repair proteins to DNA damage [274]. Although Downes *et al*. [275] found no or little involvement of topo II in excision repair of UV-induced DNA damage, DSB repair-deficient X-ray sensitive (xrs) 5 hamster cells have shown a corresponding change in total cellular topo II activity [276]. These studies have referred only to general topo II activity and not either topo II isoform specifically.

Woessner *et al*. [128] suggested that as DNA repair was more efficient in the G_0 phase, in which topo IIβ is highly expressed, that it was more likely that this isoform is involved in repairing DNA damage. This topo II isoform was also implicated in repair when it was determined that topo IIβ knock-out mice, at the late stages of embryogenesis, showed similar neural and

neuromuscular abnormalities as seen in cells lacking the repair proteins XRCC4 and ligase IV [180]. Mandraju *et al.* [277] determined that topo IIβ and not α was involved in repair, as in human cells treated with hydrogen peroxide topo IIβ expression, as determined by western blotting, increased and followed the trend of already determined repair proteins such as Ku70 and WRN (protein affected in Werner's syndrome). Also, Mielke *et al.* found that UV-irradiation caused an increase in topo IIβ expression at that site [131].

One way in which topo IIβ might be involved in repair is through its role in transcription [176], in a similar way to BRCA1, which is involved in transcription-coupled repair where BRCA1 induces transcription of p21 [29]. Topo IIβ-related DNA repair could also be indirect through the binding of the C-terminus of topo IIβ to topoisomerase II-binding protein 1 (TopBP1) [278]. TopBP1 has 8 conserved BRCT regions that bind DNA breaks [278] and its involvement in replication-related repair has been well-documented through its activation of ATR [279] after phosphorylation by ATM [280]. Also, in breast cancer TopBP1 changes its cellular localisation from the nucleus to the cytoplasm [281].

The literature reviewed above, though not completely convincing as yet, does suggest a role for topo IIβ and not α in DNA repair.

1.8 Experimental outline

As briefly mentioned at the start of this introduction, the aim of this thesis is to determine how low dose ionising radiation-induced chromatid breaks are formed and whether data support the signal model. The signal model suggests that the initial radiation-induced DSB is eventually repaired, yet still results in a chromatid break through the recruitment of as yet unknown proteins. In this thesis I have tested the involvement of topoisomerase IIα in the formation of chromatid breaks. There are several ways in which this was done. Firstly in chapter 3, I used cell lines that expressed topoisomerase IIα intrinsically at varying levels compared to each other. In chapter 4 I employed the short interfering RNA technology to 'knock down' or lower topoisomerase IIα expression and in chapter 5, I lowered topoisomerase IIα activity with the catalytic inhibitor ICRF-193. In all these cases, altered topo II expression or activity was linked with the frequency of γ-irradiation-induced chromatid breaks. In chapter 6, I looked into a way topo II might become involved in chromatid break formation, namely via the formation of $^{\cdot}$OH radicals. Hydrogen peroxide was used as a source for $^{\cdot}$OH radicals and the possible effect on DSB and chromatid break induction was determined.

CHAPTER 2

MATERIALS AND METHODS

2.1 Propagation of mammalian cells

2.1.1 HL60 and variant cell lines (MX1 and MX2)

Human promyelocytic leukaemic parental HL60 and mitoxantrone-resistant variants MX1 and MX2 cell lines (ATCC: American type culture collection, Manassas, USA) were grown in suspension in RPMI-1640 medium (Royal Park Memorial Institute medium; Gibco, Paisley, UK) containing 10% foetal calf serum (FCS) (Globefarm Ltd, Cranleigh, UK), 2 mM L-glutamine (Invitrogen Life Technologies, Paisley, UK), 50 µg/ml streptomycin (Invitrogen) and 50 units/ml penicillin (Invitrogen) at 37°C, 5% CO_2. Passaged cells were kept in 75 cm^2 tissue culture flasks (T75) (Thermo Fischer Scientific, Roskilde, Denmark) and experimental cells in 25 cm^2 flasks (T25). Cells were passaged before they reached maximum concentration to prevent differentiation into neutrophils. The cells were counted (see 2.1.3) and seeded at 200,000 cells / T75 or T25 to continue culture or start an experiment.

2.1.2 hTERT-RPE1 cell line

Human telomerase reverse transcriptase-transformed retinal pigment epithelial (hTERT-RPE1) cells were obtained from the ATCC and were maintained in exponential growth in DMEM-F12 medium (a 1:1 mixture of Dulbecco's Modified Eagle's medium and Ham's F12 medium; Gibco) containing 10% FCS, 2 mM L-glutamine, 50 µg/ml streptomycin and 50 units/ml penicillin at 37°C, 5% CO_2. hTERT-RPE1 cells are adherent and therefore were passaged by removal of medium and two washes of 4 ml trypsin/ethylenediaminetetraacetic acid (EDTA) (Sigma, 0.5 mg/500 ml). The flasks were incubated for 5 minutes at 37°C in 1 ml of the last trypsin wash and were then tapped gently. 10 ml of medium was added to neutralise the trypsin, cells were counted and cells seeded at 200,000 cells per T75 or T25 to continue culture or start an experiment. Cells were passaged up until passage number 13, when they were replaced by fresh stocks from liquid nitrogen (section 2.1.5).

2.1.3 Cell counting

Cell counts were made using the electronic Beckman Coulter Particle Counter Z1 (Coulter Particle Characterization, Hialeah, USA). 100 µl medium-suspended cells was added to 9.9 ml isoton and the number of cells was automatically determined, above or equal to a size of 275 fl.

2.1.4 Cryopreservation of cell lines

To keep stocks of cells at low passage numbers, a number of vials were cryopreserved. Cells were pelleted by centrifugation at 2000 rpm (600 x g) for 5 minutes at room temperature and

the supernatant was discarded (Heraeus Labofuge 400R, Heraeus Instruments, Hanau, Germany). 2 x 10^6 cells were resuspended in 1 ml medium (containing 10% FCS) and a final concentration of 10% dimethyl sulfoxide (DMSO). Cell suspensions were then stored in 1.5 ml cryo vials (Corning Incorporated, New York, USA). These vials were placed in a plastic holder (Nalgene Cryo 1°C Freezing Container, Roskilde, Denmark) containing a propane-1,2,-diol bath and then transferred to a -80°C freezer overnight and then to liquid nitrogen for long-term storage.

2.1.5 Defrosting cell lines

Cells were taken out of the liquid nitrogen, thawed by hand and added to a T75 culture flask. 9 ml medium was added to the cells in a drop-wise fashion and flasks were incubated for 24 hours before the medium was refreshed.

2.2 Cell lysate preparation

Lysates were prepared for immunoblotting against topoisomerase IIα or β-actin. Exponentially growing cells were washed twice in phosphate buffered saline (PBS) (Gibco) by centrifugation and resuspended in 14 μl/10^6 cells sample reducing buffer (2% sodium dodecyl sulphate (SDS) (BDH Biochemical, Poole, UK), 100 mM dithiothreitol (DTT) (Sigma-Aldrich, Poole, UK), 10% glycerol (BDH) and 60 mM Tris pH 6.8 (BDH). Protein was then denatured for 5 minutes at 100°C and stored at -20°C.

2.3 Protein quantification

The amount of protein in cell lysates was quantified to ensure equal loading in western blot gels. Here the Bio-Rad Laboratories (Hemel Hempstead, UK) Protein Assay was used in which known bovine serum albumin (BSA, Promega Corporation, Southampton, UK) concentrations, namely 0-8 μg/ml, were used as reference values. The method is based on the Bradford assay [282]. Briefly, the 5x dye reagent concentrate was diluted 1 in 5 with deionised water. The standard samples were prepared as a 1:10 dilution of 10 mg/ml stock solutions of BSA. The stock solutions were diluted in 1x protein assay solution in sterile water as follows:

BSA (1 mg/ml)	8 μl	6 μl	4 μl	2 μl	0 μl
Protein Assay Solution 1x	1 ml	1 ml	1 ml	1 ml	1 ml
Final BSA Concentration	8 μg/ml	6 μg/ml	4 μg/ml	2 μg/ml	0 μg/ml

Table 2.1 Bradford dilution solutions for standard curve.

Samples were prepared by adding 1 μl of lysate sample to 1 ml of 1x protein assay solution. Both samples and BSA controls were mixed by inversion and left at room temperature for 5 minutes. Prepared standard BSA concentration samples were read at absorbance 595 nm and a standard curve was drawn. Protein concentrations in unknown samples were extrapolated from the linear part of this curve. 100 mM DTT, found in the sample reducing buffer, does not affect the Bio-Rad Protein Assay.

2.4 Western blot

All gels were prepared freshly and for a western blot, two separate gels, namely resolving and stacking gel, needed to be prepared. This is known as the Laemmli method [283]. The same vertical electrophoresis apparatus (Thistle Scientific Ltd, Glasgow, UK) was used for electrophoresis and protein blotting.

2.4.1 Laemmli method

Firstly, glass plates (8.5 cm) were wiped with 70% ethanol, which was allowed to evaporate off, and then assembled onto a setting rig. No rubber spacers were added as they were already fixed to the glass plates. Sterile water was then applied to check that the set-up was tightly sealed. A 7% resolving gel was made first as follows:

- 5 ml sterile water
- 2.5 ml Tris (1.5 M pH 8.8) (BDH)
- 100 μl SDS (10%) (BDH)
- 2.33 ml acrylamide:bisacrylamide (37:1, 30%) (Sigma)
- 100 μl ammonium persulphate (APS) (10%) (Sigma)
- 10 μl N,N,N',N'-tetramethylethylenediamine (TEMED) (Sigma).

The tube containing the above 'ingredients' was mixed thoroughly and 7 ml added to the setting rig between the glass plates, covered with 1 ml 70% ethanol and left to set for about 30 minutes. Once set, the alcohol was poured off and the 3.4% stacking gel was prepared as follows:

- 5 ml sterile water
- 2.5 ml Tris (0.5 M pH 6.8)
- 100 μl SDS (10%)
- 1 ml acrylamide:bisacrylamide (30%)
- 100 μl APS (10%)
- 10 μl TEMED.

Again all ingredients were mixed by inversion and then 1-2 ml applied on top of the already set resolving gel and a comb put in. Once the gel was set, the comb was taken out and the wells cleaned out with sterile water to ensure the removal of all acrylamide. The 10x running buffer was prepared as follows for 1 L:

- 250 mM Tris
- 1.92 M glycine (VWR, East Grinstead, UK)
- 1% w/v SDS
- pH 8.56.

1x running buffer was made up to 1 L with 100 ml 10x stock and 900 ml sterile water mixed well. The set gels were removed from the setting rig and placed in the running rig. 1x running buffer was poured into the rig ensuring the plates were covered.

Meanwhile, 1 L of 10x blotting buffer was prepared as follows:

- 250 mM Tris
- 1.92 M glycine
- pH 8.48.

100 ml 10x blotting buffer was mixed with 50 ml methanol (VWR) and made up to 1 L with sterile water.

2.4.2 Sample preparation

Approximately 10 μg of samples were run mixed with 5 μl sample reducing buffer and 0.1% bromophenol blue (BPB). The volume of the sample to be added to the gel to get 10 μg of protein was determined from the protein concentration (see section 2.3).

2.4.3 SDS-polyacrylamide gel electrophoresis (-PAGE)

6 μl of prestained broad range protein marker (7-175 kDa) ladder (New England Biolabs Inc., Ipswich, USA) was added to the first well and samples were added to the other wells. The amount of sample or marker added to each well was made up to the same volume by adding the appropriate amount of sample reducing buffer plus BPB. The gel was run in 1x running buffer at 100 V for the first 30 minutes with a BioRad PowerPac 300 (BioRad Laboratories Ltd., Hemel Hemstead, UK) and then at 150 V until the dye had run to the bottom of the gel (approximately another hour).

2.4.4 Transfer of protein to nitrocellulose

Nitrocellulose membrane (Watman, Schleicher & Schuell, Dassel, Germany), sponges and filter paper were soaked in 1x blotting buffer. Once the gel had finished running it was removed from the running rig and glass plates. The order of layers in the transfer cassette were arranged as follows:

- black cassette
- sponge
- filter paper
- gel
- nitrocellulose membrane
- filter paper
- sponge
- red cassette.

This blot 'sandwich' was slotted into the rig with the black cassette facing the back. Blotting buffer was poured into the electrophoresis rig (Thistle Scientific Ltd, Glasgow, UK) and proteins were transferred at 100 V for 1 hour.

2.4.5 Western blot analysis

Protein transfer was checked with Ponceau S red stain (0.5% Ponceau S in 1% acetid acid) (Sigma). Membranes were blocked with 2% milk powder in PBS/Tween (0.1%) (Sigma) for 15 minutes at room temperature. Membranes were further incubated for 2 hours (or at 4°C overnight) in either rabbit anti-topoisomerase IIα or mouse anti-β-actin (Abcam, Cambridge, UK) at 1:20,000 and 1:5,000 respectively in 10 ml PBS/Tween-20. After being washed twice in 10 ml PBS/Tween for 15 minutes, the membranes were incubated in either anti-mouse or anti-rabbit antibody both of which were horse-radish peroxidase-conjugated (Pierce Biotechnology, Rockford, USA) at 1:100,000 in 10 ml PBS/Tween. Membranes were then

washed twice as before. Enchanced chemiluminescent (ECL) reagents were used for 1 minute for visualisation (Millipore, Watford, UK). Under red light, 1 piece of film (Fuji Medical X-ray film, Fujifilm USA) was placed on top of the membrane and the cassette was closed. The film was exposed to the membrane for 30 seconds. The film was then removed and placed in developer (Sigma) for approximately 3 minutes with agitated movement so as to acquire an image that was not overexposed, yet still exposed enough to allow all bands to show up. The film was then removed with forceps and placed in methanol to fix for 5 minutes and then washed in water and hung to dry. The film images were scanned to obtain a digital image and the amount of protein in samples was estimated using image analysis (Image J).

2.5 Mitotic index

2.5.1 Flow cytometry

Mitotic indices were determined by the proportion of mitotic cells labelled by an anti-phosphohistone 3 antibody. Exponentially growing cells were treated under various experimental conditions as explained in each individual chapter. Cells (1 x 10^6) were then washed in PBS, pelleted at 600 x g for 5 minutes at 20°C and fixed in 1 ml 70% ethanol for 30 minutes on ice. After centrifugation, cells were permeabilised with 90% ice-cold methanol and incubated for 30 minutes at 37°C in 1 mg/ml ribonuclease A in 0.5% donkey serum in PBS. Cells were then centrifuged as before and resuspended in 2 μg/ml propidium iodide in PBS for 30 minutes at room temperature in the dark before being washed once in 1 ml PBS. All further steps were performed in the dark. Cells were further stained for phosphohistone 3 according to the manufacturer's protocol (Cell Signalling Technology, Danvers, MA, USA). Briefly, cells were resuspended in 1 ml incubation buffer (0.5 % BSA in PBS) and centrifuged as before. 180 μl incubation buffer was then added to the pelleted cells and samples were blocked in this buffer for 10 minutes at room temperature. 20 μl of Alexa-conjugated anti-phosphohistone 3 antibody was added for 30 minutes at room temperature before cells were pelleted by centrifugation as before, resuspended in 0.5 ml PBS and acquired by FACScan (Becton-Dickinson BioSciences, Oxford, UK) with CellQuest software (San Jose, CA, USA). Data was analysed with Summit software (Dakocytomation, Glostrup, Denmark).

2.5.2 Manual counting

Mitotic indices were also determined manually to verify trends in siRNA-treated hTERT-RPE1 cells observed from flow cytometric data in a more cost effective way. Exponentially growing cells were treated under experimental conditions as explained in chapter 4. Cells were then trypsinised (section 2.1.2), pelleted by centrifugation and resuspended in 5 ml hypotonic solution (75 mM potassium chloride (KCl), Sigma) for approximately 10 minutes at room

temperature. Cells were fixed 3 times in 5 ml 3:1 methanol:acetic acid (BDH) for 10 minutes at room temperature. Cells were finally resuspended in 200 μl fixative. Metaphase spreads were then prepared by dropping 10 μl of each sample in fix onto a glass slide allowing the fix to evaporate in air. When dry, slides were stained with 10% Giemsa (BDH) in Gurr's buffer (BDH) for 10 minutes, washed in Gurr's buffer followed by water and then left to dry. Remaining samples were kept in fixative at -20°C. The number of cells in mitosis was determined at x10 magnification (Zeiss Axioplan 2, Welwyn Garden City, Hertfordshire, UK) for 1000 cells of each sample. Cells in mitosis were defined as cells with no nuclear membrane and DNA clearly condensed into chromosomes.

2.6 Chromatid break analysis

Cells underwent mostly the same protocol as described under section 2.5.2. Briefly cells were irradiated (^{137}Cs γ-rays, IBL437C; CIS UK Bio-International, High Wycombe, UK), pelleted, resuspended in hypotonic followed by fixative solution. The final volume fixative cells were resuspended in was 200 μl. Chromatid break analysis in HL60, MX1 and MX2 cells involved preparing metaphase spreads on ethanol-prewashed glass slides (BDH) using a humidity control cabinet (Hanabi, AO Science Technologies, Chiba, Japan). Metaphase spreads of hTERT-RPE1 cells were prepared in air. In all cases, 10 - 20 μl of sample was added to the slide and allowed to evaporate in air. When dry, slides were stained with 10% Giemsa in Gurr's buffer (pH 6.8) for 10 minutes, washed briefly in Gurr's buffer followed by water and left to dry. Remaining samples were kept in fixative in eppordorf tubes at -20°C. 100 metaphases were examined for chromatid breaks using oil-immersion (x100 magnification) optics (Zeiss Axioplan 2). Chromatid breaks were defined as any chromatid discontinuity i.e. gaps and breaks with either aligned or misaligned terminal fragments [65].

2.7 DNA double strand break measurements

2.7.1 DSB induction

DSB induction was measured either by low-voltage gel electrophoresis or γH$_2$AX immunocytochemistry.

Low-voltage gel electrophoresis

DSBs were determined by low voltage electrophoresis. After treatment (see relevant results chapters), exponentially growing cells were centrifuged at 600 x g for 5 minutes at 1^{o}C. Medium was aspirated and cell pellets resuspended in 160 μl of 0.8% low melting point (LMP) agarose (Sigma) in PBS at 37^{o}C. 80 μl was transferred to each of two gel plug moulds (Bio-Rad Laboratories) and placed on ice for approximately 5 minutes to set. Plugs containing

cells were extruded into 1 ml of ice-cold lysis solution (0.4 M EDTA (Sigma), 2% sodium N-lauryl sarcosine (Sigma), 1 mg/ml proteinase K (Sigma), pH 8.0) in eppendorf tubes for 30 minutes. Tubes were then incubated overnight (18 hours) at 37^{o}C. A 200 ml 0.8 % agarose gel (Life technology Ltd, Paisley, UK) was prepared in 0.5 M tris acetate EDTA (TAE: Sigma) buffer containing 1 μg/ml ethidium bromide (Serva, distributor AMS Biotechnology (Europe) Ltd, Abingdon Oxon, UK). Plugs were recovered from the lysis solution and placed in comb wells of the 200 ml agarose gel in a BioRad Sub-Cell horizontal electrophoresis apparatus. Wells were sealed using 0.8% LMP agarose in PBS, and the gel run in 0.5 M TAE buffer at 0.6 V/cm (6 mA, 8 V; constant current) for 96 hours. The fraction of DNA released from the wells during electrophoresis was used to calculate the induced double-strand breakage. DNA was quantified by ethidium bromide fluorescence, analysed using Syngene Genetools software (Syngene, Cambridge, UK). The mean fraction of DNA released (FDR) from each well (two wells per sample) was determined by the following equation:

$$FDR = DR/(DR + DW)$$

Where:

DR = DNA released
DW = DNA remaining in well

γH$_2$AX immunocytochemistry

hTERT-RPE1 cells were added as a drop of 2 x 10^5 cells in 200 μl onto a 22 x 22 mm coverslip in a 55 mm in diameter dish. Cells were allowed to attach to the coverslip surface for 3 hours after which 4 ml complete medium was added to the dish and cells were allowed to grow for 2 days. Cells were grown for another 2 days in complete medium until 90% confluent or incubated overnight in serum-free complete medium. Cells were then treated experimentally as described in the relevant results chapters in complete medium. After a fixative stage of 10 minutes in 4% formaldehyde in PBS at room temperature, cells were washed twice for 5 minutes in PBS before being permeabilised with fresh 0.2% Triton X-100 in PBS for 10 minutes. All washes, fix, permeabilisation and probe stages of the procedure were performed in a total volume of 4 ml, agitated on a rocker and at room temperature. Cells were washed as before and were then blocked four times for 15 minutes in PBS containing 1% BSA and 0.2 M glycine. 50 μl primary anti-γH$_2$AX mouse monoclonal antibody (Millipore) was added at a dilution of 1:100 in fresh 0.5% BSA in PBS with the coverslips covered in Nescofilm for 1 hour before being washed four times for 15 minutes in 0.5% BSA in PBS. Cells were further incubated in 1:250 dilution of anti-mouse-FITC-conjugated secondary goat antibody (Sigma) in the dark, with the coverslips bearing cells covered in Nescofilm for 1 hour. Control experiments were also carried out where cells were incubated with secondary antibody only. Coverslips were washed twice in PBS, applied to slides with cells face-down on

a drop of 12 μl 4',6-diamidino-2-phenylindole (DAPI) /Vectashield (Vector Laboratories Inc, Burlingame, CA, USA). Coverslips were sealed with nail-varnish and left overnight at 4°C in the dark.

2.7.2 DNA double strand break repair

HL60, MX1 and MX2 cells were irradiated and further processed in the same manner as described above in section 2.7.1 by low voltage gel electrophoresis; the only difference being that cells were allowed to repair at 37°C for a predetermined amount of time. Once a time-point was reached, cells were kept on ice until the last time-point in the series had been sampled. Cells were then centrifuged and resuspended in LMP agarose as described above. These experiments were carried out by Dr P. Bryant.

2.8 Cell cycle synchronisation

hTERT-RPE1 cells were seeded at 2 x 10^5 cells per T25 flask containing 5 ml DMEM-F12 complete medium and left to grow for 24 hours at 37°C, 5% CO_2. The next day sterile 2 mM thymidine (Sigma) in medium was added to the flasks and cells were incubated for 16 hours at 37°C and in 5% CO_2. Cells were then washed with fresh medium to remove thymidine and placed back at 37°C, 5% CO_2 in medium containing no thymidine. At certain time points cell samples were harvested by trypsinisation as described in section 2.1.2 and washed in PBS. Cell pellets were fixed in 1 ml 70% ethanol for 30 minutes on ice. Samples were stored in 70% ethanol at -20°C.

2.9 Silencing RNA treatment

hTERT-RPE1 cells were seeded at 2 x 10^5 in a T25 flask 24 hours prior to transfection. They were then transfected with various concentrations of short siRNA oligos against topoisomerase IIα or, as a control, scrambled siRNA (Negative Control siRNAs that have no significant sequence similarity to mouse, rat, or human gene sequences) (Ambion, Warrington, UK) using Dharmafect transfection reagents (Dharmacon, Chicago, IL, USA). Briefly, both 7.5 μl Dharmafect and in a separate tube, siRNA, were incubated in a total volume of 0.5 ml antibiotic- and FCS-free DMEM-F12 for 5 minutes at room temperature. The contents of the two tubes were then mixed together and incubated for 20 minutes at room temperature. Meanwhile cells were washed twice in 4 ml 10% FCS-containing DMEM-F12, and finally 1 ml siRNA mix was added to 4 ml 10% FCS-containing DMEM-F12 and subsequently added to the cells. The final concentrations of siRNAs used ranged from 0.25 – 2 nM. Cells were incubated with siRNAs for 12 hours.

2.10 Immunocytochemistry

Exponentially growing hTERT-RPE1 cells were transfected with siRNA as described in chapter 4, before trypsinisation (section 1.2.1) and centrifugation for 5 minutes at 600 x g. 10,000 cells were cytospun per slide at 50 x g, high acceleration for 7 minutes (Cytospin 2, Thermo Fischer Scientific Inc, Waltham, MA, USA) and fixed in 100% cold acetone for 15 minutes at room temperature. Cells were then washed twice for 15 minutes in PBS before permeabilisation with fresh 0.2% Triton X-100 in PBS (PBST). Cells were washed twice as before and blocked overnight at 4°C in 5% BSA in PBST in a Copland jar. Cells were then probed with primary anti-topoisomerase IIα rabbit polyclonal antibody at a dilution of 1:500 (Abcam, Cambridge, UK) in fresh 5% BSA/PBST in a moisture chamber for 1 hour at room temperature before being washed as before. Cells were further incubated in 1:160 dilution of anti-rabbit IgG-Cy3-conjugated secondary goat antibody (Abcam) in a moisture chamber for 1 hour at room temperature and in the dark. Slides were washed twice in PBS and finally 12 μl DAPI/Vectashield was added and slides were mounted, sealed with nail varnish and kept overnight in the dark at 4°C until ready the next day for observation at x63 magnification under a fluorescent microscope (Zeiss Axioskop, Welwyn Garden City, Hertfordshire, UK).

2.11 Polymerase chain reaction (PCR)

2.11.1 RNA extraction

RNA was extracted from exponentially growing hTERT-RPE1 cells according to the protocol accompanying the RNeasy mini kit (Qiagen, Crawley, UK). Briefly, 350 μl RLT lysis buffer, which contained guanidine salts at a high concentration (molar range) that denature proteins, was added to 5 x 10^5 cells. Cells were then homogenised to reduce lysate viscosity by shearing high molecular weight genomic DNA and cellular components with a 21-gauge needle (5-10 times) and mixed with 350 μl 70% ethanol. Samples were then transferred to a silica column in a 2 ml collecting tube to allow the RNA to bind to the column, and spun for 15 seconds at 8000 x g using a bench top centrifuge (centrifuge 5414D: Eppendorf, Hamburg, Germany). The flow-through was discarded and the column washed with 700 μl RW1 buffer that also contained guanidine salts. The column was then washed twice in RPE buffer containing 95% ethanol to remove salts and spun dry to ensure no liquid remained. The column was finally placed in a new 1.5 ml eppendorf tube with the lid cut off so that the eppendorfs could be placed in the bench top centrifuge. It was ensured that the lids were kept sterile. 30 μl sterile water was added to the column and after a spin for 1 minute, RNA was eluted. Samples were kept on ice to be used immediately to make complement DNA (cDNA) and the rest stored at -80°C.

2.11.2 cDNA conversion

cDNA was made following the protocol of Quantitect Reverse Transcription kit (Qiagen). Briefly, 2 μl of 7x genomic DNA wipe-out buffer, containing DNase, was added to 12 μl template RNA and left to incubate for 2 minutes at 42°C. These were then placed on ice for no longer than 10 minutes whilst the remaining solutions were prepared. 1 μl quantiscript reverse transcriptase (RT), which contained RT as well as RNase inhibitors, was added to 4 μl of 5x RT buffer, which contained deoxynucleoside triphosphates (dNTPs), 1 μl RT random primer mix and finally the 14 μl of RNA mentioned above. These were left for 15 minutes at 42°C on a PCR machine (Techgene, Techne, Cambridge, UK), before being heated at 95°C for 3 minutes to inactivate DNase and RT, and stored at -20°C. cDNA concentrations were quantified by adding 1 μl to the Nanovue spectrophotometer (Nanovue 4282 V1.7.3, GE Healthcare, Little Chalfont, UK).

2.11.3 PCR

Approximately 1 μg of cDNA was added to each polymerase chain reaction (PCR). Other components of the reaction were added as recommended by the Readymix Taq PCR kit (Sigma): 12.5 μl buffer, containing the thermostable Taq DNA polymerase from *Thermus aquaticus* and dNTPs, 11 μl dH_2O, 0.5 μl cDNA and 0.5 μl forward and reverse primers (0.5 μl of 10 μM stock per reaction; VH Bio). The primer sequences were as follows:

- Topo IIα forward primer: '5-GCGTGTTGAGCCTGAATG-3'
- Topo IIα reverse primer: '5-GGTCTTAGGTGGACTAGC-3'

- β-actin forward primer: '5-ACCCCGTGCTGCTGACC-3'
- β-actin reverse primer: '5-AGGAAGGAAGGCTGGAAGAGT-3'

Primer sequences were taken from the literature [152,284]. PCR was performed on a Techgene Thermocycler using the following conditions:

- Preheat lid to 110°C
- Initialise: 95°C for 3 minutes
- Cycle of 35 repeats
    - Denature: 94°C for 30 seconds
    - Anneal: 52°C for 30 seconds
    - Extend: 72°C for 1 minute
- Final extension: 72°C for 10 minutes.

PCR products were stored at -20°C.

2.11.4 Agarose gel

4 μl of PCR sample was loaded onto a 2% agarose gel in 175 ml TAE containing 1 μg/ml ethidium bromide buffered with TAE. 1 μl 5x DNA loading buffer blue (Bioline, London, UK) was added to each sample. 4 μl marker (Quickload 100 base pairs DNA ladder, New England Biolabs) plus 1 μl loading buffer was also run on each gel. The gel was run at 110 V (7.3 V/cm) for 1 hour and quantified by ethidium bromide fluorescence, analysed using Syngene Genetools software.

2.11.5 Sequencing

PCR products were purified (Wizard SV gel and PCR cleanup system: Promega, Southampton, UK) by adding an equal volume of membrane binding solution to the sample and adding it to a column. This was then incubated for 1 minute, spun at 16,000 x g for 1 minute, washed with 700 μl membrane wash solution containing ethanol and washed again with 500 μl membrane wash solution. The column was then transferred to a clean 1.5 ml eppendorf tube and after 50 μl nuclease-free water was added, columns were spun for 1 minute as before to elute the product and samples were stored at -20°C. The amount of DNA present in PCR products was quantified by running the samples alongside a DNA marker (Hyperladder I, Bioline) of which the quantity of DNA (ng/band) was known.

3-10 ng of PCR products in 15 μl sterile water, alongside corresponding forward and reverse primers (each 3.2 μM) was sent to be sequenced at the Sequencing Service, University of Dundee, using Applied Biosystems Big-Dye Ver3.1 chemistry on an Applied Systems Model 3730 automated capillary DNA Sequencer.

2.12 Topoisomerase II activity assay

Decatenation of kDNA minicircles from the parasite *Crithidia fasciculata* was performed according to the protocol suggested by TopoGEN, Inc. (distributed by Axorra, Nottingham, UK). Briefly, fresh 5x complete assay buffer was prepared by mixing buffer A (0.5 M Tris/ hydrogen chloride (HCl) pH8, 1.5 M sodium chloride (NaCl), 100 mM magnesium chloride ($MgCl_2$) and 5 mM DTT) with an equal volume of buffer B (20 mM ATP in water). This assay buffer was then diluted 1:5 with water to make 20 μl 1x assay buffer per sample. 0.2 μg kDNA was then added and the solution was incubated at 37°C for 30 minutes. 4 μl stop buffer/loading dye (5% Sarkosyl, 0.125% bromophenol blue and 25% glycerol) and 1.8 μg proteinase K (Sigma) was added before further incubation for 30 minutes at 37°C.

The total volume of the assay sample was loaded on to a 1% agarose gel in 175 ml TAE containing 1 μg/ml ethidium bromide buffered with TAE. 3 μl decatenated and linearised

kDNA markers (TopoGEN Inc.) were also loaded alongside the sample. The gel was run at 110 V (7.3 V/cm) for 1 hour and quantified by ethidium bromide fluorescence, analysed using Syngene Genetools software.

2.13 Single cell gel electrophoresis (SCGE, comet) assay

hTERT-RPE1 cells were seeded at 2 x 10^5 cells per T25 flask and allowed to grow for 24 hours. 300 μl 1% agarose in TAE was added to fully frosted microscope slides (Surgipath, Richmond, Illinois, USA) and covered with a 22 x 50 mm coverslip (VWR), to ensure equal spreading of the agarose across the slide. Once the agarose was set, coverslips were removed and cells were trypsinised (section 2.1.2) and spun at 600 x g to pellet cells. Meanwhile cells were counted (section 2.1.3) to ensure that 5000 cells were added to each slide. Cells were resuspended in 75 μl of 0.75% LMP agarose in PBS, which had been retained at 37°C for at least 30 minutes. As soon as the LMP agarose was added, the mixture was spread onto the first agarose layer on the slide with another 22 x 50 coverslip. Again, once the agarose was set the coverslip was removed. Cells were treated with hydrogen peroxide at 0.1 – 10 nM and then immersed in freshly prepared neutral lysing solution (2.5 M lithium chloride (LiCl) (Sigma), 10 mM Tris, 0.03 M EDTA, 0.1% lithium dodecyl sulphate (LiDS) (Sigma), 0.03 mg/ml proteinase K, pH 8.0 dissolved at 37°C) overnight at 37°C. Slides were kept in fresh cold alkaline lysing solution (2.5 M NaCl, 100 mM EDTA, 10 mM Tris, 1% triton X-100, pH10) at 4°C for 1 hour. Slides were then removed, dabbed dry and added to a horizontal electrophoresis tank side by side. The tank was filled with electrophoresis buffer (0.3 M sodium hydroxide (NaOH), 1 mM EDTA, pH>13) to cover the slides and left for 40 minutes to allow the DNA to unwind. Slides were then electrophoresed for 20 minutes at 26 V, with the buffer volume altered to maintain a constant current at 275 - 300 mA. Slides were then drained and washed 3 times in neutralisation buffer (0.4 M Tris, pH8.5) for 5 minutes each and washed once in PBS for 5 minutes. Slides were then drained and allowed to dry in air. 40 μl of 2 μg/ml propidium iodide in PBS was added to the slides and spread with a 22 x 22 mm coverslip (VWR). Slides were kept in a moisture chamber in the dark for 2 hours before analysis.

Pictures of comets were taken at x10 magnification using a fluorescent microscope (Zeiss Axioplan2). It was ensured that the head of the comet was to the left of the tail so that the analysis program Comet Assay IV (Perceptive Instruments, Suffolk, UK) could recognise the comet and the percentage of DNA in the head (cell nucleus) and tail of the comet could be analysed by densitometry. An example comet analysed by Comet Assay IV is shown below (Figure 2.1).

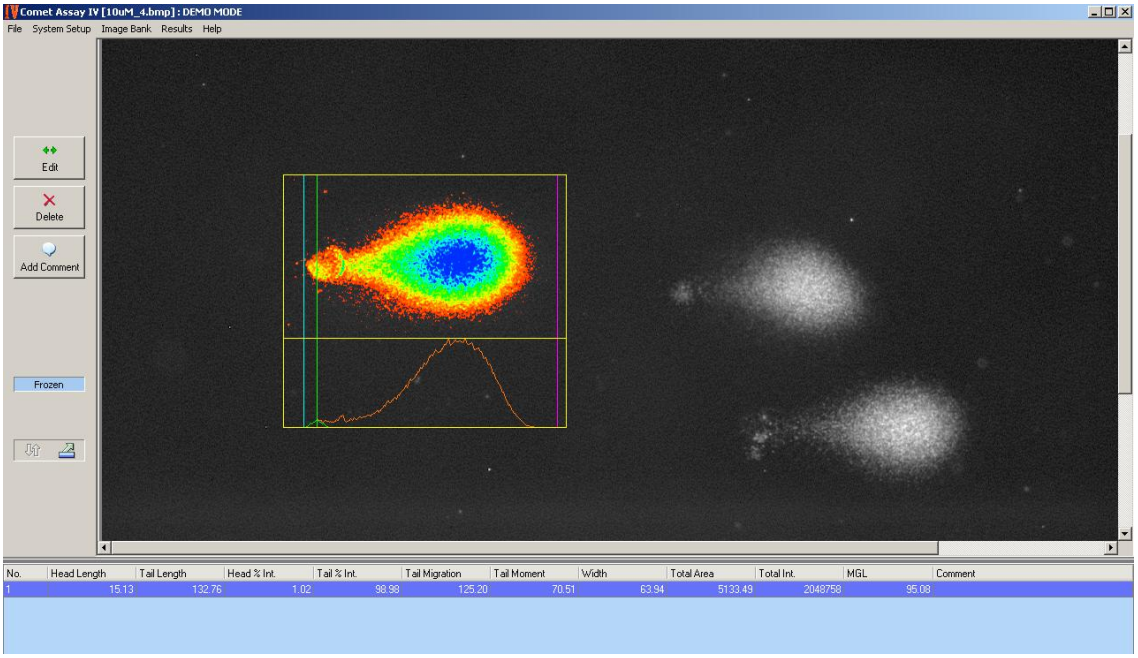

Figure 2.1: An example of a comet analysed by Comet Assay IV. The blue line represents the start of the head, the green line is the middle of the head and the purple line is the end of the tail.

Analysis was done for 50 comets per experiment and the tail moment was used to define DNA damage. The tail moment takes into account both the migration of the genetic material and the relative amount of the DNA in the tail.

CHAPTER 3

LOWER TOPO IIα LEVEL AND ACTIVITY AFFECTS CHROMATID BREAK FREQUENCY IN HUMAN CELL VARIANTS

3.1 Introduction

To determine if human topoisomerase IIα has a role in forming chromatid breaks, I first used cell lines that intrinsically show lower topo IIα levels. The parental **H**uman promyelocytic **L**eukemia cell line **HL**60 was originally derived from a 36-year old woman with acute promyelocytic leukaemia at the National Cancer Institute [285,286]. Myeloid cells are defined as leukocytes that are not lymphocytes (B- and T-cells) and the promyelocytic HL60 cells can be induced to differentiate into predominantly neutrophils with a small proportion of monocytes [285]. HL60 cells are tumorigenic and express the oncogene c-myc (cell line information provided by the ATCC), which activates telomerase [287]. C-myc is a well-known oncogene that increases cell proliferation through its activity as a transcription factor [288]. Telomerase is another protein often expressed at a higher level in cancer cells. It increases telomere length by adding TTAGGG to the 3' end of DNA strands through its reverse transcriptase activity on a RNA template [289]. Usually cells that divide without telomerase lose some telomeric sequences and when telomeres get to a critical length DNA replication can no longer occur. Due to its ability to increase telomere length and thus extend cellular lifespan [289] telomerase is often inserted into cells to produce immortalised cell lines.

HL60 cells were used by Harker *et al*. (1989) to create cell lines that were resistant to mitoxantrone (MX). MX is a known topo II poison and the MX1 and MX2 variant cell lines were produced as follows [290]. Briefly, HL60 cells were exposed to the drug for 3 days followed by a 3-7 day period of growth in the absence of MX. After 21 passages in gradually increasing concentrations of MX, a cell population, named HL60/MX1, emerged that could grow continuously in the presence of MX at a concentration of 3.9×10^{-8} M. Further exposure to the drug at successively higher concentrations led to the emergence of cells capable of growing at 1.9×10^{-7} M MX, named HL60/MX2 cells. Resistance to the drug is associated with decreased general topo II activity as well as lower topo IIα and β expression levels [154]. As explained in section 1.5.4 I have focussed on the isoform topo IIα mainly due to its role in DNA decatenation.

3.2 Aims

The aim was to verify whether lower topo IIα expression and total cellular activity levels were actually found in the MX1 and MX2 variant cell lines when compared to parental HL60 cells. Also, I aimed to determine whether the drug-resistant variants MX1 and MX2 showed lower radiation-induced chromatid break frequency and whether the lower frequencies of chromatid breaks correlated with topo II expression and/or activity.

3.3 Measurement of topo IIα expression in HL60 and variant cell lines

Procedure

HL60, MX1 and MX2 cells were grown to a high density (1 x 10^6 cells per ml) in suspension culture, cell lysates were prepared (section 2.2) and the protein concentration within these lysates quantified as described in section 2.3. Immunoblotting experiments were carried out as described in section 2.4. The data was normalised against β-actin and HL60 values were equalled to 100%. Experiments were carried out in triplicate.

Results and discussion

The relative levels of topo IIα expression in exponentially growing HL60, MX1 and MX2 cells were determined by quantitative western blotting. Figures 3.1A and B show that MX1 and MX2 cells have lowered topo IIα expression compared to HL60 cells. Protein loading was similar in comparative samples as shown by β-actin expression in Figure 3.1A. It is clear that the antibodies are specific to either topo IIα or β-actin as the corresponding bands align with the marker at their known molecular weight, namely 170 kDa and 42 kDa respectively. Although the topo IIα band in a western blot is located just above the 175 kDa marker band, it is certain that this band represents the 170 kDa protein as when purified topo IIα was added to the gel, the band occurred at exactly the same molecular weight (data not shown). Data was normalised against β-actin, although β-actin levels were similar in all cell lines, to ensure that slight changes in topo IIα expression were not a result of slightly altered protein loading within the different lanes. Following quantification by densitometry, topo IIα values obtained for HL60 were set at 100% and topo IIα values in MX1 and MX2 cells expressed as a percentage of this HL60 value. This extra normalisation step was imposed as triplicate experiments were not carried out on the same gel or membrane and values even within the HL60 cell line varied slightly after normalisation against β-actin. These different values, as visualised in Figure 3.1A as topo IIα bands in HL60 cells of different intensities, are most likely due to slight differences in antibody or blocking agent concentrations or exposure time. Increased concentrations of blocking agents alone or combined with decreased concentrations of antibodies would decrease band intensity. Also, the development of the film was done manually and the developer and fix were not always used fresh, which might have affected band intensities between experiments too.

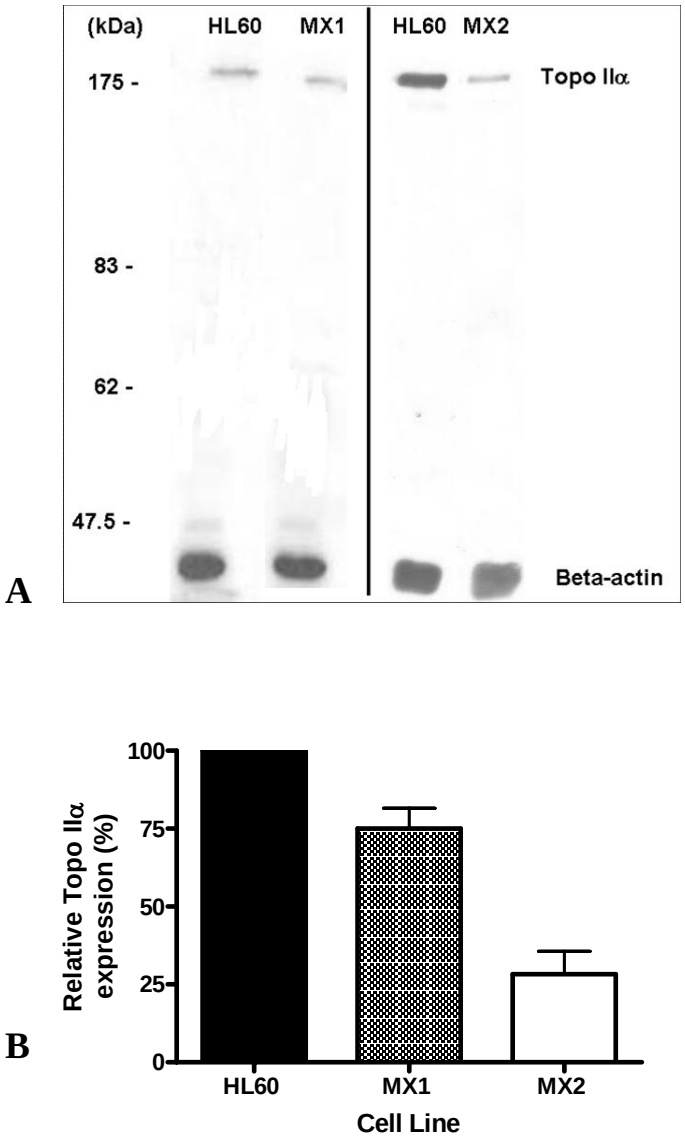

Figure 3.1: A: Whole cell lysate probed against topo IIα and β-actin showing lower topo IIα expression in MX1 and MX2 cells when compared to HL60 cells. β-actin acts to control for protein loading. To the left the molecular weights (kDa) of the marker are shown. **B:** Analysis through densitometry of western blot data probed against topo IIα and normalised against β-actin levels that represent protein loading. The data was also normalised against HL60 values. Bars represent standard errors of the mean from triplicate experiments.

Analysis of the immunoblotting data (Figure 3.1B) by densitometry confirmed that topo IIα levels are lower in MX1 and MX2 cells when compared to the parental HL60 line, with MX2 cells showing the lowest expression of topo IIα. More specifically, MX1 and MX2 cells expressed on average 25% and 72% less topo IIα than HL60 cells respectively. This verifies previous findings by Harker *et al*. who stated that MX2 cells have lowered topo IIα expression levels, which explained the increased mitoxantrone resistance found in these cells when compared to the parental HL60 lines [155]. Harker *et al*. (1995) determined through western blotting that topo IIα expression was 40% lower in nuclear extracts of MX2 cells when

compared to HL60 cells; they did not determine topo IIα expression in MX1 cells [155]. This decrease in MX2 topo IIα value is less than the decrease of 72% found here. This is most likely down to their use of nuclear extracts, whereas data here was produced only for whole cell lysates. Other factors might be the use of different antibodies or the different amount of protein loaded in each well. Harker *et al*. added 100 μg of protein per well, whereas my experiments incorporated only approximately 10 μg of protein per well.

3.4 Measurement of total topo II activity as measured by mAMSA-induced G_2 block in HL60 and variant cell lines

Procedure

Amsacrine hydrochloride, also known as mAMSA, was used to indirectly estimate topo II activity. mAMSA is a topo II poison that induces DSBs, which in turn elicits a G_2 block. Therefore an increase in mAMSA concentration should increase the number of DSBs and consequently decrease the number of cells in mitosis. It is assumed that this effect is dependent on cellular topo II activity as topo II is the only known target protein of mAMSA. Exponentially growing HL60, MX1 and MX2 cells (1×10^6) were incubated with mAMSA (Sigma, stock in 30% ethanol), ranging from 0 to 20 μM for 30 minutes at 37°C. Cells were centrifuged and washed in growth medium before being resuspended and incubated in growth medium with or without colcemid (Gibco) at 0.15 μg/ml for 2 hours at 37°C and further washed in medium by centrifugation. Mitotic indices were calculated by flow cytometry as described under section 2.5.1 for 1×10^4 cells. The mitotic index at 0 μM amsacrine was set at 100% for each cell line. The total change in mitotic indices of MX1 and MX2 cells were normalised against HL60 change in mitotic index.

Results and discussion

In addition to establishing topo IIα expression levels in HL60, MX1 and MX2 cells, it was also important to establish topo II activity. As it is impossible to distinguish between topo IIα and β activity within the cell without purifying them separately, the total enzyme activity was calculated. The ability of mAMSA to decrease the number of cells in mitosis, presumably through causing double strand breaks [230,231,291] and arresting cells in G_2, was measured. Topo II activity was assumed to be the cause of this mAMSA-induced G_2 block as this drug has not been shown to affect any other protein. Therefore, any difference in mAMSA-induced mitotic index between HL60, MX1 and MX2 cells can be related back to a difference in topo II activity.

Firstly, the combination of an antibody against phosphohistone 3, as a marker for mitotic cells, and a dye against DNA was tested. Flow cytometry is a useful, high throughput tool for detecting proteins and determining normal cell cycle distribution. Propidium iodide is used

here to label DNA. As it can bind both DNA and RNA, cells were treated with ribonuclease A prior to data acquisition to rid the cells of RNA and ensure only DNA content was measured [292]. Here I used propidium iodide (PI) alongside an Alexa-conjugated antibody against phosphohistone 3 to determine the mitotic index. If cells are labelled with PI alone, then cells in G_1, S and G_2/M could only be distinguished according to their DNA content. G_1 cells peak with a DNA content of 1x, G_2/M cells would peak at 2x the DNA content and S phase cells would be located in between the two peaks as DNA synthesis has yet to be completed. Because PI binds DNA indescriminately, it cannot distinguish between cells in G_2 or mitosis as both have the same DNA content. It is therefore essential to use a marker of mitosis, such as histone 3, which is phosphorylated at serine 10 during mitosis [293]. Figure 3.2 shows that this protocol combining PI and an antibody against phosphohistone 3 is a good way of determining mitotic index; with the addition of colcemid, the mitotic index increased from 2% to 4% [80]. As colcemid blocks cells in mitosis, they cannot proceed to G_1 and therefore the mitotic index would be expected to increase.

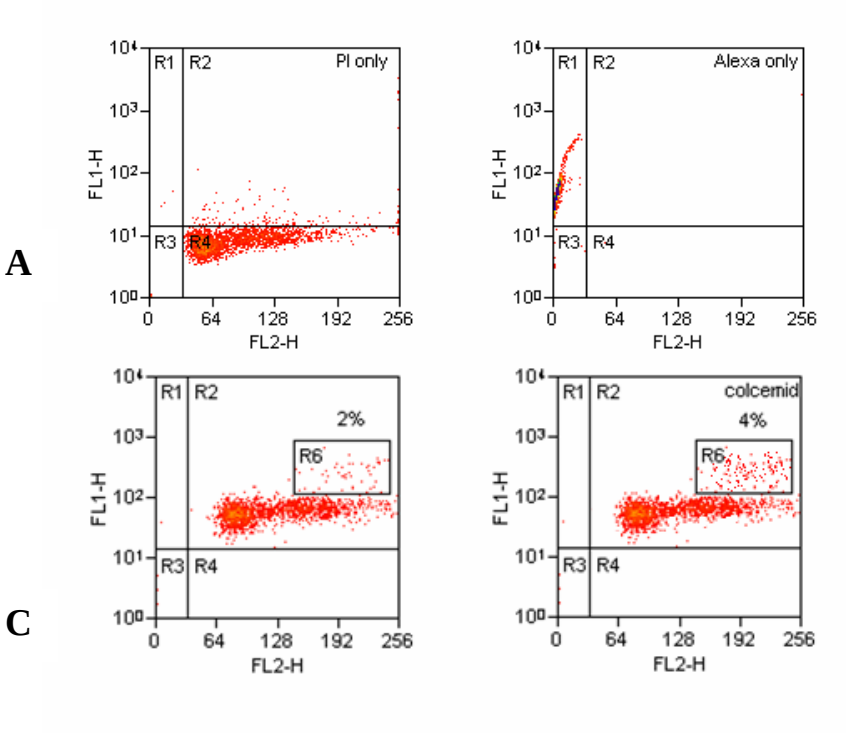

Figure 3.2: Flow cytometric analysis of non-treated (Panels A-C) or colcemid-treated (Panel D) HL60 cells. Cells were labelled with propidium iodide (PI) (FL2-H) and an Alexa-conjugated antibody against phosphohistone 3 (FL1-H), a marker of mitosis. Panels A and B are controls with single labelling with either PI (A) or anti-phosphohistone 3 (B). Panel C shows a mitotic index of 2% which increases to 4% if colcemid is added for two hours (D).

Topo II activity is usually measured through the kinetoplast DNA assay that assesses the ability of topo II to decatenate many DNA minicircles resulting in non-tangled minicircles which can be visualised by gel electrophoresis [294]. As I was unable to purify topo II from HL60 and variant cells, other ways of measuring topo II activity were explored. The assay presented here is based on the ability of mAMSA to 'poison' topo II. As amsacrine targets both topo IIα and β equally [225], activity cannot be attributed to one particular isoform. Therefore this assay only estimates total topo II activity. Amsacrine prevents the religation of the G-segment by topo II which then results in DSBs [291]. As the G_2 checkpoint is sensitive to DNA damage, amsacrine treatment halts cells in G_2 without allowing them to proceed to mitosis. Hence the higher the topo II activity is in a cell, the more DSBs will form following treatment with amsacrine and the higher the proportion of cells are found in G_2 and consequently the lower the mitotic index. Figure 3.3A shows that an increase in amsacrine concentration decreases the mitotic index until it reaches a plateau. What is important in this graph is the difference between initial values at 0 μM mAMSA and the percentage of cells in mitosis at which the response plateaus. This plateau suggests that at high amsacrine concentrations, inhibition of topo II activity is saturated and therefore the total decrease of mitotic index must be representative of total cellular topo II activity; hence the higher cellular topo II activity, the larger the difference. Figure 3.3A shows that the mitotic index decreases most in HL60 cells (96%), less in MX1 cells (77%) and least in MX2 cells (55%). These values were calculated as the difference between the mitotic index at 0 and 20 μM mAMSA. This implies that amsacrine causes less DSBs in MX1 and MX2 cells than in HL60 cells, most likely due to less topo II activity.

Harker *et al*. [154] previously determined total cellular topo II activity in HL60 and MX2 cells with the kinetoplast DNA decatenation assay and found that topo II purified from nuclear extracts was on average four times (75%) less active in MX2 cells when compared to HL60 cells. They also found that total cellular topo II activity, i.e. including both nuclear and cytosolic fractions, was decreased by 50% in MX2 cells [154,155]. These topo II activity values determined by Harker *et al*. differ from the data presented here. My assumption that the difference in mitotic index caused by mAMSA in HL60 and MX2 cells was due to altered topo II activity is therefore not completely valid as according to this method, topo II activity is only 57% less in MX2 cells when compared to HL60 cells (100%) (Figure 3.3). Harker *et al*. on the other hand had determined topo II activity to be decreased by 75% in MX2 cells for nuclear fractions. One reason for this discrepancy might be that not every single topo II-induced DSB is recognised as DNA damage. A signalling cascade that would normally result in a G_2 block might therefore not be induced. Perhaps a threshold of DNA damage is required to induce this G_2 block and therefore any values obtained through this mAMSA-induced G_2 block, which is then assumed to be equal to topo II activity, would be an underestimation. The reason I compared my values only to nuclear, and not total cellular topo II activity values obtained by Harker *et al*. is because of the nature of the kinetoplast DNA assay. This assay involves adding purified topo

II to catenated DNA. Therefore any cytoplasmic topo II if active would still decatenate the DNA, however this would not reflect the situation *in vivo* where topo II is not associated with DNA in the cytoplasm. I therefore do not believe that I should compare my results to total cellular topo II activity values as the data obtained from the mAMSA-induced G_2 block assay would not incorporate cytosolic topo II activity. Just because topo II is present and active in the cytosol, does not mean it would induce DSBs as it would not be located near the DNA.

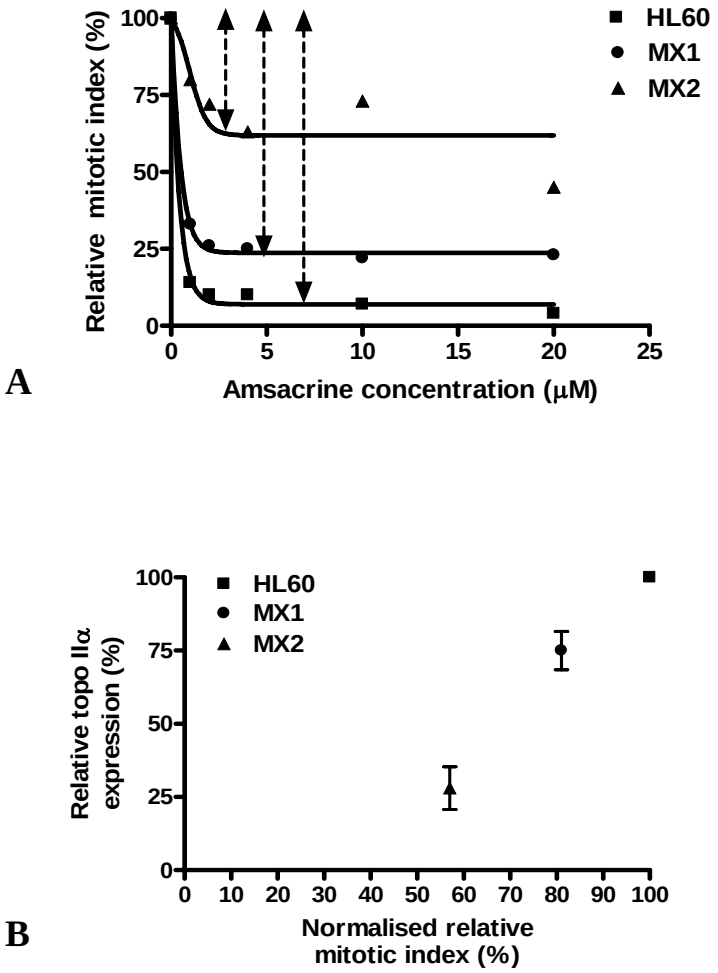

Figure 3.3A: Flow cytometric analysis of HL60, MX1 and MX2 cells treated with varying concentrations of mAMSA up to 20 μM. All cells were incubated with colcemid. Each data point represents the mean of 1 x 10^4 cells within one experiment. The mitotic index was measured through labelling of cells with propidium iodide and an Alexa-conjugated antibody against phosphohistone 3, a marker of mitosis. The mitotic index at 0 μM amsacrine was equalled to 100% for each cell line. The dashed arrows refer to the difference in mitotic index caused by mAMSA. **B**: Total difference in mitotic index (determined from Figure 3.3A) for HL60, MX1 and MX2 cells plotted against relative topo IIα expression (Figure 3.1B) showing a positive correlation. The relative mitotic indices were normalised against HL60 total change in mitotic index.

Although topo II activity was only determined within a single experiment, it does correlate well with topo IIα expression as determined by immunoblotting (Figure 3.3B). The mitotic index values are based on the values obtained from Figure 3.3A where the 96% decrease in mitotic index found in HL60 cells was equalled to 100%. This makes the decrease in mitotic index found in MX1 and MX2 cells at 20 μM mAMSA 80% and 57% respectively when compared to the decrease in mitotic index found in HL60 cells. The correlation between topo II activity as measured by mAMSA-induced G_2 block and western blot-determined topo IIα levels suggests that topo IIα is a good indicator of total cellular topo II activity and that it is in fact the dominant isoform. Also it confirms that MX1 and MX2 cells do show less topo II activity when compared to HL60 cells as previously suggested by Harker *et al*.

3.5 Chromatid break analysis

Procedure

Exponentially growing HL60, MX1 and MX2 cells were prepared for chromatid break analysis following the protocol found in section 2.6. More specifically, cells were irradiated at 0.4 Gy and alongside unirradiated controls incubated for 30 minutes at 37°C, 5% CO_2 in air before the addition of colcemid at 0.1 μg for 1.5 hours. Metaphase spreads were prepared on slides using a humidity control cabinet (Hanabi system) where 20 μl of sample was added to each slide. Slides were further stained in 50 ml Copland jars with 10% Giemsa in Gurr's buffer for 10 minutes, washed in Gurr's buffer followed by distilled water and allowed to dry in air. Experiments were carried out in duplicate.

Results and discussion

The 'G_2 assay' is a useful way to determine chromatid break frequency. It is called the G_2 assay as it is assumed that if the time between irradiation and fixation is short, metaphases were originally irradiated cells in the G_2 phase of the cell cycle. Chromatid breaks, as seen in Figure 3.4 can be seen not only after cells have been irradiated with low doses of ionising radiation; they can also occur at very low levels spontaneously. In this thesis chromatid breaks were defined as any type of discontinuity, including chromatid 'gaps', where discontinuities are smaller than the width of the chromatid, and 'breaks' where aligned or misaligned discontinuities are the width of the chromatid or larger [65].

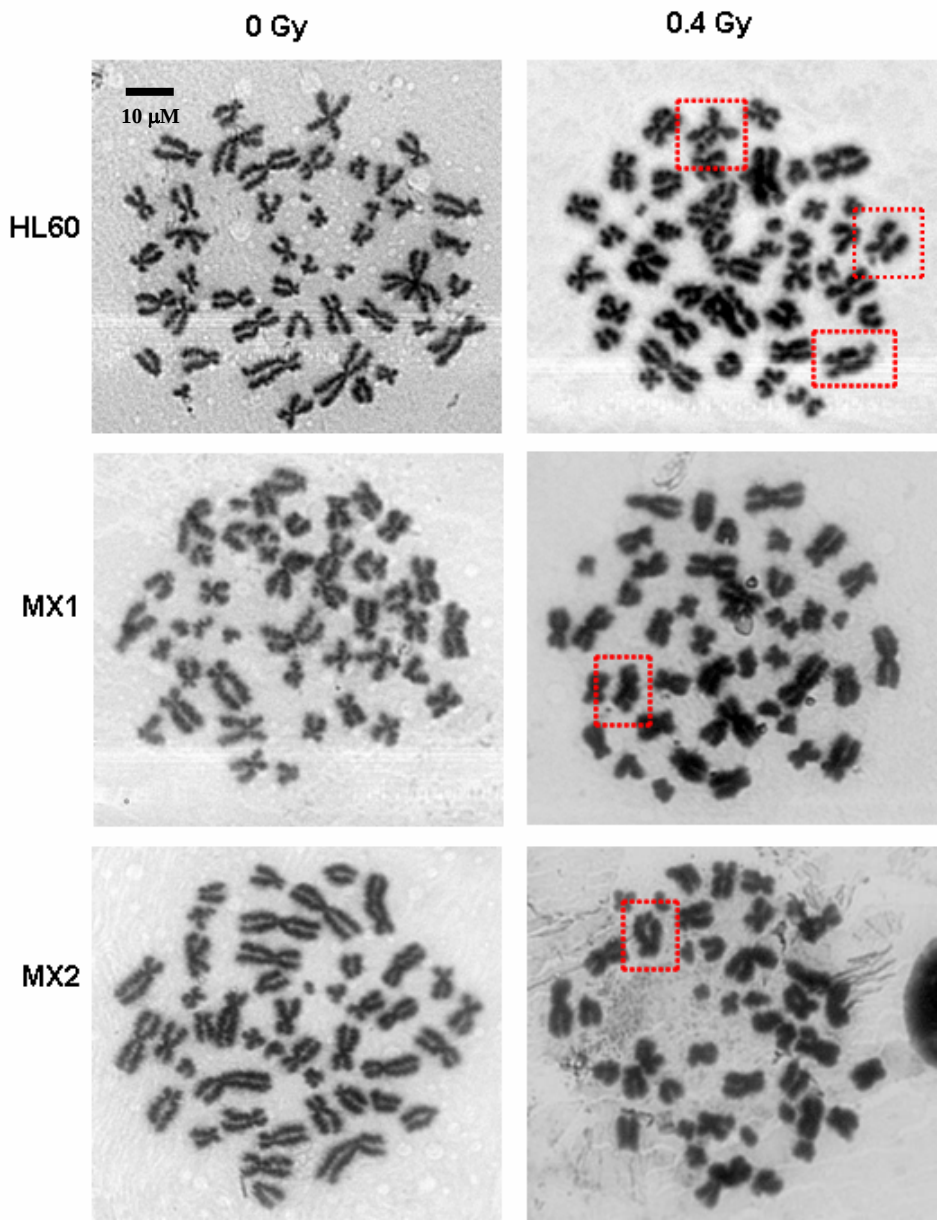

Figure 3.4: Metaphase spreads of control and irradiated (0.4 Gy γ-rays) Giemsa-stained HL60, MX1 and MX2 cells at x100 magnified. The red boxes surround chromosomes with chromatid breaks. Scale bar represents 10 μm.

The number of chromatid breaks formed in both control and irradiated cells (0.4 Gy) were calculated per 100 metaphases. Figure 3.5 shows that in all three cell lines, little (<0.2 breaks/cell) or no chromatid breaks were formed in non-irradiated controls. When irradiated at 0.4 Gy, all cell lines showed an increase in chromatid break frequency as expected. However, the chromatid break frequency in HL60 cells (1.1 breaks per metaphase) was significantly higher than in MX1 (0.8 breaks per metaphase) and MX2 cells with MX2 cells showing the lowest number of chromatid breaks (0.6 breaks per metaphase) with p=0.004 and 0.003 for MX1 and MX2 cells respectively. The p-value is defined here as the probability of obtaining

the results assuming the null hypothesis is correct. Here the significance level is taken as 5% (0.05) so any p-value obtained below 0.05 is statistically significant.

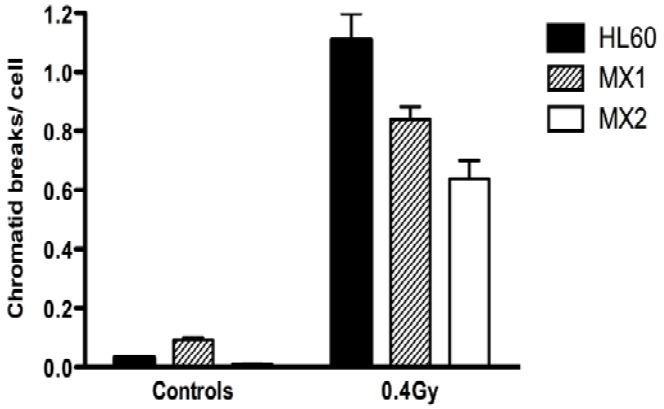

Figure 3.5: Chromatid break frequency per metaphase in control and irradiated (0.4 Gy γ-rays) HL60, MX1 and MX2 cells. Bars refer to standard deviations from the mean calculated for 100 cells per duplicate experiment.

As cells have been incubated with colcemid, it could be postulated that the chromatid breaks result from colcemid incubation rather than irradiation. It has previously been determined that colcemid treatment increases the frequency of chromosome abnormalities; however, these experiments included 5 and 17 hour incubation periods [295]. Here, colcemid was added only for 1.5 hours and therefore the effect on chromatid break frequency in itself is quite low or absent as seen in the non-irradiated controls of Figure 3.5. Although it might seem simpler to forego colcemid treatment, it is necessary to acquire sufficient numbers of metaphases to be able to measure chromatid break numbers in at least 100 cells, as not all metaphases spread well. Also the addition of colcemid has proven to aid condensation and spreading, although the mechanism behind this is still unclear. The more condensed the chromosomes (up to a point), the easier chromatid breaks can be distinguished.

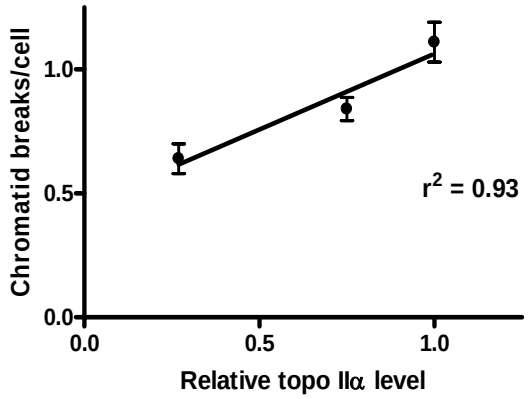

Figure 3.6: Topo IIα expression as measured by western blotting (Figure 3.1B) correlates positively with chromatid break number per cell (Figure 3.5).

Figure 3.6 was plotted to determine if chromatid break frequency (Figure 3.5) and topo IIα expression (Figure 3.1B) correlated. A significant positive correlation ($r^2 = 0.93$) shows that as topo IIα expression increases, so does chromatid break frequency. As topo IIα expression and activity are correlated (Figure 3.3B) this suggests that topo IIα activity is indeed involved in the formation of chromatid breaks. Whether or not this connection is direct is unclear from this data and remains to be determined.

3.6 Is reduced chromatid break frequency a result of less DSB repair?

Procedure

DNA DSB repair was measured in HL60, MX1 and MX2 cells as described under section 2.7.2 by Dr Peter Bryant. Cells were passaged at 2 x 10^5 per ml in RPMI medium and incubated for 2 days. 6 x 10^5 cells were transferred to 1.5 ml eppendorf tubes and cooled on ice for 30 minutes prior to irradiation. Tubes were irradiated on ice with 40 Gy of ^{137}Cs gamma-rays. The dose-rate was approximately 3.5 Gy/minute. Unirradiated controls and time zero samples were held on ice while the other samples were transferred to a water-bath running at 37^{o}C from 15 minutes up to 3 hours. After 3 hours incubation on ice or at 37^{o}C, all samples were treated as described in section 2.7.2. Samples were run in a 200 ml 0.8% agarose gel in 0.5 tris borate EDTA (TBE) buffer (Sigma) containing 0.5 μg/ml ethidium bromide. All DNA double strand break repair experiments were performed in duplicate, as well as duplicates within experiments.

Results and discussion

In some cases altered DNA repair is thought to be the cause of increased DNA damage [94,95]. Although it was previously discussed that radiosensitivity in the form of chromatid break induction might not be due to altered DNA repair, it was nonetheless important to check that the higher chromatid break frequency found in HL60 cells was not due to decreased DSB repair. DSB repair was determined by pulsed field gel electrophoresis, where the direction of the pulse changes regularly. This allows the DNA fragments caused by DSBs to be separated according to size [296]. As we were interested only in the number of DSBs caused under certain conditions, and not the size of the resulting DNA fragments, a simple, non-pulsed gel electrophoresis assay was performed by Dr P. Bryant. This technique still allows the DSBs to be separated, but it does not distinguish between different sizes of DNA, as DNA molecules larger than 15-20 kb migrate at the same rate through the gel in a size-independent manner.

To determine if HL60, MX1 and MX2 cells differ in DNA repair kinetics, irradiated cells were left to repair for up to 3 hours. Figure 3.7 shows that with time, the number of DSBs reduces, reaching a plateau at around 3 hours, implying that rejoining has been completed. The data shown in panel A does however suggest that DNA repair was not completely finished, though it would have been more conclusive had the fraction of DNA released (FDR) been measured at 4 hours. It appears that the kinetics of DSB repair is similar in HL60, MX1 and MX2 cells (Figure 3.7). Therefore altered DNA repair kinetics could not account for differences found in chromatid break frequency.

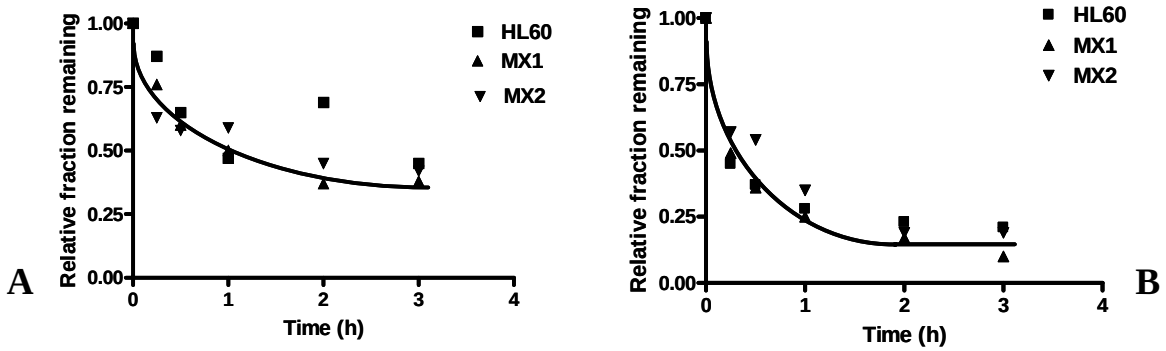

Figure 3.7: **A**: Analysis of gel electrophoresis showing a disappearance of the relative DNA fraction remaining with time in HL60, MX1 and MX2 cells. **B**: duplicate of experiment. Experiments carried out by Dr Peter Bryant.

When comparing the duplicate experiments shown in Figure 3.7, it is clear that the amount of DNA released at 3 hours is different between the two experiments, suggesting slower or less repair in cells from panel A. Although the reason for this is not apparent, it does not alter the conclusion that HL60, MX1 and MX2 cells do not differ in repair kinetics within each experiment.

3.7 Conclusion

Lower topo IIα expression and activity was seen in MX1 and MX2 cells when compared with parental HL60 cells. This correlated with decreased chromatid break frequency, which could not have been affected by altered DNA DSB repair.

CHAPTER 4

LOWERED TOPO IIα LEVELS AFFECT CHROMATID BREAK FREQUENCY

4.1 Introduction

In this chapter the effect of silencing topo IIα on the frequency of radiation-induced chromatid breaks in the **h**uman-**te**lomerase **r**everse **t**ranscriptase-transformed **r**etinal **p**igment **e**pithelial (hTERT-RPE1) cell line was examined.

Research using silencing RNA (siRNA) has soared since its optimisation by Fire *et al.* in the nematode *Caenorhabditis elegans* [297]. The authors showed that double-stranded RNA in the cell, produced through the introduction of a mix of sense and anti-sense RNAs specific to coding sequences, was more effective in interfering mRNA translation than single stranded anti-sense RNA. Experiments involving siRNA against topo IIα have confirmed many roles of topo IIα including condensation and chromosome arm localisation at the metaphase plate [169] as well as in apoptosis [173].

The siRNAs used here (purchased from Ambion) are chemically synthesised 21 nucleotide double-stranded RNA with 3' dinucleotide overhangs that are short enough to be incorporated in the RNA-induced silencing complex (RISC). This introduction of siRNAs exploits part of the RNA interference pathway that a cell uses to protect itself from viruses where long (>200 bp) double-stranded RNA species are cut to double-stranded RNA of 21-25 bp intervals with dinucleotide 3' overhangs by the RNase protein Dicer [298]. The siRNAs provided by Ambion mimic these small double-stranded RNAs already processed by Dicer and so go on to form part of the 'silencing complex'. One strand of the RNA is assembled into RISC whilst the other strand is cleaved by Argonaute (or Slicer) proteins thus allowing the target mRNA to bind the RISC-associated strand. RISC assembly involves Dicer bound to the protein R2D2 as a heterodimer guiding the siRNA to its target RNA. Dicer/R2D2 is then replaced by the endonuclease Argonaute slicer protein Ago2 and once the other single-stranded siRNA is dissociated from the siRNA/RNA complex [299], the RISC complex is activated and cleaves the mRNA [300], thus ultimately lowering protein expression.

4.2 Aims

The first aim was to determine the mitotic index response as well as the normal frequency of chromatid breaks in hTERT-RPE1 cells exposed to a low dose of radiation. The second aim was to investigate the effect of lowering topo IIα expression, by treatment with siRNA, on radiation-induced break frequency. The effect of siRNA treatment on mitotic index was also tested.

4.3 Measurement of radiation response of hTERT-RPE1 cells

The effect of radiation dose on mitotic index and chromatid break frequency was tested.

Procedure

The mitotic index for 1 x 10^4 cells was determined as described in section 2.5.1. hTERT-RPE1 cells were irradiated at 0.3, 0.4 and 0.5 Gy γ-rays. Results were normalised against the non-irradiated control with this latter value set at 100%. The number of cells in G_2 was also established through the same protocol. The number of cells in G_2 was determined as follows: (G_2/M) – M with G_2/M determined by flow cytometric analysis after staining with PI (Figure 4.1 Panel A), and M also determined by flow cytometry with an Alexa-conjugated anti-phosphohistone 3 antibody as well as PI (Figure 4.1 Panel B).

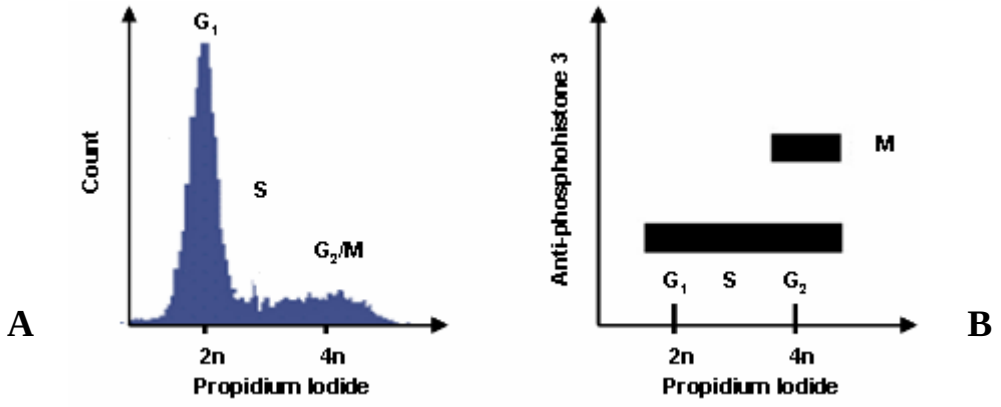

Figure 4.1 A: Representative diagram of cycling cells stained with propidium iodide. G_1, G_2/M and S phase cells can be clearly distinguished according to their DNA content (2n, 4n or in between respectively). **B**: Representative diagram of cycling cells stained with both propidium iodide and an Alexa-conjugated phosphohistone 3 antibody. Mitotic cells can now be visualised separately from G_2 cells.

Chromatid break frequency was also determined in exponentially growing hTERT-RPE1 cells. These were prepared following the protocol found in section 2.6. Briefly, cells were irradiated with a dose of 0.3 Gy and with parallel un-irradiated controls, incubated for 30 minutes at 37°C before the addition of colcemid at 0.1 μg/ml for 1.5 hours. Following fixation, metaphase spreads were prepared on slides, stained, washed, and dried in air. 100 metaphases were analysed for chromatid breaks.

Results and discussion

The effect of radiation on mitotic index was established using flow cytometry. The use of PI and anti-phosphohistone 3 labeling has already been described under section 3.4. Figure 4.2A shows that an increase in radiation dose decreases the number of cells in mitosis by 50%, 65% and 75% (Panel A) and increases the number of cells in G_2 by 8%, 17% and 32% (Panel B) at 0.3, 0.4 and 0.5 Gy respectively. This suggests that the decrease in mitotic index is due to cells being blocked at the G_2 checkpoint (section 1.3.2). It is thought that this G_2 block is necessary to allow cells to repair their DNA after 'injury' by, in this case, low doses of ionising radiation. If DNA damage repair systems are overwhelmed, cells will not progress to mitosis where damaged genetic material could be passed on to daughter cells, but instead cell checkpoints either hold cells back until repaired or signal cells to apoptose. Figure 4.2 shows that hTERT-RPE1 cells illustrate a normal reaction when treated with ionising radiation, with the mitotic index decreasing with radiation dose whilst the number of cells in G_2 increases. This result suggests that hTERT-RPE1 cells have a functional G_2 checkpoint.

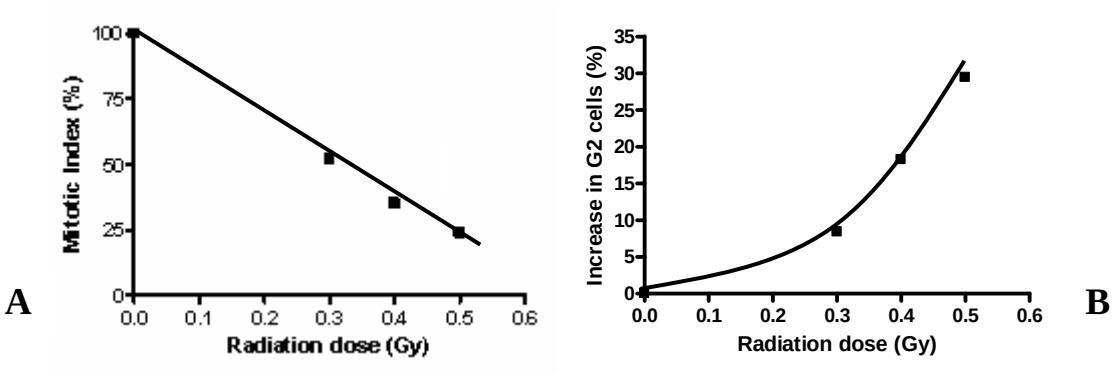

Figure 4.2: Flow cytometric analysis of hTERT-RPE1 cells irradiated with γ-rays ranging from 0.3 to 0.5 Gy. Each data point represents the mean of 1 x 10^4 cells. **A**: The mitotic index was measured through labelling of cells with PI and an Alexa-conjugated antibody against phosphohistone 3, a marker of mitosis. The mitotic index decreased with radiation dose. Results were normalised against non-irradiated controls. **B:** The number of cells in G_2 was calculated by deducting the number of cells in mitosis (determined from panel A) from the G_2/M value measured by labelling of cells with PI only.

Interestingly, the increase in G_2 cell number is non-linear over the range of 0 - 0.3 Gy (Figure 4.2B). This suggests that there is a threshold of DNA damage that is tolerated within hTERT-RPE1 cells and that if the DNA damage is increased beyond this threshold, the G_2 checkpoint is activated. The mitotic index on the other hand, does show a linear trend. Figure 4.2A shows that the mitotic index decreases with radiation dose and its linear relationship is most likely due to a low number of cells in mitosis distorting the actual trend between 0 – 0.3 Gy. Also, the 75% decrease in mitotic index seen in 0.5 Gy-irradiated cells compared to non-irradiated controls does not correspond with a 75% increase in G_2 population at 0.5 Gy, which only increased by 32%. This is most likely due to the same number of cells in mitosis representing a lower percentage of cells in G_2.

As well as looking into the effect of IR on mitotic index and number of cells in G_2, its effect on chromatid break frequency was also established. As the aim of this thesis was to look into the mechanism behind chromatid break formation, it was important to determine whether or not chromatid break induction in hTERT-RPE1 cells is linear with radiation dose as found for other types of cells [105,108,112]. The dose-effect relationship for chromatid breaks is shown in Figure 4.3 and it is clear that this relationship is linear as its R^2 value is 0.97. At 0.3, 0.4 and 0.5 Gy γ-irradiation cells averaged 0.81, 1.43 and 1.77 chromatid breaks per metaphase respectively..

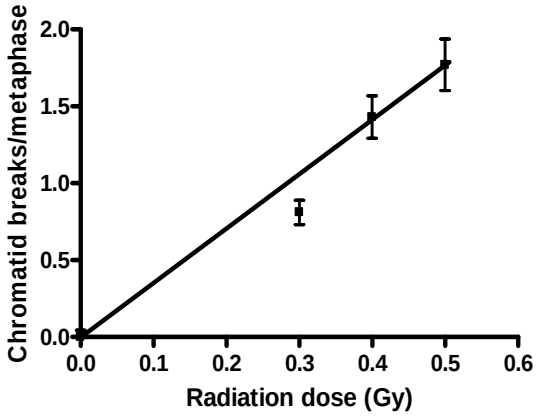

Figure 4.3: Frequency of chromatid breaks in Giemsa-stained hTERT-RPE1 metaphases treated with ^{137}Cs γ-rays at doses ranging from 0 to 0.5 Gy, as determined through the G_2 assay. Bars represent standard deviations from the mean for 100 metaphases.

4.4 Analysis of cells in the G_2 assay

I attempted to determine if when analysing metaphases for chromatid breaks as part of the G_2 assay a proportion of S-phase cells were included in the irradiated population.

Procedure

To do this, hTERT-RPE1 cells were synchronised in S-phase with a thymidine block following the protocol found under section 2.8. Samples were taken at 0, 1.5 and 2.5 hours after release from thymidine. After thymidine release samples were incubated in colcemid 0.1 μg/ml until they were harvested. A non-synchronised control was also collected at the zero time-point. The mitotic index was determined as described under section 2.5.1 for 1 x 10^4 cells per sample.

Mitotic indices of samples taken at 0, 1.5, 2.5 and 6 hours after release from thymidine were also established manually following the procedure in section 2.5.2. After thymidine release again samples were incubated in colcemid 0.1 μg/ml until they were harvested. The number of cells in mitosis was determined for 1000 cells per sample and counted at x10 magnification.

Results and discussion

It was important to determine if mitotic cells collected 1.5 – 2.5 hours after irradiation did actually acquire their original damage in the G_2 phase of the cell cycle, as hypothesised, rather than the early part of S-phase. Theoretically, if cells are in early S-phase when irradiated, metaphase spreads would show breaks in both chromatids whereas cells irradiated in late S-phase or G_2 would show breaks in only one chromatid. As breaks in only one chromatid are usually seen after 1.5 hours of irradiation, it is generally assumed that cells must have originally been in G_2 when irradiated. This was tested by synchronising cells in S-phase with excess thymidine and collecting cells at 0, 1.5 and 2.5 hours after release from thymidine, at which stage cells could progress through the cell cycle and the proportion of cells in S, G_2 and mitosis could be analysed. Excess thymidine blocks cells in S-phase as when it becomes phosphorylated to dTTP, it inhibits the reduction of CDP by ribonucleotide reductase to dCDP [301]. An increase in dTTP thus leads to the decreased reduction of the dCDP pyrimidine substrate, which is essential for DNA replication, ultimately resulting in an accumulation of cells in S-phase [301]. The use of PI and an anti-phosphohistone 3 antibody for this mitotic index assay has been previously discussed in section 3.4.

Figure 4.4A shows that the proportion of cells in S and G_2/M is 35% and 18% respectively in non-synchronised cells at the zero time-point. After synchronisation with thymidine, 56% of cells are found in S-phase and the number of cells in G_2 decreases to 6%. 1.5 and 2.5 hours after release increases this G_2/M fraction to 11% and 17% respectively. The increase in the number of cells in G_2/M from 6% to 17% from 0 to 2.5 hours after thymidine release suggests that only part of the S-phase population has cycled to G_2/M. This implies that the cycling population must originally be late S-phase cells that have not been blocked by thymidine.

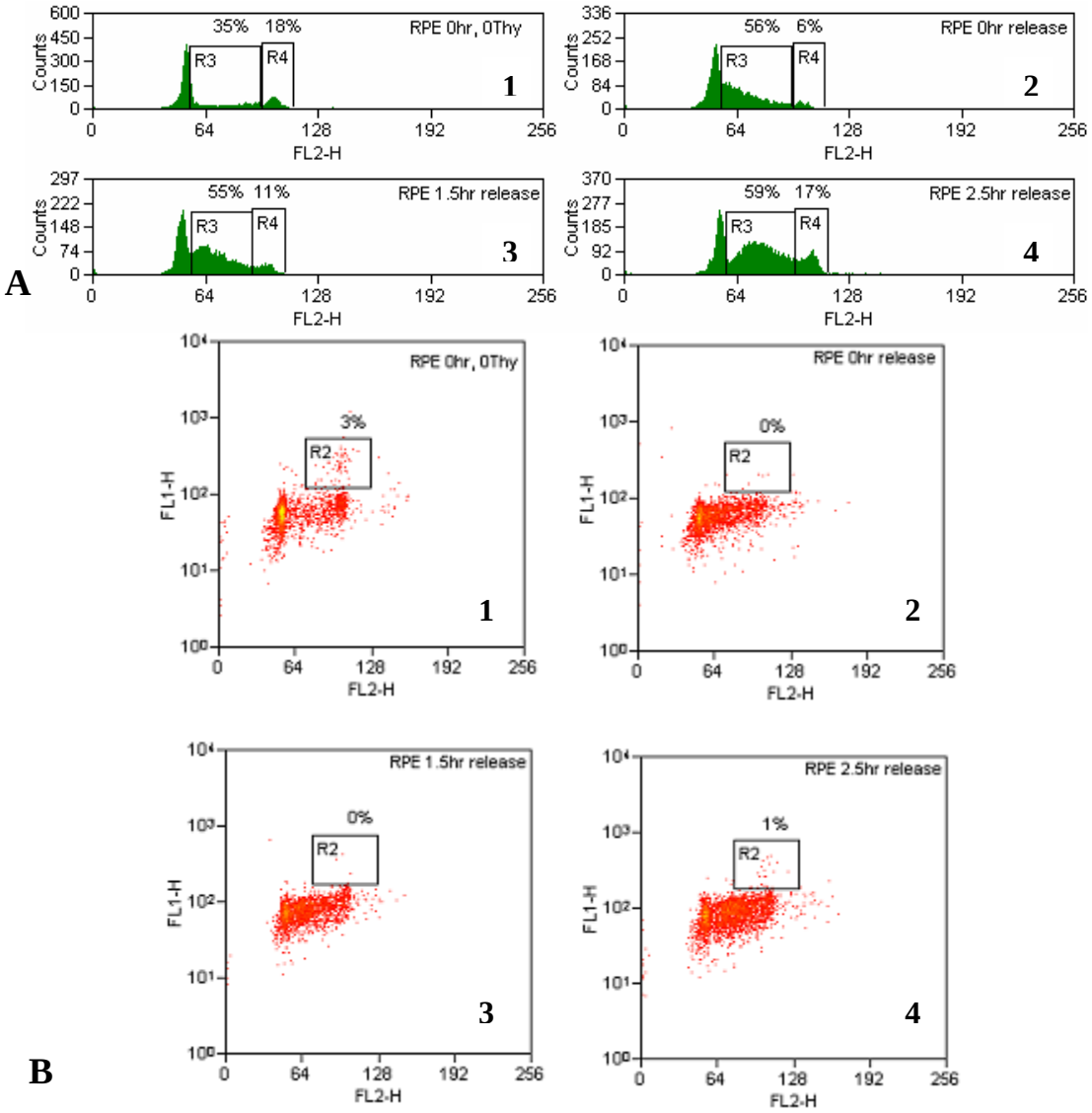

Figure 4.4 A: Flow cytometric analysis of propidium iodide-treated hTERT-RPE1 cells synchronised in S-phase with 2 mM thymidine for 16 hours and released at 0, 1.5 and 2.5 hours as shown in panels 2-4. Panel 1 shows unsynchronised cells. **B**: Flow cytometry analysis of propidium iodide and anti-phosphohistone 3-treated hTERT-RPE1 cells synchronised in S-phase with 2 mM thymidine for 16 hours and released at 0, 1.5 and 2.5 hours as shown in panel 2-4. Panel 1 shows unsynchronised cells. Boxed areas include cells in mitosis.

The mitotic index was also determined. In non-synchronised cells, the mitotic index equalled 3% (Figure 4.4B). This decreased to 0% in synchronised cells released for 0 and 1.5 hours and increased to 1% at 2.5 hours after release. These results suggest that it takes more than 1.5 hours and less than 2.5 hours for S-phase cells to accumulate in mitosis and that the increase in the G_2/M population in Figure 4.4A is mostly due to an increase of cells in G_2. More accurately, I would suggest that the S-phase cells seen in mitosis 2.5 hours after thymidine release are due to a few cells in late S-phase, as the whole synchronised S-population (56%) does not appear to have cycled that far.

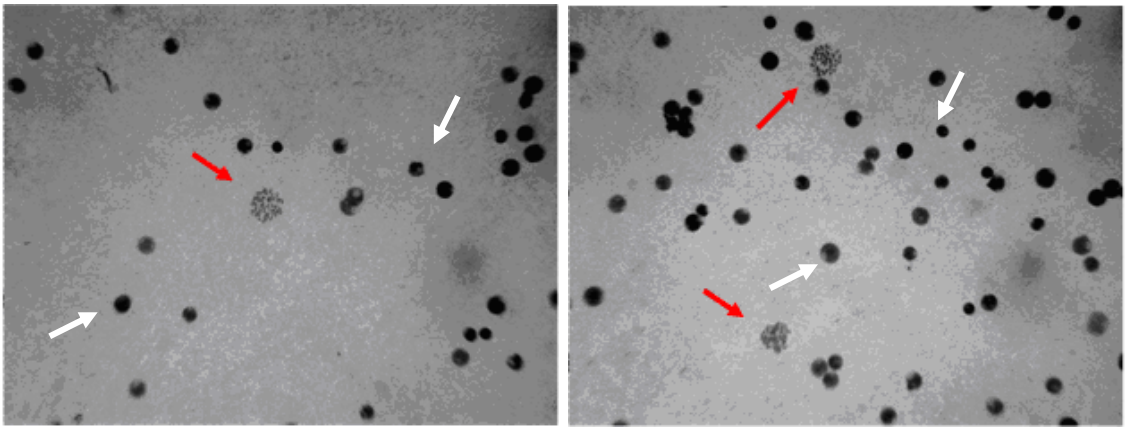

Figure 4.5: Giemsa-stained hTERT-RPE1 cells at x10 magnification. Red and white arrows point to mitotic and interphase cells respectively.

The mitotic index was also established manually. Cells were synchronised and released as before and mitotic cells could be distinguished from interphase cells (Figure 4.5 white arrows) with Giemsa staining as chromosomes without a nuclear membrane (Figure 4.5 red arrows). Table 4.1 shows that at 0, 1.5 and 2.5 hours after release from thymidine, 0.1% of cells were in mitosis. Only between 2.5 and 6 hours did the mitotic index increase to 0.9%. These numbers are lower than those obtained with the anti-phosphohistone 3 antibody (Figure 4.4) suggesting that histone 3 might be phosphorylated in late G_2 just before entry into mitosis and thus using the anti-phosphohistone 3 antibody might pick up cells in both late G_2 and mitosis. Another way in which mitotic index numbers might be altered is through the preparation of the samples. Nonetheless, the data of both the manually-established and the flow cytometry-calculated mitotic index experiments suggest that even up to 2.5 hours after S-phase, early S-phase cells have not reached mitosis and thus DNA damage seen in metaphases in the G_2 assay must have originated in G_2.

Time after release (hours)	0	1.5	2.5	6
Mitotic Index (%)	0.1	0.1	0.1	0.9

Table 4.1: Results of manual counting of mitotic index in S-phase synchronised hTERT-RPE1 cells released from 2 mM thymidine for 0, 1.5, 2.5 or 6 hours. The mitotic index was determined for 1000 cells at x10 magnification after Giemsa staining.

These synchronisation results might have been affected by the thymidine block if it caused a delay in the cycling of cells, preventing cells from immediately resuming the cell cycle after S-phase synchronisation. I cannot infer from my data that no cell cycle delay is initiated by the thymidine block. It is clear however that at 1.5 hours after release from thymidine, cells are cycling as the S-phase peak has shifted compared to the zero time-point (Figure 4.4A). As examples of thymidine-induced cell cycle delay are not found in the literature I can confidently say that the results in this cell synchronisation section are not affected by the thymidine block itself.

4.5 siRNA knock-down of topo IIα expression

4.5.1 Determining siRNA concentration

Procedure

Addition of siRNA against topo IIα

In all the following experiments topo IIα expression was lowered using siRNA. SiRNA against topo IIα was added as described under section 2.9. Two separate siRNAs were added, namely 5'-GCUCCUAACUUCUAGUAACtt-3' and 5'-CCUUCAACUAUCUUCUUGAtt-3' that target different topo IIα exons, namely 5 and 26 respectively. In both siRNA sequences, the final tt located at the 3' end denotes the dinucleotide overhang that is incorporated into RISC. SiRNA concentrations ranged from 0 to 2 nM. Also as a control, 1 nM scrambled siRNA was added parallel to the other studies. For a clear image as to where the siRNAs bind the topo IIα mRNA sequence I refer you to Appendix A.

Analysis of topo IIα expression

Once siRNA was added for 12 hours, samples were collected in sample reducing buffer (section 2.2). Protein concentrations were determined (section 2.3) and western blot analysis was carried out (section 2.4). The data was normalised against β-actin and non-siRNA-treated control values were set at to 100% topo IIα expression.

Chromosome condensation

It has been reported that reduced topo IIα expression affects chromosome condensation [124,168,302-304]. Therefore experiments were performed to test this as reduced chromosome condensation might interfere with chromatid break analysis. When looking at chromosome condensation, exponentially growing hTERT-RPE1 cells, treated with siRNA against topo IIα, were prepared and stained following the protocol in section 2.6. Cells were incubated with colcemid 0.1 μg/ml for 1.5 hours. Metaphase spreads were prepared on slides, dried in air and pictures were taken at x100 magnification.

Immunocytochemistry

After 1 nM siRNA treatment against topo IIα, exponential hTERT-RPE1 cells were also prepared for immunocytochemistry as described under section 2.10.

RNA analysis

RNA was extracted from siRNA-treated and control hTERT-RPE1 cells and cDNA formed from it as described under section 2.11. PCR was then performed as explained in the same section with forward and reverse primers against a coding region topo IIα or β-actin. A negative control was also carried out where primers against β-actin were added to a tube with no cDNA. The topo IIα and β-actin PCR reactions were performed separately and in triplicate. Primer sequences were taken from the literature [152,284]. The GC base content and melting temperatures were determined using the online oligonucleotide properties calculator Oligocalc [305].

Appendices A and B show the target DNA sequences to which the forward and reverse primers against topo IIα and β-actin bind.

PCR samples were sent, as described under section 2.11.5, to the Sequencing Service in the School of Life Sciences at Dundee University to test that the PCR products did in fact code for topo IIα or β-actin.

Results and Discussion

Firstly, it was important to determine the concentration of siRNA that lowered topo IIα expression as measured by western blotting. Figure 4.6 shows that increasing siRNA concentration, decreases topo IIα protein expression (Panel A). 1 and 2 nM siRNA incubation resulted in approximately 65% and 75% knockdown respectively (Panel B). The addition of 1 nM scrambled siRNA did not affect topo IIα protein expression (Panel A) suggesting that the process of adding siRNA does not alter protein expression. Protein loading was similar in comparative samples as shown by β-actin expression in Figure 4.6A. As discussed in chapter 3, it is clear that the antibodies are specific to either topo IIα or β-actin. As in HL60, MX1 and

MX2 samples (chapter 3), data was normalised against β-actin and following quantification by densitometry, topo IIα values obtained for control hTERT-RPE1 were set at 100% and topo IIα values in siRNA-treated cells expressed as a percentage of this hTERT-RPE1 value. This extra normalisation step was imposed as experiments were not carried out on the same gel or membrane and values even within the hTERT-RPE1 cell line varied slightly after normalisation against β-actin. Reasons behind these different values have been suggested in section 3.3.

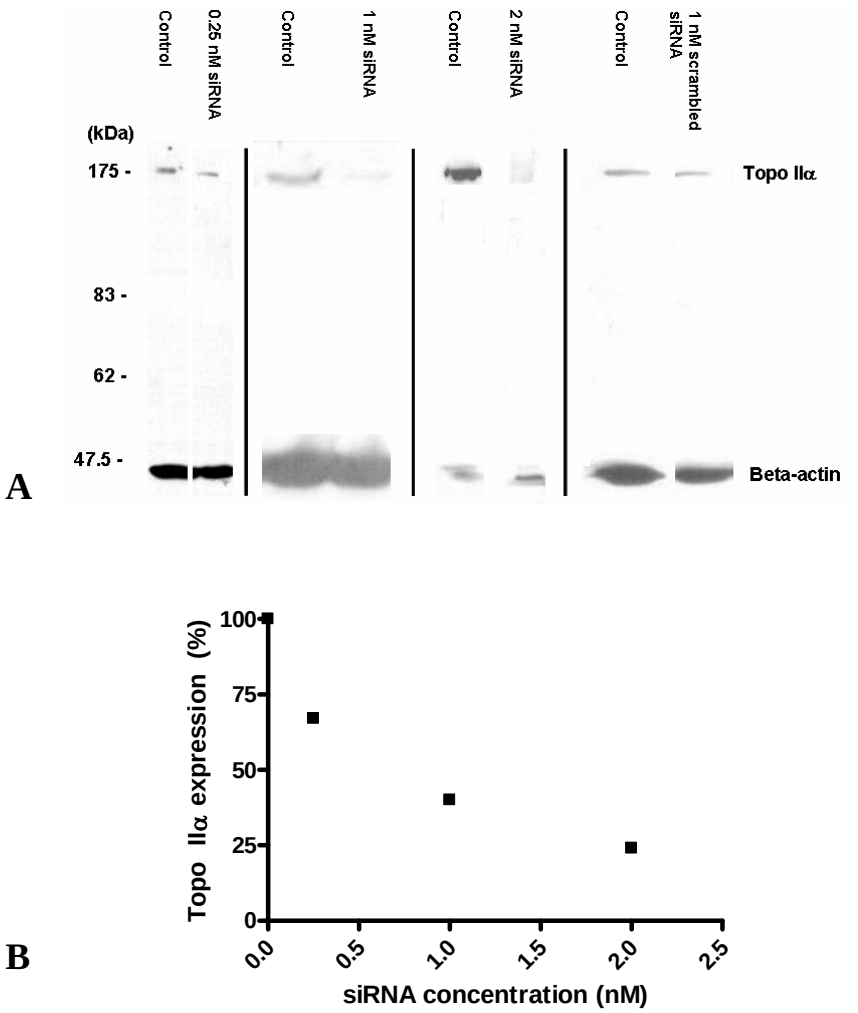

Figure 4.6 A: Western blot of anti-topo IIα siRNA-treated and control hTERT-RPE1 cells probed against topo IIα and β-actin. **B**: Data from western blots was analysed showing that increased siRNA treatment decreases topo IIα expression. Topo IIα results from Panel A were normalised against β-actin levels and these results were further normalised against 0 nM siRNA concentration with this latter value set at 100%.

Dual antibody-sandwich ELISA experiments also showed that 1 nM siRNA against topo IIα decreased protein expression by approximately 70% (P. Bryant, personal communication). Generally, a siRNA experiment is deemed successful when the target protein expression level has decreased by approximately 80%. For this reason, 2 nM siRNA against topo IIα was chosen as the concentration to use for further chromatid break experiments.

When trying to determine if 2 nM siRNA against topo IIα had any effect on chromatid break frequency, it became clear that this concentration of siRNA was affecting chromosome structure and was therefore too high. Chromatid breaks could not be determined at 2 nM siRNA as chromosomes appeared less condensed as well as more entangled (Figure 4.7). This confirms a role for topo IIα in chromosome condensation. The addition of 1 nM scrambled siRNA did not affect chromosomal structure.

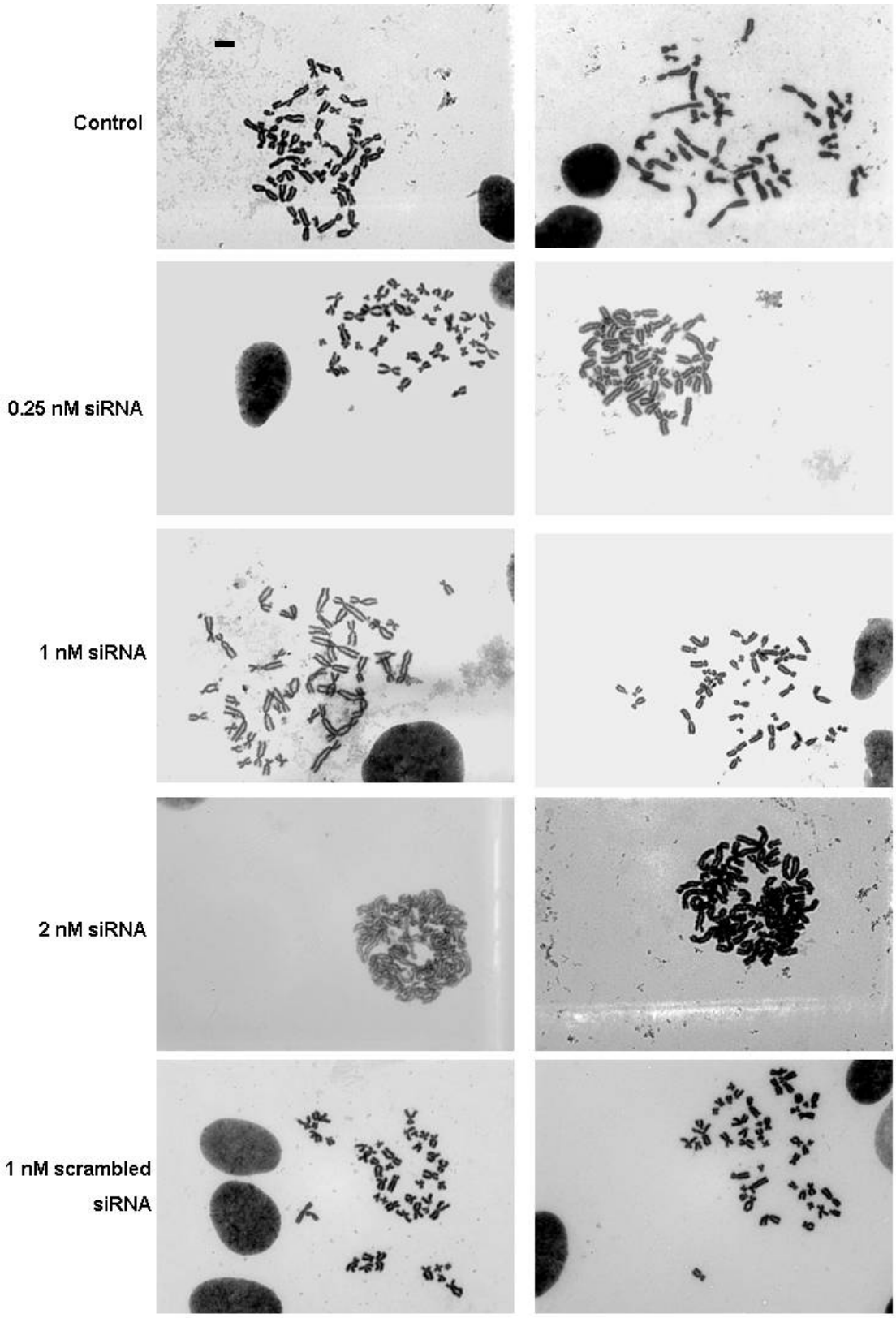

Figure 4.7: Metaphase spreads of Giemsa-stained hTERT-RPE1 cells treated with 0, 0.25, 1 and 2 nM siRNA against topo IIα. Two metaphases are shown for each experimental treatment. The lowest panels show hTERT-RPE1 cells treated with 1 nM scrambled siRNA. The bar in the top left panel represents 10 μm. Pictures were taken at x100 magnification.

Rather than using 2 nM siRNA, I decided that 1 nM siRNA against topo IIα would be a better concentration for chromatid break frequency studies as it provided not only a good topo IIα protein knockdown, but it also did not affect chromosome condensation or individualisation. Figure 4.7 shows that 1 nM, unlike 2 nM, siRNA against topo IIα had no effect on chromosomal structure, nor did 0.25 nM.

It was determined microscopically via immunocytochemistry that knockdown of topo IIα with 1 nM siRNA was homogenous as lowered topo IIα expression appeared universal across all cells (data not shown). Also the addition of 2 nM siRNA against topo IIα caused abnormal chromosome structure, as shown in Figure 4.7, in all metaphases, again suggesting a universal knockdown.

Another method used to determine topo IIα knockdown was PCR. Table 4.2 shows not only the sequence of the primers used, but also their % GC content and melting temperatures. Generally, the GC content should be between 40% and 60%. This % GC content determines the melting temperatures of the forward and reverse primers which should differ by no more than 5°C. Although the forward β-actin primer has a GC content of 72%, its melting temperature is only 3°C higher than that of the reverse primer and therefore these two primers can be used together. As the forward and reverse primers had been selected from the literature [152,284] but had not been used in conjunction with each other previously, it was important to ensure that their melting points made them compatible. The melting points are used to determine the annealing temperature during the PCR cycles. Here, an annealing temperature of 52°C was used which gives clear bands when the PCR products are run on an agarose gel as seen in Figure 4.8.

Target	Forward or reverse	Primer Sequence	GC Content	Melting temperature
Topo IIα	Forward	'5-GCGTGTTGAGCCTGAATG-3'	56%	50°C
Topo IIα	Reverse	'5-GCTAGTCCACCTAAGACC-3'	56%	50°C
β-actin	Forward	'5-ACCCCGTGCCTGCTGACC-3'	72%	57°C
β-actin	Reverse	'5-AGGAAGGAAGGCTGGAGAGT-3'	55%	54°C

Table 4.2: Sequence of forward and reverse primers targeted to either topo IIα or β-actin along with their % GC content and melting temperature as determined using Oligocalc [305].

As siRNA theoretically targets mRNA, PCR is a useful way to check that the lowered protein knockdown (Figure 4.6) is in fact due to altered mRNA levels, rather than posttranslational modifications. Figure 4.8 shows that 1 nM siRNA treatment against topo IIα of hTERT-RPE1 lowered topo IIα mRNA. This was found when treating cells with the second siRNA as well

(data not shown). As the extracted RNA was converted into cDNA in preparation for the PCR, and the cDNA was used as a template for PCR, the results only indirectly relate to mRNA levels. Although it appears that no topo IIα mRNA is present in siRNA-treated cells, I believe this is due to sensitivity issues with detection as cells lacking topo IIα cannot separate sister chromatids in mitosis [124,170] and are therefore not viable.

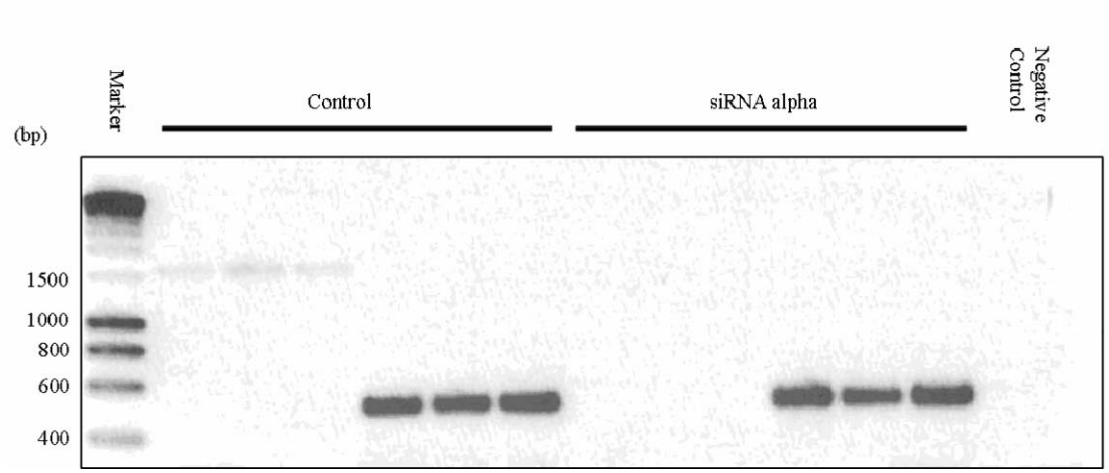

Figure 4.8: PCR products of cDNA, converted from mRNA, extracted from control hTERT-RPE1 cells or treated with 1 nM siRNA against topo IIα. Experiments were performed in triplicate with forward and reverse primers against either topo IIα or β-actin. The negative control does not contain cDNA. DNA was labelled with ethidium bromide.

It was important to run β-actin controls alongside topo IIα to ensure, just as in western blots, that the same amount of DNA was added to each PCR reaction so that the results from topo IIα in different samples could be compared. Figure 4.8 shows that β-actin mRNA levels were in fact the same in control and siRNA-treated cells. As well as running β-actin controls, a negative control was run, which did not contain any cDNA. As no band was present, it proves that bands produced in the cDNA–containing samples were not due to any contamination. It was found that the single bands were in fact topo IIα or β-actin mRNA as PCR products were sent for sequencing and the results corresponded very well with known topo IIα or β-actin sequences (Appendix C and D respectively). The product sequences showed 94.4 and 97.8% identity for forward and reverse primers against topo IIα respectively as determined by LALIGN and 95% and 98% identity for human topo IIα mRNA as determined by BLAST. Sequences showed 99.7 and 98.7% identity for forward and reverse primer against β-actin respectively as determined by LALIGN and 99% identity with human β-actin mRNA for both primers as determined by BLAST.

Also, the migration of the PCR products correlated well with the predicted size of the bands, with topo IIα- and β-actin-amplified mRNA equalling 1573 bp (Appendix A) and 499 bp (Appendix B) respectively. It was also determined that primers did not amplify genomic DNA.

Not only was genomic DNA removed in the process of converting mRNA to cDNA; in case some still remained, it was also ensured that the forward and reverse primers targeted different exons (Appendix A and B). As the PCR products were the same size as that predicted from the coding mRNA sequence of each protein, I can confidently say that no introns and therefore no genomic DNA were amplified.

4.5.2 Chromatid break analysis

Procedure

Exponentially growing hTERT-RPE1 cells were treated with siRNA (for sequences see section 4.5.1) as described under section 2.9. Here cells were incubated with 0, 0.25 or 1 nM siRNA against topo IIα. Alongside these experiments, cells were also treated with a second siRNA against topo IIα targeting a different exon (1 nM) or 1 nM scrambled siRNA. Once incubated with siRNA for 12 hours, cells were irradiated at 0.3 Gy γ-rays and metaphase spreads prepared as mentioned under section 2.6. Non-irradiated controls were run alongside irradiated samples. Cells were added to slides and air dried before staining with 10% Giemsa in Gurr's buffer and chromatid break frequencies counted in 100 metaphase cells.

Results and discussion

The number of chromatid breaks formed in both control and irradiated (0.3 Gy) cells were calculated in 100 metaphases. The effect of colcemid incubation has already been discussed in section 3.5. Figure 4.9 shows that in all cells (control and siRNA-treated) little or no chromatid breaks were formed in non-irradiated controls. When irradiated at 0.3 Gy, all cells showed an increase in chromatid break frequency as expected. Panel A shows that 1 nM scrambled siRNA does not alter chromatid break frequency from control cells. Both the control and scrambled siRNA-treated cells exhibit approximately 1 chromatid break per metaphase after γ-irradiation at 0.3 Gy. This suggests that the process of adding 1 nM siRNA to cells does not cause or prevent chromatid break formation. 0.25 nM siRNA against topo IIα also did not affect chromatid break frequency (Panel B). This is very interesting as Figure 4.6 clearly shows that 0.25 nM siRNA does lower topo IIα expression. This suggests either a threshold or a separate pool of topo IIα involved in the formation of chromatid breaks. Another reason might be the non-synchronised nature of the cells as siRNA incorporation into G_2 cells might be 'diluted' by cells in other phases of the cell-cycle.

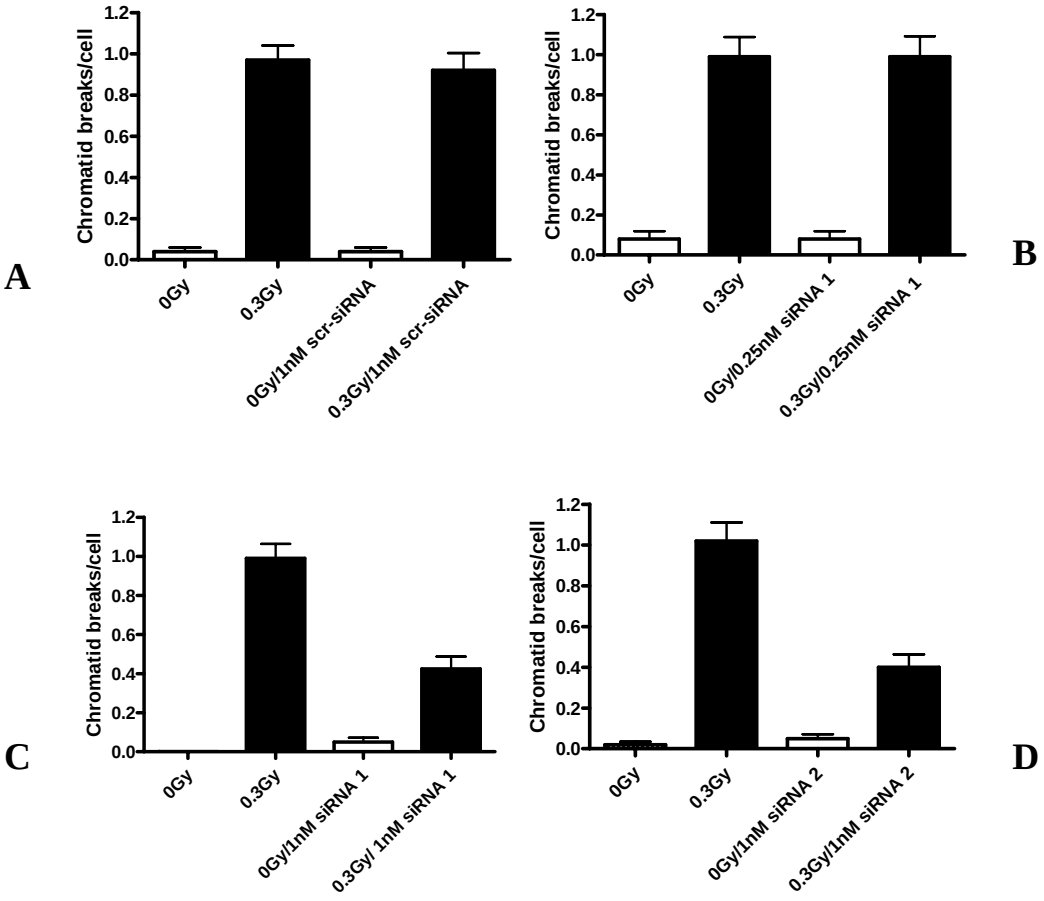

Figure 4.9: Chromatid break frequency per cell in control and irradiated (0.3 Gy γ-rays) siRNA-treated hTERT-RPE1 cells. **A**: Cells treated with or without 1 nM scrambled siRNA. **B**: Cells treated with or without 0.25 nM siRNA1 against topo IIα. **C**: Cells treated with or without 1 nM siRNA1 against topo IIα. **D**: Cell treated with or without 1 nM siRNA2 against topo IIα. Bars indicate standard deviations from the mean calculated for 100 cells.

Panels C and D however do show that the addition of 1 nM siRNA targeted against different exons of topo IIα decreased chromatid break frequency in irradiated cells ($p \leq 0.0001$). As discussed in Chapter 3 the p-value is defined as the probability of obtaining the results assuming the null hypothesis is correct. The significance level is taken as 5% (0.05) so any p-value obtained below 0.05 is statistically significant. Irradiated cells initially showed approximately 1 chromatid break per metaphase, however the addition of 1 nM of siRNA against topo IIα decreased this value by approximately 60% (Panels C and D). This suggests that topo IIα must be involved in the formation of chromatid breaks. Although chromatid break frequency was counted only once for 100 cells, the data is reproducible as treatment with either siRNA against topo IIα had acquired the same results. Also, the number of chromatid breaks obtained in radiation (0.3 Gy) -only cells in Figure 4.9 compare well with the radiation dose effect results of Figure 4.3. In both cases, the number of chromatid breaks, which was

low in non-irradiated control cells, increased to approximately 0.8 - 1 chromatid break per metaphase when irradiated at 0.3 Gy.

4.6 Is reduced chromatid breakage due to the G_2/M checkpoint?

It was important to test the effect of anti-topo IIα siRNA treatment on the mitotic index as I wanted to ensure that the lowered chromatid break frequency seen in siRNA-treated cells was not due to cells with high chromatid break frequencies being blocked in G_2.

Procedure

hTERT-RPE1 cells were treated, alongside controls, with 1 nM siRNA against exon 5 of topo IIα (for sequence see section 4.5) for 12 hours as described under section 2.9. Cells were then irradiated at 0.3 Gy γ-rays alongside controls and prepared for mitotic index studies as explained under section 2.5.1. The proportion of cells in mitotis was determined with anti-phosphohistone 3 for 1 x 10^4 cells in duplicate experiments. Results were normalised against values obtained from the control sample.

Results and discussion

Figure 4.10 shows that the addition of 1 nM siRNA against topo IIα in non-irradiated cells decreases the proportion of cells in mitosis by 40%. This confirms a role for topo IIα in normal G_2 checkpoint function [303] and verifies normal checkpoint activity in the hTERT-RPE1 cells. Irradiated, non-treated cells also showed a lowered mitotic index, again confirming normal checkpoint function. However, no significant lowering of mitotic index was seen in these irradiated cells when incubated with 1 nM siRNA against topo IIα (41%) as compared with untreated, irradiated controls (36%) (Figure 4.10).

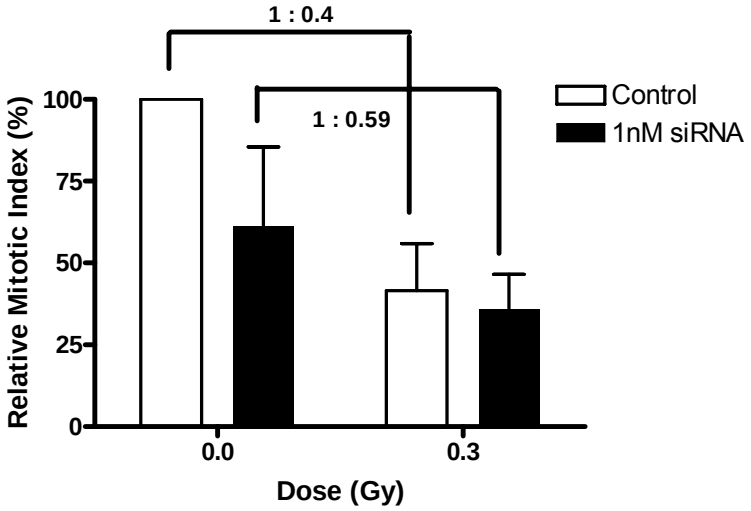

Figure 4.10: Mitotic index of control (unirradiated) and irradiated (0.3 Gy) hTERT-RPE1 cells treated with or without 1 nM siRNA against topo IIα as measured by flow cytometry. Cells were labelled with PI and an Alexa-conjugated antibody against phosphohistone 3 (FL1-H), a marker of mitosis. 1 x 10^4 cells per duplicate experiment were analysed per sample. Bars represent standard deviation for duplicate experiments. Results were normalised against the non-irradiated non-treated control.

Interestingly, the relative decrease in mitotic index from 0 to 0.3 Gy was not reduced further by siRNA incubation. Control samples showed a reduction by 60% (ratio 1:0.4) whereas the mitotic index in siRNA-treated cells decreased by only 40% (ratio 1:0.59) when irradiated at 0.3 Gy (Figure 4.10). This suggests that siRNA incubation in fact not only inhibits further reduction in mitotic index when irradiated, but actually increases the ratio. Also, previous data suggests that at low doses (such as here: 0.3 Gy) the minor cell-cycle block induced does not significantly affect chromatid break frequency [306]. It can therefore be argued that anti-topo IIα siRNA incubation at 1 nM does not lower mitotic index frequency and therefore the lowered chromatid break frequency cannot be explained by cells with a high chromatid break frequency being blocked in G_2.

4.7 Conclusion

The main finding of this results chapter was that lowered topo IIα expression, through the introduction of siRNA, in hTERT-RPE1 cells correlated with decreased radiation-induced chromatid breaks. It was clearly shown that 1 nM siRNA against topo IIα was sufficient to reduce not only mRNA, but also topo IIα protein levels and that the process of adding siRNA did not affect topo IIα protein levels. Also, 1 nM siRNA did not affect chromosome condensation therefore allowing chromatid break analysis. It was also determined that ionising radiation induces a G_2 checkpoint response in hTERT-RPE1 cells as well as a linear induction of chromatid breaks. These results suggest that this cell line not only has a functional G_2 checkpoint, but also that it was suitable for chromatid break analysis. siRNA incubation in irradiated (0.3 Gy) cells however, had no significant effect on the mitotic index, suggesting that the lowered chromatid break frequency seen in these cells was not due to cells with high DNA damage being halted in G_2. It was also suggested that metaphases analysed in the G_2 assay were originally in G_2 and not in S phase.

CHAPTER 5

INHIBITING TOPO IIα ACTIVITY WITH ICRF-193

DECREASES CHROMATID BREAK FREQUENCY

5.1 Introduction

This chapter is based around experiments where topo IIα activity is lowered using the catalytic inhibitor ICRF-193. As already mentioned briefly in the introduction (section 1.6.7), ICRF-193 is a compound that targets topo II without stabilising the cleavable complex. As ICRF-193 actually traps the enzyme in the closed clamp form by inhibiting ATPase activity, it does not cause DSBs and can therefore be referred to as a catalytic inhibitor [224]. Also, ICRF-193 preferentially targets topo IIα rather than β, as experiments where topo IIα– or β-containing plasmids were grown in yeast that were then treated with the inhibitor suggest a different range of active ICRF-193 specific to either topoisomerase IIα or β, namely 0.32 - 3.2 μM and 10 - 100 μM respectively [225].

Studies with ICRF-193 have already inferred a role for topo II in transcription [163], chromosome condensation and kinetochore structure [189], G_2 checkpoint activity [54,226,307-309], anaphase chromosome segregation [170], early stages of neuronal differentiation [179] and re-entry into G_1 from a quiescent cell state [310]. Also, experiments with ICRF-193 have provided further evidence for the specific action of drugs such as etoposide on topo II as treatment with ICRF-193 before incubation with etoposide lowered topo II-induced DNA damage [234].

5.2 Aims

The first aim of this chapter was to determine whether lowering topo IIα activity with ICRF-193 affected chromatid break frequency. Secondly, the way in which ICRF-193 might affect chromatid break formation was tested.

5.3 Determining ICRF-193 concentration

ICRF-193 was used as a catalytic topo IIα inhibitor to determine if this isoform was involved in the formation of chromatid breaks. Before this could be achieved it was important to determine whether the condensation of chromosomes was affected by this inhibitor.

5.3.1 Effect on chromosome structure

Procedure

ICRF-193 was added at 0, 100 nM, 1 and 32 μM to exponentially growing hTERT-RPE1 cells immediately before irradiation (0.3 Gy) with γ-rays. These, along with non-irradiated controls were then incubated for 30 minutes before the addition of colcemid 0.1 μg/ml for a further 2 hours. Cells were incubated with ICRF-193 for 2.5 hours in total. Metaphase spreads were made following the protocol in section 2.6. Metaphase spreads were prepared on slides, stained with Giemsa, washed and dried in air.

Results and discussion

hTERT-RPE1 cells were originally treated with ICRF-193 at 1 and 32 μM, concentrations that were chosen as they fell within ranges that targeted either topo IIα alone or topo IIα and β together respectively [225]. It was previously determined that less ICRF-193 was required to affect topo IIα than β, and it can therefore be assumed that concentrations below 10 μM ICRF-193 would affect topo IIα only whereas concentrations higher than 10 μM must affect both isoforms [225].

Cells treated with 1 μM ICRF-193 showed abnormal chromosome condensation and spreading (Figure 5.1). No metaphases were present in metaphase spreads of 32 μM ICRF-193-treated cells. Chromosome condensation and chromatid break frequency could therefore not be analysed at this high concentration, most likely due to activation of the intact G_2 checkpoint. The effects of 1 μM ICRF-193 and 2 nM anti-topo IIα siRNA-treated cells (section 4.5.1) on chromosome structure, suggest that topo IIα has a role in not only decatenation but also chromosome condensation. Analysis of chromatid break frequency in cells where topo IIα activity is inhibited with ≥1 μM ICRF-193 is therefore impossible.

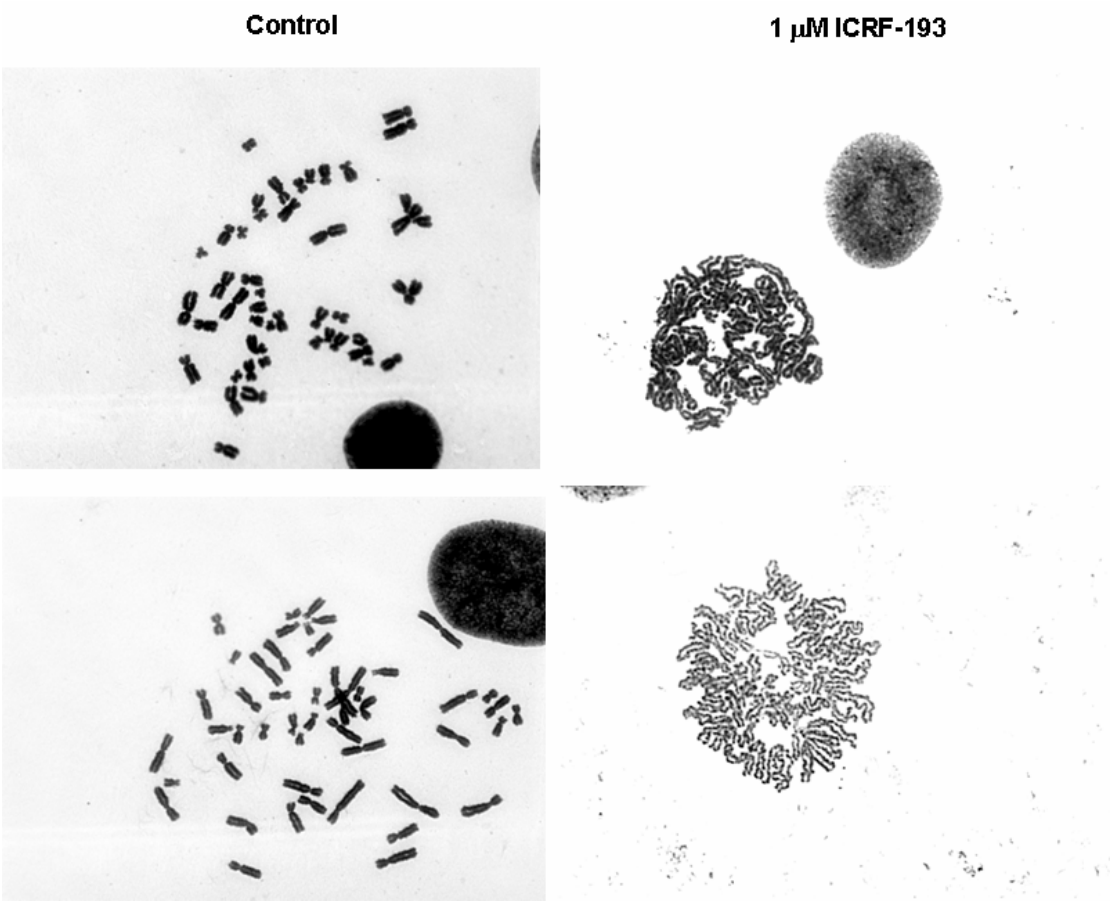

Figure 5.1: Two examples of metaphase spreads of Giemsa-stained hTERT-RPE1 cells treated without (left) or with 1 μM ICRF-193 (right) showing the de-condensing effect of the drug. Pictures were taken at x100 magnification.

When cells were treated with 100 nM ICRF-193, no de-condensing effect was seen on chromosomes (Figure 5.2). This suggested that if 100 nM ICRF-193 does inhibit topo IIα and affect chromatid break frequency, then there must be a topo IIα activity threshold, that if passed, affects chromosome condensation and spreading. Figure 5.2 also shows that unlike 1 μM ICRF-193, the frequency of IR-induced chromatid breaks can be determined after incubation with 100 nM ICRF-193 as chromatids are clearly visible.

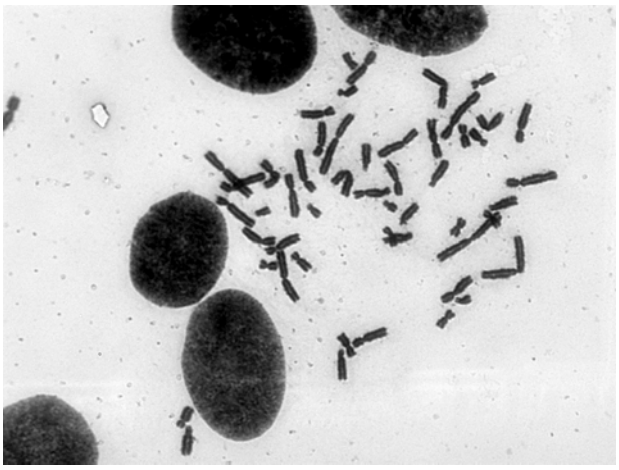

Figure 5.2: Metaphase spread of Giemsa-stained hTERT-RPE1 cells treated with 100 nM ICRF-193 for 2.5 hours (x 100 magnification).

5.3.2 Effect of ICRF-193 on mitotic index

Having established a concentration (100 nM) of ICRF-193 that does not reduce chromosome condensation in the hTERT-RPE1 cell line, the effect of 100 nM ICRF-193 on mitotic index was tested.

Procedure

1 x 10^6 exponentially growing hTERT-RPE1 cells were incubated with or without 100 nM ICRF-193, for a total of 2.5 hours, immediately before γ-irradiation at 0 or 0.3 Gy. Cells were then left to recover at 37°C for 30 minutes and incubated with 0.1 μg/ml colcemid for another 2 hours. Cells were then trypsinised (section 2.1.2) and pelleted by centrifugation at 600 x g. Mitotic indices were determined by flow cytometry (section 2.5.1). The number of cells in mitosis was determined for 1 x 10^4 cells per sample within each of the duplicate experiments. Results were expressed as a percentage of control values.

Results and discussion

As in chapter 4, I wanted to ensure that any effect that ICRF-193 might have on chromatid break frequency was not due to cells with high chromatid break frequencies being blocked in G_2. The use of PI and anti-phosphohistone 3 labelling has already been described under section 3.4. Figure 5.3 shows that in non-ICRF-193-treated control cells the mitotic index decreased after irradiation (0.3 Gy) compared to non-irradiated controls from 100% to 40%. This 60% decrease in mitotic index after irradiation confirms results found in Chapter 4 (section 4.6). Irradiation of cells after treatment with 100 nM ICRF-193 for 2.5 hours caused an additional depression of mitotic index (Figure 5.3). The mitotic index was reduced by 71% (radiation plus 100 nM ICRF-193) rather than 60% (radiation alone) when compared to the

non-irradiated, non-ICRF-193-treated control (100%). However, Figure 5.3 also shows that although ICRF-193 does reduce the mitotic index, it does not do so significantly as the ratio between non-irradiated and irradiated in both control and 100 nM ICRF-193-treated samples was still 1:0.4. Therefore the relative amount of cells proceeding to mitosis after irradiation in control and ICRF-193-treated cells is the same.

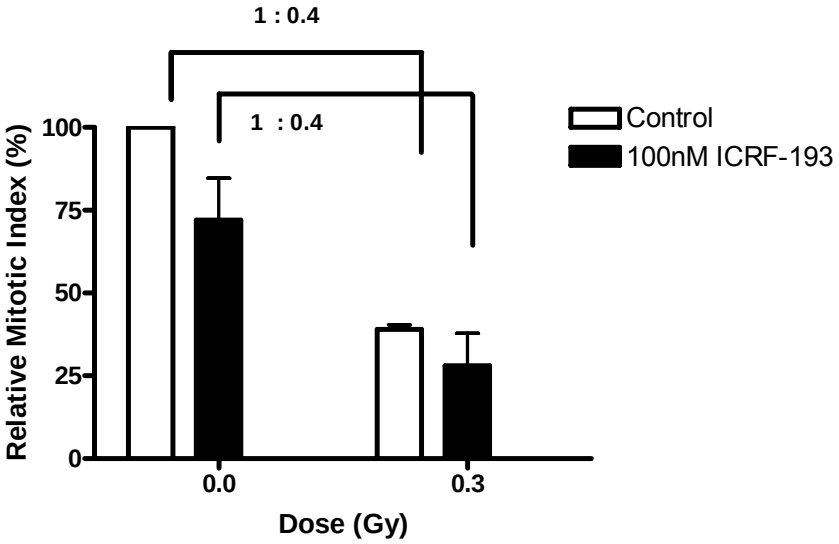

Figure 5.3: Mitotic index of control and irradiated (0.3 Gy) hTERT-RPE1 cells treated with or without 100 nM ICRF-193 as measured by flow cytometric analysis cells labelled with an Alexa-conjugated antibody against phosphohistone 3, a marker of mitosis, and PI. 1 x 10^4 cells per duplicate experiment were analysed per sample. Bars represent standard deviations for duplicate experiments. Results were normalised against control samples.

5.3.3 Is the lab-stock of ICRF-193 active?

As the inhibitor ICRF-193 used in the experiments described here had been stored at -20°C for several years, it was important to ensure that it was still active. This was achieved by determining if it lowered the ability of topo IIα to decatenate minicircles of kinetoplast DNA (kDNA) of the trypanosome *Chritidia fasciculata*.

Procedure

The kDNA decatenation assay was performed as described under section 2.12. Samples included the following:

- kDNA only

  or

- kDNA and 5 μl purified topo IIα (TopoGEN Inc.)

  or

- kDNA, 100 nM ICRF-193 and 5 μl purified topo IIα.

Results and discussion

To check that our batch of ICRF-193 did indeed inhibit topo IIα activity, 100 nM ICRF-193 was added to purified topo IIα *in vitro*. Figure 5.4 shows that kDNA alone stayed in the well and did not migrate (Lane 1). When purified topo IIα was added to kDNA, the minicircles migrated and the distances corresponded to the decatenated nicked and circular kDNA markers (Lanes 4, 2 and 3 respectively). When 100 nM ICRF-193 was added (Lane 5), this effect by topo IIα decreased with more interlocked kDNA remaining in the well and less DNA migration showing that less decatenation was achieved by topo IIα. This verified that ICRF-193 was active and does decrease topo IIα activity. It is important to stress though that this experiment was performed *in vitro* and that 100 nM ICRF-193 concentration *in vivo* might not achieve an equal inhibitory effect. Figure 5.4 therefore only shows that ICRF-193 is active at 100 nM *in vitro*, although the addition of 1 μM ICRF-193 *in vivo* which affected chromosome condensation (Figure 5.1), also suggests that at this concentration ICRF-193 is active.

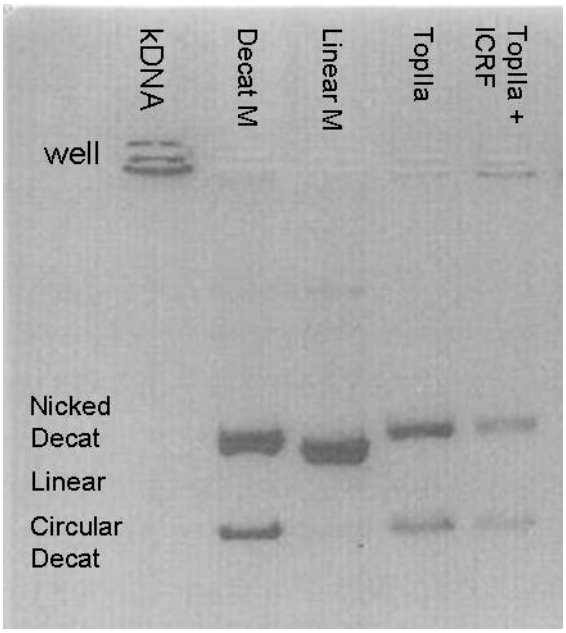

Figure 5.4: UV-trans-illuminated image of 1% TAE gel electrophoresis plus 1 μg/ml ethidium bromide. Lane 1: kDNA only. Lane 2: decatenated marker. Lane 3: linear marker. Lane 4: purified topo IIα and kDNA. Lane 5: purified topo IIα, kDNA and 100 nM ICRF-193.

5.4 Effect of ICRF-193 on chromatid break frequency in irradiated cells

Procedure

Exponentially growing hTERT-RPE1 cells were incubated with 25 or 100 nM ICRF-193 in medium immediately before irradiation (0.3 Gy). These along with un-irradiated or non-treated controls were incubated at 37°C for 30 minutes after irradiation before the addition of colcemid 0.1 μg/ml for 2 hours. Thus, cells were exposed to ICRF-193 for a total of 2.5 hours. Metaphase spreads were prepared as described in section 2.6. 10 μl of the fixed samples were dropped on to slides and air dried before staining with 10% Giemsa in Gurr's buffer and chromatid break frequencies counted for 100 metaphase cells. Combined results from graphs A and B were normalised in graph C by setting the value of 0.3 Gy in each experiment at 100%.

Results and discussion

The number of chromatid breaks formed in both control and irradiated cells (0.3 Gy) were averaged for 100 metaphases. As discussed in section 4.4, it is unlikely that 2.5 hours after irradiation early S-phase cells have progressed to mitosis and it is generally assumed that the metaphases analysed for chromatid breaks were originally in G_2 when irradiated. The effect of colcemid incubation was discussed in section 3.5. It is shown in Figure 5.5 that in all cells (control and ICRF-193-treated) few or no chromatid breaks were formed in non-irradiated

controls. This suggests that incubation with ICRF-193 does not of itself affect chromatid break frequency in non-irradiated cells. The data presented in Graphs 5.5A and B were acquired in separate experiments and this might explain why irradiated cells in both graph A and B showed a chromatid break frequency of 0.8 and 0.6 per metaphase respectively. The value for irradiated only cells in Figure 5.5A confirms results seen in Figure 4.3 where 0.3 Gy also resulted in 0.8 chromatid breaks per metaphase. The lower chromatid break frequency (0.6 per metaphase) in irradiation-only cells found Figure 5.5B is most likely due to altered growth of cells with a high passage number. Nonetheless, as all samples within this experiment were carried out under the same circumstances and were seeded at the same concentration from the same batch of cells, the data is still held to be valid.

Graph 5.5A shows that incubation of cells with 25 nM ICRF-193, a dose that, as explained previously, I assume only affected topo IIα, reduced chromatid break frequency after irradiation by 24% (p=0.01). This reduction was even more substantial in hTERT-RPE1 cells treated with 100 nM ICRF-193 (Figure 5.5B, p=0.003) where chromatid break frequency was lowered by 40% when compared to irradiation-only cells. As discussed in Chapter 3 the p-value is here defined as the probability of obtaining the results assuming the null hypothesis is correct. Here the significance level is taken as 5% (0.05) so any p-value obtained below 0.05 is statistically significant. To be able to compare the data between graphs 5.5A and B, the values of IR-induced chromatid break frequencies in ICRF-193-treated cells was normalised against the radiation-alone cells within each experiment with the latter value set at 100%. Graph 5.5C shows this normalised data and demonstrates that the effect on chromatid break frequency is ICRF-193 dose-dependent. The data presented here not only shows that 100 nM ICRF-193 is an active concentration *in vivo* but also provides more evidence for the role of topo IIα in the formation of chromatid breaks.

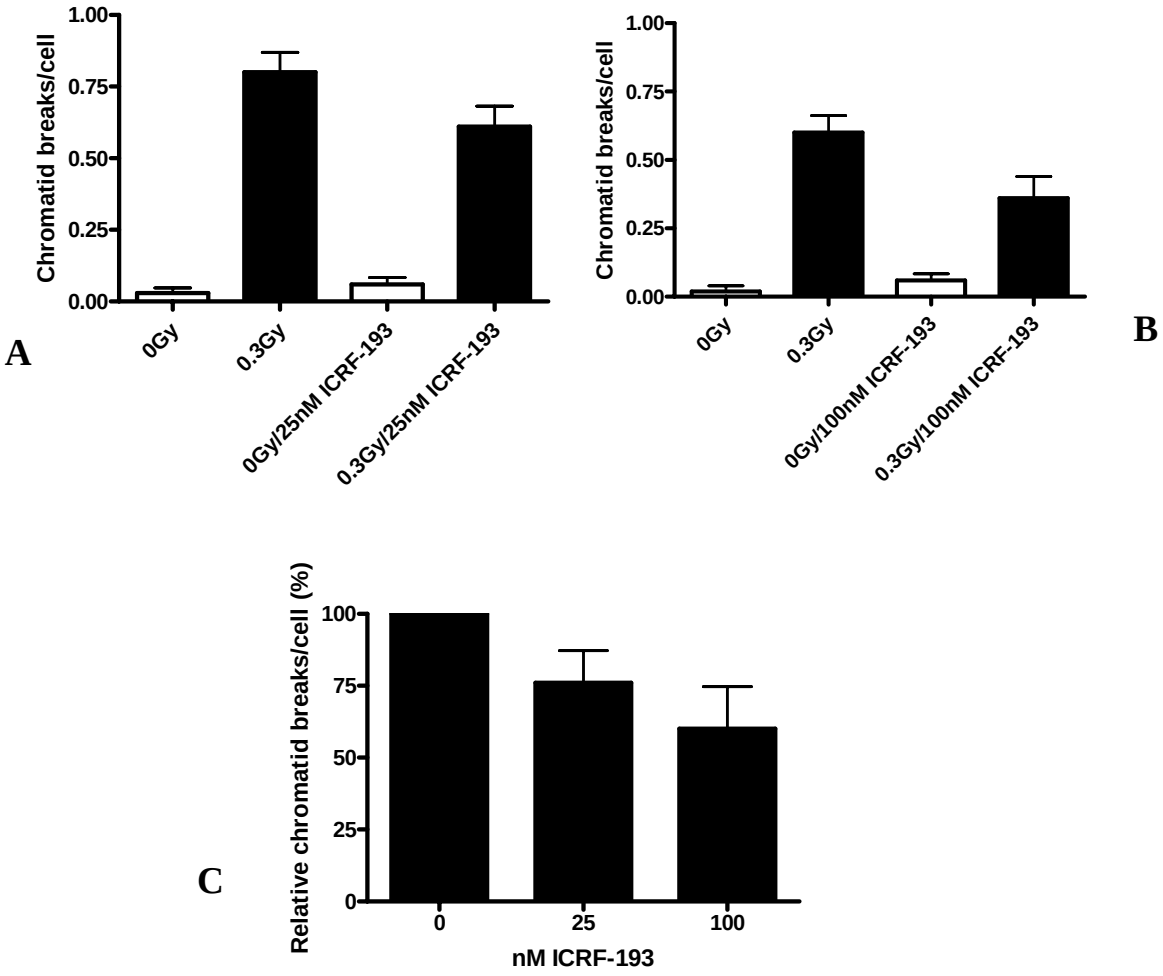

Figure 5.5: Frequencies of chromatid breaks in two separate experiments (A and B) using the G_2 assay in control (unirradiated) and irradiated hTERT-RPE metaphases incubated with or without 25 nM (graph **A**) or 100 nM (graph **B**) ICRF-193. Bars indicate standard errors from the mean for 100 metaphases. Combined results from graphs A and B have been normalised in graph **C** by setting the value of 0.3 Gy in each experiment at 100%.

It appears that ICRF-193 affects both chromatid break frequency (Figure 5.5) and kDNA decatenation (Figure 5.4) almost instantaneously, most likely due to the way in which ICRF-193 inhibits topo IIα, namely by trapping the protein [224]. Interestingly, treatment of hTERT-RPE1 cells with 100 nM ICRF-193 before irradiation affected chromatid break frequency suggesting that it does inhibit topo IIα at this concentration, yet it does not affect chromosome condensation. However, 1 μM ICRF-193 clearly does alter chromosomal condensation, suggesting that there must be a minimal topo II activity threshold, which if crossed decreases chromosomal condensation. This was already implied by experiments in Chapter 4 where cells treated with 0.25 nM siRNA against topo IIα decreased topo IIα expression, but did not affect chromosome condensation, unlike higher siRNA concentrations.

5.5 Does topo II affect radiation-induced DNA damage?

Having determined that ICRF-193 lowers chromatid break frequency, the next step was to determine wether it affected DSB induction too as DSBs are known to cause chromatid breaks [10,109]. Firstly the dose-effect relationship for radiation-induced DSBs in hTERT-RPE1 cells was established. Next, the effect of ICRF-193 on radiation-induced DSBs was tested. In these experiments DSB induction was determined firstly by low voltage gel electrophoresis and then by immunocytochemistry against γH_2AX.

Procedure

DSB induction as measured by low-voltage gel electrophoresis

DNA double-strand break induction by radiation (γ-rays) was determined by low voltage electrophoresis. hTERT-RPE1 cells were seeded the day before an experiment at 2 x 10^5 per T25 flask in 5 ml complete DMEM-F12 medium to ensure cells were growing exponentially when used for the experiment the following day. After approximately 24 hours 4 x 10^5 cells were then irradiated at 0, 10, 20, 30 and 40 Gy on ice, trypsinised (section 1.2.1) and pelleted by centrifugation at 600 x g. The remaining protocol is fully explained under section 2.7.1. Briefly, the cells, embedded in agarose plugs, were slotted into a 200 ml ethidium bromide-containing agarose gel that was run in 0.4 TAE buffer. Experiments were carried out in duplicate.

To test the effect of ICRF-193 on radiation-induced DSBs, hTERT-RPE1 cells were seeded at 2 x 10^5 in a T25 flask and 5 ml complete DMEM-F12 medium. A day later, cells were treated with or without 100 nM ICRF-193 for 2 hours at 37°C and 5% CO_2. Cells were then irradiated at 0.3 or 10 Gy γ-irradiation on ice and DSBs estimated as described under section 2.7.1. Briefly, the agarose gel contained 1 μg/ml ethidium bromide and was run in a 0.4 TAE buffer for 96 hours. Experiments were performed in duplicate.

DSB induction as measured by γH_2AX foci

Exponentially growing hTERT-RPE1 cells were also prepared for immunocytochemistry against γH_2AX foci as described under section 2.7.1. After cells were grown to 90% confluency or serum-starved overnight, they were treated with 100 nM ICRF-193 for 2 hours then irradiated at 0.3 Gy. In another experiment cells were serum-starved overnight and then treated with 0, 5, 10 or 32 μM etoposide for 1 hour. In all cases cells were then allowed to recover for 20 minutes at 37°C, 5% CO_2 with etoposide-treated cells allowed to recover in fresh medium containing no drug. Control experiments, where cells were not irradiated nor treated with ICRF-193 or etoposide, were carried out simultaneously. Cells were further fixed, blocked and stained as described in section 2.7.1. Experiments were performed in triplicate.

Results and discussion

The effect of low dose IR on DSB induction in hTERT-RPE1 cells was tested. It was important to not only check that the DSB assay could be applied to hTERT-RPE1 cells but also to make sure that DSB induction was linear as found in other cell lines [11]. The theory behind the low-voltage gel electrophoresis DSB assay was discussed under section 3.6. Figure 5.6A shows that the DNA fragments in irradiated hTERT-RPE1 cells were clearly visible as a secondary band below the wells. Also, an increase in radiation dose caused an increase in the fraction of DNA released from the well (Figure 5.6A); the amount of DNA released is attributed to the number of DSBs that are formed. Densitometry analysis of Figure 5.6A determined the fraction of DNA released from the well due to DSBs to be 0, 0.05, 0.14, 0.22 and 0.26 at radiation doses of 0, 10, 20, 30 and 40 Gy respectively (Figure 5.6B). The linear induction of DSBs, with R^2=0.9872, confirms studies in the literature in other cell lines [11] and signifies that this assay is a valid method of measuring DSB induction in hTERT-RPE1 cells.

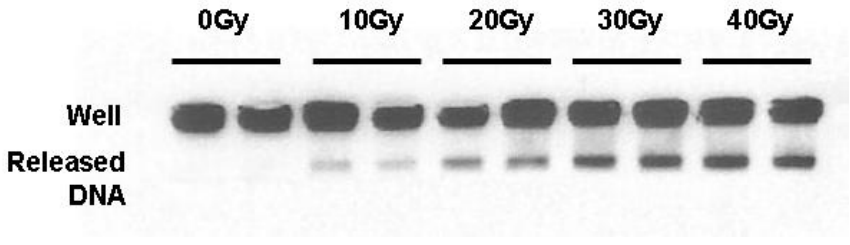

A

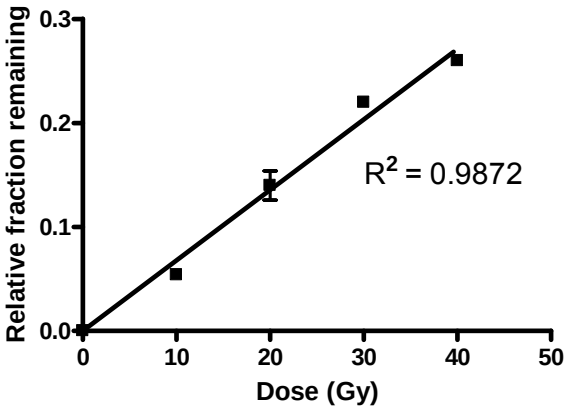

B

Figure 5.6 A: 4-day low voltage gel electrophoresis of DNA in hTERT-RPE1 cells irradiated from 0 to 40 Gy of γ-rays in duplicate experiments. DNA was labelled with ethidium bromide. **B**: Analysis of Figure 5.6A showing a linear response between fraction of DNA released with an increase in radiation dose (Gy), with R^2 = 0.9872. Bars are standard deviations from duplicate experiments.

As it has been shown that topo IIα is involved in the formation of chromatid breaks, and it has previously been shown that chromatid breaks arise from single DSBs [10]. It was important to determine if topo IIα played a role in the formation of DSBs. Using electrophoresis no DSBs

were seen in 0.3 Gy irradiated hTERT-RPE1 cells, whether treated with ICRF-193 or not (Figure 5.7). However, cells irradiated with 10 Gy γ-rays showed DSB induction with the fraction of DNA released equal to 0.14. Addition of 100 nM ICRF-193 to 10 Gy-irradiated cells did not significantly lower DSB induction (p=0.72), suggesting that topo IIα is not involved in the formation of the initial DSB. Whether this is due to the relative insensitivity of the assay is unclear. What is certain however is that 100 nM ICRF-193 does not cause significant numbers of DSBs. Although ICRF-193 was thought to only act as a catalytic inhibitor, it could at high doses cause DNA damage [226,311]. However, Figure 5.7 suggests that the concentration at which ICRF-193 has been used throughout this thesis does not induce DNA damage and therefore does act as a true catalytic inhibitor.

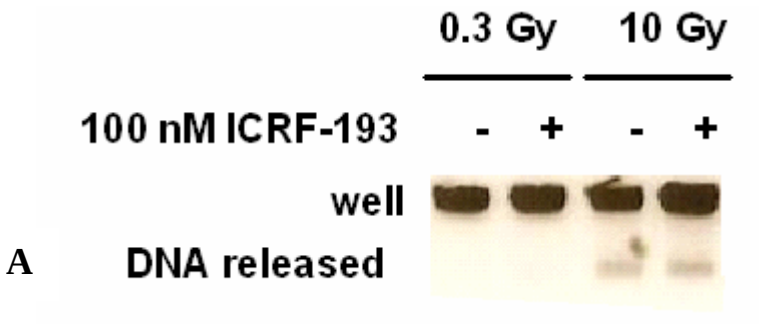

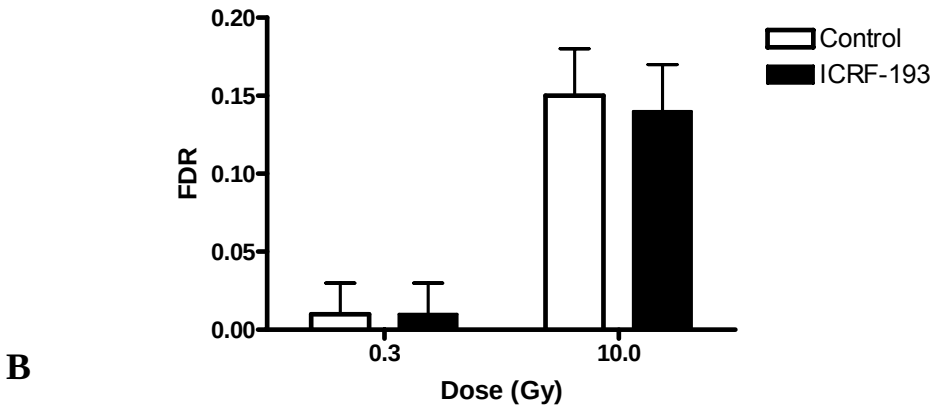

Figure 5.7 A: Induction of DSBs in hTERT-RPE1 cells treated with or without 100 nM ICRF-193 followed by γ-irradiation at 0.3 and 10 Gy. DNA was labelled with ethidium bromide. **B**: Analysis of figure 5.7A with FDR equal to the fraction of DNA released (from well) determined as described in section 2.7.1. Bars are standard deviations from the mean in duplicate experiments.

Another method to measure DSB induction is immunocytochemistry for γH_2AX. As mentioned in the introduction, the histone H_2AX is phosphorylated at serine 139 by ATM shortly after irradiation in response to DSBs [23]. This makes γH_2AX a useful marker for DSBs and therefore measuring γH_2AX foci can provide a measure of the number of DSBs per cell. The γH_2AX assay requires the synchronisation of cells in G_0 which is usually obtained by growing the cell population until it reaches confluency. The reason for this is to avoid cells in S-phase as generally replication processes induce many replication fork-associated DSBs, which would interfere with the analysis of radiation-induced DSBs. As the white arrows in Figure 5.8A show, using this method of synchronisation, in both control and irradiated cells, also picked up many cells that were still cycling and S-phase cells could be easily recognised as cells with a high number of DSBs (equal to approximately 40). It is even clearer from Figure 5.8B that some of these cells are still cycling as both cells in anaphase (left panel) and metaphase (right panel) are clearly visible. In this situation, it can easily be imagined that including the number of DSBs in S-phase cells would distort the calculated number of radiation-induced DSBs. It could be argued that as S-phase cells are quite obvious to spot, as they have such a high number of DSBs, they could simply be left out of the analysis. In doing this however, non-S-phase cells possibly with a true high radiation-induced DSB frequency would not be included.

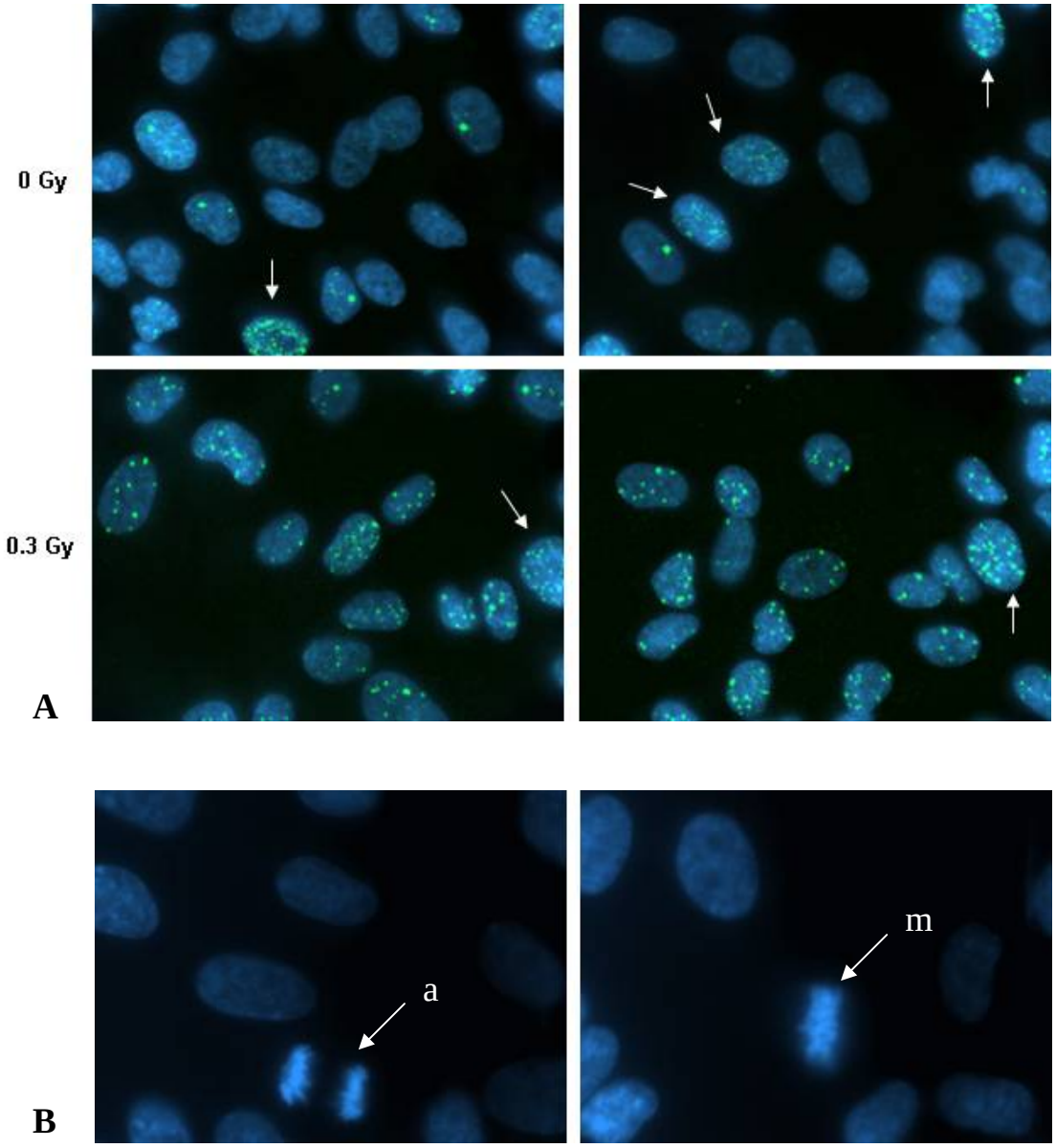

Figure 5.8: Two examples of hTERT-RPE1 cells grown to 90% confluency probed with anti-mouse-FITC-conjugated secondary antibodies against the primary mouse anti-γH_2AX antibody as well as DAPI. **A**: Control and 0.3 Gy-irradiated cells at x63 magnification. White arrows indicate S-phase cells. **B**: Control unirradiated cells at x100 magnification. The left and right panels show cells in anaphase (a) and metaphase (m) respectively.

hTERT-RPE1 cells were therefore synchronised in G_0 by serum-starvation. This method yielded almost no cells in S-phase or mitosis suggesting that most cells had remained in G_0/G_1 (Figure 5.9). The γH_2AX immunocytochemistry method is much more sensitive than gel electrophoresis, as DSBs are visible in cells irradiated at 0.3 Gy (Figure 5.8 and bottom panels of Figure 5.9), a dose where DSBs could not be measured by low-voltage gel electrophoresis (Figure 5.7). Figure 5.9 shows that control (non-irradiated) cells (top panels) or irradiated cells (middle panels panels) probed only with the secondary FITC-conjugated antibody (top panels) have little or no γH_2AX foci.

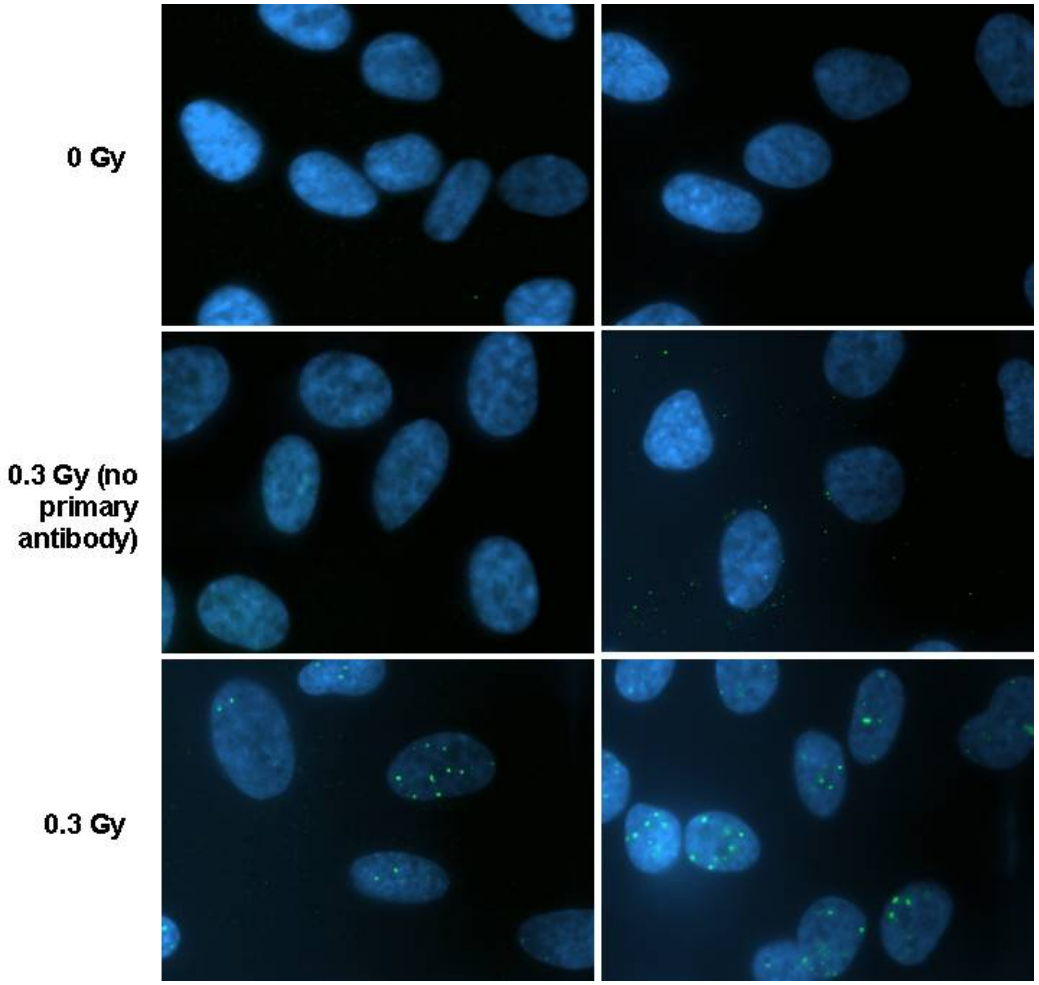

Figure 5.9: Immunocytochemistry of serum-starved hTERT-RPE1 cells probed with γH_2AX (FITC) and stained with DAPI (nucleus) (x100 magnification). The top two panels show non-irradiated cells. The middle and bottom panels show irradiated (0.3 Gy) cells respectively, with cells in the middle panels probed only with the secondary anti-mouse FITC-conjugated antibody, whereas cells in the bottom and top panels were probed with both primary (mouse anti-γH_2AX) and secondary antibodies.

Figure 5.10 shows the quantification of γH_2AX foci per cell, calculated as the mean frequency of foci in 100 cells in each of the triplicate experiments performed. In both control and ICRF-193-treated non-irradiated samples, almost no foci were found, suggesting that no DSBs were formed. This confirms the conclusion derived from gel electrophoresis (Figure 5.7) as 100 nM ICRF-193 also did not induce any γH_2AX foci. When irradiated at 0.3 Gy, the number of DSBs increased to a mean of 11 γH_2AX foci per cell in both radiation-only and ICRF-193-treated plus irradiated cells. Thus, no significant difference was found in cells treated with 0.3 Gy or ICRF-193 plus 0.3 Gy. This again confirms the finding in Figure 5.7 that ICRF-193 does not lower DSB formation in irradiated cells, suggesting that topo IIα is not involved in the induction of DSBs. The number of foci corresponds well to other findings as it was previously determined that approximately 40 DSBs are formed per Gy in each cell [9,11,12]. Accordingly, a dose of 0.3 Gy should result in 12 γH_2AX foci per cell. The value obtained here for 0.3 Gy, namely 11 DSBs per cell, is not far from the expected result suggesting that this assay fits the

data found in the literature well. Also, it appears that the 20 minute recovery period after irradiation is long enough to initiate the signalling cascade as exemplified by the accumulation of the γH_2AX foci at the sites of DNA damage.

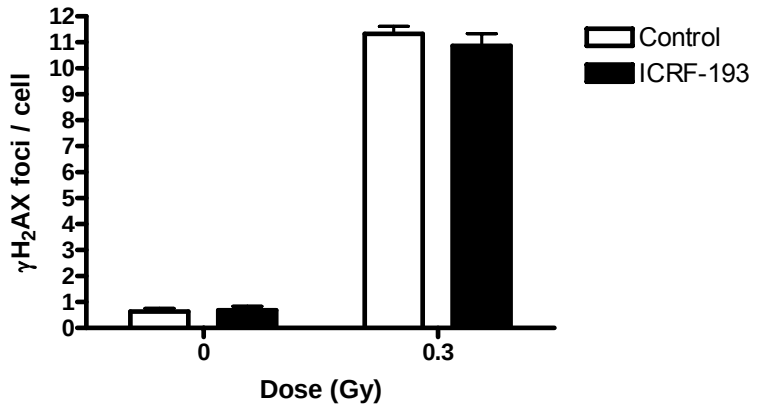

Figure 5.10: Number of γH_2AX foci per cell in control and irradiated (0.3 Gy) hTERT-RPE1 cells treated without or with 100 nM ICRF-193. The number of foci for each sample was determined for 100 cells in triplicate by immunocytochemistry. Cells were probed with anti-mouse-FITC-conjugated secondary antibodies against the primary mouse anti-γH_2AX antibody as well as DAPI. Bars represent standard errors from the mean for triplicate experiments.

In view of the fact that topo IIα expression may be relatively low in G_0, the question arises as to whether the experiments behind figure 5.10 are valid for cells in other phases of the cell cycle. To test this, the drug etoposide was used to determine whether topo IIα is active in G_0. Etoposide preferentially targets topo IIα rather than β, as experiments where topo IIα or β-containing plasmids were grown in yeast that were then treated with the poison suggest a different range in which etoposide is specific to either topoisomerase IIα or β, namely 10 - 100 μM and 100 - >100 μM respectively [225]. Thus the concentration used here (32 μM) should target just topo IIα. This drug is a classic topo II 'poison' that acts in a similar way to mAMSA and stabilises the cleavable complex thus increasing the number of DSBs formed by topo II [222]. The results shown in Figure 5.11 suggests that γH_2AX foci in G_0 can be used to test the role of topo IIα in the formation of radiation-induced DSBs because etoposide (32 μM) increased the number of γH_2AX foci per cell significantly, more so than after irradiation at 0.3 Gy. Treatment with only 5 or 10 μM etoposide also increased the number of γH_2AX foci per cell when compared to non-treated cells (data not shown). Therefore etoposide, used at doses that affect only topo IIα, increased the number of γH_2AX foci per cell thus suggesting that topo IIα in G_0 is active at a level that could be affected by etoposide.

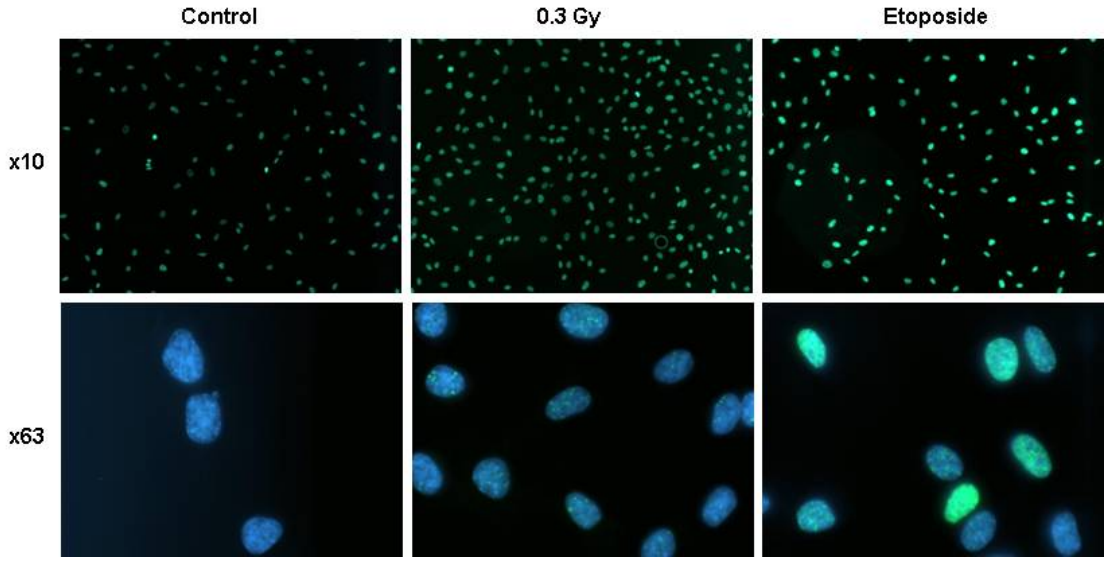

Figure 5.11: Image of immunocytochemistry against γH_2AX in control, irradiated (0.3 Gy) and etoposide-treated (32 μM) hTERT-RPE1 cells at x10 and x63 magnification. Cells were probed with anti-mouse-FITC-conjugated secondary antibodies against the primary mouse anti-γH_2AX antibody as well as DAPI.

One might suggest that 100 nM ICRF-193 could never affect DSB induction as the probability of the inhibitor-affected topo II sites and 0.3 Gy-irradiation-affected DNA sites overlapping might be quite small; therefore radiation and inhibitor are unlikely to interact in the cell at this radiation dose. This however does not explain the results seen at the high IR dose (10 Gy) in Figure 5.7 where the probability of the two factors interacting is quite high, yet DSB induction is still not affected. Also, as lowered chromatid break frequency after irradiation at 0.3 Gy, it is unlikely that ICRF-193 and irradiation sites do not overlap.

The effect of ICRF-193 on chromatid break frequency could theoretically be explained by its property to create a physical block when bound to topo II so that the DNA associated with topo II is shielded from radiation-induced damage. However, if this was the case, one would also expect DSB numbers to be affected in the same way as chromatid breaks i.e. lowered, as DSBs are more frequent in cells than chromatid breaks. DSB frequency however was not lowered by ICRF-193 after radiation suggesting that the effect of ICRF-193 on chromatid breaks is not simply a physical block and must be due to it specifically altering topo IIα activity.

If ICRF-193 does not affect DSB frequency in cells, what is the mechanism behind its effect on chromatid breaks? I am suggesting that ICRF-193 lowers the conversion of the original radiation-induced DSB to chromatid breaks, which provides further evidence for the signal model [112]. Thus not only is topo IIα involved in the formation of chromatid breaks, but it may be key in converting the original radiation-induced DSBs to chromatid breaks.

5.6 Conclusion

Treatment of hTERT-RPE1 cells with 25 or 100 nM ICRF-193, concentrations that do not significantly affect chromosome condensation or mitotic index, decreased the frequency of radiation-induced chromatid breaks. This is indicative of a role for topo IIα in the formation of radiation-induced chromatid breaks. Also, the data supports the signal model suggesting that topo IIα is involved in converting radiation-induced DSBs into chromatid breaks.

CHAPTER 6

INHIBITING TOPO IIα AFFECTS HYDROGEN PEROXIDE-INDUCED CHROMOSOMAL DAMAGE

6.1 Introduction

Oxidative stress is involved in the initiation of many diseases and causes reactive oxygen species (ROS) that can target cellular DNA, proteins and lipids. The ROS hydrogen peroxide (H_2O_2) has been shown to be involved in apoptosis [6]. H_2O_2 occurs naturally as a by-product of oxygen metabolism and is usually decomposed into water and oxygen by peroxidases [6]. Due to its oxidising abilities, H_2O_2 has also been manufactured to be used domestically as a source for bleaching and therapeutically to sterilise or combat acne.

In this chapter, H_2O_2, rather than ionising radiation, was used as a source of chromosomal and DNA damage. It is known that γ-rays can result in DNA damage indirectly through the production of $^{\cdot}OH$ radicals [3], which is also an endogenous product of H_2O_2 [6]. It has previously been determined that H_2O_2 is radiomimetic [5] and can cause both single and double strand breaks. Treatment of cells with $^{\cdot}OH$ scavengers, such as DMSO or mannitol, reduces DNA [5] damage.

Hydrogen peroxide treatment (from 10 μM to 0.5 mM) has also been associated with chromosomal damage after 10 minute [312] or 3 hour [313] treatments resulting in chromosome-type aberrations (dicentrics, acentric fragments) and chromatid-type aberrations (breaks, exchanges and gaps) respectively which were absent if cells were treated with ROS scavengers [312,313].

Interest in hydrogen peroxide in this chapter is based not only on its radiomimetic and DNA or chromosome damaging properties but also for its potential to affect topo IIα activity. $^{\cdot}OH$ radicals can result in the 'poisoning' of topo II [126], which might provide an explanation of action of topo IIα in the signal model of chromatid break formation. Cells appear more sensitive to H_2O_2 in S-phase than in G_1 due to not only the more open and thus susceptible state of the DNA chromatin structure [314], but also the higher level of expression of topo IIα [128].

6.2 Aim

The aim of this chapter was to determine if topo IIα is involved in H_2O_2-induced chromosomal and DNA damage.

6.3 Does H_20_2 induce chromosomal damage?

As a first approach the extent of chromosomal damage caused by hydrogen peroxide was tested.

Procedure

Exponentially growing hTERT-RPE1 cells were treated with 0, 10, 50 and 100 μM H_20_2 for 20 minutes on ice. They were then left to recover in fresh medium for 30 minutes at 37°C and further incubated with colcemid 0.1 μg/ml for 1 hour. Metaphase spreads were prepared as described in section 2.6. 10 μl of the samples were dropped on to slides and air dried before being stained with 10% Giemsa in Gurr's buffer, washed in first Gurr's buffer and then water and finally air dried again. Other metaphase spreads were stained with 12 μl DAPI/vectashield.

Results and discussion

The effect of colcemid incubation was discussed in section 3.5. Incubation of cells with 50 or 100 μM H_20_2 did not result in any cells visible in mitosis suggesting that the amount of DNA damage caused by H_20_2 induced the G_2 checkpoint. Figure 6.1 shows the effect of 10 μM H_20_2 on hTERT-RPE1 cells. Unlike non-treated cells, after 10 μM H_20_2 treatment chromosomes appeared fragmented and entangled, and chromosomal 'dots' (red arrows in Figure 6.1) were also seen. It has been shown that H_20_2 can excise chromatin loops through its effect on topo IIα [126]. I thought that these 'dots' might be equivalent to excised chromatin loops. In order to confirm that these 'dots' were composed of DNA, cells were stained with the DNA-binding fluorescent dye DAPI rather than Giemsa. Figure 6.2 shows that the 'dots' do indeed stain with DAPI and so can definitely be identified as DNA.

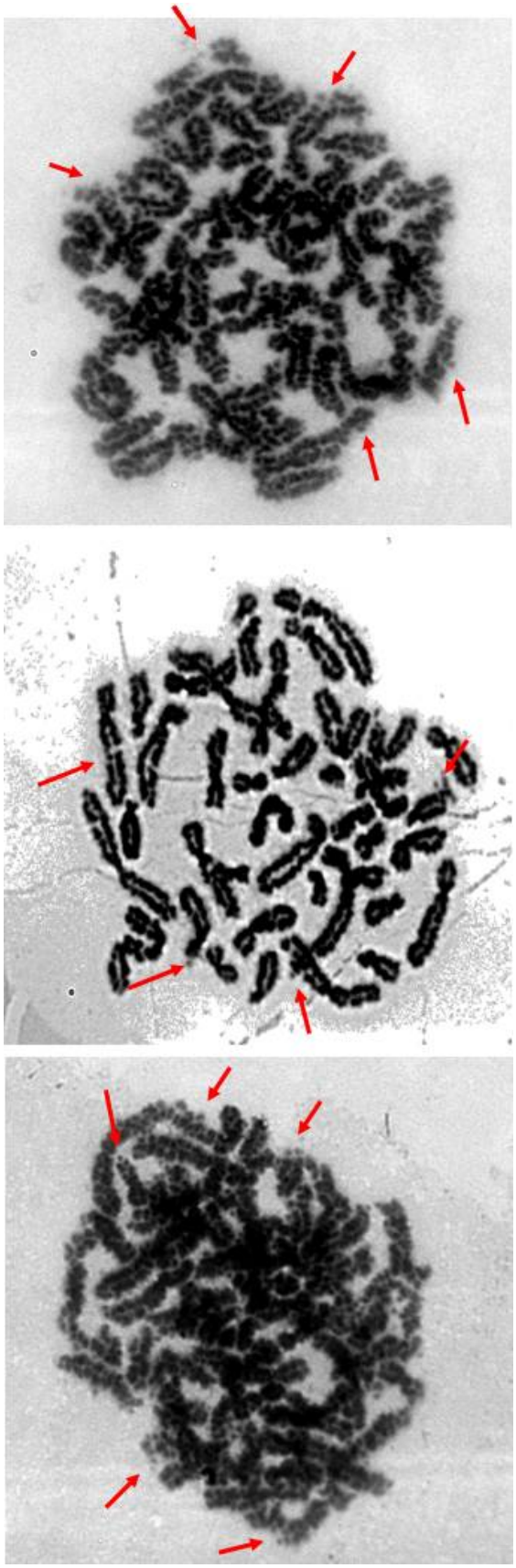

Figure 6.1: Photomicrographs of Giemsa-stained 10 μM H_20_2-treated hTERT-RPE1 cells at x100 magnification. The red arrows point to chromosomal damage that appear as 'dots'.

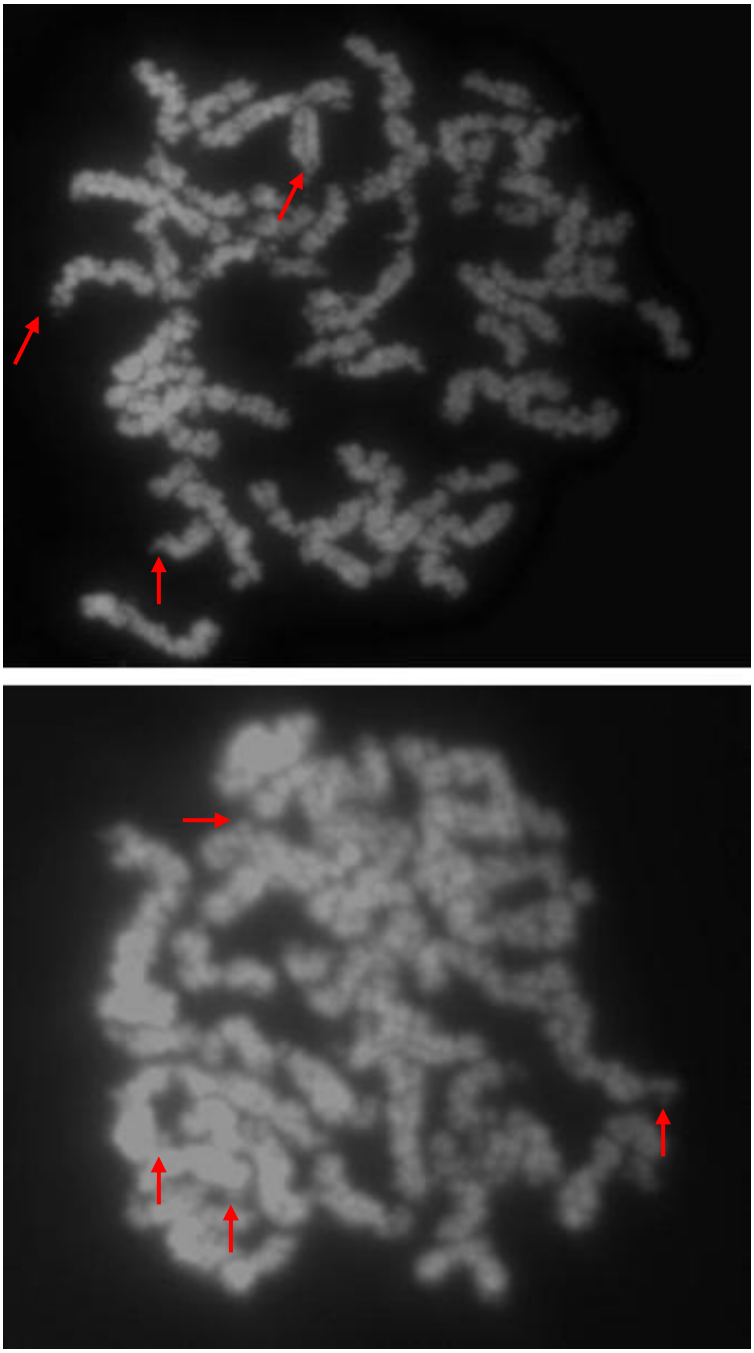

Figure 6.2: Photomicrograph of DAPI-stained 10 μM H_20_2-treated hTERT-RPE1 cells at x100 magnification. The red arrows point to some chromosomal damage that appear as 'dots'.

6.4 Are chromosome 'dots' produced by H_2O_2 excised chromatin loops?

To determine if chromosome 'dots' seen in H_20_2-treated cells were excised chromatin loops, metaphases were analysed by atomic force microscopy (AFM) in order to greatly increase resolution.

Procedure

Exponentially growing hTERT-RPE1 cells were treated with 0 or 10 μM H_20_2 for 20 minutes on ice. Cells were then left to recover in fresh medium for 30 minutes at 37°C and further incubated with colcemid 0.1 μg/ml for 1 hour. Metaphase spreads were prepared as described in section 2.6. 10 μl of the samples were added to slides and air dried before being stained with 1% or 10% Giemsa in Gurr's buffer for 10 minutes at room temperature, washed first in Gurr's buffer followed by water and finally air dried again.

The prepared samples were imaged at room temperature using AFM. This was done in collaboration with Francis McCarthy working for Georg Haehner at the School of Chemistry, University of St Andrews. Figure 6.3 shows a schematic of the underlying principles of an AFM. The AFM was used in contact mode, where the force between the tip and the sample surface was kept constant during scanning. In AFM when a force is exerted on the cantilever, any change in sample surface 'bends' the cantilever so as to maintain a constant force. Laser light is reflected off the cantilever onto a photodiode detector, which with appropriate electronics produces voltage from incident light. A change in sample surface causes the cantilever to bend, resulting in reflection angle variation. A change of the position of the light on the photodiode ultimately changes the voltage output. The sample was scanned using a piezoelectric translation stage scanner, which is made with piezoelectric crystals that can expand and contract when voltage is applied allowing for very fine control of movement.

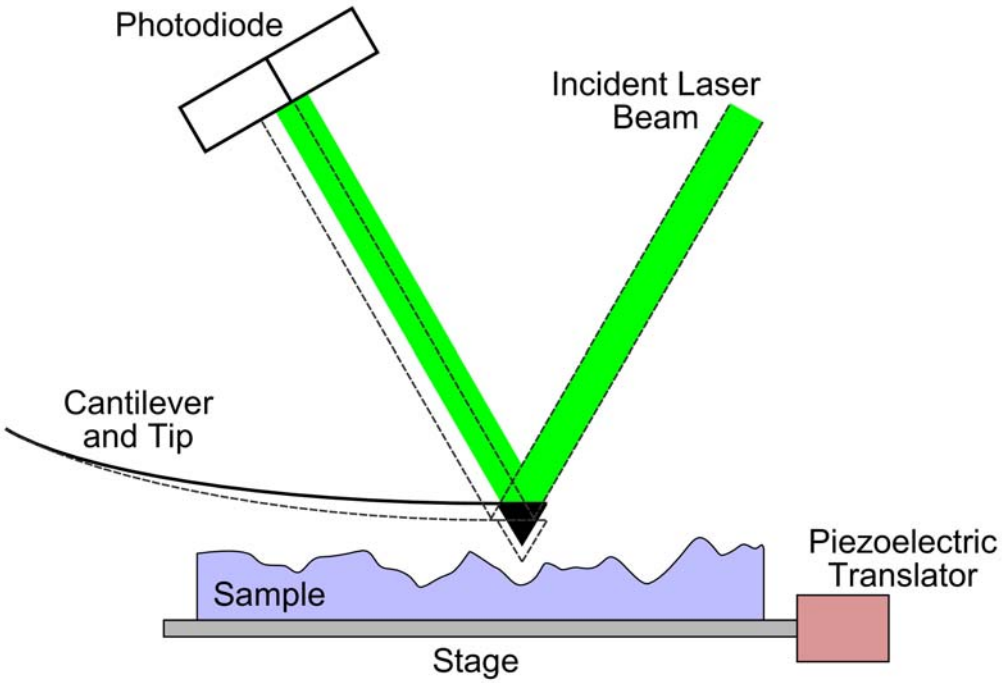

Figure 6.3: Diagram of AFM imaging. The dashed lines indicate a movement of the cantilever due to altered sample surface which in turn changes the reflection of the laser onto the photodiode.

The load applied to the sample ranged from 5 – 10 nN but was constant within each scan. Data was analysed with Gwyddion 2.12 that was developed by David Nečas and Petr Klapetek and supported by the Czech Metrology Institute. Most images were flattened with the provided software to eliminate low-frequency background noise during scanning detection. 3-dimensional (3D) images were acquired with the same software.

The AFM was invented by Binnig *et al.* [315] and has become a very useful tool for the analysis of biological samples. It was used here as it did not require any complex treatment of the sample and therefore chromosomal structures would remain unaltered. It was ensured that forces applied to the cantilever were low as high forces in contact mode AFM can move or affect the surface structure. AFM has been used for chromosomal analysis before, such as looking at the surface of ring chromosomes after 10 Gy X-irradiation (Figure 6.4) [316]. Figure 6.4 clearly shows that ring structures can be visualised with AFM. Chromatid gaps induced by a neon beam have also been observed by AFM [317]. The AFM had also been used to look at plasmid DNA linearisation after γ-irradiation [318].

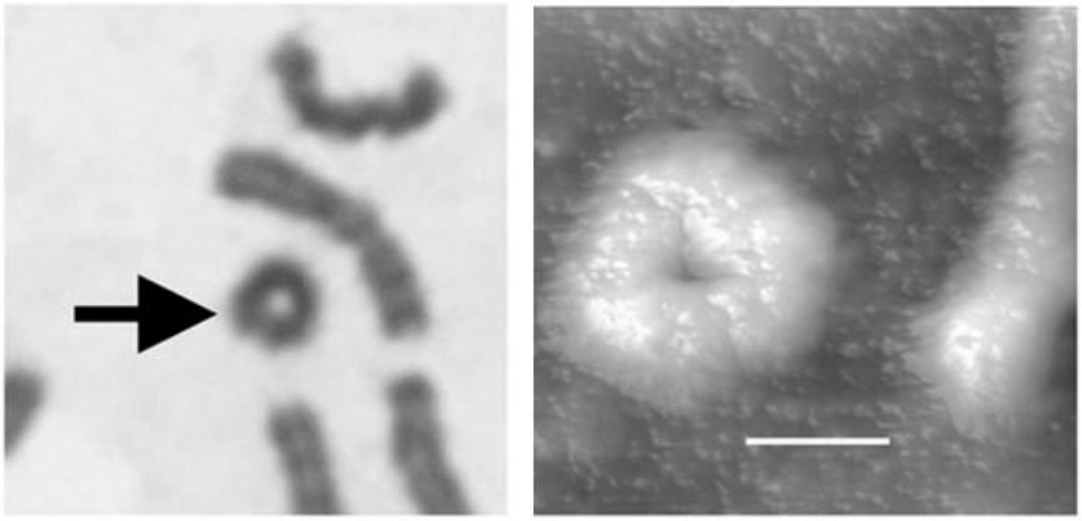

Figure 6.4: Giemsa-stained light microscopy (**A**) and AFM image (**B**) of a ring chromosome induced by X-irradiation (10 Gy). Reprinted from Murakami *et al*. 2004 [316] (with permission from Elsevier Inc. publisher). Bar = 1 μm.

Results and discussion

Figure 6.5A shows chromosomes from 10 μM H_2O_2-treated hTERT-RPE1 cells imaged by AFM. Consecutive images zoom in on a chromosomal 'dot'. The AFM allowed the imaging of sample surfaces with increasing spatial resolution starting from 80 x 80 μm down to 3.5 x 3.5 μm in multiple increments. The 3D images in 6.5B allowed for even more interesting chromosome structure analysis. Focussing in on a chromosome 'dot' using AFM might have allowed us to determine if this 'dot' was in fact a chromosomal loop that had been excised in these cells. However this was not possible here as the resolution below 3.5 μm x 3.5 μm was not good enough to determine the topography of the chromosome. We showed that the chromosomal 'dots' were approximately 0.4 μm in length. The third picture of Figure 6.5A shows horizontal scratches (red arrow) that were due to the tip having picked up some debris that was then dragged along during scanning.

It is possible that the resolution was affected by the 10% Giemsa stain. Murakami *et al*. [317] found that Giemsa staining reduced the resolution of AFM imaging such that analysis at the nanometer level was not possible. They did not however specify the percentage of Giemsa used nor the incubation time. Others [319] however have managed to compare Chinese hamster ovary and human chromosomal structure with AFM at the nanometer level after 10% Giemsa staining for 8 minutes. Therefore the effect of 10% Giemsa on chromosomal analysis by AFM is still unclear. Although perhaps chromosomal analysis by AFM might best be achieved in non-stained samples, this would be extremely challenging as without phase-contrast microscopy attached to the AFM, metaphases could not be located. Also scanning a whole non-stained slide to find a 'well-spread' metaphase was not a possibility as the maximum

range that could be scanned using this AFM set-up was 80 μm x 80 μm. The remaining experiments were therefore carried out using only 1% Giemsa.

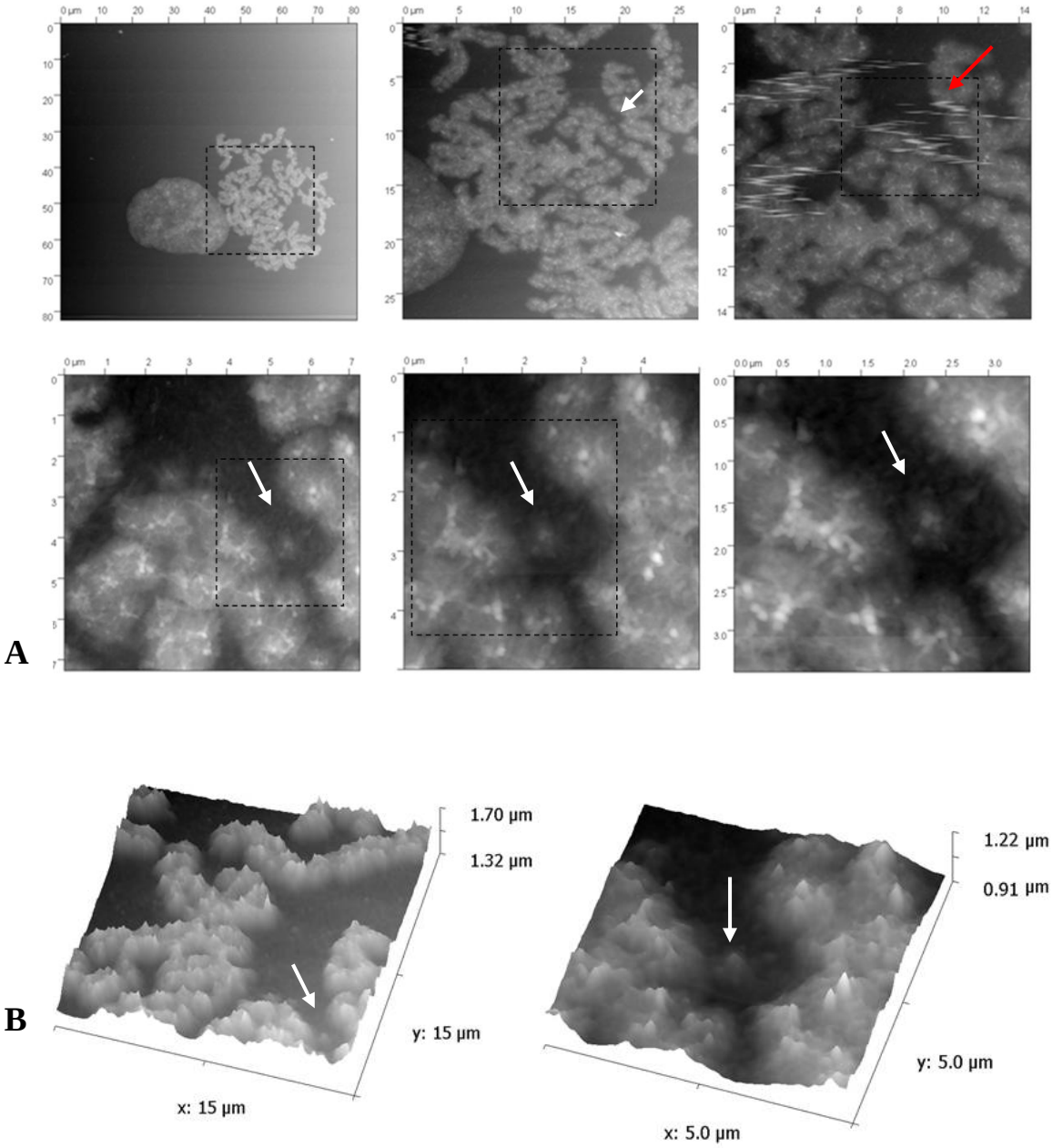

Figure 6.5: AFM images (**A**) and 3D chromosomal images (**B**) of hTERT-RPE1 cells treated with 10 μM H_20_2 and stained with 10% Giemsa. The boxed area defines the total area scanned in the next image. White arrows point to chromosomal 'dots'. The red arrow points to a scratched area.

Next, untreated control metaphases stained with 1% Giemsa were analysed by AFM. Figure 6.6 shows that the AFM technique does not affect chromosomal structure as cells not treated with H_2O_2 show no chromosomal damage and this confirms that the chromosomal 'dots' seen in Figure 6.5 were caused by H_2O_2. Also chromosomes stained with 1% Giemsa could be

analysed by the AFM with increased accuracy when compared to chromosomes stained with 10% Giemsa as structures were clearly distinguishable at 2 μm x 2 μm or lower. The change of shade of the image at 45 μm x 45 μm was a result of increasing the force slightly to get a clearer picture.

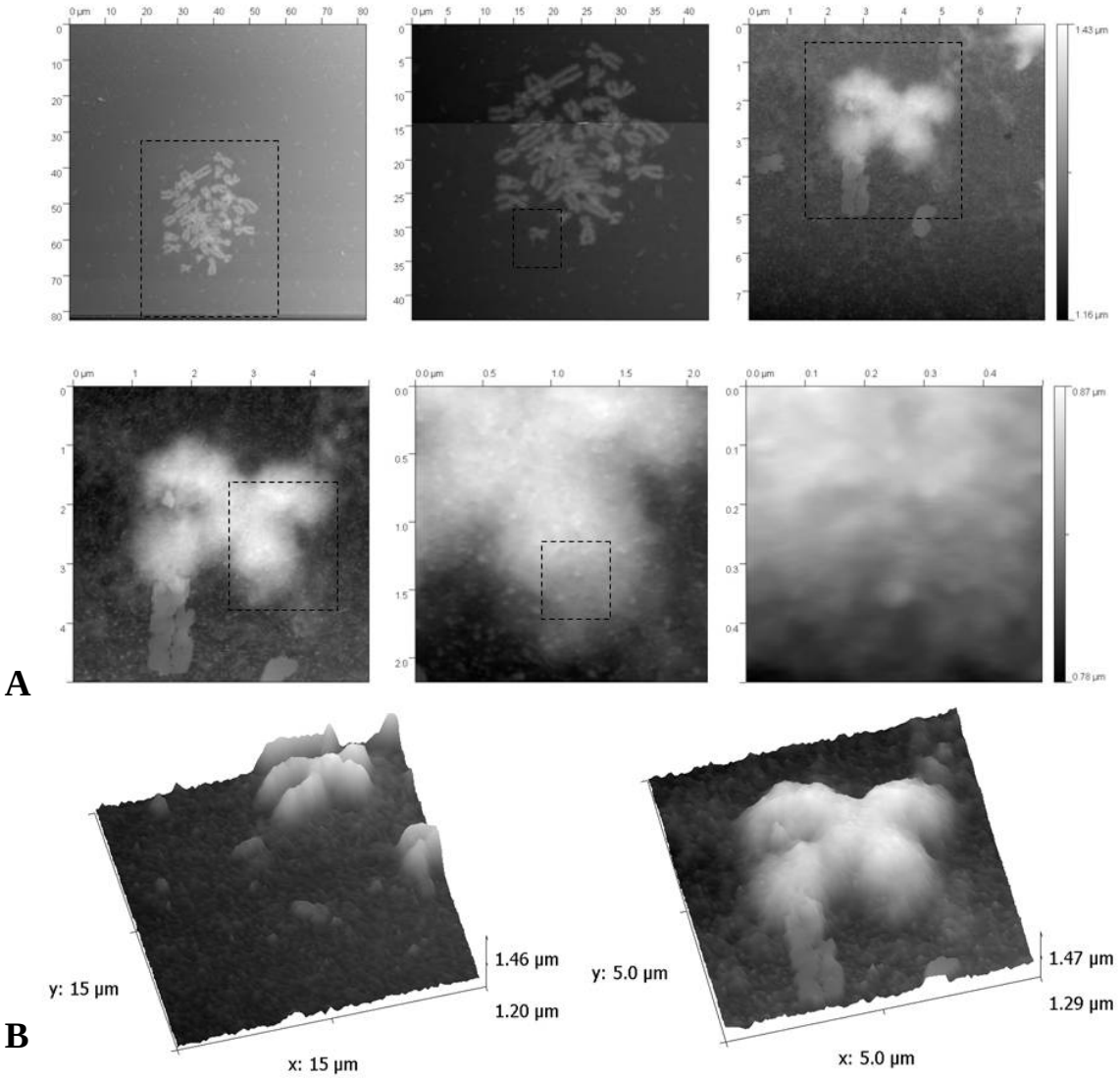

Figure 6.6: AFM images (**A**) and 3D chromosomal images (**B**) of control hTERT-RPE1 cells stained with 1% Giemsa. The boxed area defines the total area scanned in the next image.

Finally 10 μM H_20_2-treated cells stained with 1% Giemsa were analysed by AFM. Figure 6.7 shows that chromosomes were damaged and that 'dots' were formed again. The last of the consecutive images shows a 'dot' at a high resolution. Interestingly, the 'dot' does look as though it might be a ring. The height profiles in Figure 6.7B indicate that the dot's surface does indeed decrease in height which might refer to the 'hole' of a loop even though it is not in the middle of the 'dot'. This might perhaps be due to the preparation of the sample. Given

the experimental time available, the results presented here are not ideal, therefore it is not possible to say that Figure 6.7 confirms that H_2O_2-induced chromosomal 'dots' are excised chromatin loops. They do however indicate what might be achieved with AFM in the analysis of H_2O_2-induced DNA damage in future experiments.

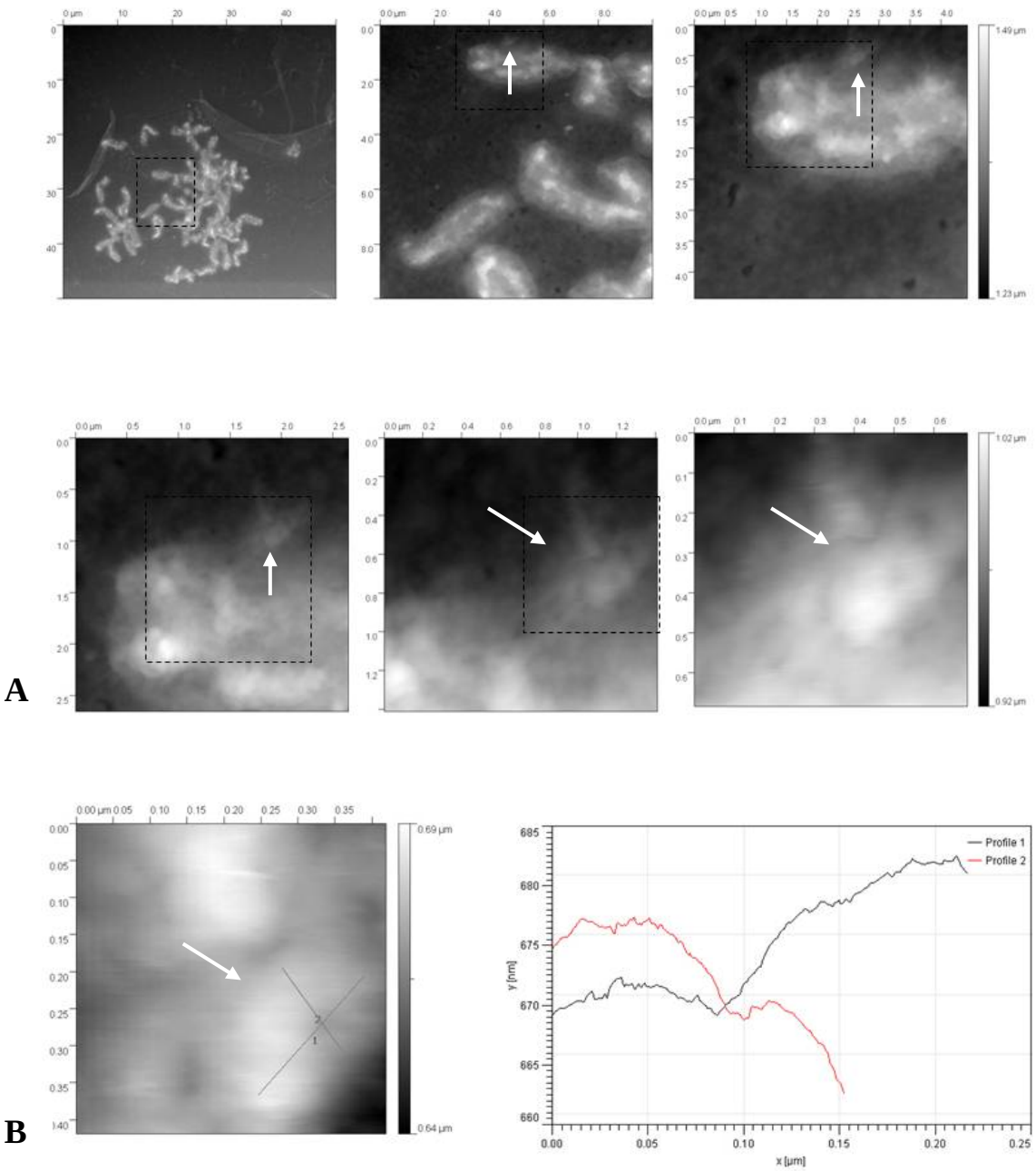

Figure 6.7: AFM images (**A**) and height profiles (**B**) of hTERT-RPE1 cells treated with 10 μM H_20_2 and stained with 1% Giemsa. The boxed area defines the total area scanned in the next image. White arrows point to chromosomal 'dots'.

6.5 Does H_2O_2 induce chromosomal and DNA damage via topo IIα?

It is clear that hydrogen peroxide induces chromosomal damage. To try to confirm that the 'dots' (putative loops) were a result of topo IIα, the effect of the catalytic topo IIα inhibitor ICRF-193 on chromosomal damage was tested. A role for topo IIα in hydrogen peroxide-induced DNA damage was also investigated.

6.5.1 Chromosomal damage

Procedure

hTERT-RPE1 cells were treated with 0 or 10 μM H_20_2 for 20 minutes on ice after incubation with 100 nM ICRF-193. Cells were allowed to recover from H_20_2 treatment in fresh medium still containing 0 or 100 nM ICRF-193 for 30 minutes at 37°C and further incubated with colcemid 0.1 μg/ml for 1 hour. Total ICRF-193 treatment was 2 hours. Metaphase spreads were prepared as described in section 2.6. 10 μl of the samples were added to slides and air dried before being stained with 10% Giemsa in Gurr's buffer for 10 minutes at room temperature, washed first in Gurr's buffer and then water and finally air dried again.

Exponentially growing hTERT-RPE1 cells were also treated with H_20_2 ranging from 1 nM to 1 mM and incubated on ice for 20 minutes. Cells were then left to recover in fresh medium for 30 minutes at 37°C and further incubated with colcemid 0.1 μg/ml for 1 hour. Metaphase spreads were prepared as described above. Other metaphase spreads were stained with 12 μl DAPI/vectashield.

Results and discussion

It was found that metaphases of cells treated with 100 nM ICRF-193 still demonstrated normal chromosomal structure (section 5.3.1). As discussed in section 5.3, 100 nM ICRF-193 targets only topo IIα. Figure 6.8 shows that although chromosomes still appeared damaged and entangled as seen in Figure 6.1, the frequency of not only hydrogen peroxide-induced 'dots' but also chromosomal fragmentation was severely reduced by ICRF-193. Therefore, although only qualitative observations were made, the results presented here do suggest that topo IIα is not only involved in the formation of the DNA 'dots' but also in chromosomal fragmentation.

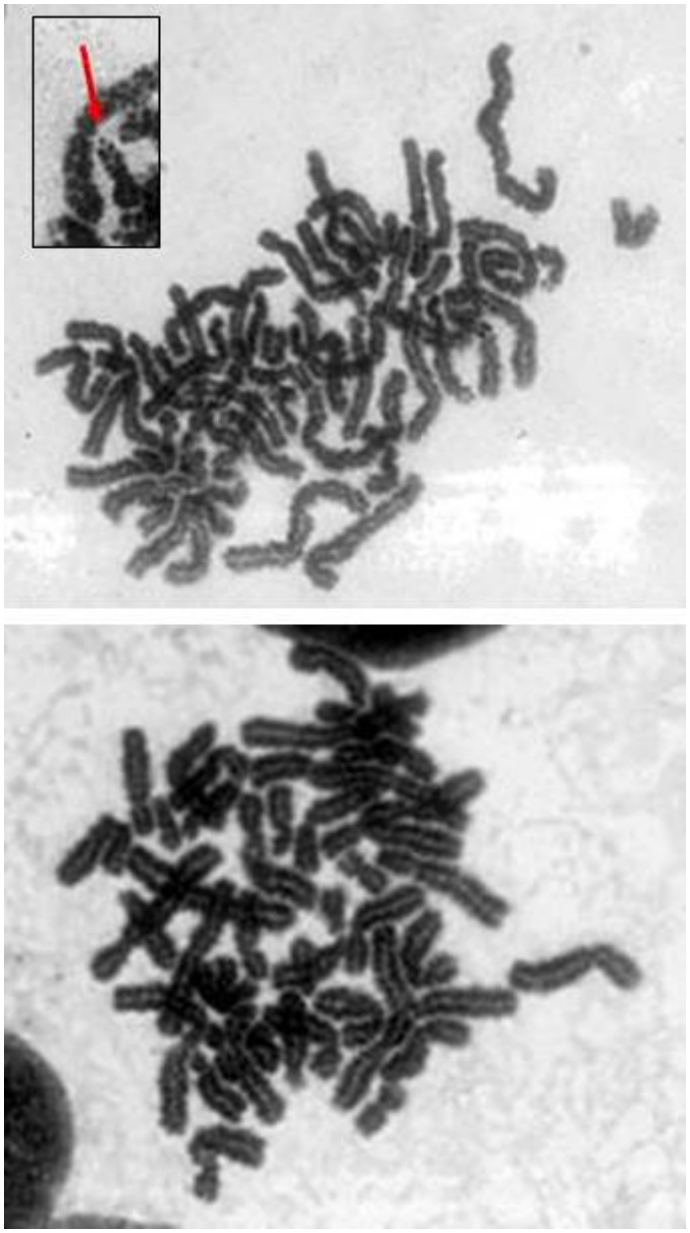

Figure 6.8: Photomicrograph of Giemsa-stained 10 μM H_20_2-treated hTERT-RPE1 cells after 100 nM ICRF-193 incubation at x100 magnification. The inset picture is an example of chromosomal damage after incubation with 10 μM H_20_2 in hTERT-RPE1 cells (derived from bottom panel in Figure 6.1). The red arrow indicates a chromosomal 'dot'.

Originally I aimed to determine the range of H_2O_2 concentrations where chromatid breaks were formed so as to calculate the number of chromatid breaks per cell and how ICRF-193 affected this. However the ideal range of H_2O_2 concentration to produce just chromatid breaks was never quite determined, as at the lower doses (1 and 10 nM H_2O_2) no damage occurred, yet at the higher dose (>0.1 μM) damage was too high to calculate chromatid break frequency as DNA became fragmented. However, the red arrows in figure 6.9 show that at 0.1 μM H_2O_2, many chromosomal 'dots' are already visible that were also evident in cells treated with 10 μM

H_2O_2 (Figures 6.1 and 6.2). Chromatid breaks, such as those formed after IR, were not typically seen after incubation with 0.1 μM H_2O_2. As in the previous figures, these chromosomal 'dots' were proven to be DNA when stained with DAPI (Figure 6.10). In the previous section the effect of 100 nM ICRF-193 on H_2O_2-induced chromosomal damage was tested. Here however, a lower frequency of these 'dots after treatment with H_2O_2 at 0.1 μM would be hard to quantify and hence chromosomal structure was not looked at after cells were treated with both ICRF-193 and 0.1 μM H_2O_2.

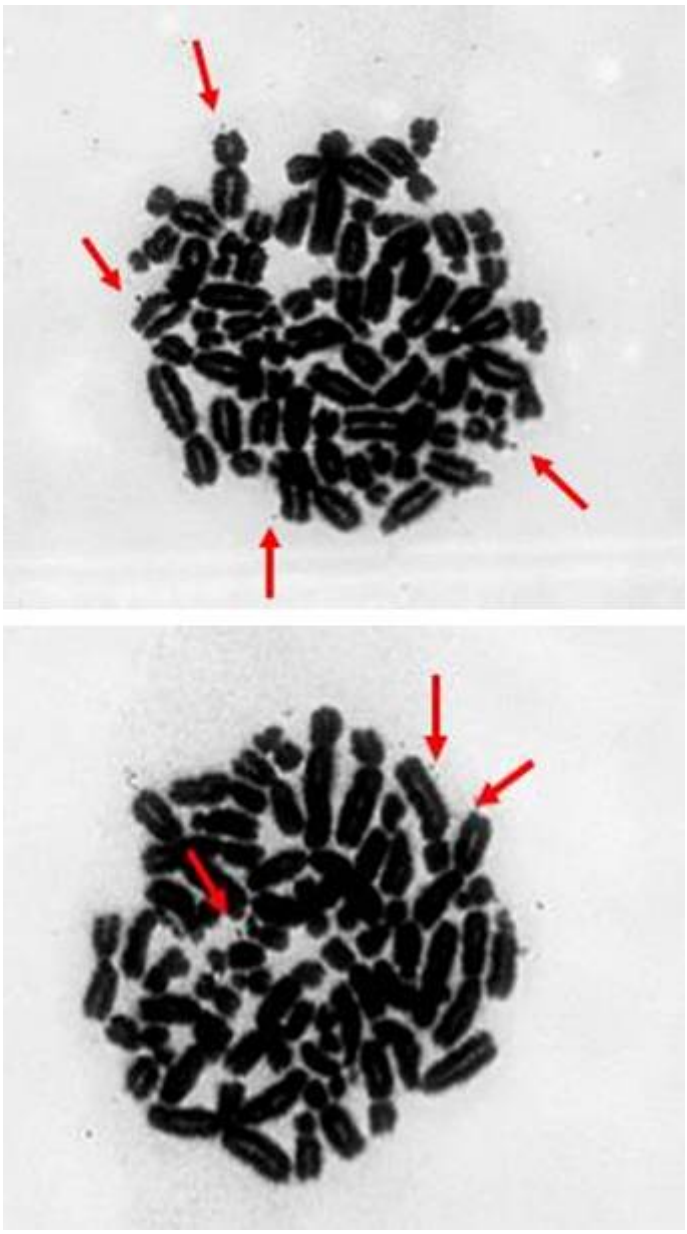

Figure 6.9: Photomicrograph of Giemsa-stained 0.1 μM H_20_2-treated hTERT-RPE1 cells at x100 magnification. The red arrows point to chromosomal damage that appear as 'dots'.

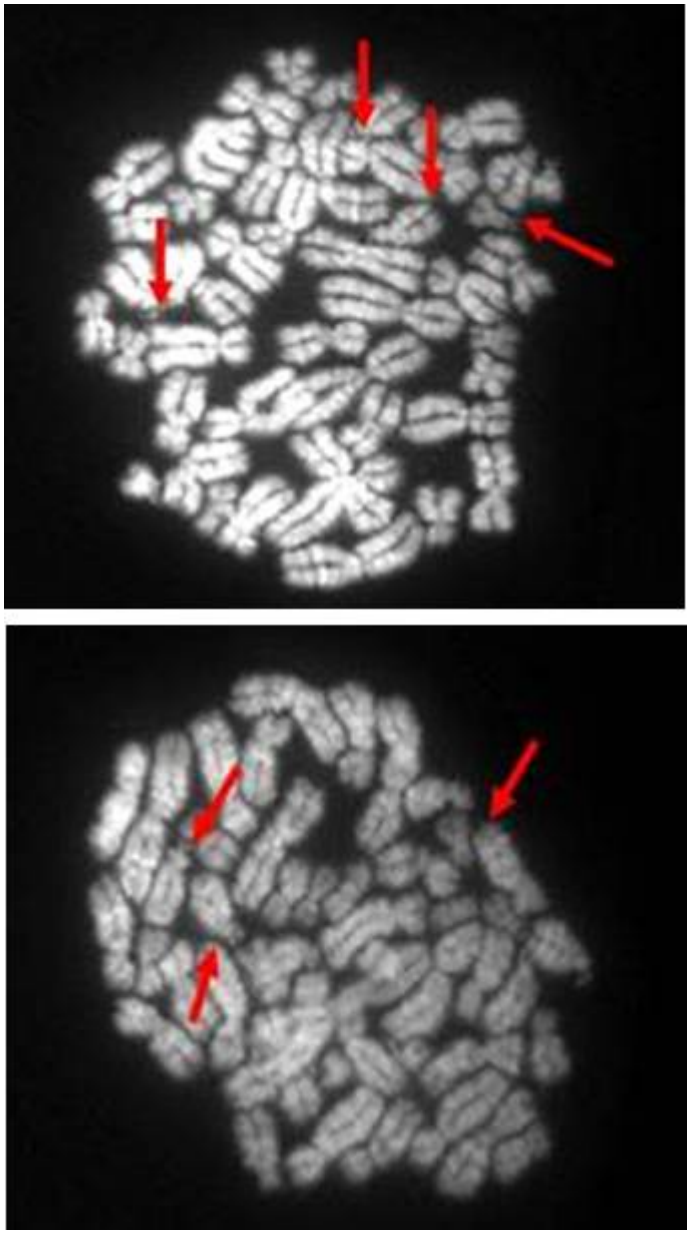

Figure 6.10: Photomicrograph of DAPI-stained 0.1 μM H_20_2-treated hTERT-RPE1 cells at x100 magnification. The red arrows point to chromosomal damage that appear as dots.

It has previously been shown that topo IIα is involved in the excision of chromosomal loops after oxidative stress [126]. It is therefore possible that the 'dots' are excised chromosomal loops. If topo IIα is able to excise chromosomal loops, it would confirm the possibility of topo IIα being involved in chromatid break formation too as 'omega' loops (Figure 1.7) can be thought of as chromosomal loops not yet excised.

6.5.2 DNA damage

Procedure

The single or double strand break origin of chromosomal damage at 0.1 μM H_20_2 was also investigated. SSB induction in 0, 0.1, 1 and 10 nM H_2O_2-treated hTERT-RPE1 cells was measured by the alkaline comet assay described in section 2.13. Hydrogen peroxide was added for 20 minutes on ice. The tail moment in control cells was subtracted from the results of H_20_2-treated cells. Experiments were carried out in duplicate.

DSB break induction was measured by low voltage gel electrophoresis in exponentially growing hTERT-RPE1 cells treated with 0, 0.01, 0.1, 1, 10, 100 and 1000 μM H_2O_2 for 20 minutes on ice. Cells were then trypsinised and DSBs measured as described in section 2.7.1. DSB induction in 0.1 μM H_2O_2-treated cells, synchronised in G_0 by serum starvation, was also measured with immunocytochemistry against γH_2AX after 20 minutes recovery as described in section 2.7.1. All DSB experiments were carried out in triplicate.

hTERT-RPE1 cells were also treated with or without 0.1 μM H_2O_2 for 0, 5, 10, 20 and 40 minutes on ice or 1 mM H_2O_2 for 20 minutes on ice which served as a positive control. In other experiments cells were treated with 1 mM or 10 μM H_2O_2 for 20 minutes. Certain samples treated with 1 mM H_2O_2 were allowed to recover in H_2O_2-free medium at 37°C for 0, 15 or 30 minutes. In all experiments, cells had previously been incubated with or without 100 nM ICRF-193 for 2 hours. Cells were then trypsinised (section 2.1.2) and DSBs measured by either low voltage gel electrophoresis or immunocytochemistry against γH_2AX as described in section 2.7.1.

Results and discussion

Chromosomal damage is generally attributed to DSBs. This is also the case here where damage to chromosomes in metaphases are analysed only 2 hours after H_2O_2 treatment. As mentioned in section 4.4, it is unlikely that metaphases analysed at the time interval used here include S-phase cells. Therefore most of the damage seen in chromatids must be due to DSBs rather than SSBs, as SSBs could not have been transformed into DSBs after replication. It was important to establish which doses of H_20_2 caused SSBs only or both SSBs and DSBs in hTERT-RPE1 cells, as I wanted to determine if the chromosomal damage seen at 0.1 μM H_20_2 was caused by SSBs or DSBs.

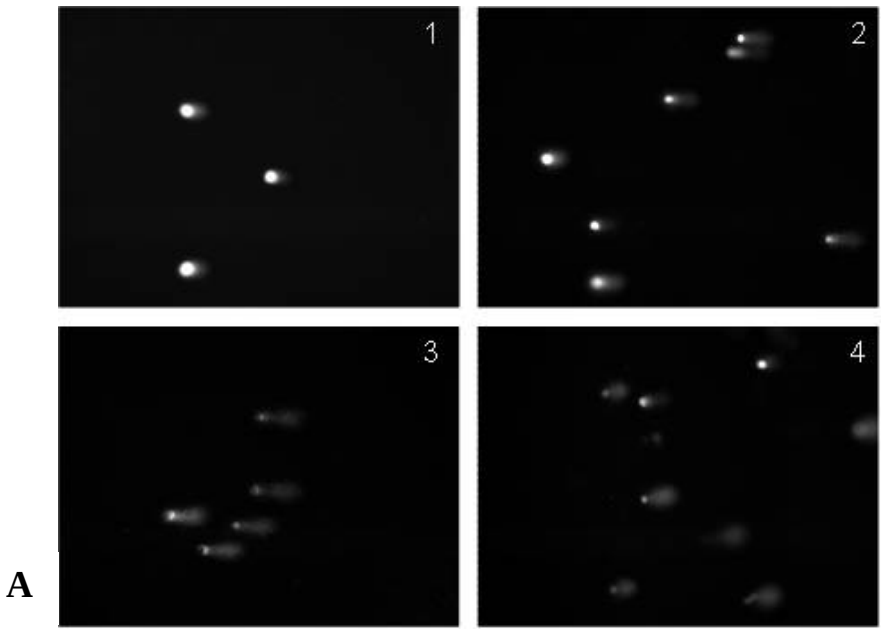

A

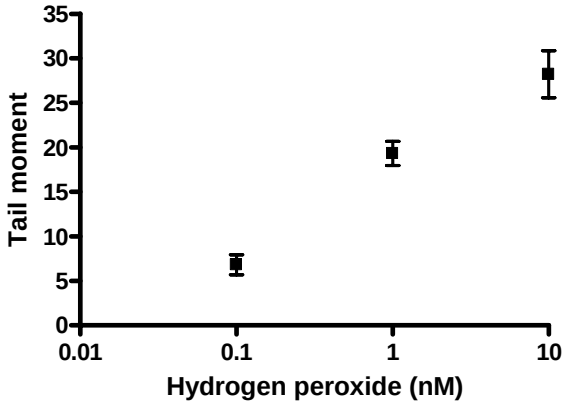

B

Figure 6.11 A: Induction of single strand breaks as determined by the alkaline comet assay in hTERT-RPE1 cells treated with 0 (panel 1), 0.1 (panel 2), 1 (panel 3) and 10 nM (panel 4) H_2O_2. DNA was labelled with propidium iodide. Pictures were taken at x10 magnification. **B**: Analysis of Figure 6.11A. The background value determined in control (non-treated) cells was subtracted from all samples. Error bars represent standard errors of the mean for 50 cells in duplicate experiments.

SSB induction was measured using the alkaline comet assay. Figure 6.11A shows that H_2O_2 at 0.1 nM caused SSBs and that the number of SSBs increased with H_2O_2 dose. Tail moments as quantified by Comet Assay IV (Figure 6.11B) were 6.8, 19.3 and 28.2 at 0.1, 1 and 10 nM H_2O_2 respectively. Therefore at 0.1 μM H_2O_2, the concentration that induced chromosomal damage in Figures 6.9 and 6.10, many SSBs were formed.

Figure 6.12 shows that the number of DSBs increased with H_20_2 dose between 10, 100 and 1000 μM with the fraction of DNA released (FDR) equal to 0.09, 0.14 and 0.34 respectively. This shows that higher concentrations of H_2O_2 are needed to induce DSBs than SSBs. DSB induction was visible only at concentrations ≥10 μM H_20_2. This is interesting as previous studies have shown that DSBs are formed at concentrations ≥ 100 μM H_20_2 [320] and therefore no DSBs would be formed at 10 μM H_20_2 unlike here. This is most likely due to the neutral elution assay being less sensitive than the low voltage gel electrophoresis assay. When comparing the FDR at 10 μM H_2O_2 with data collected from Figure 5.6, it can be determined that this concentration is equal to a dose of approximately 13 Gy γ-radiation in terms of DSB induction. To confirm that no DSBs were present at 0.1 μM H_2O_2, cells were also probed against γH_2AX as this assay is more sensitive than the low voltage gel electrophoresis assay as discussed in section 5.5.

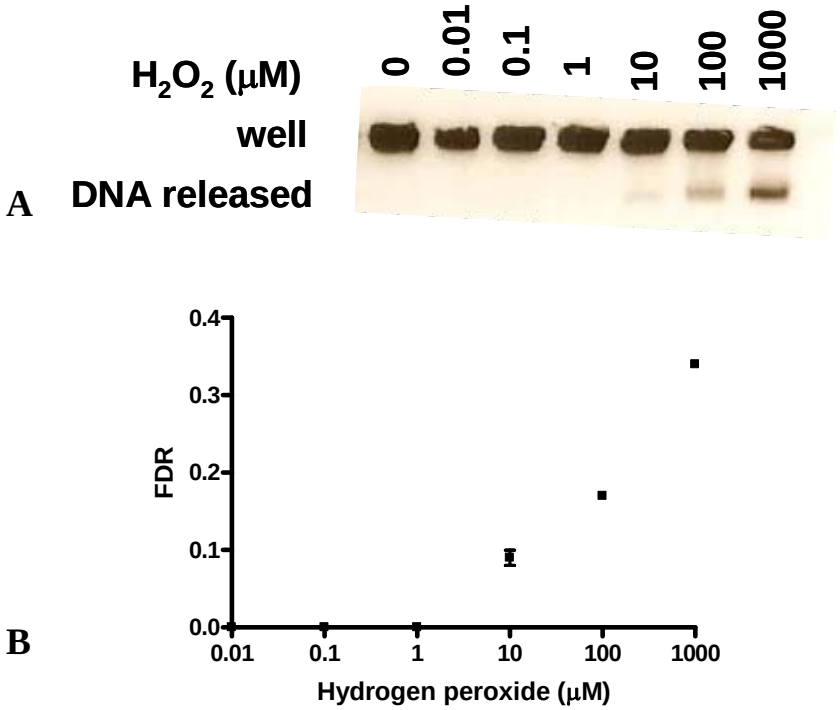

Figure 6.12 A: Induction of DSBs in hTERT-RPE1 cells treated with varying concentrations of H_2O_2. DNA was labelled with ethidium bromide. **B**: Analysis of figure 6.12A with FDR is equal to frequency of DNA released (from well) and was determined as described in section 2.7.1. Error bars represent standard deviations from the mean in triplicate experiments.

Figure 6.13 confirms that 0.1 μM H_2O_2 does not induce DSBs as H_2O_2-treated cells averaged 0.69 γH_2AX foci per cell, a value close to that found in control cells (0.64 foci per cell). The results shown in Figure 6.13 pose some interesting questions about the formation of H_2O_2-induced chromosomal damage. How is chromosomal damage such as the formation of chromosomal 'dots' and fragmentation caused in the absence of DSBs? Also the damage caused at 10 μM H_2O_2, where chromosomes looked fragmented and 'dots' were formed, seems disproportionate with the damage at 0.1 μM H_2O_2, where only chromosomal 'dots' were visible. It is possible that topo IIα is involved as $^{\cdot}$OH radicals are known to 'poison' topo II which as mentioned earlier is an enzyme that under these conditions causes DSBs [126]. At 10 μM H_2O_2 one might consider that the effect of $^{\cdot}$OH radicals on topo IIα is much larger than at 0.1 μM resulting in more complex chromosomal damage. The role of topo IIα in the formation of DSBs will be the focus of the latter part of this chapter.

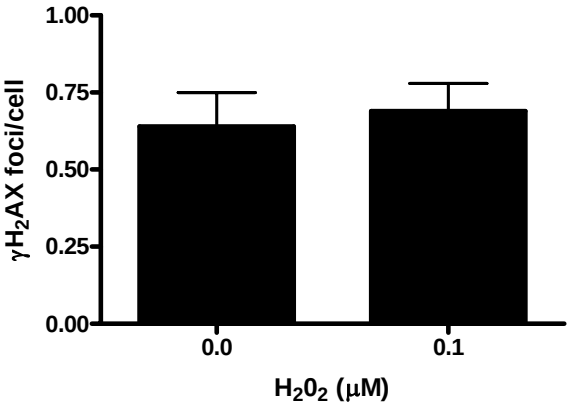

Figure 6.13: Number of γH_2AX foci per cell in control and H_2O_2-treated (0.1 μM) hTERT-RPE1 cells. The number of foci for each sample was determined for 100 cells in triplicate by immunocytochemistry. Cells were probed with anti-mouse-FITC-conjugated secondary antibodies against the primary mouse anti-γH_2AX antibody as well as DAPI. Error bars represent standard errors from the mean for triplicate experiments.

If topo IIα is indeed involved in causing chromosomal damage after incubation with 0.1 μM H_2O_2 where no DSBs are formed, perhaps increased incubation time of H_2O_2 would result in the formation of DSBs due to topo IIα poisoning and ICRF-193 would inhibit this. Figure 6.14 shows that even after 40 minutes incubation with 0.1 μM H_2O_2 still no DSBs were formed. This was not due to experimental error as incubation with 1 mM H_2O_2 for 20 minutes did result in DSBs. As no DSBs were formed at 0.1 μM H_2O_2, the role of topo IIα could not be established through ICRF-193 treatment. Figure 6.14 does however again confirm that 100 nM ICRF-193 does not induce DSBs. Perhaps the time period of this experiment (40 minutes) was too short to see any DSBs formed at 0.1 μM H_2O_2 as observation of the spread chromosomes was carried out 1.5 hours after a 20 minute H_2O_2 treatment.

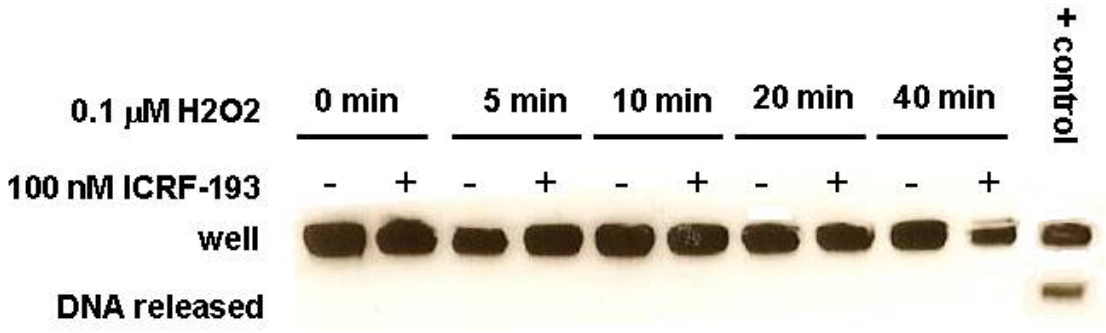

Figure 6.14: DSB induction in hTERT-RPE1 cells incubated with or without 100 nM ICRF-193 and then treated with 0.1 μM H_2O_2 for 0, 5, 10, 20 or 40 minutes. The positive control is DNA from cells treated with 1 mM H_2O_2 for 20 minutes. DNA was labelled with ethidium bromide.

Next, the effect of ICRF-193 on 1 mM H_2O_2 treatment was tested. It was already established that 1 mM H_2O_2 causes DSBs (Figure 6.12) and if topo IIα is involved in causing chromosomal damage, which is usually caused by DSBs, perhaps inhibition of DSB formation by ICRF-193 might be visualised. Figure 6.15 shows that treatment of cells with 100 nM ICRF-193 before incubation with 1 mM H_2O_2 decreases DSB induction. The FDR at 1 mM H_2O_2 decreased significantly ($p=0.04$) from 0.28 to 0.22 after ICRF-193 incubation. As discussed in Chapter 3 the p-value is defined here as the probability of obtaining the results assuming the null hypothesis is correct. Here the significance level is taken as 5% (0.05) so any p-value obtained below 0.05 is statistically significant. These DSB induction results suggest that topo IIα is involved in the formation of H_2O_2-induced DSBs.

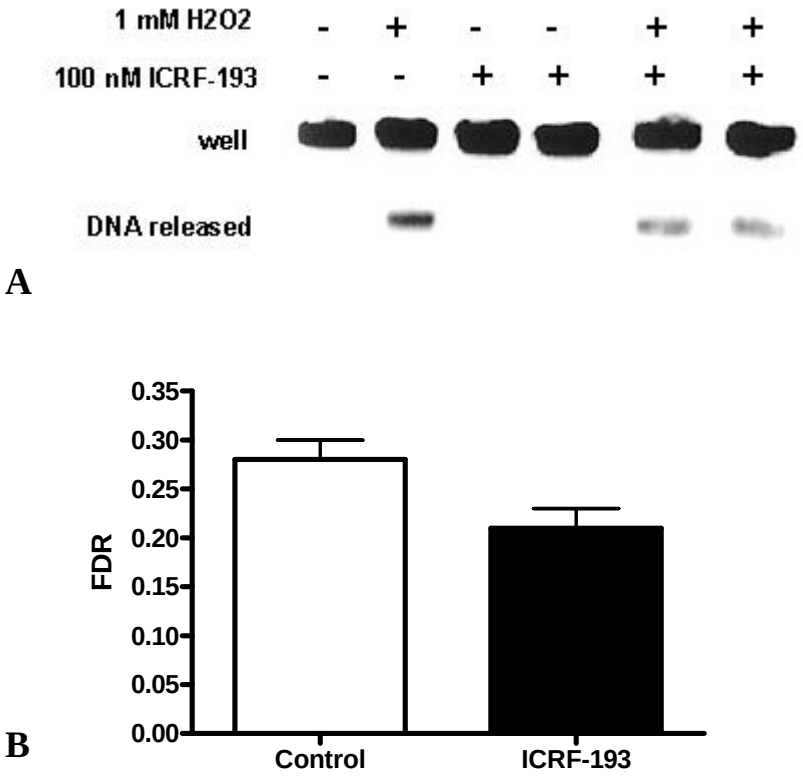

Figure 6.15 A: Induction of DSBs in hTERT-RPE1 cells treated with or without 1 mM H_2O_2 or 100 nM ICRF-193. DNA was labelled with ethidium bromide. **B**: Analysis of figure 6.15A with FDR equal to frequency of DNA released (from well). The FDR was determined as described in section 2.7.1. Error bars represent standard errors of the mean from duplicate experiments.

If H_2O_2 does cause DSBs, does the number of DSBs increase with time after treatment because topo IIα is poisoned by the $^{\cdot}OH$ radicals? Figure 6.16 shows the fraction of DNA released in cells incubated with or without ICRF-193, then treated with 1 mM H_2O_2 for 20 minutes, and then left to recover for different lengths of time in fresh medium. Figure 6.16 shows that recovery after H_2O_2 treatment decreased the number of DSBs found suggesting that DSB repair occurred. It therefore suggests that topo IIα is not involved in H_2O_2-induced DSB formation after H_2O_2 treatment of 20 minutes as the number of DSBs did not increase with time. Perhaps topo IIα did induce further DSBs, but they took longer to form than to be rejoined. As in Figure 6.15, inhibiting topo IIα with ICRF-193 decreased the number of DSBs formed after 1 mM H_2O_2 treatment. What is interesting is that ICRF-193 still decreased DSB formation even after 30 minutes of recovery from H_2O_2 when compared to H_2O_2-alone treated samples.

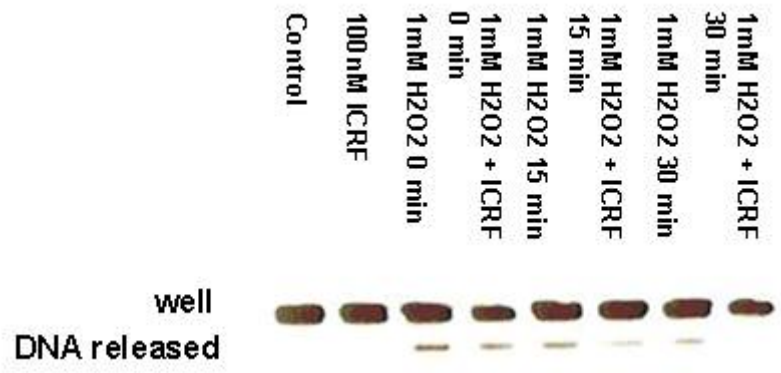

Figure 6.16: DSB induction in hTERT-RPE1 cells incubated with or without 100 nM ICRF-193 and then treated with 1 mM H_2O_2 for 20 minutes on ice and allowed to recover in H_20_2-free medium for 0, 15 or 30 minutes. DNA was labelled with ethidium bromide.

As ICRF-193 affected the number of DSBs after 1 mM H_2O_2 treatment, perhaps the same trend would be seen in cells treated with 10 μM H_2O_2, another dose that causes DSBs (Figure 6.12). DSB induction was first measured by immunocytochemistry against γH_2AX as this method is far more sensitive than low voltage gel electrophoresis. The reason the γH_2AX method was not used to measure DSB induction in 1 mM H_2O_2-treated cells was because the number of foci per cell would have been too high to measure accurately. Figure 6.17 shows that the number of γH_2AX foci increases after 10 μM H_2O_2-treatment from 0.5 foci per cell to 19 foci per cell. Incubation with 100 nM ICRF-193 alone did not increase DSB frequency (0.5 foci per cell) and also did not affect DSB frequency after 10 μM H_2O_2 treatment either (19 foci per cell). This lack of effect of ICRF-193 on 10 μM H_2O_2-treated cells was also found with low voltage gel electrophoresis (data not shown).

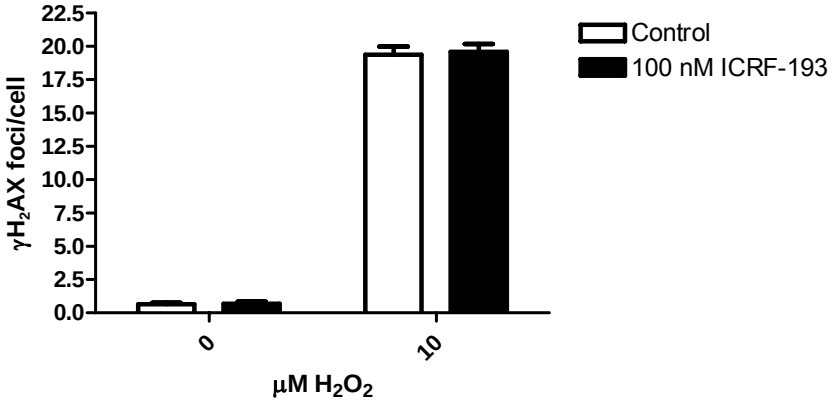

Figure 6.17: Number of γH_2AX foci per cell in control and 100 nM ICRF-193-treated hTERT-RPE1 cells then incubated with 0 or 10 μM H_20_2. The number of foci for each sample was determined for 100 cells in triplicate by immunocytochemistry. Cells were probed with anti-mouse-FITC-conjugated secondary antibodies against the primary mouse anti-γH_2AX antibody as well as DAPI. Error bars represent standard errors from the mean for triplicate experiments.

The next question to answer was why does ICRF-193 treatment affect DSB induction after 1 mM H_2O_2 treatment, but not 10 μM H_2O_2? This inconsistency might be related to the amount of $^{\cdot}OH$ radicals produced by H_2O_2. Perhaps higher levels of ROS, such as those induced by 1 mM H_2O_2, are required to trigger topo II-induced DNA damage, whereas lower ROS levels, induced by ≤10 μM H_2O_2, do not poison topo II to such levels that DSBs are caused. This might relate to the concept of 'cellular barometers' [242] mentioned in section 1.6 where DNA damage poisons topo II to amplify damage to the DNA which in turn might initiate apoptosis if the damage is beyond repair. DNA fragmentation [321] is a 'symptom' of apoptosis and as topo IIα is known to be involved in apoptosis [173], the decrease of DSBs after ICRF-193 treatment at 1 mM H_2O_2 is most likely due to the apoptotic pathway signalling further DSB induction by topo IIα. Although it might follow that as chromosomes look fragmented at 10 μM H_2O_2 cells are going through apoptosis, this I think is unlikely as DSB numbers should also have decreased with ICRF-193 incubation yet they did not. This does not exclude the possibility that topo IIα is involved in the formation of chromosomal 'dots' at concentrations where H_2O_2 does not induced apoptosis (0.1 μM) as it is possible that mis-exchange by topo IIα, a mechanism also suggested for chromatid break formation, might not be detected with assays that measure DSB induction.

6.6 Conclusion

Hydrogen peroxide, presumably through $^{\cdot}OH$ radicals, induces chromosomal fragmentation and 'dots' that can be visualised using AFM. For further imaging by AFM, staining and set-up conditions need to be optimised. The chromosomal 'dots' are still apparent at doses of H_2O_2 where only SSBs were produced which suggests the involvement of a DNA-damaging protein such as topo IIα which magnifies the damage to the chromosomal level. Only H_2O_2 concentrations higher than 10 μM caused DSBs that were reduced when topo IIα activity was inhibited. A role for topo IIα in H_2O_2-induced chromosomal damage at levels that do not induce apoptosis seems likely but remains uncertain. The role of $^{\cdot}OH$ radicals in altering topo IIα activity after γ-irradiation in such a way as to induce chromatid breaks is therefore still unclear.

CHAPTER 7

FINAL DISCUSSION

7.1 Final discussion

The aim of this study was to determine if topo IIα plays a role in low dose IR-induced chromatid breaks as suggested by the signal model [112]. The results presented in chapters 3 - 5 support the hypothesis that topo IIα is involved in forming chromatid breaks after γ-irradiation. I also showed that this involvement of topo IIα was not due to perturbation of the cell cycle or induction of the G_2/M checkpoint nor altered DSB repair. The results also suggested a role for topo IIα in altering chromatid break frequency by lowering the conversion of the initial DNA damage to chromatid breaks.

The signal model of chromatid breakage [112] was originally proposed to account for both a linear induction of chromatid breaks and the finding that DSB repair was not directly linked to chromatid break rejoining. The signal model proposes that chromatid breaks are essentially mis-exchanges within and between chromatids that have been interrupted by fixing the cells during experiments thus rendering the exchanges incomplete [112]. Perhaps the role of topo IIα in chromatid break formation, as suggested by the results in this thesis, is in the mis-exchange of damage at the base of the chromatin loop which, in the case of intra-chromosomal exchanges, would lead to the appearance of intermediate 'omega' figures. If so, how might topo II accomplish this mechanistically? Figure 1.9 shows that topo IIα forms a dimer with each monomer bound to a strand of the gated DNA helix whilst the T-segment is passed through the break of the G-segment to allow for DNA decatenation. This G-segment break is usually religated, except after incubation with topo II poisons such as mAMSA [231] and etoposide [322]. One possibility is therefore that topo IIα is involved in creating chromatid breaks through acting irregularly, leading to a mis-exchange of the genetic material between the two double helices ultimately forming a chromatid break. Thus topo IIα might cause a mis-exchange if two topo II molecules are located near each other at the base of a chromatin loop, each bound to two separate areas of one helix and inducing one DSB in each area of the strand. It has been shown that topo IIα is bound at the base of chromatin loops [121] so the occurrence of two dimers near each other is possible. If bonds between the dimers and DNA helices were cut and somehow the dimers were consequently bound to the wrong part of the helix, exchange between the two areas could occur. However, under which endogenous conditions two dimers might lose their connections with DNA is unclear.

Perhaps a more realistic theory of chromatid breakage involving topo IIα is mis-exchange of genetic material accomplished by DNA repair mechanisms after topo II-induced DNA damage. Such mis-repair of topo II-induced DNA damage has also previously been suggested to result in chromosomal translocations as discussed in section 1.7.2. It is known that topo II creates protein-associated DSBs, which form irreversible DSBs after collision with a replication fork [243]. Perhaps topo II creates protein-associated DSBs after low dose ionising radiation which are

not religated. However, how these are converted in G_2, where DNA replication is absent, into irreversible DSBs is not clear. Collision of transcription forks with topo II-associated DSBs might induce irreversible DSBs in a similar manner to that suggested by Radford [122] . Another possibility might be that endogenous poisons, such as $^{\cdot}OH$ radicals, affect topo IIα [126] catalytically, resulting in DSBs.

Although the data here suggest that topo IIα is involved in chromatid break formation as proposed by the signal model [112], the nature of the signal is still unclear. To determine how topo IIα is involved or recruited in radiation-induced chromatid break formation, the role of $^{\cdot}OH$ radicals was tested in chapter 6. It was shown that topo IIα is involved in H_2O_2-induced chromosomal damage and chromatin 'dots'. Interestingly, chromatin 'dots', thought to be excised chromatin loops, occur even at H_2O_2 concencentrations where no DSBs were produced suggesting that, as with chromatid breaks, topo IIα might be key in forming other types of chromosomal damage.

These results have highlighted some interesting issues. Why did treatment of cells with 0.1 μM H_2O_2 produce only chromosomal 'dots' and no obvious chromatid breaks (chapter 6) whereas irradiation at 0.3 Gy produced only chromatid breaks (chapters 3 – 5) if topo IIα is involved in both? Most likely the amount of $^{\cdot}OH$ radicals present after low dose ionising radiation and H_2O_2 treatment alters the effect of topo IIα in such a way that it either creates chromatid breaks or in rarer cases completely excises the chromatin loop.

If $^{\cdot}OH$ radicals are involved in altering topo IIα activity after γ-irradiation as suggested here, how could this explain the formation of chromatid breaks after DSB induction by restriction endonucleases [10]? Restriction endonucleases would not induce $^{\cdot}OH$ radicals. However, it is feasible that cells might have a high endogenous background of topo IIα poisons that produce topo II-associated DSBs, the same effect as $^{\cdot}OH$ radicals, and that chromatid breaks might still be formed in this way. The endogenous poisons might alternatively be abasic sites. It is known that $^{\cdot}OH$ radicals frequently induce abasic sites [323] and they can be present endogenously at a high level [239]. Therefore although restriction endonucleases do not themselves induce $^{\cdot}OH$ radicals, they might still form chromatid breaks due to a background level of abasic sites leading to irregular topo IIα decatenation.

The signal model of chromatid breakage proposes that damage at the base of a chromatin loop would need to consist of at least two non-IR-induced DSBs as seen in Figure 1.7. I, however, view chromatid breakage as a result of an original IR-induced-DSB located

randomly along a chromatin loop or at its base followed by an interaction of the original DSB and a separate topo II-induced DSB at the base of the loop. The topo II-induced DSB would result from the presence of abasic sites, which poison topo IIα. This theory of two DSBs interacting might appear to contradict data suggesting a linear induction of chromatid breaks with radiation dose [106]. However, if one assumes a very high background of abasic sites, any DSBs induced by low dose radiation would have the same chance of being located next to an abasic site and therefore the induction of chromatid breaks would still appear linear with dose.

7.2 Future outlooks

The work presented here has increased our understanding of IR-induced chromatid breakage in showing that IR-induced DSBs interact with topo IIα in causing chromatid breaks. It is therefore a possibility that the inter-individual variation in chromatid radiosensitivity of lymphocytes of normal healthy individuals and between normals and breast-cancer patients [70,86] could be attributed to variations in topo IIα expression, as shown here. Future studies could therefore be aimed at measuring topo IIα levels, expression or cellular localisation in these individuals and relating these to IR-induced chromatid break frequency. If a significant inter-relationship were found, measurement of topo IIα expression for example could form the basis of a possible future test or marker of IR-induced chromosomal radiosensitivity and cancer susceptibility.

Inter- and intra-individual differences in radiosensitivity could be attributed to changes in diet. When taking into account the data presented here it is likely that an increase of topo II poisons such as genestein and quercetein (found in normal diets) induces different levels of topo IIα activity which would results in changes in radiosensitivity. It is therefore possible, with further investigation, that topo IIα can be used as a marker of not only inter- and intra-individual differences in radiosensitivity but also of sporadic and heritable breast cancer cases.

Also in this thesis only the effect of lowered topo IIα activity and expression on chromatid break frequency was tested. To further confirm the involvement of topo IIα in chromatid break formation overexpression studies should be conducted. It would also be interesting to see if topo IIα expression or activity is affected after either IR or incubation with H_2O_2. The role of $^{\cdot}OH$ radicals and abasic sites in creating chromatid breaks as well as the nature of chromosomal ‘dots’ should also be further investigated.

REFERENCES

1. Hall, A.J. *Radiobiology for the radiobiologist.*, (J.B Lippincott Company, Philadelphia, 1994).
2. Muller, H.J. Artificial Transmutation of the Gene. *Science* **66**, 84-87 (1927).
3. Sasaki, M.S. & Matsubara, S. Free radical scavenging in protection of human lymphocytes against chromosome aberration formation by gamma-ray irradiation. *Int J Radiat Biol Relat Stud Phys Chem Med* **32**, 439-45 (1977).
4. Balasubramanian, B., Pogozelski, W.K. & Tullius, T.D. DNA strand breaking by the hydroxyl radical is governed by the accessible surface areas of the hydrogen atoms of the DNA backbone. *Proc Natl Acad Sci U S A* **95**, 9738-43 (1998).
5. Meneghini, R. & Hoffmann, M.E. The damaging action of hydrogen peroxide on DNA of human fibroblasts is mediated by a non-dialyzable compound. *Biochim Biophys Acta* **608**, 167-73 (1980).
6. Schroder, E. & Eaton, P. Hydrogen peroxide as an endogenous mediator and exogenous tool in cardiovascular research: issues and considerations. *Curr Opin Pharmacol* **8**, 153-9 (2008).
7. Tubiana, M., Dutreix, J. & Wambersie, A. *Introduction to radiobiology*, 1st edition (Taylor and Francis, 1990).
8. Frankenberg, D., Frankenberg-Schwager, M., Blocher, D. & Harbich, R. Evidence for DNA double-strand breaks as the critical lesions in yeast cells irradiated with sparsely or densely ionizing radiation under oxic or anoxic conditions. *Radiat Res* **88**, 524-32 (1981).
9. Blocher, D. & Pohlit, W. DNA double strand breaks in Ehrlich ascites tumour cells at low doses of x-rays. II. Can cell death be attributed to double strand breaks? *Int J Radiat Biol Relat Stud Phys Chem Med* **42**, 329-38 (1982).
10. Bryant, P.E. Enzymatic restriction of mammalian cell DNA using Pvu II and Bam H1: evidence for the double-strand break origin of chromosomal aberrations. *Int J Radiat Biol Relat Stud Phys Chem Med* **46**, 57-65 (1984).
11. Rothkamm, K. & Lobrich, M. Evidence for a lack of DNA double-strand break repair in human cells exposed to very low x-ray doses. *Proc Natl Acad Sci U S A* **100**, 5057-62 (2003).
12. Ahnstrom, G. & Bryant, P.E. DNA double-strand breaks generated by the repair of X-ray damage in Chinese hamster cells. *Int J Radiat Biol Relat Stud Phys Chem Med* **41**, 671-6 (1982).
13. von Sonntag, C. *The chemical basis of radiation biology.*, (Taylor and Francis Ltd., London, 1987).
14. Ward, J.F. Biochemistry of DNA lesions. *Radiat Res Suppl* **8**, S103-11 (1985).
15. Culotta, E. & Koshland, D.E., Jr. DNA repair works its way to the top. *Science* **266**, 1926-9 (1994).
16. Dianov, G.L. & Parsons, J.L. Co-ordination of DNA single strand break repair. *DNA Repair (Amst)* **6**, 454-60 (2007).
17. Pardo, B., Gomez-Gonzalez, B. & Aguilera, A. DNA repair in mammalian cells: DNA double-strand break repair: how to fix a broken relationship. *Cell Mol Life Sci* **66**, 1039-56 (2009).
18. Mahaney, B.L., Meek, K. & Lees-Miller, S.P. Repair of ionizing radiation-induced DNA double-strand breaks by non-homologous end-joining. *Biochem J* **417**, 639-50 (2009).
19. Pastink, A., Eeken, J.C. & Lohman, P.H. Genomic integrity and the repair of double-strand DNA breaks. *Mutat Res* **480-481**, 37-50 (2001).

20. Ahnesorg, P., Smith, P. & Jackson, S.P. XLF interacts with the XRCC4-DNA ligase IV complex to promote DNA nonhomologous end-joining. *Cell* **124**, 301-13 (2006).
21. Rubnitz, J. & Subramani, S. The minimum amount of homology required for homologous recombination in mammalian cells. *Mol Cell Biol* **4**, 2253-8 (1984).
22. van den Bosch, M., Bree, R.T. & Lowndes, N.F. The MRN complex: coordinating and mediating the response to broken chromosomes. *EMBO Rep* **4**, 844-9 (2003).
23. Burma, S., Chen, B.P., Murphy, M., Kurimasa, A. & Chen, D.J. ATM phosphorylates histone H2AX in response to DNA double-strand breaks. *J Biol Chem* **276**, 42462-7 (2001).
24. Rogakou, E.P., Boon, C., Redon, C. & Bonner, W.M. Megabase chromatin domains involved in DNA double-strand breaks in vivo. *J Cell Biol* **146**, 905-16 (1999).
25. Stucki, M. et al. MDC1 directly binds phosphorylated histone H2AX to regulate cellular responses to DNA double-strand breaks. *Cell* **123**, 1213-26 (2005).
26. Huen, M.S. et al. RNF8 transduces the DNA-damage signal via histone ubiquitylation and checkpoint protein assembly. *Cell* **131**, 901-14 (2007).
27. Ruffner, H., Joazeiro, C.A., Hemmati, D., Hunter, T. & Verma, I.M. Cancer-predisposing mutations within the RING domain of BRCA1: loss of ubiquitin protein ligase activity and protection from radiation hypersensitivity. *Proc Natl Acad Sci U S A* **98**, 5134-9 (2001).
28. Cohn, M.A. & D'Andrea, A.D. Chromatin recruitment of DNA repair proteins: lessons from the fanconi anemia and double-strand break repair pathways. *Mol Cell* **32**, 306-12 (2008).
29. Somasundaram, K. Breast cancer gene 1 (BRCA1): role in cell cycle regulation and DNA repair--perhaps through transcription. *J Cell Biochem* **88**, 1084-91 (2003).
30. Cousineau, I., Abaji, C. & Belmaaza, A. BRCA1 regulates RAD51 function in response to DNA damage and suppresses spontaneous sister chromatid replication slippage: implications for sister chromatid cohesion, genome stability, and carcinogenesis. *Cancer Res* **65**, 11384-91 (2005).
31. Ellisen, L.W. & Haber, D.A. Hereditary breast cancer. *Annu Rev Med* **49**, 425-36 (1998).
32. Wang, B., Matsuoka, S., Carpenter, P.B. & Elledge, S.J. 53BP1, a mediator of the DNA damage checkpoint. *Science* **298**, 1435-8 (2002).
33. Paull, T.T. et al. A critical role for histone H2AX in recruitment of repair factors to nuclear foci after DNA damage. *Curr Biol* **10**, 886-95 (2000).
34. Celeste, A. et al. Genomic instability in mice lacking histone H2AX. *Science* **296**, 922-7 (2002).
35. Fillingham, J., Keogh, M.C. & Krogan, N.J. GammaH2AX and its role in DNA double-strand break repair. *Biochem Cell Biol* **84**, 568-77 (2006).
36. Kim, S.T., Xu, B. & Kastan, M.B. Involvement of the cohesin protein, Smc1, in Atm-dependent and independent responses to DNA damage. *Genes Dev* **16**, 560-70 (2002).
37. Baumann, P. & West, S.C. Role of the human RAD51 protein in homologous recombination and double-stranded-break repair. *Trends Biochem Sci* **23**, 247-51 (1998).

38. Liu, Y., Tarsounas, M., O'Regan, P. & West, S.C. Role of RAD51C and XRCC3 in genetic recombination and DNA repair. *J Biol Chem* **282**, 1973-9 (2007).
39. Park, M.S., Ludwig, D.L., Stigger, E. & Lee, S.H. Physical interaction between human RAD52 and RPA is required for homologous recombination in mammalian cells. *J Biol Chem* **271**, 18996-9000 (1996).
40. Rossi, M.J. & Mazin, A.V. Rad51 protein stimulates the branch migration activity of Rad54 protein. *J Biol Chem* **283**, 24698-706 (2008).
41. Dronkert, M.L. et al. Mouse RAD54 affects DNA double-strand break repair and sister chromatid exchange. *Mol Cell Biol* **20**, 3147-56 (2000).
42. Fekairi, S. et al. Human SLX4 is a Holliday junction resolvase subunit that binds multiple DNA repair/recombination endonucleases. *Cell* **138**, 78-89 (2009).
43. Munoz, I.M. et al. Coordination of structure-specific nucleases by human SLX4/BTBD12 is required for DNA repair. *Cell* **138**, 116-127 (2009).
44. Svendsen, J.M. et al. Mammalian BTBD12/SLX4 assembles a Holliday junction resolvase and is required for DNA repair. *Cell* **138**, 63-77 (2009).
45. Grawunder, U. et al. Activity of DNA ligase IV stimulated by complex formation with XRCC4 protein in mammalian cells. *Nature* **388**, 492-5 (1997).
46. Riballo, E. et al. A pathway of double-strand break rejoining dependent upon ATM, Artemis, and proteins locating to gamma-H2AX foci. *Mol Cell* **16**, 715-24 (2004).
47. Gu, J. et al. XRCC4:DNA ligase IV can ligate incompatible DNA ends and can ligate across gaps. *Embo J* **26**, 1010-23 (2007).
48. Jackson, S.P. & Jeggo, P.A. DNA double-strand break repair and V(D)J recombination: involvement of DNA-PK. *Trends Biochem Sci* **20**, 412-5 (1995).
49. Wang, H., Wang, X., Iliakis, G. & Wang, Y. Caffeine could not efficiently sensitize homologous recombination repair-deficient cells to ionizing radiation-induced killing. *Radiat Res* **159**, 420-5 (2003).
50. Rothkamm, K., Kruger, I., Thompson, L.H. & Lobrich, M. Pathways of DNA double-strand break repair during the mammalian cell cycle. *Mol Cell Biol* **23**, 5706-15 (2003).
51. Golding, S.E. et al. Double strand break repair by homologous recombination is regulated by cell cycle-independent signaling via ATM in human glioma cells. *J Biol Chem* **279**, 15402-10 (2004).
52. Yun, M.H. & Hiom, K. CtIP-BRCA1 modulates the choice of DNA double-strand-break repair pathway throughout the cell cycle. *Nature* **459**, 460-3 (2009).
53. Mladenov, E., Kalev, P. & Anachkova, B. The complexity of double-strand break ends is a factor in the repair of pathway choice. *Radiat Res* **171**, 397-404 (2009).
54. Deming, P.B. et al. The human decatenation checkpoint. *Proc Natl Acad Sci U S A* **98**, 12044-9 (2001).
55. Terzoudi, G.I., Manola, K.N., Pantelias, G.E. & Iliakis, G. Checkpoint abrogation in G2 compromises repair of chromosomal breaks in ataxia telangiectasia cells. *Cancer Res* **65**, 11292-6 (2005).
56. Bucher, N. & Britten, C.D. G2 checkpoint abrogation and checkpoint kinase-1 targeting in the treatment of cancer. *Br J Cancer* **98**, 523-8 (2008).

57. Lobrich, M. & Jeggo, P.A. The impact of a negligent G2/M checkpoint on genomic instability and cancer induction. *Nat Rev Cancer* **7**, 861-9 (2007).
58. Stark, G.R. & Taylor, W.R. Control of the G2/M transition. *Mol Biotechnol* **32**, 227-48 (2006).
59. Clifford, B., Beljin, M., Stark, G.R. & Taylor, W.R. G2 arrest in response to topoisomerase II inhibitors: the role of p53. *Cancer Res* **63**, 4074-81 (2003).
60. Taylor, W.R. & Stark, G.R. Regulation of the G2/M transition by p53. *Oncogene* **20**, 1803-15 (2001).
61. Khanna, K.K. et al. ATM associates with and phosphorylates p53: mapping the region of interaction. *Nat Genet* **20**, 398-400 (1998).
62. Sanford, K.K. et al. Factors affecting and significance of G2 chromatin radiosensitivity in predisposition to cancer. *Int J Radiat Biol* **55**, 963-81 (1989).
63. Papworth, R. BSc Honours Thesis: The spectrum of G2 chromatid aberrations induced by X-rays. *Bute Medical School, University of St Andrews, UK* (1993).
64. MacLeod, R.A. & Bryant, P.E. Effects of adenine arabinoside and coformycin on the kinetics of G2 chromatid aberrations in X-irradiated human lymphocytes. *Mutagenesis* **7**, 285-90 (1992).
65. Bryant, P.E. et al. The G2 chromosomal radiosensitivity assay. *Int J Radiat Biol* **78**, 863-6 (2002).
66. Haering, C.H., Farcas, A.M., Arumugam, P., Metson, J. & Nasmyth, K. The cohesin ring concatenates sister DNA molecules. *Nature* **454**, 297-301 (2008).
67. Gruber, S., Haering, C.H. & Nasmyth, K. Chromosomal cohesin forms a ring. *Cell* **112**, 765-77 (2003).
68. Gimenez-Abian, J.F. et al. Regulation of sister chromatid cohesion between chromosome arms. *Curr Biol* **14**, 1187-93 (2004).
69. Smart, V., Curwen, G.B., Whitehouse, C.A., Edwards, A. & Tawn, E.J. Chromosomal radiosensitivity: a study of the chromosomal G(2) assay in human blood lymphocytes indicating significant inter-individual variability. *Mutat Res* **528**, 105-10 (2003).
70. Riches, A.C. et al. Chromosomal radiosensitivity in G2-phase lymphocytes identifies breast cancer patients with distinctive tumour characteristics. *Br J Cancer* **85**, 1157-61 (2001).
71. Scott, D., Spreadborough, A., Levine, E. & Roberts, S.A. Genetic predisposition in breast cancer. *Lancet* **344**, 1444 (1994).
72. Parshad, R., Sanford, K.K., Jones, G.M. & Tarone, R.E. G2 chromosomal radiosensitivity of ataxia-telangiectasia heterozygotes. *Cancer Genet Cytogenet* **14**, 163-8 (1985).
73. Scott, D., Spreadborough, A.R. & Roberts, S.A. Radiation-induced G2 delay and spontaneous chromosome aberrations in ataxia-telangiectasia homozygotes and heterozygotes. *Int J Radiat Biol* **66**, S157-63 (1994).
74. Pandita, T.K. & Hittelman, W.N. Initial chromosome damage but not DNA damage is greater in ataxia telangiectasia cells. *Radiat Res* **130**, 94-103 (1992).
75. Taylor, A.M. Unrepaired DNA strand breaks in irradiated ataxia telangiectasia lymphocytes suggested from cytogenetic observations. *Mutat Res* **50**, 407-18 (1978).
76. Lehman, A.R. & Stevens, S. The production and repair of double strand breaks in cells from normal humans and from patients with ataxia telangiectasia. *Biochim Biophys Acta* **474**, 49-60 (1977).

77. Foray, N., Arlett, C.F. & Malaise, E.P. Dose-rate effect on induction and repair rate of radiation-induced DNA double-strand breaks in a normal and an ataxia telangiectasia human fibroblast cell line. *Biochimie* **77**, 900-5 (1995).
78. Painter, R.B. & Young, B.R. Radiosensitivity in ataxia-telangiectasia: a new explanation. *Proc Natl Acad Sci U S A* **77**, 7315-7 (1980).
79. Scott, D. & Zampetti-Bosseler, F. Cell cycle dependence of mitotic delay in X-irradiated normal and ataxia-telangiectasia fibroblasts. *Int J Radiat Biol Relat Stud Phys Chem Med* **42**, 679-83 (1982).
80. Rieder, C.L. & Palazzo, R.E. Colcemid and the mitotic cycle. *J Cell Sci* **102 (Pt 3)**, 387-92 (1992).
81. Terzoudi, G.I. et al. Increased G2 chromosomal radiosensitivity in cancer patients: the role of cdk1/cyclin-B activity level in the mechanisms involved. *Int J Radiat Biol* **76**, 607-15 (2000).
82. Cadwell, K. Masters, University of Central Lancashire in collaboration with Westlakes Research Institute (2009).
83. Curwen, G.B. PhD, University of St Andrews (2007).
84. Mozdarani, H. & Bryant, P.E. Kinetics of chromatid aberrations in G2 ataxia-telangiectasia cells exposed to X-rays and ara A. *Int J Radiat Biol* **55**, 71-84 (1989).
85. Bryant, P.E., Gray, L.J. & Peresse, N. Progress towards understanding the nature of chromatid breakage. *Cytogenet Genome Res* **104**, 65-71 (2004).
86. Scott, D., Barber, J.B., Spreadborough, A.R., Burrill, W. & Roberts, S.A. Increased chromosomal radiosensitivity in breast cancer patients: a comparison of two assays. *Int J Radiat Biol* **75**, 1-10 (1999).
87. Baria, K., Warren, C., Roberts, S.A., West, C.M. & Scott, D. Chromosomal radiosensitivity as a marker of predisposition to common cancers? *Br J Cancer* **84**, 892-6 (2001).
88. Roberts, S.A. et al. Heritability of cellular radiosensitivity: a marker of low-penetrance predisposition genes in breast cancer? *Am J Hum Genet* **65**, 784-94 (1999).
89. Howe, O.L. et al. Elevated G2 chromosomal radiosensitivity in Irish breast cancer patients: a comparison with other studies. *Int J Radiat Biol* **81**, 373-8 (2005).
90. Buchholz, T.A. & Wu, X. Radiation-induced chromatid breaks as a predictor of breast cancer risk. *Int J Radiat Oncol Biol Phys* **49**, 533-7 (2001).
91. Baeyens, A. et al. Chromosomal radiosensitivity in breast cancer patients with a known or putative genetic predisposition. *Br J Cancer* **87**, 1379-85 (2002).
92. Baeyens, A. et al. Chromosomal radiosensitivity in breast cancer patients: influence of age of onset of the disease. *Oncol Rep* **13**, 347-53 (2005).
93. Docherty, Z. et al. Is chromosome radiosensitivity and apoptotic response to irradiation correlated with cancer susceptibility? *Int J Radiat Biol* **83**, 1-12 (2007).
94. Parshad, R. et al. Deficient DNA repair capacity, a predisposing factor in breast cancer. *Br J Cancer* **74**, 1-5 (1996).
95. Helzlsouer, K.J. et al. DNA repair proficiency: potential susceptiblity factor for breast cancer. *J Natl Cancer Inst* **88**, 754-5 (1996).
96. Baeyens, A. et al. Chromosomal radiosensitivity in BRCA1 and BRCA2 mutation carriers. *Int J Radiat Biol* **80**, 745-56 (2004).
97. Peto, J. et al. Prevalence of BRCA1 and BRCA2 gene mutations in patients with early-onset breast cancer. *J Natl Cancer Inst* **91**, 943-9 (1999).

98. Baria, K. et al. Chromosomal radiosensitivity in young cancer patients: possible evidence of genetic predisposition. *Int J Radiat Biol* **78**, 341-6 (2002).
99. Curwen, G.B. et al. G(2) chromosomal radiosensitivity in Danish survivors of childhood and adolescent cancer and their offspring. *Br J Cancer* **93**, 1038-45 (2005).
100. Pharoah, P.D. et al. Polygenic susceptibility to breast cancer and implications for prevention. *Nat Genet* **31**, 33-6 (2002).
101. Renwick, A. et al. ATM mutations that cause ataxia-telangiectasia are breast cancer susceptibility alleles. *Nat Genet* **38**, 873-5 (2006).
102. De Ruyck, K. et al. Chromosomal radiosensitivity in head and neck cancer patients: evidence for genetic predisposition? *Br J Cancer* **98**, 1723-38 (2008).
103. Papworth, R., Slevin, N., Roberts, S.A. & Scott, D. Sensitivity to radiation-induced chromosome damage may be a marker of genetic predisposition in young head and neck cancer patients. *Br J Cancer* **84**, 776-82 (2001).
104. Lisowska, H. et al. Enhanced chromosomal radiosensitivity in peripheral blood lymphocytes of larynx cancer patients. *Int J Radiat Oncol Biol Phys* **66**, 1245-52 (2006).
105. Sax, K. Chromosome Aberrations Induced by X-Rays. *Genetics* **23**, 494-516 (1938).
106. Sax, K. An Analysis of X-Ray Induced Chromosomal Aberrations in Tradescantia. *Genetics* **25**, 41-68 (1940).
107. Bender, M.A., Griggs, H.G. & Bedford, J.S. Mechanisms of chromosomal aberration production. 3. Chemicals and ionizing radiation. *Mutat Res* **23**, 197-212 (1974).
108. Bryant, P.E. Mechanisms of radiation-induced chromatid breaks. *Mutat Res* **404**, 107-11 (1998).
109. Natarajan, A.T. & Obe, G. Molecular mechanisms involved in the production of chromosomal aberrations. III. Restriction endonucleases. *Chromosoma* **90**, 120-7 (1984).
110. Harvey, A.N. & Savage, J.R. Investigating the nature of chromatid breaks produced by restriction endonucleases. *Int J Radiat Biol* **71**, 21-8 (1997).
111. Natarajan, A.T. & Obe, G. Molecular mechanisms involved in the production of chromosomal aberrations. I. Utilization of Neurospora endonuclease for the study of aberration production in G2 stage of the cell cycle. *Mutat Res* **52**, 137-49 (1978).
112. Bryant, P.E. The signal model: a possible explanation for the conversion of DNA double-strand breaks into chromatid breaks. *Int J Radiat Biol* **73**, 243-51 (1998).
113. Venter, J.C. et al. The sequence of the human genome. *Science* **291**, 1304-51 (2001).
114. Bryant, P.E., Jones, C., Armstrong, G., Frankenberg-Schwager, M. & Frankenberg, D. Induction of chromatid breaks by carbon K-shell ultrasoft X rays. *Radiat Res* **159**, 247-50 (2003).
115. Revell, S.H. The accurate estimation of chromatid breakage, and its relevance to a new interpretation of chromatid aberrations induced by ionizing radiations. *Proc R Soc Lond B Biol Sci* **150**, 563-89 (1959).
116. Perry, P. & Wolff, S. New Giemsa method for the differential staining of sister chromatids. *Nature* **251**, 156-8 (1974).
117. Heddle, J.A. & Bodycote, D.J. On the formation of chromosomal aberrations. *Mutat Res* **9**, 117-26 (1970).

118. Heddle, J.A., Whissell, D. & Bodycote, D.J. Changes in chromosome structure induced by radiations: a test of the two chief hypotheses. *Nature* **221**, 1158-60 (1969).
119. Rogers-Bald, M., Sargent, R.G. & Bryant, P.E. Production of chromatid breaks by single dsb: evidence supporting the signal model. *Int J Radiat Biol* **76**, 23-9 (2000).
120. Iborra, F.J., Pombo, A., Jackson, D.A. & Cook, P.R. Active RNA polymerases are localized within discrete transcription "factories' in human nuclei. *J Cell Sci* **109 (Pt 6)**, 1427-36 (1996).
121. Gasser, S.M., Laroche, T., Falquet, J., Boy de la Tour, E. & Laemmli, U.K. Metaphase chromosome structure. Involvement of topoisomerase II. *J Mol Biol* **188**, 613-29 (1986).
122. Radford, I.R. Transcription-based model for the induction of interchromosomal exchange events by ionizing irradiation in mammalian cell lines that undergo necrosis. *Int J Radiat Biol* **78**, 1081-93 (2002).
123. Gimenez-Abian, J.F. et al. Premitotic chromosome individualization in mammalian cells depends on topoisomerase II activity. *Chromosoma* **109**, 235-44 (2000).
124. Uemura, T. et al. DNA topoisomerase II is required for condensation and separation of mitotic chromosomes in S. pombe. *Cell* **50**, 917-25 (1987).
125. Earnshaw, W.C. & Heck, M.M. Localization of topoisomerase II in mitotic chromosomes. *J Cell Biol* **100**, 1716-25 (1985).
126. Li, T.K. et al. Activation of topoisomerase II-mediated excision of chromosomal DNA loops during oxidative stress. *Genes Dev* **13**, 1553-60 (1999).
127. Pommier, Y., Kerrigan, D., Covey, J.M., Kao-Shan, C.S. & Whang-Peng, J. Sister chromatid exchanges, chromosomal aberrations, and cytotoxicity produced by antitumor topoisomerase II inhibitors in sensitive (DC3F) and resistant (DC3F/9-OHE) Chinese hamster cells. *Cancer Res* **48**, 512-6 (1988).
128. Woessner, R.D., Mattern, M.R., Mirabelli, C.K., Johnson, R.K. & Drake, F.H. Proliferation- and cell cycle-dependent differences in expression of the 170 kilodalton and 180 kilodalton forms of topoisomerase II in NIH-3T3 cells. *Cell Growth Differ* **2**, 209-14 (1991).
129. Shibuya, M.L., Ueno, A.M., Vannais, D.B., Craven, P.A. & Waldren, C.A. Megabase pair deletions in mutant mammalian cells following exposure to amsacrine, an inhibitor of DNA topoisomerase II. *Cancer Res* **54**, 1092-7 (1994).
130. Gromova, II, Thomsen, B. & Razin, S.V. Different topoisomerase II antitumor drugs direct similar specific long-range fragmentation of an amplified c-MYC gene locus in living cells and in high-salt-extracted nuclei. *Proc Natl Acad Sci U S A* **92**, 102-6 (1995).
131. Mielke, C., Christensen, M.O., Barthelmes, H.U. & Boege, F. Enhanced processing of UVA-irradiated DNA by human topoisomerase II in living cells. *J Biol Chem* **279**, 20559-62 (2004).
132. Wang, J.C. Cellular roles of DNA topoisomerases: a molecular perspective. *Nat Rev Mol Cell Biol* **3**, 430-40 (2002).
133. Wang, J.C. DNA topoisomerases. *Annu Rev Biochem* **54**, 665-97 (1985).
134. Wang, J.C. DNA topoisomerases. *Annu Rev Biochem* **65**, 635-92 (1996).
135. Gellert, M. DNA topoisomerases. *Annu Rev Biochem* **50**, 879-910 (1981).

136. Watt, P.M. & Hickson, I.D. Structure and function of type II DNA topoisomerases. *Biochem J* **303 (Pt 3)**, 681-95 (1994).
137. Deweese, J.E. & Osheroff, N. The DNA cleavage reaction of topoisomerase II: wolf in sheep's clothing. *Nucleic Acids Res* **37**, 738-48 (2009).
138. Brown, P.O. & Cozzarelli, N.R. Catenation and knotting of duplex DNA by type 1 topoisomerases: a mechanistic parallel with type 2 topoisomerases. *Proc Natl Acad Sci U S A* **78**, 843-7 (1981).
139. Tse, Y. & Wang, J.C. E. coli and M. luteus DNA topoisomerase I can catalyze catenation of decatenation of double-stranded DNA rings. *Cell* **22**, 269-76 (1980).
140. Miller, K.G., Liu, L.F. & Englund, P.T. A homogeneous type II DNA topoisomerase from HeLa cell nuclei. *J Biol Chem* **256**, 9334-9 (1981).
141. Liu, L.F., Liu, C.C. & Alberts, B.M. Type II DNA topoisomerases: enzymes that can unknot a topologically knotted DNA molecule via a reversible double-strand break. *Cell* **19**, 697-707 (1980).
142. Uemura, T. & Yanagida, M. Isolation of type I and II DNA topoisomerase mutants from fission yeast: single and double mutants show different phenotypes in cell growth and chromatin organization. *Embo J* **3**, 1737-44 (1984).
143. Goto, T. & Wang, J.C. Cloning of yeast TOP1, the gene encoding DNA topoisomerase I, and construction of mutants defective in both DNA topoisomerase I and DNA topoisomerase II. *Proc Natl Acad Sci U S A* **82**, 7178-82 (1985).
144. Wyckoff, E., Natalie, D., Nolan, J.M., Lee, M. & Hsieh, T. Structure of the Drosophila DNA topoisomerase II gene. Nucleotide sequence and homology among topoisomerases II. *J Mol Biol* **205**, 1-13 (1989).
145. Tsai-Pflugfelder, M. et al. Cloning and sequencing of cDNA encoding human DNA topoisomerase II and localization of the gene to chromosome region 17q21-22. *Proc Natl Acad Sci U S A* **85**, 7177-81 (1988).
146. Tan, K.B. et al. Topoisomerase II alpha and topoisomerase II beta genes: characterization and mapping to human chromosomes 17 and 3, respectively. *Cancer Res* **52**, 231-4 (1992).
147. Drake, F.H. et al. Biochemical and pharmacological properties of p170 and p180 forms of topoisomerase II. *Biochemistry* **28**, 8154-60 (1989).
148. Drake, F.H. et al. Purification of topoisomerase II from amsacrine-resistant P388 leukemia cells. Evidence for two forms of the enzyme. *J Biol Chem* **262**, 16739-47 (1987).
149. Chung, T.D. et al. Characterization and immunological identification of cDNA clones encoding two human DNA topoisomerase II isozymes. *Proc Natl Acad Sci U S A* **86**, 9431-5 (1989).
150. Jenkins, J.R. et al. Isolation of cDNA clones encoding the beta isozyme of human DNA topoisomerase II and localisation of the gene to chromosome 3p24. *Nucleic Acids Res* **20**, 5587-92 (1992).
151. Sng, J.H. et al. Molecular cloning and characterization of the human topoisomerase IIalpha and IIbeta genes: evidence for isoform evolution through gene duplication. *Biochim Biophys Acta* **1444**, 395-406 (1999).
152. Lang, A.J. et al. Structural organization of the human TOP2A and TOP2B genes. *Gene* **221**, 255-66 (1998).

153. Davies, S.L., Jenkins, J.R. & Hickson, I.D. Human cells express two differentially spliced forms of topoisomerase II beta mRNA. *Nucleic Acids Res* **21**, 3719-23 (1993).
154. Harker, W.G., Slade, D.L., Drake, F.H. & Parr, R.L. Mitoxantrone resistance in HL-60 leukemia cells: reduced nuclear topoisomerase II catalytic activity and drug-induced DNA cleavage in association with reduced expression of the topoisomerase II beta isoform. *Biochemistry* **30**, 9953-61 (1991).
155. Harker, W.G. et al. Alterations in the topoisomerase II alpha gene, messenger RNA, and subcellular protein distribution as well as reduced expression of the DNA topoisomerase II beta enzyme in a mitoxantrone-resistant HL-60 human leukemia cell line. *Cancer Res* **55**, 1707-16 (1995).
156. Harker, W.G., Slade, D.L., Parr, R.L. & Holguin, M.H. Selective use of an alternative stop codon and polyadenylation signal within intron sequences leads to a truncated topoisomerase II alpha messenger RNA and protein in human HL-60 leukemia cells selected for resistance to mitoxantrone. *Cancer Res* **55**, 4962-71 (1995).
157. Prosperi, E., Negri, C., Marchese, G. & Ricotti, G.C. Expression of the 170-kDa and 180-kDa isoforms of DNA topoisomerase II in resting and proliferating human lymphocytes. *Cell Prolif* **27**, 257-67 (1994).
158. Dereuddre, S., Frey, S., Delaporte, C. & Jacquemin-Sablon, A. Cloning and characterization of full-length cDNAs coding for the DNA topoisomerase II beta from Chinese hamster lung cells sensitive and resistant 9-OH-ellipticine. *Biochim Biophys Acta* **1264**, 178-82 (1995).
159. Heck, M.M. & Earnshaw, W.C. Topoisomerase II: A specific marker for cell proliferation. *J Cell Biol* **103**, 2569-81 (1986).
160. Jarvinen, T.A. et al. Amplification and deletion of topoisomerase IIalpha associate with ErbB-2 amplification and affect sensitivity to topoisomerase II inhibitor doxorubicin in breast cancer. *Am J Pathol* **156**, 839-47 (2000).
161. Bermejo, R. et al. Top1- and Top2-mediated topological transitions at replication forks ensure fork progression and stability and prevent DNA damage checkpoint activation. *Genes Dev* **21**, 1921-36 (2007).
162. Cuvier, O., Stanojcic, S., Lemaitre, J.M. & Mechali, M. A topoisomerase II-dependent mechanism for resetting replicons at the S-M-phase transition. *Genes Dev* **22**, 860-5 (2008).
163. Mondal, N. & Parvin, J.D. DNA topoisomerase IIalpha is required for RNA polymerase II transcription on chromatin templates. *Nature* **413**, 435-8 (2001).
164. Yang, L., Wold, M.S., Li, J.J., Kelly, T.J. & Liu, L.F. Roles of DNA topoisomerases in simian virus 40 DNA replication in vitro. *Proc Natl Acad Sci U S A* **84**, 950-4 (1987).
165. Abdurashidova, G. et al. Functional interactions of DNA topoisomerases with a human replication origin. *Embo J* **26**, 998-1009 (2007).
166. Champoux, J.J. DNA topoisomerases: structure, function, and mechanism. *Annu Rev Biochem* **70**, 369-413 (2001).
167. McClendon, A.K., Rodriguez, A.C. & Osheroff, N. Human topoisomerase IIalpha rapidly relaxes positively supercoiled DNA: implications for enzyme action ahead of replication forks. *J Biol Chem* **280**, 39337-45 (2005).
168. Belmont, A.S. Mitotic chromosome structure and condensation. *Curr Opin Cell Biol* **18**, 632-8 (2006).

169. Chang, C.J., Goulding, S., Earnshaw, W.C. & Carmena, M. RNAi analysis reveals an unexpected role for topoisomerase II in chromosome arm congression to a metaphase plate. *J Cell Sci* **116**, 4715-26 (2003).
170. Clarke, D.J., Johnson, R.T. & Downes, C.S. Topoisomerase II inhibition prevents anaphase chromatid segregation in mammalian cells independently of the generation of DNA strand breaks. *J Cell Sci* **105 (Pt 2)**, 563-9 (1993).
171. Holm, C., Goto, T., Wang, J.C. & Botstein, D. DNA topoisomerase II is required at the time of mitosis in yeast. *Cell* **41**, 553-63 (1985).
172. DiNardo, S., Voelkel, K. & Sternglanz, R. DNA topoisomerase II mutant of Saccharomyces cerevisiae: topoisomerase II is required for segregation of daughter molecules at the termination of DNA replication. *Proc Natl Acad Sci U S A* **81**, 2616-20 (1984).
173. Yoshida, K. et al. Protein kinase C delta activates topoisomerase IIalpha to induce apoptotic cell death in response to DNA damage. *Mol Cell Biol* **26**, 3414-31 (2006).
174. Grue, P. et al. Essential mitotic functions of DNA topoisomerase IIalpha are not adopted by topoisomerase IIbeta in human H69 cells. *J Biol Chem* **273**, 33660-6 (1998).
175. Jensen, S., Redwood, C.S., Jenkins, J.R., Andersen, A.H. & Hickson, I.D. Human DNA topoisomerases II alpha and II beta can functionally substitute for yeast TOP2 in chromosome segregation and recombination. *Mol Gen Genet* **252**, 79-86 (1996).
176. Ju, B.G. et al. A topoisomerase IIbeta-mediated dsDNA break required for regulated transcription. *Science* **312**, 1798-802 (2006).
177. Kondapi, A.K., Mulpuri, N., Mandraju, R.K., Sasikaran, B. & Subba Rao, K. Analysis of age dependent changes of Topoisomerase II alpha and beta in rat brain. *Int J Dev Neurosci* **22**, 19-30 (2004).
178. Sugimoto, K. et al. Temporal and spatial distribution of DNA topoisomerase II alters during proliferation, differentiation, and apoptosis in HL-60 cells. *Blood* **91**, 1407-17 (1998).
179. Tsutsui, K., Tsutsui, K., Sano, K., Kikuchi, A. & Tokunaga, A. Involvement of DNA topoisomerase IIbeta in neuronal differentiation. *J Biol Chem* **276**, 5769-78 (2001).
180. Yang, X., Li, W., Prescott, E.D., Burden, S.J. & Wang, J.C. DNA topoisomerase IIbeta and neural development. *Science* **287**, 131-4 (2000).
181. Constantinou, A., Henning-Chubb, C. & Huberman, E. Novobiocin- and phorbol-12-myristate-13-acetate-induced differentiation of human leukemia cells associated with a reduction in topoisomerase II activity. *Cancer Res* **49**, 1110-7 (1989).
182. Blasquez, V.C., Sperry, A.O., Cockerill, P.N. & Garrard, W.T. Protein:DNA interactions at chromosomal loop attachment sites. *Genome* **31**, 503-9 (1989).
183. Bauman, M.E., Holden, J.A., Brown, K.A., Harker, W.G. & Perkins, S.L. Differential immunohistochemical staining for DNA topoisomerase II alpha and beta in human tissues and for DNA topoisomerase II beta in non-Hodgkin's lymphomas. *Mod Pathol* **10**, 168-75 (1997).
184. Juenke, J.M. & Holden, J.A. The distribution of DNA topoisomerase II isoforms in differentiated adult mouse tissues. *Biochim Biophys Acta* **1216**, 191-6 (1993).
185. Austin, C.A. & Marsh, K.L. Eukaryotic DNA topoisomerase II beta. *Bioessays* **20**, 215-26 (1998).

186. Mirski, S.E., Bielawski, J.C. & Cole, S.P. Identification of functional nuclear export sequences in human topoisomerase IIalpha and beta. *Biochem Biophys Res Commun* **306**, 905-11 (2003).
187. Mirski, S.E. et al. Topoisomerase II binds importin alpha isoforms and exportin/CRM1 but does not shuttle between the nucleus and cytoplasm in proliferating cells. *Exp Cell Res* **313**, 627-37 (2007).
188. Tavormina, P.A. et al. Rapid exchange of mammalian topoisomerase II alpha at kinetochores and chromosome arms in mitosis. *J Cell Biol* **158**, 23-9 (2002).
189. Rattner, J.B., Hendzel, M.J., Furbee, C.S., Muller, M.T. & Bazett-Jones, D.P. Topoisomerase II alpha is associated with the mammalian centromere in a cell cycle- and species-specific manner and is required for proper centromere/kinetochore structure. *J Cell Biol* **134**, 1097-107 (1996).
190. Mo, Y.Y. & Beck, W.T. Association of human DNA topoisomerase IIalpha with mitotic chromosomes in mammalian cells is independent of its catalytic activity. *Exp Cell Res* **252**, 50-62 (1999).
191. Christensen, M.O. et al. Dynamics of human DNA topoisomerases IIalpha and IIbeta in living cells. *J Cell Biol* **157**, 31-44 (2002).
192. Meyer, K.N. et al. Cell cycle-coupled relocation of types I and II topoisomerases and modulation of catalytic enzyme activities. *J Cell Biol* **136**, 775-88 (1997).
193. Warburton, P.E. & Earnshaw, W.C. Untangling the role of DNA topoisomerase II in mitotic chromosome structure and function. *Bioessays* **19**, 97-9 (1997).
194. Maeshima, K. & Laemmli, U.K. A two-step scaffolding model for mitotic chromosome assembly. *Dev Cell* **4**, 467-80 (2003).
195. Poljak, L. & Kas, E. Resolving the role of topoisomerase II in chromatin structure and function. *Trends Cell Biol* **5**, 348-54 (1995).
196. Gasser, S.M. & Laemmli, U.K. The organisation of chromatin loops: characterization of a scaffold attachment site. *Embo J* **5**, 511-518 (1986).
197. Adolph, K.W., Cheng, S.M. & Laemmli, U.K. Role of nonhistone proteins in metaphase chromosome structure. *Cell* **12**, 805-16 (1977).
198. Paulson, J.R. & Laemmli, U.K. The structure of histone-depleted metaphase chromosomes. *Cell* **12**, 817-28 (1977).
199. Marsden, M.P. & Laemmli, U.K. Metaphase chromosome structure: evidence for a radial loop model. *Cell* **17**, 849-58 (1979).
200. Rattner, J.B. & Lin, C.C. Radial loops and helical coils coexist in metaphase chromosomes. *Cell* **42**, 291-6 (1985).
201. Earnshaw, W.C., Halligan, B., Cooke, C.A., Heck, M.M. & Liu, L.F. Topoisomerase II is a structural component of mitotic chromosome scaffolds. *J Cell Biol* **100**, 1706-15 (1985).
202. Adachi, Y., Kas, E. & Laemmli, U.K. Preferential, cooperative binding of DNA topoisomerase II to scaffold-associated regions. *Embo J* **8**, 3997-4006 (1989).
203. Null, A.P., Hudson, J. & Gorbsky, G.J. Both alpha and beta isoforms of mammalian DNA topoisomerase II associate with chromosomes in mitosis. *Cell Growth Differ* **13**, 325-33 (2002).
204. Hirano, T. & Mitchison, T.J. Topoisomerase II does not play a scaffolding role in the organization of mitotic chromosomes assembled in Xenopus egg extracts. *J Cell Biol* **120**, 601-12 (1993).

205. Berger, J.M. Type II DNA topoisomerases. *Curr Opin Struct Biol* **8**, 26-32 (1998).
206. Biersack, H. et al. Active heterodimers are formed from human DNA topoisomerase II alpha and II beta isoforms. *Proc Natl Acad Sci U S A* **93**, 8288-93 (1996).
207. Wigley, D.B., Davies, G.J., Dodson, E.J., Maxwell, A. & Dodson, G. Crystal structure of an N-terminal fragment of the DNA gyrase B protein. *Nature* **351**, 624-9 (1991).
208. Isaacs, R.J. et al. Physiological regulation of eukaryotic topoisomerase II. *Biochim Biophys Acta* **1400**, 121-37 (1998).
209. Osheroff, N. Role of the divalent cation in topoisomerase II mediated reactions. *Biochemistry* **26**, 6402-6 (1987).
210. Dong, K.C. & Berger, J.M. Structural basis for gate-DNA recognition and bending by type IIA topoisomerases. *Nature* **450**, 1201-5 (2007).
211. Bechert, T., Diekmann, S. & Arndt-Jovin, D.J. Human 170 kDa and 180 kDa topoisomerases II bind preferentially to curved and left-handed linear DNA. *J Biomol Struct Dyn* **12**, 605-23 (1994).
212. Burden, D.A. & Osheroff, N. Mechanism of action of eukaryotic topoisomerase II and drugs targeted to the enzyme. *Biochim Biophys Acta* **1400**, 139-54 (1998).
213. Muller, M.T. et al. Single-strand DNA cleavages by eukaryotic topoisomerase II. *Biochemistry* **27**, 8369-79 (1988).
214. Zechiedrich, E.L., Christiansen, K., Andersen, A.H., Westergaard, O. & Osheroff, N. Double-stranded DNA cleavage/religation reaction of eukaryotic topoisomerase II: evidence for a nicked DNA intermediate. *Biochemistry* **28**, 6229-36 (1989).
215. Sander, M. & Hsieh, T. Double strand DNA cleavage by type II DNA topoisomerase from Drosophila melanogaster. *J Biol Chem* **258**, 8421-8 (1983).
216. Liu, L.F., Rowe, T.C., Yang, L., Tewey, K.M. & Chen, G.L. Cleavage of DNA by mammalian DNA topoisomerase II. *J Biol Chem* **258**, 15365-70 (1983).
217. Downes, C.S., Mullinger, A.M. & Johnson, R.T. Inhibitors of DNA topoisomerase II prevent chromatid separation in mammalian cells but do not prevent exit from mitosis. *Proc Natl Acad Sci U S A* **88**, 8895-9 (1991).
218. Osheroff, N., Shelton, E.R. & Brutlag, D.L. DNA topoisomerase II from Drosophila melanogaster. Relaxation of supercoiled DNA. *J Biol Chem* **258**, 9536-43 (1983).
219. Osheroff, N. Eukaryotic topoisomerase II. Characterization of enzyme turnover. *J Biol Chem* **261**, 9944-50 (1986).
220. Roca, J., Berger, J.M., Harrison, S.C. & Wang, J.C. DNA transport by a type II topoisomerase: direct evidence for a two-gate mechanism. *Proc Natl Acad Sci U S A* **93**, 4057-62 (1996).
221. Graille, M. et al. Crystal structure of an intact type II DNA topoisomerase: insights into DNA transfer mechanisms. *Structure* **16**, 360-70 (2008).
222. Liu, L.F. DNA topoisomerase poisons as antitumor drugs. *Annu Rev Biochem* **58**, 351-75 (1989).
223. Epstein, R.J. Topoisomerases in human disease. *Lancet* **1**, 521-4 (1988).
224. Roca, J., Ishida, R., Berger, J.M., Andoh, T. & Wang, J.C. Antitumor bisdioxopiperazines inhibit yeast DNA topoisomerase II by trapping the

enzyme in the form of a closed protein clamp. *Proc Natl Acad Sci U S A* **91**, 1781-5 (1994).
225. Perrin, D., van Hille, B. & Hill, B.T. Differential sensitivities of recombinant human topoisomerase IIalpha and beta to various classes of topoisomerase II-interacting agents. *Biochem Pharmacol* **56**, 503-7 (1998).
226. Park, I. & Avraham, H.K. Cell cycle-dependent DNA damage signaling induced by ICRF-193 involves ATM, ATR, CHK2, and BRCA1. *Exp Cell Res* **312**, 1996-2008 (2006).
227. Hande, K.R. Etoposide: four decades of development of a topoisomerase II inhibitor. *Eur J Cancer* **34**, 1514-21 (1998).
228. Houlbrook, S. et al. Relationship between expression of topoisomerase II isoforms and intrinsic sensitivity to topoisomerase II inhibitors in breast cancer cell lines. *Br J Cancer* **72**, 1454-61 (1995).
229. Orlando, L. et al. Topoisomerase IIalpha gene status and prediction of pathological complete remission after anthracycline-based neoadjuvant chemotherapy in endocrine non-responsive Her2/neu-positive breast cancer. *Breast* **17**, 506-11 (2008).
230. Nelson, E.M., Tewey, K.M. & Liu, L.F. Mechanism of antitumor drug action: poisoning of mammalian DNA topoisomerase II on DNA by 4'-(9-acridinylamino)-methanesulfon-m-anisidide. *Proc Natl Acad Sci U S A* **81**, 1361-5 (1984).
231. Pommier, Y., Minford, J.K., Schwartz, R.E., Zwelling, L.A. & Kohn, K.W. Effects of the DNA intercalators 4'-(9-acridinylamino)methanesulfon-m-anisidide and 2-methyl-9-hydroxyellipticinium on topoisomerase II mediated DNA strand cleavage and strand passage. *Biochemistry* **24**, 6410-6 (1985).
232. McClendon, A.K. & Osheroff, N. DNA topoisomerase II, genotoxicity, and cancer. *Mutat Res* **623**, 83-97 (2007).
233. Drake, F.H. et al. In vitro and intracellular inhibition of topoisomerase II by the antitumor agent merbarone. *Cancer Res* **49**, 2578-83 (1989).
234. Tanabe, K., Ikegami, Y., Ishida, R. & Andoh, T. Inhibition of topoisomerase II by antitumor agents bis(2,6-dioxopiperazine) derivatives. *Cancer Res* **51**, 4903-8 (1991).
235. Jensen, P.B. et al. Antagonistic effect of aclarubicin on the cytotoxicity of etoposide and 4'-(9-acridinylamino)methanesulfon-m-anisidide in human small cell lung cancer cell lines and on topoisomerase II-mediated DNA cleavage. *Cancer Res* **50**, 3311-6 (1990).
236. Sabourin, M. & Osheroff, N. Sensitivity of human type II topoisomerases to DNA damage: stimulation of enzyme-mediated DNA cleavage by abasic, oxidized and alkylated lesions. *Nucleic Acids Res* **28**, 1947-54 (2000).
237. Kingma, P.S. & Osheroff, N. Apurinic sites are position-specific topoisomerase II poisons. *J Biol Chem* **272**, 1148-55 (1997).
238. Kingma, P.S., Corbett, A.H., Burcham, P.C., Marnett, L.J. & Osheroff, N. Abasic sites stimulate double-stranded DNA cleavage mediated by topoisomerase II. DNA lesions as endogenous topoisomerase II poisons. *J Biol Chem* **270**, 21441-4 (1995).
239. Kingma, P.S. & Osheroff, N. Spontaneous DNA damage stimulates topoisomerase II-mediated DNA cleavage. *J Biol Chem* **272**, 7488-93 (1997).
240. Felix, C.A., Kolaris, C.P. & Osheroff, N. Topoisomerase II and the etiology of chromosomal translocations. *DNA Repair (Amst)* **5**, 1093-108 (2006).

241. Cantero, G., Campanella, C., Mateos, S. & Cortes, F. Topoisomerase II inhibition and high yield of endoreduplication induced by the flavonoids luteolin and quercetin. *Mutagenesis* **21**, 321-5 (2006).
242. Kingma, P.S. & Osheroff, N. The response of eukaryotic topoisomerases to DNA damage. *Biochim Biophys Acta* **1400**, 223-32 (1998).
243. Cortes, F., Pinero, J. & Ortiz, T. Importance of replication fork progression for the induction of chromosome damage and SCE by inhibitors of DNA topoisomerases. *Mutat Res* **303**, 71-6 (1993).
244. Noviello, E. et al. Sister-chromatid exchanges, chromosomal aberrations and cytotoxicity produced by topoisomerase II-targeted drugs in sensitive (A2780) and resistant (A2780-DX3) human ovarian cancer cells: correlations with the formation of DNA double-strand breaks. *Mutat Res* **311**, 21-9 (1994).
245. Suzuki, H., Tarumoto, Y. & Ohsawa, M. Topoisomerase II inhibitors fail to induce chromosome-type aberrations in etoposide-resistant cells: evidence for essential contribution of the cleavable complex formation to the induction of chromosome-type aberrations. *Mutagenesis* **12**, 29-33 (1997).
246. Suzuki, H. & Nakane, S. Differential induction of chromosomal aberrations by topoisomerase inhibitors in cultured Chinese hamster cells. *Biol Pharm Bull* **17**, 222-6 (1994).
247. Suzuki, H. et al. Efficient induction of chromosome-type aberrations by topoisomerase II inhibitors closely associated with stabilization of the cleavable complex in cultured fibroblastic cells. *Mutat Res* **328**, 151-61 (1995).
248. Sung, P.A., Libura, J. & Richardson, C. Etoposide and illegitimate DNA double-strand break repair in the generation of MLL translocations: new insights and new questions. *DNA Repair (Amst)* **5**, 1109-18 (2006).
249. Kingma, P.S., Greider, C.A. & Osheroff, N. Spontaneous DNA lesions poison human topoisomerase IIalpha and stimulate cleavage proximal to leukemic 11q23 chromosomal breakpoints. *Biochemistry* **36**, 5934-9 (1997).
250. Kantidze, O.L. & Razin, S.V. Chemotherapy-related secondary leukemias: A role for DNA repair by error-prone non-homologous end joining in topoisomerase II - Induced chromosomal rearrangements. *Gene* **391**, 76-9 (2007).
251. Coiteux, V., Onclercq-Delic, R., Fenaux, P. & Amor-Gueret, M. Predisposition to therapy-related acute leukemia with balanced chromosomal translocations does not result from a major constitutive defect in DNA double-strand break end joining. *Leuk Res* **31**, 353-8 (2007).
252. Chadwick, K.H. & Leenhouts, H.P. The rejoining of DNA double-strand breaks and a model for the formation of chromosomal rearrangements. *Int J Radiat Biol Relat Stud Phys Chem Med* **33**, 517-29 (1978).
253. Withoff, S. et al. DNA topoisomerase IIalpha and -beta expression in human ovarian cancer. *Br J Cancer* **79**, 748-53 (1999).
254. McLeod, H.L. et al. Topoisomerase I and II activity in human breast, cervix, lung and colon cancer. *Int J Cancer* **59**, 607-11 (1994).
255. Segawa, E. et al. Expression of cyclooxygenase-2 and DNA topoisomerase II alpha in precancerous and cancerous lesions of the oral mucosa. *Oral Oncol* **44**, 664-71 (2008).
256. Hannemann, J. et al. Molecular subtypes of breast cancer and amplification of topoisomerase II alpha: predictive role in dose intensive adjuvant chemotherapy. *Br J Cancer* **95**, 1334-41 (2006).

257. Kalogeraki, A. et al. Topoisomerase II alpha expression in breast ductal invasive carcinomas and correlation with clinicopathological variables. *In Vivo* **19**, 837-40 (2005).
258. Smith, P.J. & Makinson, T.A. Cellular consequences of overproduction of DNA topoisomerase II in an ataxia-telangiectasia cell line. *Cancer Res* **49**, 1118-24 (1989).
259. Davies, S.M., Harris, A.L. & Hickson, I.D. Overproduction of topoisomerase II in an ataxia telangiectasia fibroblast cell line: comparison with a topoisomerase II-overproducing hamster cell mutant. *Nucleic Acids Res* **17**, 1337-51 (1989).
260. Antoccia, A., Palitti, F., Raggi, T., Catena, C. & Tanzarella, C. Lack of effect of inhibitors of DNA synthesis/repair on the ionizing radiation-induced chromosomal damage in G2 stage of ataxia telangiectasia cells. *Int J Radiat Biol* **66**, 309-17 (1994).
261. Singh, S.P., Mohamed, R., Salmond, C. & Lavin, M.F. Reduced DNA topoisomerase II activity in ataxia-telangiectasia cells. *Nucleic Acids Res* **16**, 3919-29 (1988).
262. Rosselli, F., Duchaud, E., Averbeck, D. & Moustacchi, E. Comparison of the effects of DNA topoisomerase inhibitors on lymphoblasts from normal and Fanconi anemia donors. *Mutat Res* **325**, 137-44 (1994).
263. Poot, M. & Hoehn, H. DNA topoisomerases and the DNA lesion in human genetic instability syndromes. *Toxicol Lett* **67**, 297-308 (1993).
264. Malik, M., Nitiss, K.C., Enriquez-Rios, V. & Nitiss, J.L. Roles of nonhomologous end-joining pathways in surviving topoisomerase II-mediated DNA damage. *Mol Cancer Ther* **5**, 1405-1414 (2006).
265. Ayene, I.S., Ford, L.P. & Koch, C.J. Ku protein targeting by Ku70 small interfering RNA enhances human cancer cell response to topoisomerase II inhibitor and gamma radiation. *Mol Cancer Ther* **4**, 529-36 (2005).
266. Adachi, N., Iiizumi, S., So, S. & Koyama, H. Genetic evidence for involvement of two distinct nonhomologous end-joining pathways in repair of topoisomerase II-mediated DNA damage. *Biochem Biophys Res Commun* **318**, 856-61 (2004).
267. Bromberg, K.D., Burgin, A.B. & Osheroff, N. A two-drug model for etoposide action against human topoisomerase IIalpha. *J Biol Chem* **278**, 7406-12 (2003).
268. Martensson, S., Nygren, J., Osheroff, N. & Hammarsten, O. Activation of the DNA-dependent protein kinase by drug-induced and radiation-induced DNA strand breaks. *Radiat Res* **160**, 291-301 (2003).
269. Labib, K. & Hodgson, B. Replication fork barriers: pausing for a break or stalling for time? *EMBO Rep* **8**, 346-53 (2007).
270. Montecucco, A. & Biamonti, G. Cellular response to etoposide treatment. *Cancer Lett* **252**, 9-18 (2007).
271. Mao, Y., Desai, S.D., Ting, C.Y., Hwang, J. & Liu, L.F. 26 S proteasome-mediated degradation of topoisomerase II cleavable complexes. *J Biol Chem* **276**, 40652-8 (2001).
272. Zhang, A. et al. A protease pathway for the repair of topoisomerase II-DNA covalent complexes. *J Biol Chem* **281**, 35997-6003 (2006).
273. Bae, Y.S., Kawasaki, I., Ikeda, H. & Liu, L.F. Illegitimate recombination mediated by calf thymus DNA topoisomerase II in vitro. *Proc Natl Acad Sci U S A* **85**, 2076-80 (1988).

274. Mateos, S., Hajji, N., Pastor, N. & Cortes, F. Modulation of radiation response by inhibiting topoisomerase II catalytic activity. *Mutat Res* **599**, 105-15 (2006).
275. Downes, C.S., Mullinger, A.M. & Johnson, R.T. Action of etoposide (VP-16-123) on human cells: no evidence for topoisomerase II involvement in excision repair of u.v.-induced DNA damage, nor for mitochondrial hypersensitivity in ataxia telangiectasia. *Carcinogenesis* **8**, 1613-8 (1987).
276. Pastor, N. & Cortes, F. DNA topoisomerase activities in Chinese hamster radiosensitive mutants after X-ray treatment. *Cell Biol Int* **26**, 547-55 (2002).
277. Mandraju, R.K., Kannapiran, P. & Kondapi, A.K. Distinct roles of Topoisomerase II isoforms: DNA damage accelerating alpha, double strand break repair promoting beta. *Arch Biochem Biophys* **470**, 27-34 (2008).
278. Yamane, K., Kawabata, M. & Tsuruo, T. A DNA-topoisomerase-II-binding protein with eight repeating regions similar to DNA-repair enzymes and to a cell-cycle regulator. *Eur J Biochem* **250**, 794-9 (1997).
279. Mordes, D.A., Glick, G.G., Zhao, R. & Cortez, D. TopBP1 activates ATR through ATRIP and a PIKK regulatory domain. *Genes Dev* **22**, 1478-89 (2008).
280. Yoo, H.Y., Kumagai, A., Shevchenko, A., Shevchenko, A. & Dunphy, W.G. Ataxia-telangiectasia mutated (ATM)-dependent activation of ATR occurs through phosphorylation of TopBP1 by ATM. *J Biol Chem* **282**, 17501-6 (2007).
281. Going, J.J. et al. Aberrant expression of TopBP1 in breast cancer. *Histopathology* **50**, 418-24 (2007).
282. Bradford, M.M. A rapid and sensitive method for the quantitation of microgram quantities of protein utilizing the principle of protein-dye binding. *Anal Biochem* **72**, 248-54 (1976).
283. Laemmli, U.K. Cleavage of structural proteins during the assembly of the head of bacteriophage T4. *Nature* **227**, 680-5 (1970).
284. Xu, J. et al. Identification of differentially expressed genes in human prostate cancer using subtraction and microarray. *Cancer Res* **60**, 1677-82 (2000).
285. Gallagher, R. et al. Characterization of the continuous, differentiating myeloid cell line (HL-60) from a patient with acute promyelocytic leukemia. *Blood* **54**, 713-33 (1979).
286. Collins, S.J., Gallo, R.C. & Gallagher, R.E. Continuous growth and differentiation of human myeloid leukaemic cells in suspension culture. *Nature* **270**, 347-9 (1977).
287. Wang, J., Xie, L.Y., Allan, S., Beach, D. & Hannon, G.J. Myc activates telomerase. *Genes Dev* **12**, 1769-74 (1998).
288. Knoepfler, P.S. Myc goes global: new tricks for an old oncogene. *Cancer Res* **67**, 5061-3 (2007).
289. Shay, J.W., Zou, Y., Hiyama, E. & Wright, W.E. Telomerase and cancer. *Hum Mol Genet* **10**, 677-85 (2001).
290. Harker, W.G., Slade, D.L., Dalton, W.S., Meltzer, P.S. & Trent, J.M. Multidrug resistance in mitoxantrone-selected HL-60 leukemia cells in the absence of P-glycoprotein overexpression. *Cancer Res* **49**, 4542-9 (1989).
291. Robinson, M.J. & Osheroff, N. Effects of antineoplastic drugs on the post-strand-passage DNA cleavage/religation equilibrium of topoisomerase II. *Biochemistry* **30**, 1807-13 (1991).
292. Deitch, A.D., Law, H. & deVere White, R. A stable propidium iodide staining procedure for flow cytometry. *J Histochem Cytochem* **30**, 967-72 (1982).

293. Wei, Y., Mizzen, C.A., Cook, R.G., Gorovsky, M.A. & Allis, C.D. Phosphorylation of histone H3 at serine 10 is correlated with chromosome condensation during mitosis and meiosis in Tetrahymena. *Proc Natl Acad Sci U S A* **95**, 7480-4 (1998).
294. Marini, J.C., Miller, K.G. & Englund, P.T. Decatenation of kinetoplast DNA by topoisomerases. *J Biol Chem* **255**, 4976-9 (1980).
295. Marquez, C., Egozcue, J., Martorell, M.R., Moreno, V. & Templado, C. Colcemid increases the frequency of chromosome abnormalities in human sperm. *Cytogenet Cell Genet* **72**, 164-70 (1996).
296. Schwartz, D.C. & Cantor, C.R. Separation of yeast chromosome-sized DNAs by pulsed field gradient gel electrophoresis. *Cell* **37**, 67-75 (1984).
297. Fire, A. et al. Potent and specific genetic interference by double-stranded RNA in Caenorhabditis elegans. *Nature* **391**, 806-11 (1998).
298. Bernstein, E., Caudy, A.A., Hammond, S.M. & Hannon, G.J. Role for a bidentate ribonuclease in the initiation step of RNA interference. *Nature* **409**, 363-6 (2001).
299. Leuschner, P.J., Ameres, S.L., Kueng, S. & Martinez, J. Cleavage of the siRNA passenger strand during RISC assembly in human cells. *EMBO Rep* **7**, 314-20 (2006).
300. Liu, J. et al. Argonaute2 is the catalytic engine of mammalian RNAi. *Science* **305**, 1437-41 (2004).
301. Eriksson, S., Thelander, L. & Akerman, M. Allosteric regulation of calf thymus ribonucleoside diphosphate reductase. *Biochemistry* **18**, 2948-52 (1979).
302. Adachi, Y., Luke, M. & Laemmli, U.K. Chromosome assembly in vitro: topoisomerase II is required for condensation. *Cell* **64**, 137-48 (1991).
303. Anderson, H. & Roberge, M. Topoisomerase II inhibitors affect entry into mitosis and chromosome condensation in BHK cells. *Cell Growth Differ* **7**, 83-90 (1996).
304. Wood, E.R. & Earnshaw, W.C. Mitotic chromatin condensation in vitro using somatic cell extracts and nuclei with variable levels of endogenous topoisomerase II. *J Cell Biol* **111**, 2839-50 (1990).
305. Kibbe, W.A. OligoCalc: an online oligonucleotide properties calculator. *Nucleic Acids Res* **35**, W43-6 (2007).
306. Pretazzoli, V., Salone, B., Bosi, A. & Olivieri, G. Variability of G(2) checkpoint sensitivity to low doses of X-rays (2 cGy): correlation with G(2) chromatid aberrations but not with an adaptive response. *Mutagenesis* **15**, 531-5 (2000).
307. Downes, C.S. et al. A topoisomerase II-dependent G2 cycle checkpoint in mammalian cells. *Nature* **372**, 467-70 (1994).
308. Robinson, H.M., Bratlie-Thoresen, S., Brown, R. & Gillespie, D.A. Chk1 is required for G2/M checkpoint response induced by the catalytic topoisomerase II inhibitor ICRF-193. *Cell Cycle* **6**, 1265-7 (2007).
309. Luo, K., Yuan, J., Chen, J. & Lou, Z. Topoisomerase IIalpha controls the decatenation checkpoint. *Nat Cell Biol* **11**, 204-10 (2009).
310. Hossain, M.S., Akimitsu, N., Takaki, T., Hirai, H. & Sekimizu, K. ICRF-193, a catalytic inhibitor of DNA topoisomerase II, inhibits re-entry into the cell division cycle from quiescent state in mammalian cells. *Genes Cells* **7**, 285-94 (2002).

311. Hajji, N., Pastor, N., Mateos, S., Dominguez, I. & Cortes, F. DNA strand breaks induced by the anti-topoisomerase II bis-dioxopiperazine ICRF-193. *Mutat Res* **530**, 35-46 (2003).
312. Oya, Y., Yamamoto, K. & Tonomura, A. The biological activity of hydrogen peroxide. I. Induction of chromosome-type aberrations susceptible to inhibition by scavengers of hydroxyl radicals in human embryonic fibroblasts. *Mutat Res* **172**, 245-53 (1986).
313. Tsuda, H. Chromosomal aberrations induced by hydrogen peroxide in cultured mammalian cells. *Jpn J Genet* **56**, 1-8 (1981).
314. Frankenberg-Schwager, M., Becker, M., Garg, I., Wolf, H. & Frankenberg, D. The role of nonhomologous DNA end joining, conservative homologous recombination, and single-strand annealing in the cell cycle-dependent repair of DNA double-strand breaks induced by H2O2 in mammalian cells. *Radiat Res* **170**, 784-793 (2008).
315. Binnig, G., Quate, C.F. & Gerber, C. Atomic force microscope. *Phys Rev Lett* **56**, 930-933 (1986).
316. Murakami, M., Kanda, R., Minamihisamatsu, M. & Hayata, I. Characterization of ionizing radiation-induced ring chromosomes by atomic force microscopy. *Anal Biochem* **334**, 251-6 (2004).
317. Murakami, M., Minamihisamatsu, M., Sato, K. & Hayata, I. Structural analysis of heavy ion radiation-induced chromosome aberrations by atomic force microscopy. *J Biochem Biophys Methods* **48**, 293-301 (2001).
318. Murakami, M., Hirokawa, H. & Hayata, I. Analysis of radiation damage of DNA by atomic force microscopy in comparison with agarose gel electrophoresis studies. *J Biochem Biophys Methods* **44**, 31-40 (2000).
319. Wu, Y., Cai, J., Cheng, L., Wang, C. & Chen, Y. Chromosome imaging by atomic force microscopy: influencing factors and comparative evaluation. *J Genet* **85**, 141-5 (2006).
320. Prise, K.M., Davies, S. & Michael, B.D. Cell killing and DNA damage in Chinese hamster V79 cells treated with hydrogen peroxide. *Int J Radiat Biol* **55**, 583-92 (1989).
321. Elmore, S. Apoptosis: a review of programmed cell death. *Toxicol Pathol* **35**, 495-516 (2007).
322. Osheroff, N. Effect of antineoplastic agents on the DNA cleavage/religation reaction of eukaryotic topoisomerase II: inhibition of DNA religation by etoposide. *Biochemistry* **28**, 6157-60 (1989).
323. Cadet, J. et al. Hydroxyl radicals and DNA base damage. *Mutat Res* **424**, 9-21 (1999).

APPENDICES

Appendix A – Topo IIα mRNA sequence data

Acquired from: National Center for Biotechnology Information (NCBI)
Reference number: >gi|19913405|ref|NM_001067.2| Homo sapiens topoisomerase (DNA) II alpha 170kDa (TOP2A), mRNA)

Altered to show exon boundaries (determined from Lang *et al.* 1998 [152]) so exons alternate from bold to normal font.

ATGGAAGTGTCACCATTGCAGCCTGTAAATGAAAATATGCAAGTCAACAAAATAAAGAAAAATGAAGAT
GCTAAGAAAAGACTGTCTGTTGAAAGAATCTATCAAAAGAAAACACAATTGGAACATATTTTGCTCCGC
CCAGACACCTACATTGGTTCTGTGGAATTAGTGACCCAG**CAAATGTGGGTTTACGATGAAGATGTTGGC**
ATTAACTATAGGGAAGTCACTTTTGTTCCTGGTTTGTACAAAATCTTTGATGAGATTCTAGTTAATGCT
GCGGACAACAAACAAAGGGACCCAAAAATGTCTTGTATTAGAGTCACAATTGATCC**GGAAAACAATTTA**
ATTAGTATATGGAATAATGGAAAAGGTATTCCTGTTGTTGAACACAAAGTTGAAAAGATGTATGTCCCA
GCTCTCATATTTGGACAGCTCCTAACTTCTAGTAACTATGATGATGATGAAAAGAAAGTGACAGGTGGT
CGAAATGGCTATGGAGCCAAATTGTGTAACATATTCAGTACCAAATTTACTGTGGAAACAGCCAGTAGA
GAATACAAGAAAATGTTCAAACAG**ACATGGATGGATAATATGGGAAGAGCTGGTGAGATGGAACTCAAG**
CCCTTCAATGGAGAAGATTATACATGTATCACCTTTCAGCCTGATTTGTCTAAGTTTAAAATGCAAAGC
CTGGACAAAGATATTGTTGCACTAATGGTCAGAAGAGCATATGATATTGCTGGATCCACCAAAGATGTC
AAAGTCTTTCTTAATGGAAATAAACTGCCAGTAAAAGGATTTCGTAGTTATGTGGACATGTATTTGAAG
GACAAGTTGGATGAAACTGGTAACTCCTTGAAAGTAATACATGAACAAGTAAACCACAGGTGGGAAGTG
TGTTTAACTATGAGTGAAAAAGGCTTTCAGCAAATTAGCTTTGTCAACAGCATTGCTACATCCAAG**GGT**
GGCAGACATGTTGATTATGTAGCTGATCAGATTGTGACTAAACTTGTTGATGTTGTGAAGAAGAAGAAC
AAGGGTGGTGTTGCAGTAAAAGCACATCAGGTGAAAAATCACATGTGGATTTTTGTAAATGCCTTAATT
GAAAACCCAACCTTTGACTCTCAGACAAAAGAAAACATGACTTTACAACCCAAGAGCTTTGGATCAACA
TGCCAATTGAGTGAAAAATTTATCAAAGCT**GCCATTGGCTGTGGTATTGTAGAAAGCATACTAAACTGG**
GTGAAGTTTAAGGCCCAAGTCCAGTTAAACAAGAAGTGTTCAGCTGTAAAACATAATAGAATCAAGGGA
ATTCCCAAACTCGATGATGCCAATGATGCAGGGGGCCGAAACTCCACTGAGTGTACGCTTATCCTGACT
GAGGGAGATTCAGCCAAAACTTTGGCTGTTTCAGGCCTTGGTGTGGTTGGGAGAGACAAATATGGGGTT
TTCCCTCTTAGAGGAAAAATACTCAATGTTCGAGAAGCTTCTCATAAGCAG**ATCATGGAAAATGCTGAG**
ATTAACAATATCATCAAGATTGTGGGTCTTCAGTACAAGAAAAACTATGAAGATGAAGATTCATTGAAG
ACGCTTCGTTATGGGAAGATAATGATTATGACAGATCAGGACCAAGATGGTTCCCACATCAAAGGCTTG
CTGATTAATTTTATCCATCACAACTGGCCCTCTCTTCTGCGACATCGTTTTCTGGAGGAATTTATCACT
CCCATTGTAAAG**GTATCTAAAAACAAGCAAGAAATGGCATTTTACAGCCTTCCTGAATTTGAAGAGTGG**
AAGAGTTCTACTCCAAATCATAAAAAATGGAAAGTCAAATATTACAAAGGTTTGGGCACCAGCACATCA
AAGGAAGCTAAAGAATACTTTGCAGATATGAAAAGACATCGTATCCAGTTCAAATATTCTGGTCCTGAA
GATGATGCTGCTATCAGCCTG**GCCTTTAGCAAAAAACAGATAGATGATCGAAAGGAATGGTTAACTAAT**
TTCATGGAGGATAGAAGACAACGAAAGTTACTTGGGCTTCCTGAGGATTACTTGTATGGACAAACTACC
ACATATCTGACATATAATGACTTCATCAACAAGGAACTTATCTTGTTCTCAAATTCTGATAACGAGAGA
TCTATCCCTTCTATGGTGGATG**GTTTGAAACCAGGTCAGAGAAAGGTTTTGTTTACTTGCTTCAAACGG**
AATGACAAGCGAGAAGTAAAGGTTGCCCAATTAGCTGGATCAGTGGCTGAAATGTCTTCTTATCATCAT
GGTGAGATGTCACTAATGATGACCATTATCAATTTGGCTCAGAATTTTGTGGGTAGCAATAATCTAAAC
CTCTTGCAGCCCATTGGTCAGTTTGGTACCAGGCTACATGGTGGCAAGGATTCTGCTAGTCCACGATAC
ATCTTTACAATGCTCAG**CTCTTTGGCTCGATTGTTATTTCCACCAAAAGATGATCACACGTTGAAGTTT**
TTATATGATGACAACCAGCGTGTTGAGCCTGAATG**GTACATTCCTATTATTCCCATGGTGCTGATAAAT**
GGTGCTGAAGGAATCGGTACTGGGTGGTCCTGCAAAATCCCCAACTTTGATGTGCGTGAAATTGTAAAT
AACATCAGGCGTTTGATGGATGGAGAAGAACCTTTGCCAATGCTTCCAAGTTACAAGAACTTCAAGGGT
ACTATTGAAGAACTGGCTCCAAATCAATATGTGATTAGTGGTGAAGTAGCTATTCTTAATTCTACAACC
ATTGAAATCTCAGAGCTTCCCGTCAGAACATGGACCCAG**ACATACAAAGAACAAGTTCTAGAACCCATG**
TTGAATGGCACCGAGAAGACACCTCCTCTCATAACAGACTATAGGGAATACCATACAGATACCACTGTG
AAATTTGTTGTGAAGATGACTGAAGAAAAACTGGCAGAGGCAGAGAGAGTTGGACTACACAAAGTCTTC
AAACTCCAAACTAGTCTCACATGCAACTCTATGGTGCTTTTTGACCACGTAGGCTGTTTAAAGAAATAT
GACACGGTGTTGGATATTCTAAGAGACTTTTTTGAACTCAGACTTAAATATTATGGATTAAGAAAAGAA

Start codon

Exon 5 siRNA α 1

Forward Primer Topo IIα

TGGCTCCTAGGAATGCTTGGTGCTGAATCTGCTAAACTGAATAATCAGGCTCGCTTTATCTTAGAGAAA
ATAGATGGCAAAATAATCATTG**AAAATAAGCCTAAGAAAGAATTAATTAAAGTTCTGATTCAGAGGGGA**
TATGATTCGGATCCTGTGAAGGCCTGGAAAGAAGCCCAGCAAAAGGTTCCAGATGAAGAAGAAAATGAA
GAGAGTGACAACGAAAAGGAAACTGAAAAGAGTGACTCCGTAACAGATTCTGGACCAACCTTCAACTAT
CTTCTTGATATGCCCCTTTGGTATTTAACCAAGGAAAAGAAAGATGAACTCTGCAGGCTAAGAAATGAA
AAA**GAACAAGAGCTGGACACATTAAAAAGAAAGAGTCCATCAGATTTGTGGAAAGAAGACTTGGCTACA**
TTTATTGAAGAATTGGAGGCTGTTGAAGCCAAGGAAAAACAAGATGAACAAGTCGGACTTCCTGGGAAA
GGGGGGAAGGCCAAGGGGAAAAAAACACAAATGGCTGAAGTTTTGCCTTCTCCGCGTGGTCAAAGAGTC
ATTCCACGAATAACCATAGAAATGAAAGCAGAGGCAGAAAAGAAAAATAAAAAGAAAATTAAG**AATGAA**
AATACTGAAGGAAGCCCTCAAGAAGATGGTGTGGAACTAGAAGGCCTAAAACAAAGATTAGAAAAGAAA
CAGAAAAGAGAACCAGGTACAAAGACAAAGAAACAAACTACATTGGCATTTAAGCCAATCAAAAAAGGA
AAGAAGAGAAATCCCTGGTCTGATTCAGAATCAGATAGGAGCAGTGACGAAAGTAATTTTGATGTCCCT
CCACGAGAAACAGAGCCACGGAGAGCAGCAA**CAAAAACAAAATTCACAATGGATTTGGATTCAGATGAA**
GATTTCTCAGATTTTGATGAAAAAACTGATGATGAAGATTTTGTCCCATCAGATGCTAGTCCACCTAAG
ACCAAAACTTCCCCAAAACTTAGTAACAAAGAACTGAAACCACAGAAAAGTGTCGTGTCAG**ACCTTGAA**
GCTGATGATGTTAAGGGCAGTGTACCACTGTCTTCAAGCCCTCCTGCTACACATTTCCCAGATGAAACT
GAAATTACAAACCCAGTTCCTAAAAAGAATGTGACAGTGAAGAAGACAGCAGCAAAAAGTCAGTCTTCC
ACCTCCACTACCGGTGCCAAAAAAAGGGCTGCCCCAAAAGGAACTAAAAGGGATCCAGCTTTGAATTCT
GGTGTCTCTCAAAAGCCTGATCCTGCCAAAACCAAGAATCGCCGCAAAAGGAAGCCATCCACTTCTGAT
GATTCTGACTCTAATTTTGAGAAAATTGTTTCGAAAGCAGTCACAAGCAAG**AAATCCAAGGGGGAGAGT**
GATGACTTCCATATGGACTTTGACTCAGCTGTGGCTCCTCGGGCAAAATCTGTACGGGCAAAGAAACCT
ATAAAGTACCTGGAAGAGTCAGATGAAGATGATCTGTTTTAA

Exon 26 siRNA α 2

Reverse Primer Topo IIα

Stop codon

Difference in coding length between forward and reverse primer for topo IIα: **1573** nucleotides

Appendix B – β-actin mRNA sequence data

Acquired from: National Center for Biotechnology Information (NCBI)
Reference number: > gi|5016088|ref|NM_001101.2| Homo sapiens actin, beta (ACTB), mRNA

Altered to show exon boundaries (determined from NCBI/CCDS ID CCDS5341.1) so exons alternate from bold to normal font.

ATGGATGATGATATCGCCGCGCTCGTCGTCGACAACGGCTCCGGCATGTGCAAGGCCGGCTTCGCGGGC
GACGATGCCCCCCGGGCCGTCTTCCCCTCCATCGTGGGGCGCCCCAGGCACCAGGGCGTGATGGTGGGC
ATGGGTCAGAAGGATTCCTATGTGGGCGACGAGGCCCAGAGCAAGAGAGGCATCCTCACCCTGAAGTAC
CCCATCGAGCACGGCATCGTCACCAACTGGGACGACATGGAGAAAATCTGGCACCACACCTTCTACAAT
GAGCTGCGTGTGGCTCCCGAGGAGCACCCCGTGCTGCTGACCGAGGCCCCCCTGAACCCCAAGGCCAAC
CGCGAGAAGATGACCCAG**ATCATGTTTGAGACCTTCAACACCCCAGCCATGTACGTTGCTATCCAGGCT**
GTGCTATCCCTGTACGCCTCTGGCCGTACCACTGGCATCGTGATGGACTCCGGTGACGGGGTCACCCAC
ACTGTGCCCATCTACGAGGGGTATGCCCTCCCCCATGCCATCCTGCGTCTGGACCTGGCTGGCCGGGAC
CTGACTGACTACCTCATGAAGATCCTCACCGAGCGCGGCTACAGCTTCACCACCACGGCCGAGCGGGAA
ATCGTGCGTGACATTAAGGAGAAGCTGTGCTACGTCGCCCTGGACTTCGAGCAAGAGATGGCCACGGCT
GCTTCCAGCTCCTCCCTGGAGAAGAGCTACGAGCTGCCTGACGGCCAGGTCATCACCATTGGCAATGAG
CGGTTCCGCTGCCCTGAGGCACTCTTCCAGCCTTCCTTCCT**GG**GCATGGAGTCCTGTGGCATCCACGAA
ACTACCTTCAACTCCATCATGAAGTGTGACGTGGACATCCGCAAAGACCTGTACGCCAACACAGTGCTG
TCTGGCGGCACCACCATGTACCCTGGCATTGCCGACAGGATGCAGAAGGAGATCACTGCCCTGGCACCC
AGCACAATGAAGATCAAG**ATCATTGCTCCTCCTGAGCGCAAGTACTCCGTGTGGATCGGCGGCTCCATC**
CTGGCCTCGCTGTCCACCTTCCAGCAGATGTGGATCAGCAAGCAGGAGTATGACGAGTCCGGCCCCTCC
ATCGTCCACCGCAAATGCTTCTAG

Start codon

Forward Primer β-actin

Reverse Primer β-actin

Stop codon

Difference in coding length between forward and reverse primer for β-actin: **499** nucleotides

Appendix C – Dundee sequencing results

Topo IIα

Forward primer PCR product

Dundee result

ATTGTTCCGGTGTCTCAGATGCTGATAGTGGTGCTGAAGGAATCGGTACTGGGTGGTCCTGCAAAATCC
CCAACTTTGATGTGCGTGAAATTGTAAATAACATCAGGCGTTTGATGGATGGAGAAGAACCTTTGCCAA
TGCTTCCAAGTTACAAGAACTTCAAGGGTACTATTGAAGAACTGGCTCCAAATCAATATGTGATTAGTG
GTGAAGTAGCTATTCTTAATTCTACAACCATTGAAATCTCAGAGCTTCCCGTCAGAACATGGACCCAGA
CATACAAAGAACAAGTTCTAGAACCCATGTTGAATGGCACCGAGAAGACACCTCCTCTCATAACAGACT
ATAGGGAATACCATACAGATACCACTGTGAAATTTGTTGTGAAGATGACTGAAGAAAAACTGGCAGAGG
CAGAGAGAGTTGGACTACACAAAGTCTTCAAACTCCAAACTAGTCTCACATGCAACTCTATGGTGCTTT
TTGACCACGTAGGCTGTTTAAAGAAATATGACACGGTGTTGGATATTCTAAGAGACTTTTTTGAACTCA
GACTTAAATATTATGGATTAAGAAAAGAATGGCTCCTAGGAATGCTTGGTGCTGAATCTGCTAAACTGA
ATAATCAGGCTCGCTTTATCTTAGAGAAAATAGATGGCAAAATAATCATTGAAAATAAGCCTAAGAAAG
AATTAATTAAAGTTCTGATTCAGAGGGGATATGATTCGGATCCTGTGAAGGCCTGGAAAGAAGCCCAGC
AAAAGGCTCCAGATGAAGAAGAAAATGAAGAGAGTGACAACGAAAAGGAAACTGAAAAGAGTGACTCCG
TAACAGATTCTGGACCAACCTTCAACTATCTTCTTGATATGCCCCTTTGTATTTAACCAAGGAAAGAAA
GATGAACTCTGCAGGCTAAGAAATGAAAAGACAGAGCTGGACACATTAAAAGAAGAGTCCATCAGATTG
TGGAAGAGACTGCTACATTTATTGAGATGGAGCTGTGAGCAGAAAACAGATGACAGTCGACTCTGGGAA
GGGGAGCAGGGAAAAAAACACAATTGCTGAGTTTGCCTCTCCGCGGTGTCAAGAGTCATCCGATACTGA
TGAGCGAAGGCGGAAGGAATAAGAATAGATGAAATCTGAGAGCCTTAGAGAGTGTGTGGCACAGAGGCT
ACCAAGTGGAGGACCGAAAGGAC

LALIGN result: Dundee result vs expected for topo IIα

```
ulimit -t 30; /usr/molbio/bin/lalign -f -14 -g -
4 ./wwwtmp/.4737.1.seq ./wwwtmp/.4737.2.seq 3 > ./wwwtmp/.4737.out LALIGN finds the
best local alignments between two sequences version 2.1u09 December 2006 Please cite:
X. Huang and W. Miller (1991) Adv. Appl. Math. 12:373-381 resetting to DNA matrix
alignments < E( 0.05):score: 80 (50 max)
 Comparison of:
(A) ./wwwtmp/.4737.1.seq Result primer F2 1196 bp                          - 1196 nt
(B) ./wwwtmp/.4737.2.seq Expected 1283 bp                                  - 1283 nt
 using matrix file: DNA (5/-4), gap-open/ext: -14/-4 E(limit)   0.05
```

94.4% identity in 1123 nt overlap (18-1098:40-1162); score: 4754 E(10000):0

```
         20         30         40         50         60         70
Result GATGCTGATAG-TGGTGCTGAAGGAATCGGTACTGGGTGGTCCTGCAAAATCCCCAACTT
       : ::::::::  ::::::::::::::::::::::::::::::::::::::::::::::::
Expect GGTGCTGATAAATGGTGCTGAAGGAATCGGTACTGGGTGGTCCTGCAAAATCCCCAACTT
      40         50         60         70         80         90

         80         90        100        110        120        130
Result TGATGTGCGTGAAATTGTAAATAACATCAGGCGTTTGATGGATGGAGAAGAACCTTTGCC
       ::::::::::::::::::::::::::::::::::::::::::::::::::::::::::::
Expect TGATGTGCGTGAAATTGTAAATAACATCAGGCGTTTGATGGATGGAGAAGAACCTTTGCC
     100        110        120        130        140        150

        140        150        160        170        180        190
Result AATGCTTCCAAGTTACAAGAACTTCAAGGGTACTATTGAAGAACTGGCTCCAAATCAATA
       ::::::::::::::::::::::::::::::::::::::::::::::::::::::::::::
```

```
Expect AATGCTTCCAAGTTACAAGAACTTCAAGGGTACTATTGAAGAACTGGCTCCAAATCAATA
     160       170       180       190       200       210

        200       210       220       230       240       250
Result TGTGATTAGTGGTGAAGTAGCTATTCTTAATTCTACAACCATTGAAATCTCAGAGCTTCC
       ::::::::::::::::::::::::::::::::::::::::::::::::::::::::::::
Expect TGTGATTAGTGGTGAAGTAGCTATTCTTAATTCTACAACCATTGAAATCTCAGAGCTTCC
     220       230       240       250       260       270

        260       270       280       290       300       310
Result CGTCAGAACATGGACCCAGACATACAAAGAACAAGTTCTAGAACCCATGTTGAATGGCAC
       ::::::::::::::::::::::::::::::::::::::::::::::::::::::::::::
Expect CGTCAGAACATGGACCCAGACATACAAAGAACAAGTTCTAGAACCCATGTTGAATGGCAC
     280       290       300       310       320       330

        320       330       340       350       360       370
Result CGAGAAGACACCTCCTCTCATAACAGACTATAGGGAATACCATACAGATACCACTGTGAA
       ::::::::::::::::::::::::::::::::::::::::::::::::::::::::::::
Expect CGAGAAGACACCTCCTCTCATAACAGACTATAGGGAATACCATACAGATACCACTGTGAA
     340       350       360       370       380       390

        380       390       400       410       420       430
Result ATTTGTTGTGAAGATGACTGAAGAAAAACTGGCAGAGGCAGAGAGAGTTGGACTACACAA
       ::::::::::::::::::::::::::::::::::::::::::::::::::::::::::::
Expect ATTTGTTGTGAAGATGACTGAAGAAAAACTGGCAGAGGCAGAGAGAGTTGGACTACACAA
     400       410       420       430       440       450

        440       450       460       470       480       490
Result AGTCTTCAAACTCCAAACTAGTCTCACATGCAACTCTATGGTGCTTTTTGACCACGTAGG
       ::::::::::::::::::::::::::::::::::::::::::::::::::::::::::::
Expect AGTCTTCAAACTCCAAACTAGTCTCACATGCAACTCTATGGTGCTTTTTGACCACGTAGG
     460       470       480       490       500       510

        500       510       520       530       540       550
Result CTGTTTAAAGAAATATGACACGGTGTTGGATATTCTAAGAGACTTTTTTGAACTCAGACT
       ::::::::::::::::::::::::::::::::::::::::::::::::::::::::::::
Expect CTGTTTAAAGAAATATGACACGGTGTTGGATATTCTAAGAGACTTTTTTGAACTCAGACT
     520       530       540       550       560       570

        560       570       580       590       600       610
Result TAAATATTATGGATTAAGAAAAGAATGGCTCCTAGGAATGCTTGGTGCTGAATCTGCTAA
       ::::::::::::::::::::::::::::::::::::::::::::::::::::::::::::
Expect TAAATATTATGGATTAAGAAAAGAATGGCTCCTAGGAATGCTTGGTGCTGAATCTGCTAA
     580       590       600       610       620       630

        620       630       640       650       660       670
Result ACTGAATAATCAGGCTCGCTTTATCTTAGAGAAAATAGATGGCAAAATAATCATTGAAAA
       ::::::::::::::::::::::::::::::::::::::::::::::::::::::::::::
Expect ACTGAATAATCAGGCTCGCTTTATCTTAGAGAAAATAGATGGCAAAATAATCATTGAAAA
     640       650       660       670       680       690

        680       690       700       710       720       730
Result TAAGCCTAAGAAAGAATTAATTAAAGTTCTGATTCAGAGGGGATATGATTCGGATCCTGT
       ::::::::::::::::::::::::::::::::::::::::::::::::::::::::::::
Expect TAAGCCTAAGAAAGAATTAATTAAAGTTCTGATTCAGAGGGGATATGATTCGGATCCTGT
     700       710       720       730       740       750

        740       750       760       770       780       790
Result GAAGGCCTGGAAAGAAGCCCAGCAAAAGGCTCCAGATGAAGAAGAAAATGAAGAGAGTGA
       :::::::::::::::::::::::::: :::::::::::::::::::::::::::::::::
Expect GAAGGCCTGGAAAGAAGCCCAGCAAAAGGTTCCAGATGAAGAAGAAAATGAAGAGAGTGA
```

```
     760       770       780       790       800       810

        800       810       820       830       840       850
Result CAACGAAAAGGAAACTGAAAAGAGTGACTCCGTAACAGATTCTGGACCAACCTTCAACTA
       ::::::::::::::::::::::::::::::::::::::::::::::::::::::::::::
Expect CAACGAAAAGGAAACTGAAAAGAGTGACTCCGTAACAGATTCTGGACCAACCTTCAACTA
     820       830       840       850       860       870

        860       870        880       890        900       910
Result TCTTCTTGATATGCCCCTTTG-TATTTAACCAAGGAAA-GAAAGATGAACTCTGCAGGCT
       :::::::::::::::::::: ::::::::::::::: :::::::::::::::::::::
Expect TCTTCTTGATATGCCCCTTTGGTATTTAACCAAGGAAAAGAAAGATGAACTCTGCAGGCT
     880       890       900       910       920       930

          920          930       940          950       960
Result AAGAAATGAAAA-GAC--AGAGCTGGACACATTAAAAG--AAGAGTCCATCAGATT-GTG
       :::::::::::: ::   ::::::::::::::::::   ::::::::::::::: :::
Expect AAGAAATGAAAAAGAACAAGAGCTGGACACATTAAAAAGAAAGAGTCCATCAGATTTGTG
     940       950       960       970       980       990

      970           980       990          1000             1010
Result GAAG--AGACT--GCTACATTTATTGA-GA--TGGAG-CTGTG-------AGCAGAAAAC
       :::   :::::  :::::::::::::: ::  ::::: ::::         :: : :::
Expect GAAAGAAGACTTGGCTACATTTATTGAAGAATTGGAGGCTGTTGAAGCCAAGGAAAAACA
    1000      1010      1020      1030      1040      1050

         1020          1030      1040              1050      1060
Result AGATGAC--AGTCG-ACT--CTGGGAAGGGGAGCA--------GGGAAAAAAACACAATT
       ::::::   ::::: :::  ::::::: ::: : :        ::::::::::::::: :
Expect AGATGAACAAGTCGGACTTCCTGGGAAAGGGGGGAAGGCCAAGGGGAAAAAAACACAAAT
    1060      1070      1080      1090      1100      1110

               1070       1080       1090
Result G-CTGAG--TTTGCCT-CTCCGCGGTGTCAA-GAGTCATCCGA
       : ::::   ::::::: :::::::  ::::: ::::::: : :
Expect GGCTGAAGTTTTGCCTTCTCCGCGTGGTCAAAGAGTCATTCCA
    1120      1130      1140      1150      1160
```

BLAST result: Dundee result

Accession	Description	Max score	Total score	Query coverage	E value	Max ident	Links
	Transcripts						
NM_001067.2	Homo sapiens topoisomerase (DNA) II alpha 170kDa (TOP2A), mRNA	1764	1764	89%	0.0	**95%**	UE GM

Reverse primer PCR product

Dundee result

```
CCGTTGCTTTTTCCTCTTAGTTTTTTCTCAAAATCTGAGAAATCTTCATCTGAATCCAAATCCATTGTG
AATTTTGATTTTGTTGCTGCTCTCCGTGGCTCTGTTTCTCGTGGAGGGACATCAAAATTACTTTCGTCA
CTGCTCCTATCTGATTCTGAATCAGACCAGGGATTTCTCTTCTTTCCTTTTTTGATTGGCTTAAATGCC
AATGTAGTTTGTTTCTTTGACTTTGTACCTGGTTCTCTTTTCTGTTTCTTTTCTAATCTTTGTTTTAGG
CCTTCTAGTTCCACACCATCTTCTTGAGGGCTTCCTTCAGTATTTTCATTCTTAATTTTCTTTTTATTT
TTCTTTTCTGCCTCTGCTTTCATTTCTATGGTTATTCGTGGAATGACTCTTTGACCACGCCAA
```

LALIGN result: Dundee result vs expected for topo IIα

LALIGN finds the best local alignments between two sequences version 2.1u09 December 2006 Please cite: X. Huang and W. Miller (1991) Adv. Appl. Math. 12:373-381 resetting to DNA matrix alignments < E(0.05):score: 68 (50 max)

```
 Comparison of:
(A) ./wwwtmp/.18363.1.seq Ideal Topo II alpha sequence 408 bp              - 408 nt
(B) ./wwwtmp/.18363.2.seq Result with topo II alpha reverse primer 408 bp   - 408 nt
 using matrix file: DNA (5/-4), gap-open/ext: -14/-4 E(limit)   0.05
```

97.8% identity in 400 nt overlap (1-399:4-400); score: 1863 E(10000): 1.1e-147

```
               10        20        30        40        50        60
Ideal  GCGTGGTCAAAGAGTCATTCCACGAATAACCATAGAAATGAAAGCAGAGGCAGAAAAGAA
       ::::::::::::::::::::::::::::::::::::::::::::::::::::::::::::
Result GCGTGGTCAAAGAGTCATTCCACGAATAACCATAGAAATGAAAGCAGAGGCAGAAAAGAA
            10        20        30        40        50        60

               70        80        90       100       110       120
Ideal  AAATAAAAAGAAAATTAAGAATGAAAATACTGAAGGAAGCCCTCAAGAAGATGGTGTGGA
       ::::::::::::::::::::::::::::::::::::::::::::::::::::::::::::
Result AAATAAAAAGAAAATTAAGAATGAAAATACTGAAGGAAGCCCTCAAGAAGATGGTGTGGA
            70        80        90       100       110       120

              130       140       150       160       170       180
Ideal  ACTAGAAGGCCTAAAACAAAGATTAGAAAAGAAACAGAAAAGAGAACCAGGTACAAAGAC
       ::: ::::::::::::::::::::::::::::::::::::::::::::::::::::: :
Result ACT-GAAGGCCTAAAACAAAGATTAGAAAAGAAACAGAAAAGAGAACCAGGTACAAAGTC
            130       140       150       160       170       180

              190       200       210        220       230
Ideal  AAAGAAACAAACTACATTGGCATTTAAGCCAAT-CAAAAAAGGAAAGAAGAGAAATCCCT
       :::::::::::::::::::::::::::::::: :::::::::::::::::::::::::
Result AAAGAAACAAACTACATTGGCATTTAAGCCAATTCAAAAAAGGAAAGAAGAGAAATCCCT
            190       200       210       220       230       240

     240       250       260       270       280       290
Ideal  GGTCTGATTCAGAATCAGATAGGAGCAGTGACGAAAGTAATTTTGATGTCCCTCCACGAG
       ::::::::::::::::::::::::::::::::::::::::::::::::::::::::::::
Result GGTCTGATTCAGAATCAGATAGGAGCAGTGACGAAAGTAATTTTGATGTCCCTCCACGAG
            250       260       270       280       290       300

     300       310       320       330       340       350
Ideal  AAACAGAGCCACGGAGAGCAGCAACAAAAACAAAATTCACAATGGATTTGGATTCAGATG
       :::::::::::::::::::::::::::: :::::::::::::::::::::::::::::
Result AAACAGAGCCACGGAGAGCAGCAACAAAATCAAAATTCACAATGGATTTGGATTCAGATG
            310       320       330       340       350       360
```

```
     360       370       380       390
Ideal  AAGATTTCTCAGATTTTGATGAAAAAACTGATGATGAAGA
       :::::::::::::::::: ::::::::: : :: ::: :
Result AAGATTTCTCAGATTTTGA-GAAAAAACT-AAGAGGAAAA
            370       380        390        400
```

BLAST result: Dundee result

Accession	Description	Max score	Total score	Query coverage	E value	Max ident	Links
			Transcripts				
NM_001067.2	Homo sapiens topoisomerase (DNA) II alpha 170kDa (TOP2A), mRNA	688	688	94%	0.0	**98%**	

Appendix D – Dundee sequencing results

β-actin

Forward primer PCR product

Dundee result

```
CGAACAAGCAACCGCGAGAAGTGACCCAGATCATGTTTGAGACCTTCAACACCCCAGCCATGTACGTTG
CTATCCAGGCTGTGCTATCCCTGTACGCCTCTGGCCGTACCACTGGCATCGTGATGGACTCCGGTGACG
GGGTCACCCACACTGTGCCCATCTACGAGGGGTATGCCCTCCCCCATGCCATCCTGCGTCTGGACCTGG
CTGGCCGGGACCTGACTGACTACCTCATGAAGATCCTCACCGAGCGCGGCTACAGCTTCACCACCACGG
CCGAGCGGGAAATCGTGCGTGACATTAAGGAGAAGCTGTGCTACGTCGCCCTGGACTTCGAGCAAGAGA
TGGCCACGGCTGCTTCCAGCTCCTCCCTGGAGAAGAGCTACGAGCTGCCTGACGGCCAGGTCATCACCA
TTGGCAATGAGCGGTTCCGCTGCCCTGAGGCACTCTCCGCTT
```

LALIGN result: Dundee result vs expected for β-actin

LALIGN finds the best local alignments between two sequences version 2.1u09 December 2006 Please cite: X. Huang and W. Miller (1991) Adv. Appl. Math. 12:373-381 resetting to DNA matrix alignments < E(0.05):score: 69 (50 max)

```
 Comparison of:
(A) ./wwwtmp/.14327.1.seq results dundee forward beta-actin primer 456 bp    - 456 nt
(B) ./wwwtmp/.14327.2.seq ideal result beta-actin 435 bp                     - 435 nt
 using matrix file: DNA (5/-4), gap-open/ext: -14/-4 E(limit)   0.05
```

99.7% identity in 395 nt overlap (9-402:41-435); score: 1952 E(10000): 5e-155

```
       10        20         30        40        50        60
result CAACCGCGAGAAG-TGACCCAGATCATGTTTGAGACCTTCAACACCCCAGCCATGTACGT
       :::::::::::: :::::::::::::::::::::::::::::::::::::::::::::
ideal  CAACCGCGAGAAGATGACCCAGATCATGTTTGAGACCTTCAACACCCCAGCCATGTACGT
               50        60        70        80        90       100

        70        80        90       100       110       120
result TGCTATCCAGGCTGTGCTATCCCTGTACGCCTCTGGCCGTACCACTGGCATCGTGATGGA
       ::::::::::::::::::::::::::::::::::::::::::::::::::::::::::::
ideal  TGCTATCCAGGCTGTGCTATCCCTGTACGCCTCTGGCCGTACCACTGGCATCGTGATGGA
              110       120       130       140       150       160

       130       140       150       160       170       180
result CTCCGGTGACGGGGTCACCCACACTGTGCCCATCTACGAGGGGTATGCCCTCCCCCATGC
       ::::::::::::::::::::::::::::::::::::::::::::::::::::::::::::
ideal  CTCCGGTGACGGGGTCACCCACACTGTGCCCATCTACGAGGGGTATGCCCTCCCCCATGC
              170       180       190       200       210       220

       190       200       210       220       230       240
result CATCCTGCGTCTGGACCTGGCTGGCCGGGACCTGACTGACTACCTCATGAAGATCCTCAC
       ::::::::::::::::::::::::::::::::::::::::::::::::::::::::::::
ideal  CATCCTGCGTCTGGACCTGGCTGGCCGGGACCTGACTGACTACCTCATGAAGATCCTCAC
              230       240       250       260       270       280

       250       260       270       280       290       300
result CGAGCGCGGCTACAGCTTCACCACCACGGCCGAGCGGGAAATCGTGCGTGACATTAAGGA
       ::::::::::::::::::::::::::::::::::::::::::::::::::::::::::::
```

```
ideal  CGAGCGCGGCTACAGCTTCACCACCACGGCCGAGCGGGAAATCGTGCGTGACATTAAGGA
              290       300       310       320       330       340

       310       320       330       340       350       360
result GAAGCTGTGCTACGTCGCCCTGGACTTCGAGCAAGAGATGGCCACGGCTGCTTCCAGCTC
       ::::::::::::::::::::::::::::::::::::::::::::::::::::::::::::
ideal  GAAGCTGTGCTACGTCGCCCTGGACTTCGAGCAAGAGATGGCCACGGCTGCTTCCAGCTC
              350       360       370       380       390       400

       370       380       390       400
result CTCCCTGGAGAAGAGCTACGAGCTGCCTGACGGCC
       ::::::::::::::::::::::::::::::::
ideal  CTCCCTGGAGAAGAGCTACGAGCTGCCTGACGGCC
              410       420       430
```

BLAST result: Dundee result

Accession	Description	Max score	Total score	Query coverage	E value	Max ident	Links
		Transcripts					
NM_001101.2	Homo sapiens actin, beta (ACTB), mRNA	811	811	96%	0.0	**99%**	GM

Reverse primer PCR product

Dundee result

```
CCAGCCGGACGCTCTTGCCATGGTGATGACCTGGCCGTCAGGCAGCTCGTAGCTCTTCTCCAGGGAGGA
GCTGGAAGCAGCCGTGGCCATCTCTTGCTCGAAGTCCAGGGCGACGTAGCACAGCTTCTCCTTAATGTC
ACGCACGATTTCCCGCTCGGCCGTGGTGGTGAAGCTGTAGCCGCGCTCGGTGAGGATCTTCATGAGGTA
GTCAGTCAGGTCCCGGCCAGCCAGGTCCAGACGCAGGATGGCATGGGGGAGGGCATACCCCTCGTAGAT
GGGCACAGTGTGGGTGACCCCGTCACCGGAGTCCATCACGATGCCAGTGGTACGGCCAGAGGCGTACAG
GGATAGCACAGCCTGGATAGCAACGTACATGGCTGGGGTGTTGAAGGTCTCAAACATGATCTGGGTCAT
CTTCTCGCGGTTGGCCTTGGGGTTCAGGGGGGCCTCGGGCTTTTAGCGCCCACGGCTTCAACATCGCAC
TTACTTGATTATACCCTACCAGGGGTAAAATCCGCGG
```

LALIGN result: Dundee result vs expected for β-actin

LALIGN finds the best local alignments between two sequences version 2.1u09 December 2006 Please cite: X. Huang and W. Miller (1991) Adv. Appl. Math. 12:373-381 resetting to DNA matrix alignments < E(0.05):score: 71 (50 max)

```
 Comparison of:
(A) ./wwwtmp/.6108.1.seq results dundee reverse beta-actin primer 520 bp    - 520 nt
(B) ./wwwtmp/.6108.2.seq ideal result beta-actin 495 bp                     - 495 nt
 using matrix file: DNA (5/-4), gap-open/ext: -14/-4 E(limit)   0.05
```

98.7% identity in 456 nt overlap (67-519:10-465); score: 2184
E(10000): 3e-174

```
         70        80        90       100       110       120
result GCCCGAGGCCCCCCTGAACCCCAAGGCCAACCGCGAGAAGATGACCCAGATCATGTTTGA
       : ::::::::::::::::::::::::::::::::::::::::::::::::::::::::::::
```

```
ideal  GACCGAGGCCCCCCTGAACCCCAAGGCCAACCGCGAGAAGATGACCCAGATCATGTTTGA
      10        20        30        40        50        60

        130       140       150       160       170       180
result GACCTTCAACACCCCAGCCATGTACGTTGCTATCCAGGCTGTGCTATCCCTGTACGCCTC
       ::::::::::::::::::::::::::::::::::::::::::::::::::::::::::::
ideal  GACCTTCAACACCCCAGCCATGTACGTTGCTATCCAGGCTGTGCTATCCCTGTACGCCTC
      70        80        90       100       110       120

        190       200       210       220       230       240
result TGGCCGTACCACTGGCATCGTGATGGACTCCGGTGACGGGGTCACCCACACTGTGCCCAT
       ::::::::::::::::::::::::::::::::::::::::::::::::::::::::::::
ideal  TGGCCGTACCACTGGCATCGTGATGGACTCCGGTGACGGGGTCACCCACACTGTGCCCAT
     130       140       150       160       170       180

        250       260       270       280       290       300
result CTACGAGGGGTATGCCCTCCCCCATGCCATCCTGCGTCTGGACCTGGCTGGCCGGGACCT
       ::::::::::::::::::::::::::::::::::::::::::::::::::::::::::::
ideal  CTACGAGGGGTATGCCCTCCCCCATGCCATCCTGCGTCTGGACCTGGCTGGCCGGGACCT
     190       200       210       220       230       240

        310       320       330       340       350       360
result GACTGACTACCTCATGAAGATCCTCACCGAGCGCGGCTACAGCTTCACCACCACGGCCGA
       ::::::::::::::::::::::::::::::::::::::::::::::::::::::::::::
ideal  GACTGACTACCTCATGAAGATCCTCACCGAGCGCGGCTACAGCTTCACCACCACGGCCGA
     250       260       270       280       290       300

        370       380       390       400       410       420
result GCGGGAAATCGTGCGTGACATTAAGGAGAAGCTGTGCTACGTCGCCCTGGACTTCGAGCA
       ::::::::::::::::::::::::::::::::::::::::::::::::::::::::::::
ideal  GCGGGAAATCGTGCGTGACATTAAGGAGAAGCTGTGCTACGTCGCCCTGGACTTCGAGCA
     310       320       330       340       350       360

        430       440       450       460       470       480
result AGAGATGGCCACGGCTGCTTCCAGCTCCTCCCTGGAGAAGAGCTACGAGCTGCCTGACGG
       ::::::::::::::::::::::::::::::::::::::::::::::::::::::::::::
ideal  AGAGATGGCCACGGCTGCTTCCAGCTCCTCCCTGGAGAAGAGCTACGAGCTGCCTGACGG
     370       380       390       400       410       420

        490       500         510
result CCAGGTCATCACCAT-GGCAA-GAGCG-TCCGGCTG
       :::::::::::::: ::::: ::::: : : ::::
ideal  CCAGGTCATCACCATTGGCAATGAGCGGTTCCGCTG
     430       440       450       460
```

BLAST result: Dundee result

Accession	Description	Max score	Total score	Query coverage	E value	Max ident	Links
		Transcripts					
NM_001101.2	Homo sapiens actin, beta (ACTB), mRNA	809	809	85%	0.0	**99%**	GM